Politecnico di Torino

Master’s Degree In Mechanical Engineering
A.a. 2022/2023
December 2022

Modeling and CFD analysis of piston compressor valve

Relatori:
Prof. Carlo Rosso
Ing. Marco Esposito
Ing. Chenye Jian

Candidati:
Lorenzo Giordano

Table of Contents

List of Figures

List of Tables

1 Introduction

Reciprocal compressors are one of the most common types of compressors. They may be found in a wide range of applications, including the oil and gas sector and the chemical industry, where these compressors are primarily employed for their capacity to deliver high-pressure gas. Because piston compressors play an important role in every process in which they are used, their dependability has sparked broad attention.

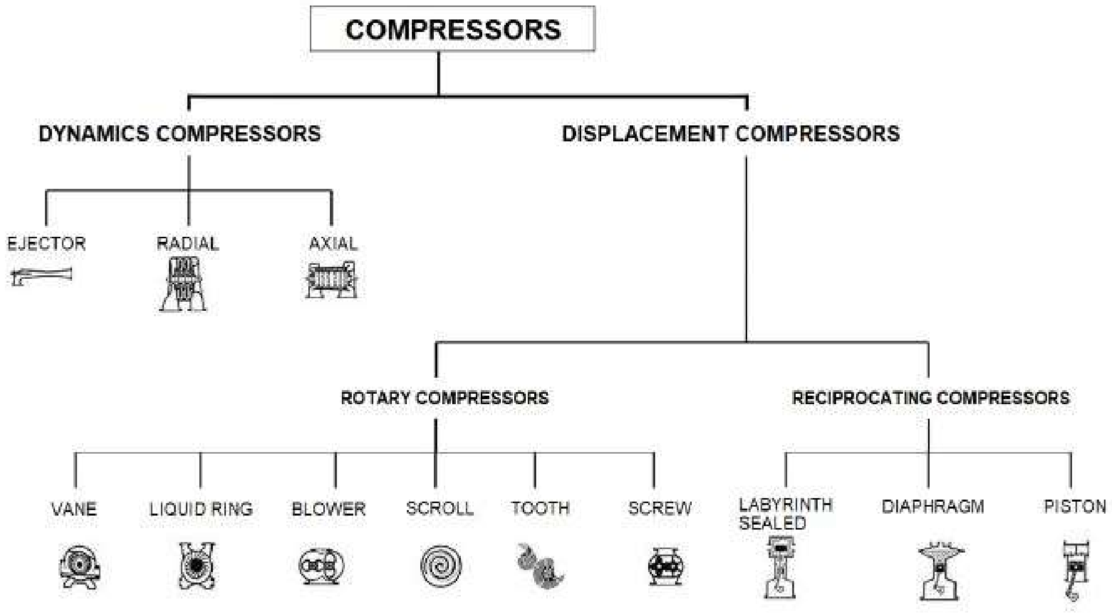

Figure 1.1 Compressor types

The primary distinction between displacement and dynamic compressors is how the fluid pressure inside them is increased [1].

The pressure rises with the flow of gas in a dynamic compressor, which accelerates significantly due to the revolving blades of a fan.

When the gas decelerates by expanding in a diffuser, its velocity is converted into static pressure. These compressors are classified as radial or axial depending on the principal direction of the gas flow. At constant rotational speed, the pressure and flow curve for a turbo-compressor is significantly different from an equivalent curve of a positive displacement compressor. The turbo-compressor is a machine with variable flow and variable pressure, whereas a positive displacement compressor is a machine with constant flow and variable pressure.
The compression ratio of a positive displacement volumetric compressor is also higher at low speed. Turbochargers are designed for large air volumes.

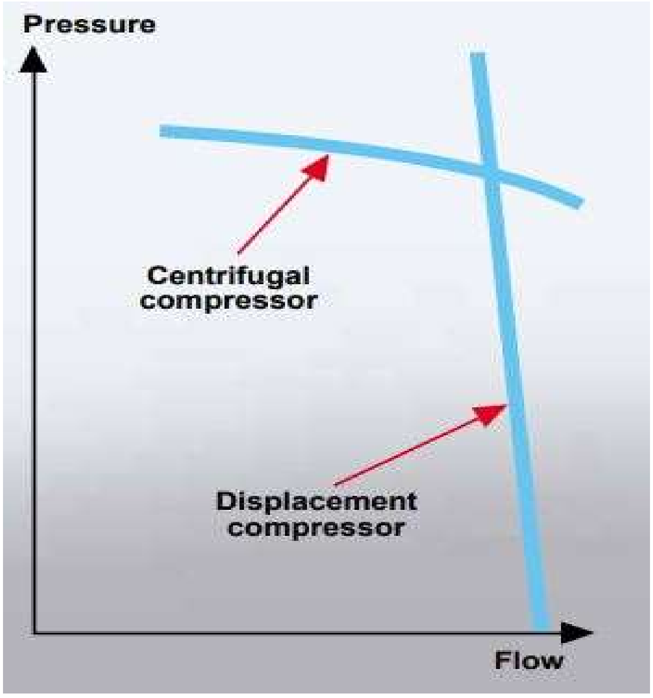

Figure 1.2 Pressure- Flow rate curve

A reciprocating or piston compressor (Fig1.3) is a compressor that is piston-driven by a crankshaft in order to deliver high-pressure gas. The compressor draws a volume of gas from a suction port and transports it to a cylinder, where it is trapped and compressed by a piston, reducing its volume. The pressurised gas is then expelled into the discharge pipe through the exhaust port. Valves regulate the flow of gas through the cylinder.

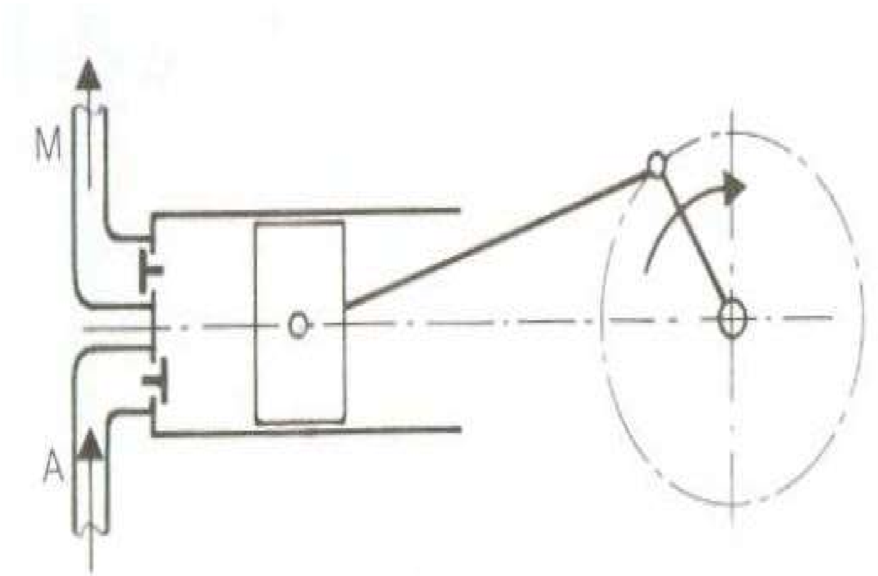

Figure 1.3 Piston Compressor Layout[2]

The compressor valves can be seen as limiting factors in the design of the reciprocating compressor. They are sometimes referred to as the compressor's heart because if they fail, the compressor will shut down, resulting in costly downtimes. Even at low rates of 700 rpm, a compressor's valves must open and close over one million times every day.

Dresser-Rand performed an industrial inquiry to identify and assess the causes of these shutdowns [3]. Fig. 2 displays an overview of these findings. Dresser-Rand states that among the most common causes of valve failures are high impact velocities, wear, corrosion, and application conditions.

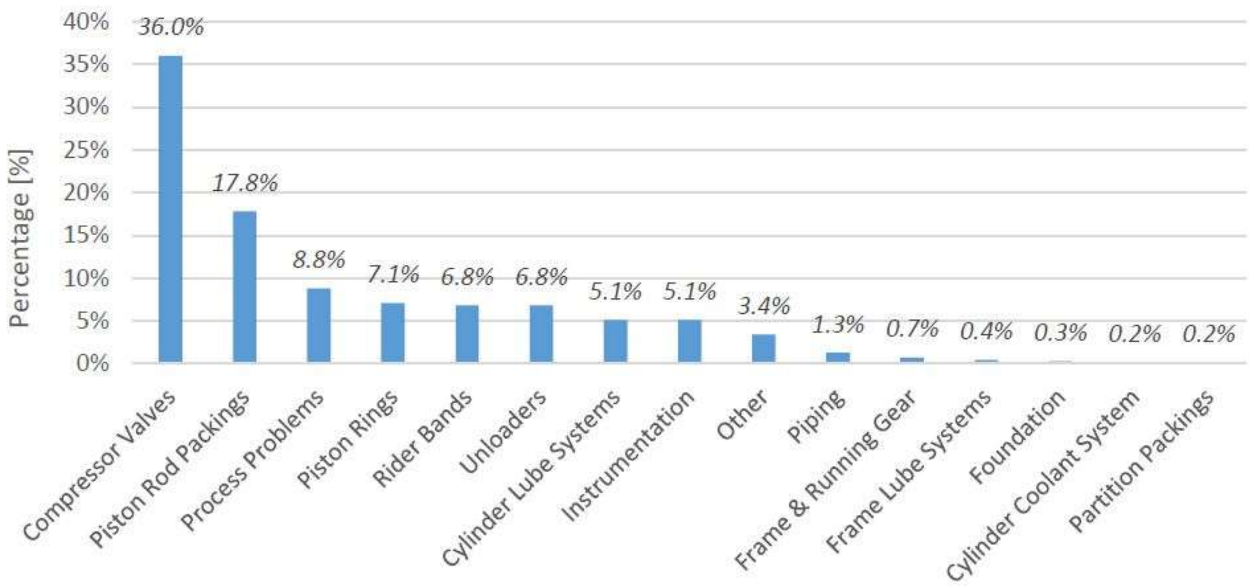

Figure 1.4 major causes of piston compressor failure

Figure 1.5a illustrates the relationship between pressure and volume for a theoretical compressor, while Figure 1.5b shows a diagram of a real piston compressor.
The stroke volume is the volume of the cylinder traversed by the piston during the suction phase.
The dead space is the volume immediately below the inlet and outlet valves and above the piston, which must remain at the upper inversion point of the piston for mechanical reasons.
The difference between the stroke volume and the volume intake of the air that remains in the dead space before the start of suction.
The difference between the theoretical p/V diagram and the actual diagram depends on the model of compressor (e.g. piston).

Valves are never totally sealed, so there is always a certain degree of leakage between the piston shell and the cylinder wall. Valves also cannot open and close completely without a slight delay, so that when gas flows into the channels, a pressure drop occurs. When flows into the cylinder, the gas also heats up.

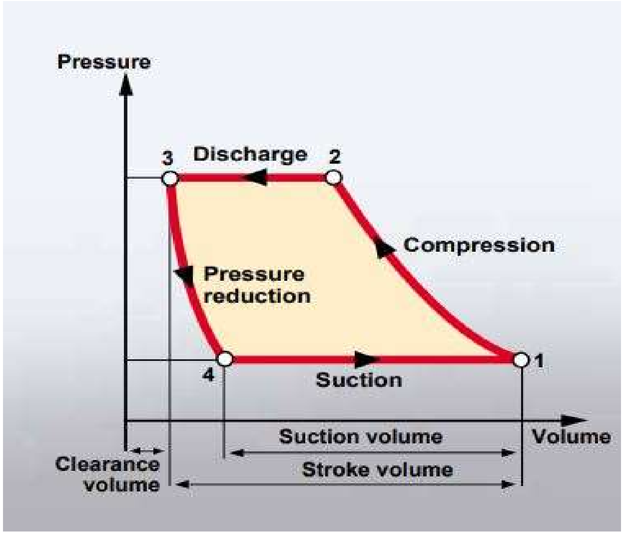

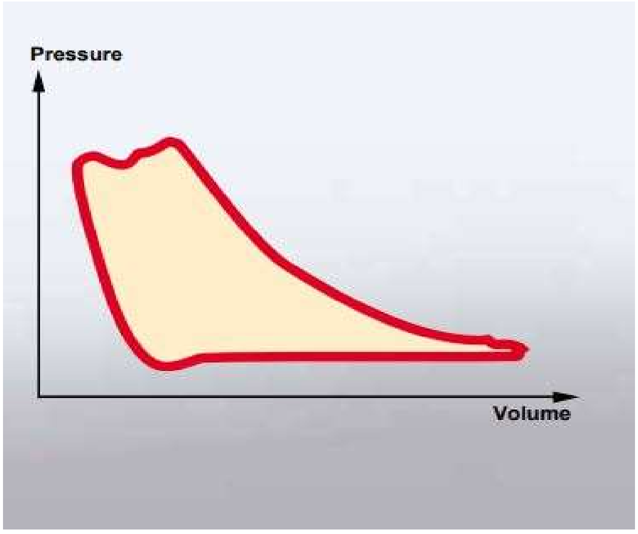

Figure 1.5 a P-V Ideal Diagram *Figure 1.5 b P-V Real Diagram*

1.1Piston compressor valves

This chapter will explain the relevance of automated valves, which are the focus of this research. Following that, we will briefly detail the valves that are typically used in modern reciprocating compressors, and at the end of this chapter, we will cover the valve design language that will be utilised throughout this thesis.

Compressor valves are classified into two categories based on their operating principle: automatic (self-acting) valves and mechanically operated valves. The pressure differential in front of and behind the valve activates automatic valves, and the motion of the latter is related to the action of the piston.

They are so called because of their capability to self-adapt to different working condition without the use of any actuating device. With respect to the mechanically-operated ones, these are so characterized by low costs and less problem of maintenance.
Mechanically operated valves have the benefit of being independent of forces arising from a gas flow, ensuring a complete valve opening under all operating conditions.

Their usage is now relatively limited because to the requirement of an actuation mechanism, which raises purchase prices. As a result, the great majority of compressors nowadays are equipped with automated valves. The working principle of automatic valves is described below,referring to the Thermodynanic phase illustrated in Fig. 1.6.

When the piston moves from the top dead centre (TDC) to the bottom dead centre (BDC), the gas expands, and when the pressure drops below the suction pressure, the valve lifts, enabling the gas to be sucked into the chamber. As the piston approaches the BDC, the pressure force can no longer compensate for the spring load, the suction valve closes, and compression begins.

The cylinder capacity decreases when the piston returns to TDC, raising pressure and temperature inside the chamber. When the pressure reaches the desired delivery pressure, the discharge valve opens, allowing the gas to escape. At the TDC, the discharge valve closes automatically in the same manner.

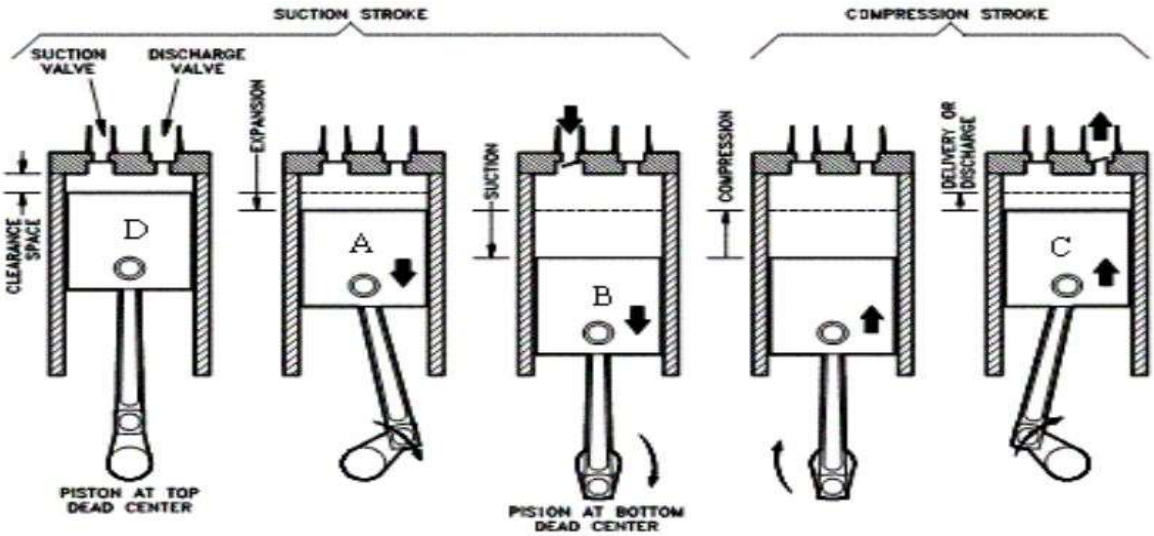

Figure 1.6 Piston Compressor Phases

The lift of the valves is clearly connected to the pressure within the cylinder and vice versa [4], as demonstrad in Fig.1.7 where the relationship between the cylinder pressure and the suction valve lift is shown.

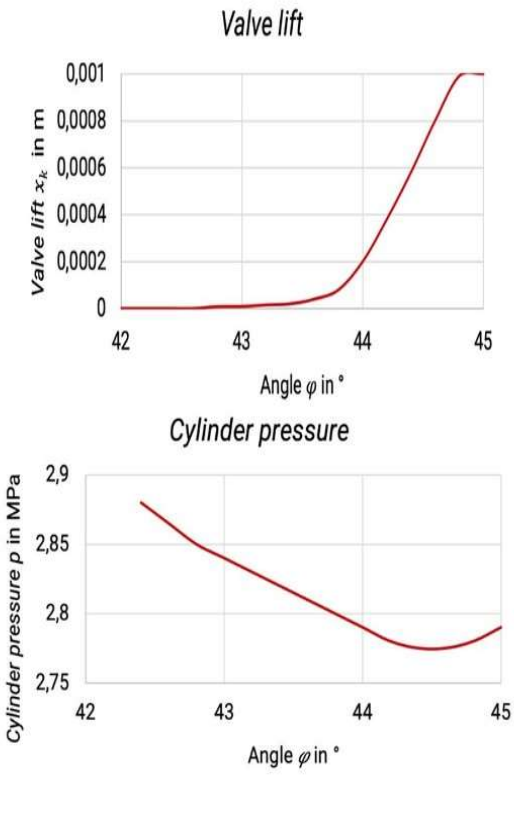

Figure 1.7 Relationship between Cylinder pressure and Suction valve lift

On the other hand, an uneven and discontinuous motion of the sealing element might create pulsing pressure behaviour, which increases losses during the discharge and suction phases.

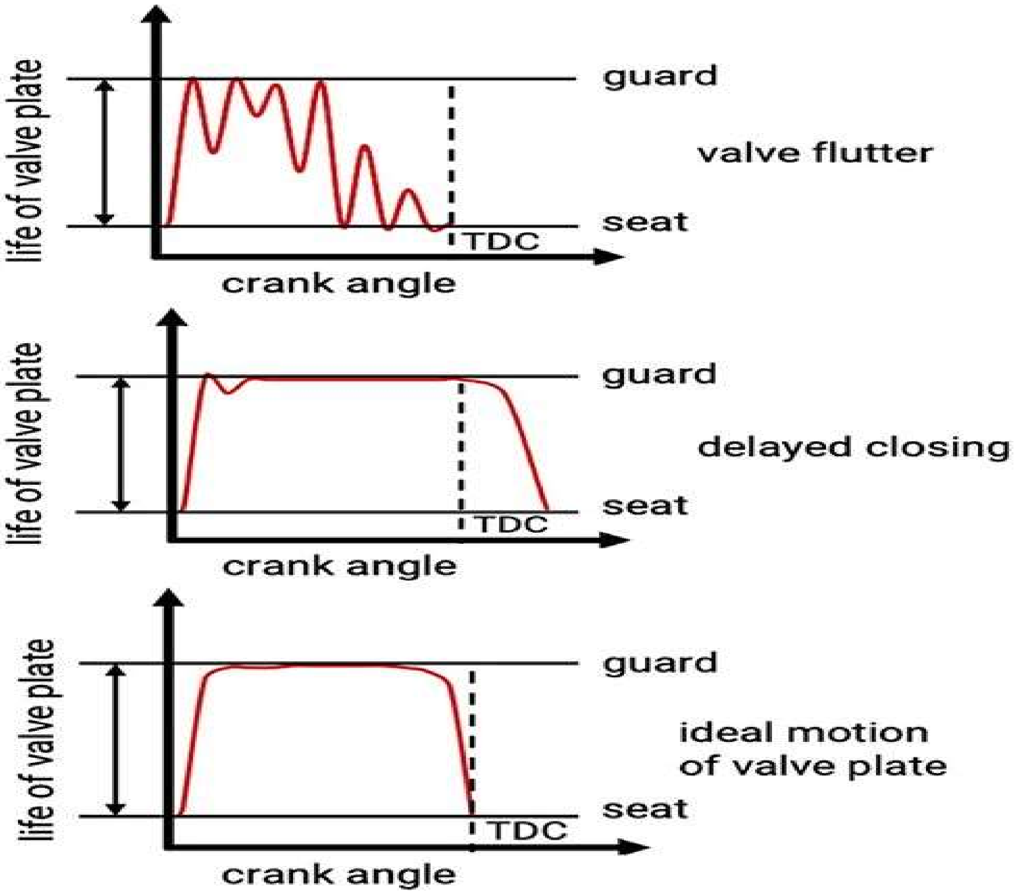

Figure 1.8 Ideal motion of valve plate in comparison to delayed closing and valve flutter

It is critical to carefully select and construct the valves so that the opening and closure happens optimally and the motion is as regular as possible.

The valve lift does not always behave like a step function but often shows oscillations (flutter) visible in Fig. 1.7 or the lift is characterised by a delayed opening or closure which can affect the capability of the compressor. In addition, oscillations of the reed repeatedly hitting the limiter could lead to high stresses and the phenomenon of impact fatigue failure, a phenomenon that has not been included in this work.

1.1.1 Valve terminology

All automated valves are distinguished by a few key components that, when combined, create the valve assembly. These are summed up as follows:

- Limiter
- Valve Port
- Valve seat
- Valve Plate

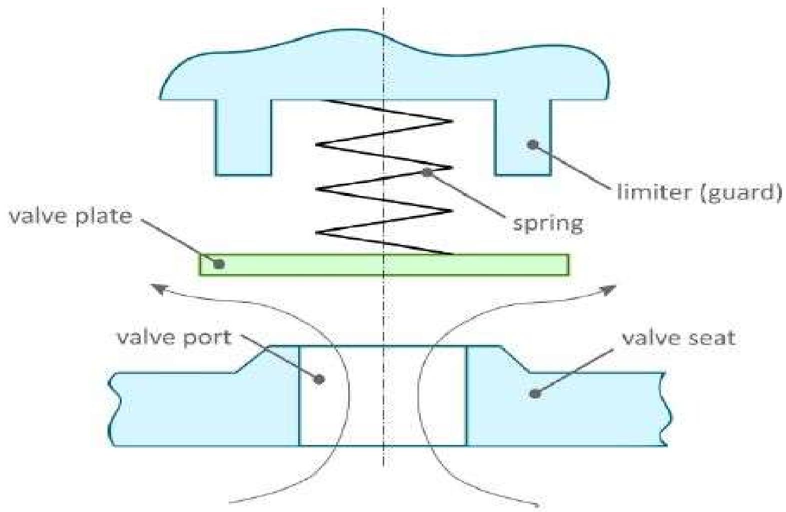

Figure 1.9 Generic Model of a valve assembly

Valve plates or, more broadly, sealing elements are considered moving components. This is the component that elevates during operation to cover the valve port, the passageway through which gas flows. The limiter (or guard) serves as a boundary for the sealing element's motion, and a spring regulates it by forcing it into contact with the valve seat when the valve is fully closed.

In other cases, the valve plate itself serves as the spring element (reed) since it elastically deflects in response to the pressure difference, as will be detailed below when the automatic valve types will be described below.

1.1.2 Automatic Valve Types

An automated valve theoretically consists of a movable sealing element, a device to restrict the lift of the moveable element when the valve is fully open, and a device to provide a force operating on the movable element to close it and then press it against the seat when the valve is closed.

- **Ring Valve.**

The movable elements in the ring valve (Figure 1.10) are concentrically arranged narrow rings around the axis of the valve. The independent rings make maintaining uniform flow control somewhat difficult, but they do have the advantage of low-stress levels due to the lack of stress concentration points.

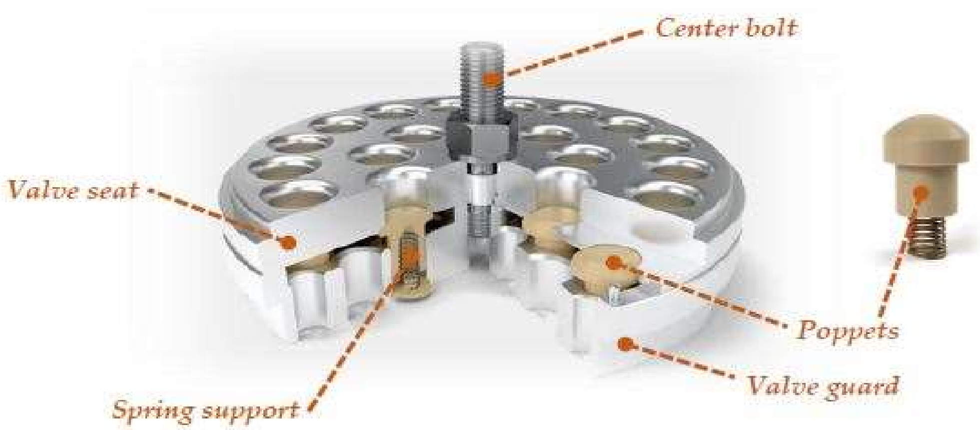

Figure 1.10 Ring Valve Assembly

- **Plate valve**

The plate valve design is identical to the preceding one, but the rings are connected to form a single moving element. This sealing element design change allows for the insertion of a second, non-sealing dampening disc. Between the valve body and the main moveable disc, the dampening disc is softly spring-loaded. Its purpose is to slow the sealing element as it approaches the valve guard, reducing the force of the impact.

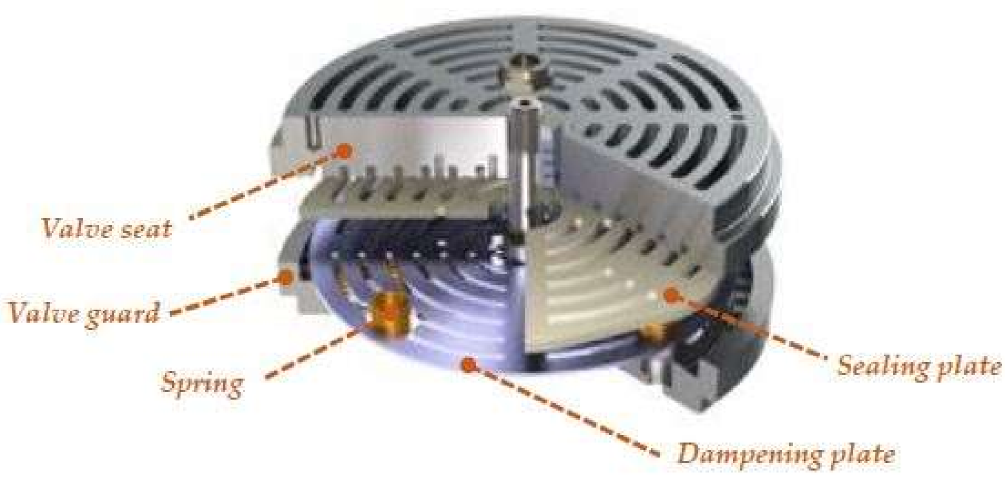

Figure 1.11 Plate Valve Assembly

- **Reed valve**

A reed valve usually consists of a valve reed, valve seat, limiter, gasket, and a spring. It is actuated due to the pressure difference acting across the valve. The hinged type of reed valve resembles a cantilever beam because in this case the reed is fixed on one side. For this type and the following one the spring is represented by the reed itself

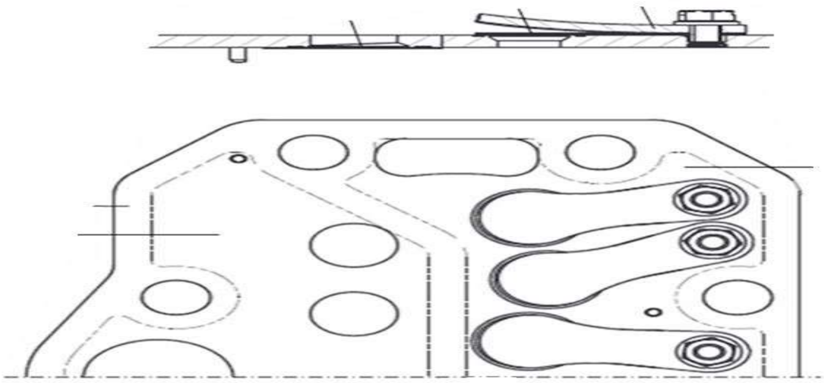

Figure 1.12 Reed Valve Assembly

- **Feather Valve**

The sealing element, called leaf, is represented by a long strip that opens as a simply supported beam. The strips, when in the seated position, completely cover the slots that form the air passages through the seat whereby the valve will be in the closed condition.

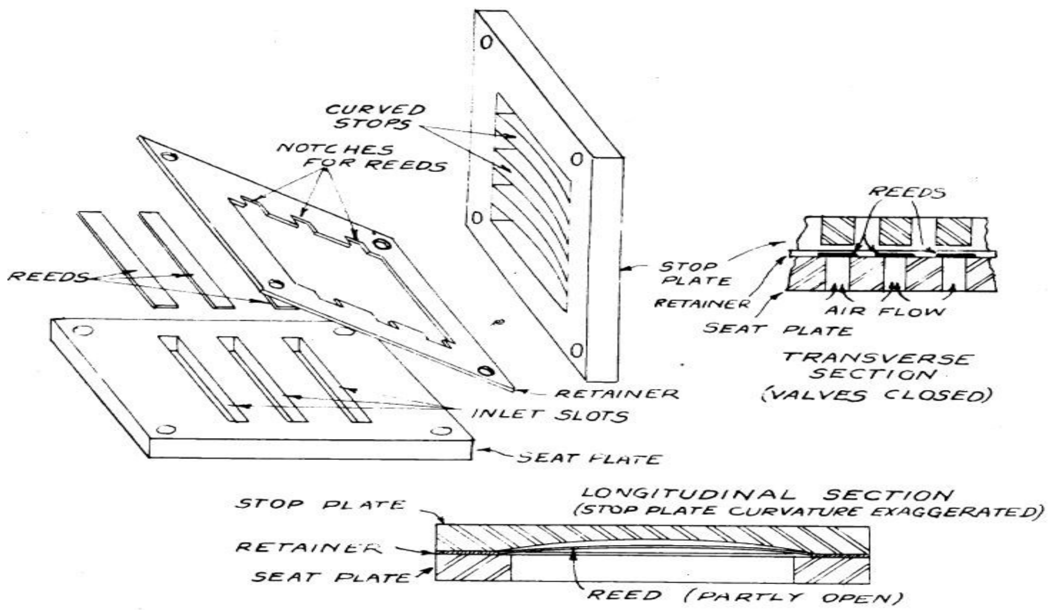

Figure 1.13 Feather Valve Assembly

1.2 Survey of Literature

Until the early twentieth century, valve design was little referenced in literature. However, the early attempts to explain valve behaviour were essentially empirical, despite the fact that experimental methods for recording valve activity, such as measuring lift as a function of time, were few. After the mid-20th century mathematical models appeared [5] [6] in the literature providing a thorough mathematical description of gas flow through valves and the thermodynamic process in a compressor cylinder. Computational fluid dynamics (CFD) has been utilised as a significant technique for compressor valve study since 1994.

There are three ways used in the development process: an experiment, computational fluid dynamics, and a simplified (analytical) model. Because tests are costly and time-consuming, they are only used in the later phases of valve development.

Using CFD to evaluate turbulent flow through valves, thermodynamic processes in the cylinder, and so on can give us with fairly precise findings even in three dimensions; nevertheless, even this technique to researching valve behaviour cannot be used adequately in the very early phases of development. This is mostly due to the lengthy preparation phase, which includes geometry preparation and discretization prior to performing the simulation itself. In [7] the valve study was carried out by both the analytical model and CFD showing that the error on the compressor flow rate of the analytical model can be neglected. Even because ,in those early phases, having a tool that can forecast the effect of broad characteristics on valve behaviour, such as valve mass, spring type, maximum valve lift, area through which gas flows, and so on, is quite important.

1.3 Thesis Structure

This thesis investigates the valve dynamics of a reciprocating compressor. To do this, a one-dimensional mathematical model of the valve is presented which includes the fluid-structure interaction as well as the effect of the whole compression cycle, including the processes in the cylinder, suction chamber, and discharge chamber, among others.

This approach to this mathematical model is distinguished by its adaptability and ease of customization.

A quick overview is provided. The contents of the several chapters of this paper are listed below.

The Chapter II was wholly devoted to the creation of a mathematical model capable of simulating valve dynamics in connection to the compression operating cycle. The goal was to design a tool that could be used to examine the impact of a given valve assembly on compressor performance.

Research focused on the simplified systems and associated equations that regulate this model, with a special emphasis on the underlying assumptions.

Chapter III describes the software through which the valve modeling is done how to connect the various submodels, and describes the outputs and their physical meaning.

In Chapter IV the model described in the previous chapters is used for the Reed valve, found in abundance in the literature from the modeling point of view, described above , focusing mainly on how to model the valve according to its geometric parameters. At the end of the chapter, a comparison is made between model outputs and measurements made in the laboratory to understand in the first instance whether the Methodology is able to achieve a certain degree of accuracy.

In Chapter V the feather valve is described in more detail than the description given in this introductory chapter. While In Chapter VI, a static CFD analysis is conducted in order to extrapolate some experimental coefficients that could be found in the literature for the reed valve.

Finally, in the last Chapter, the model is used for the feather valve, emphasizing the different performance compared with the reed valve. Since this valve is in the prototyping phase at the end a sensitivity analysis is conducted in order to improve some aspects of it.

2 Reciprocating Compressor model

This chapter describes the model with which the performance of the compressor is to be measured, focusing on the performance of the suction and discharge valves.

These two components are crucial in the operation of the piston compressor, since as we have seen during the modelling phase, a slight variation in the parameters of the valve assembly leads to a variation in volumetric efficiency, required power and the overpressure reached inside the compressor with respect to the pressure in the discharge and discharge reservoir.

In order to theoretically examine the behaviour of the valve, it is crucial to draft a model, in which real-life events can be reproduced with the goal of obtaining information about them.

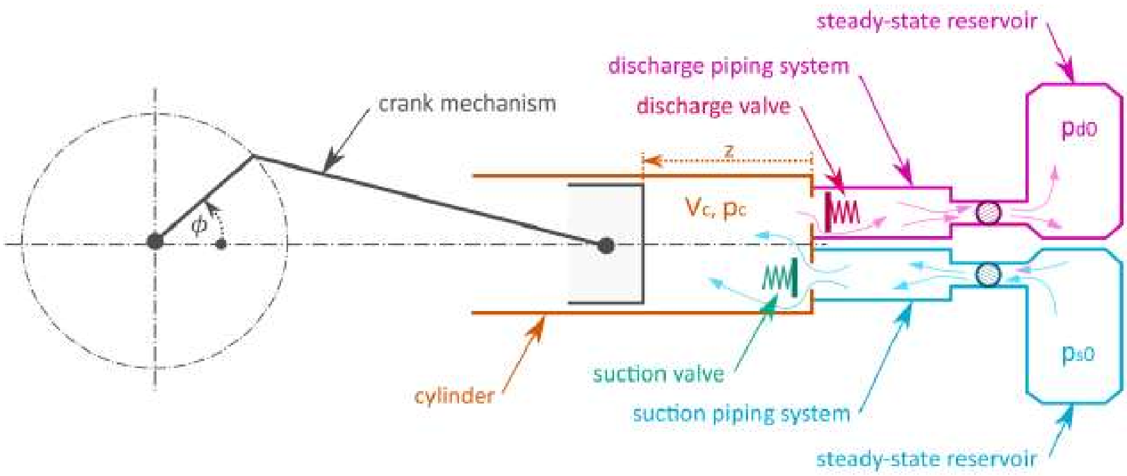

Figure 2.1 Compressor Layout Model

The model proposed (Fig.2.1) here consists of:

1. Compressor cylinder
2. Piston
3. Crankshaft Mechanism
4. Compressor head
5. Intake and discharge valves
6. the tanks
7. Pipes

Given the large number of sub-models forming the entire system, Simscape [8] , produced by Mathwoks, was chosen as the simulation software.

Simscape™ software is a set of block libraries and special simulation features for modelling physical systems in the Simulink® environment. It employs the Physical Network approach, which differs from the standard Simulink modelling approach and is particularly suited to simulating systems that consist of real physical components.

Simulink blocks represent basic mathematical operations. When you connect Simulink blocks together, the resulting diagram is equivalent to the mathematical model, or representation, of the system under design. Simscape technology lets you create a network representation of the system under design, based on the Physical Network approach. According to this approach, each system is represented as consisting of functional elements that interact with each other by exchanging energy through their ports.

These connection ports are nondirectional. They mimic physical connections between elements. Connecting Simscape blocks together is analogous to connecting real components, such as pumps, valves, and so on. In other words, Simscape diagrams mimic the physical system layout. If physical components can be connected, their models can be connected, too. You do not have to specify flow directions and information flow when connecting Simscape blocks, just as you do not have to specify this information when you connect real physical components. The Physical Network approach, with its Through and Across variables and nondirectional physical connections, automatically resolves all the traditional issues with variables, directionality, and so on.

Physical Network approach supports two types of variables:

Through — Variables that are measured with a gauge connected in series to an element.

Across — Variables that are measured with a gauge connected in parallel to an element.

The following table lists the Through and Across variables associated with each type of physical domain in Simscape software

Physical domain	**Through variable**	**Across variable**
Electrical	Current	Voltage
Gas	Mass flow rate	Pressure and Temperature
Mechanical translational	Force	Translational velocity
Mechanical rotational	Torque	Angular velocity
Thermal	Heat flow	Temperature

Table 2.1 Type of Simscape Variable

Some of these domains will be directly involved in the compressor model. As will be seen later when the Simscape model is presented, it is not possible in this software to link blocks with links of different domains that are characterised by a specific colour (i.e., it is not possible to connect a rotational mass with a translational force source)

After this brief description of the syntax of the software used, the components listed above and the equations governing their behaviour will be described below.

2.1 Crank mechanism

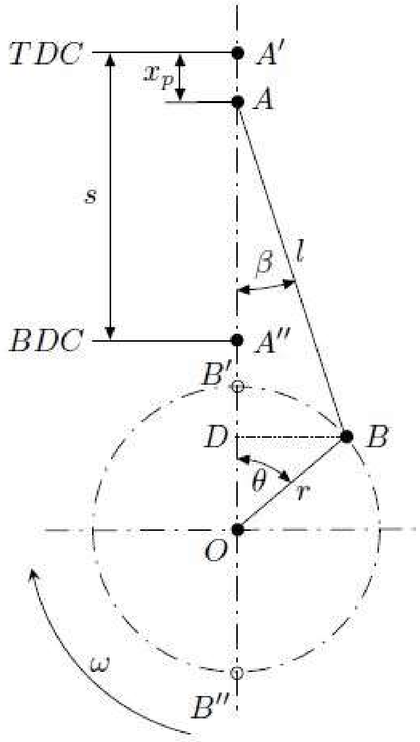

Figure 2.2 Crankshaft Layout

The conversion of rotational motion of the crankshaft in reciprocating movement of the piston in is obtained through the so-called crank mechanism [3] [9] which substantially consists of a crank coupled to a connecting rod . This mechanism is used mainly in piston compressor and combustion engine.

With the kinematics of the crankshaft mechanism, it is possible to calculate the position of the end of the connecting rod, which is firmly connected to the position of the piston inside the cylinder, on which certain physical quantities of the thermodynamic process depend (i.e., the volume between the piston and the cylinder).

To formulate the equation of the instantaneous piston position, assume a set of generalized coordinates, as follows:

$$\vec{q} = [x, \beta, \theta]$$

where x is the position of the connecting rod foot relative to top dead centre, θ is the crank angle and β is the angle of the connecting rod relative to the centre axis

Since the crank mechanism has one degree of freedom, only one of these coordinates can be independent. Let the θ coordinate be the independent one and then the remaining two coordinates can be expressed as a function of θ.

Using the theory of rigid body kinematics and trigonometric considerations it's possible to write

$$x_p = (r + l) - lcos\beta - rcos\theta \quad 2.1)$$

$$rsin\theta = lsin\beta \quad 2.2)$$

In order to simplify the model, it is possible to consider the angular speed of the crank constant

$$\theta = \omega t \quad 2.3)$$

By replacing 2.3 in 2.1, it is possible to link the position x_p and the velocity of the piston $\dot{x_p}$ as a function of the angular velocity ω .

$$x_p = (r + l) - \sqrt{l^2 - r^2 sin(\omega t)} - rcos(\omega t) \quad 2.4)$$

$$\dot{x_p} = r\omega cos(\omega t)(1 + \frac{rcos(\omega t)}{\sqrt{l^2 - r^2 sin(\omega t)}}) \quad 2.5)$$

All equations for crankshaft kinematics can be found within the Crank-Slider block in the Simscape library

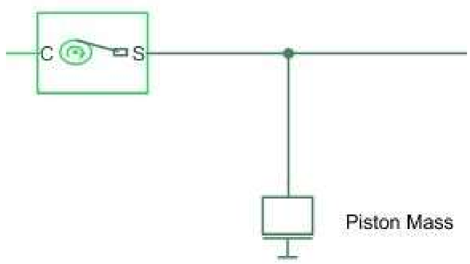

Figure 2.3 Crankshaft Mechanism

Where port C is associated with the rotation domain while S is a mechanical port that connected to the piston. The parameters required to model the Simscape block are listed below:

- Crank radius
- Rod length
- Crank Inertia
- Slider Stiffness
- Slider damping

2.2 Cylinder

The thermodynamic transformations taking place inside the cylinder are closely linked to the behaviour of the valve

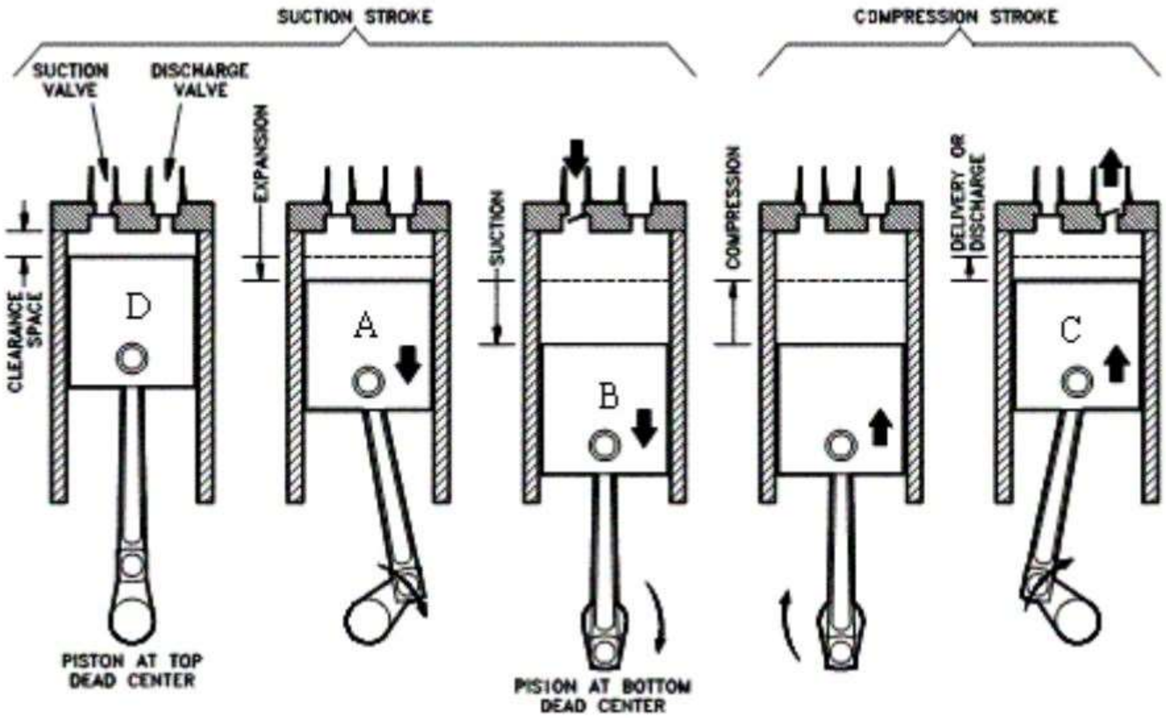

Figure 2.4 Phases during the working cycle

During the suction phase, when the suction valve is opened, the gas flows into the cylinder, where it is trapped after both valves are closed and thus the compression phase takes place. During this process, the pressure of the gas inside the cylinder, as well as its temperature, rises due to the reduction of the cylinder volume.

Moreover, heat transfer through the cylinder walls and the piston is also present. Initially, when the temperature of the gas is lower than the temperature of the walls, the temperature of the gas will rise; however, should its temperature increase such, so that it is higher than that of the wall's, the heat transfer will take place the other way around and thus the gas will start to be cooled.

If the pressure in the cylinder reaches sufficiently high values, the discharge valve plate will be pushed away, and the compressed gas will be forced out of cylinder. Finally, when both of the valves are closed again, the pressure inside the cylinder decreases due to the expansion of the remaining compressed gas in the clearance volume.

Many models already in the literature [6], [10], [7] and [11] contain simplifying assumptions in order to derive the equations governing the physics inside the cylinder some of which can be eliminated using Simscape.

Despite the use of this software, the main assumptions that remain are:

- The kinetic and potential energy of the gas is neglected
- Homogenous system
- Heat exchange Between Compressor and the environment is forced

The block that simulates cylinder behaviour is illustrated below and it is called Translational Mechanical Converter. Translational Mechanical Converter (G) block models an interface between a gas network and a mechanical translational network. The block converts gas pressure into mechanical force and vice versa. It is characterized by 4 ports:

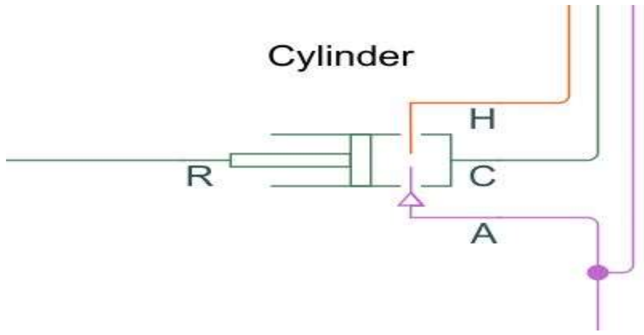

Figure 2.5 Cylinder block in Simscape Library

The converter contains a variable volume of gas. The pressure and temperature evolve based on the compressibility and thermal capacity of this gas volume. The Mechanical orientation parameter lets you specify whether an increase in the gas volume results in a positive or negative displacement of port R relative to port C.

Port A is the gas conserving port associated with the converter inlet. Port H is the thermal conserving port associated with the temperature of the gas inside the converter. Ports R and C are the mechanical translational conserving ports associated with the moving interface and converter casing, respectively.

The input parameters are:

- Mechanical orientation
- Interface displacement
- Initial interface displacement
- Interface cross sectional area
- Dead volume
- Cross sectional area at port A

The equations describing the behaviour of the gas inside the cylinder, regardless of phase, are :

- the mass conservation equation
- the energy balance
- Adiabatic control volume

The mass conservation equation

$$\frac{\delta M}{\delta p}\frac{\delta p}{\delta t}+\frac{\delta M}{\delta T}\frac{\delta T}{\delta t}+\rho\frac{dV}{dt}=\dot{m}_A \quad 2.6)$$

Where

- $\frac{\delta M}{\delta p}$ is the partial derivative of the mass of the gas volume with respect to pressure at constant temperature and volume.
- $\frac{\delta M}{\delta T}$ is the partial derivative of the mass of the gas volume with respect to temperature at constant pressure and volume.
- p is the pressure of the gas volume. Pressure at port **A** is assumed equal to this pressure, $p_A = p$.
- T is the temperature of the gas volume. Temperature at port **H** is assumed equal to this temperature, $T_H = T$.
- ρ is the density of the gas volume.
- V is the volume of gas.
- t is time.
- $\dot{m}_A$ is the mass flow rate at port **A**. Flow rate associated with a port is positive when it flows into the block

The energy balance

$$\frac{\delta U}{\delta p}\frac{\delta p}{\delta t}+\frac{\delta U}{\delta T}\frac{\delta T}{\delta t}+\rho h\frac{dV}{dt}=\dot{\Phi}_A+Q_H \quad 2.7)$$

where:

- $\frac{\delta U}{\delta p}$ is the partial derivative of the internal energy of the gas volume with respect to pressure at constant temperature and volume.
- $\frac{\delta U}{\delta T}$ is the partial derivative of the internal energy of the gas volume with respect to temperature at constant pressure and volume.
- $\dot{\Phi}_A$ is the energy flow rate at port A.
- Q_H is the heat flow rate at port H.
- h is the specific enthalpy of the gas volume.

The partial derivatives of the mass *M* and the internal energy *U* of the gas volume, with respect to pressure and temperature at constant volume, depend on the gas property model. In Simscape it's possible to chose between 3 model gas by setting the block "Gas Properties" (i.e Perfect gas, Semi-perfect gas and real gas).

For our purpose the medium will be modelled as a perfect gas, whose governing equations are

$$Pv = RT \quad 2.8)$$

$$du = c_v dT \quad 2.9)$$

$$c_p = c_v + R \quad 2.10)$$

The Equation 2.7) can be modified according to the phase it is in, as described in the image above:

- Suction phase
- Delivery phase
- Expansion and compression phase

2.2.1 Suction Phase

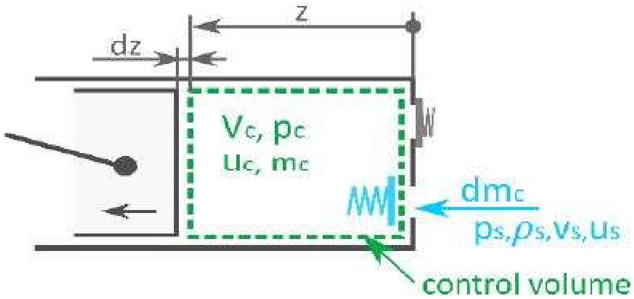

Figure 2.6 Control Volume During Suction Phase

To apply the law of conservation of energy as stated above onto the cylinder, assume a control volume, as depicted in Figure above. This control volume is valid for the suction phase and hence it has one inlet and no outlet.

One of the assumptions to simplify the discussion is not to include the heat exchange that occurs between the gas and the cylinder wall. In this way, by substituting the constitutive equations of perfect gases into the energy equation, it is possible to derive the differential equation that describes the pressure trend inside the cylinder.

By using the subscript c for the thermodynamic quantities relating to the interior of the cylinder, and the subscript s for the quantities of the discharge environment, it is possible to write:

$$\frac{dp_c}{dt} = \gamma\left(\frac{p_s}{\rho_s A_c x_p}\frac{dm_c}{dt} - \frac{p_c \dot{x_p}}{x_p}\right) \quad 2.11)$$

Some terms in Eq.2.11) derive from the kinematics of the crankshaft (i.e. $\dot{x_p}$, x_p) while other terms such as the mass entering the system m_c depends on the valve subsystem that will be introduced later

2.2.2 Discharge Phase

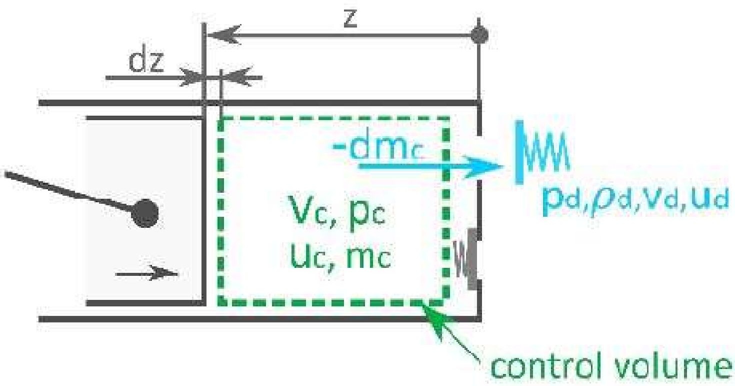

Figure 2.7 Control Volume during Discharge Phase

The mathematical treatment for the discharge phase is entirely analogous to the previous one with the exception of the sign given to the outgoing flow rate due to the convention of signs for open thermodynamic systems.

$$\frac{dp_c}{dt} = -\gamma\left(\frac{p_s}{\rho_s A_c x_p} * \left(-\frac{dm_c}{dt}\right)\right) \quad - \frac{p_c \dot{x}_p}{x_p} \quad 2.12)$$

2.2.3 Expansion and Compression Phase

Whether during the suction or discharge phase, the mass transfer and its influence on the thermodynamic state of the gas inside the cylinder were required to have been considered. However, both the expansion and compression phases are characterized by both the suction and discharge valve being closed and thus no mass transfer occurs. It follows that

$$\frac{dm_c}{dt}_{\substack{suction \\ discharge}} = 0 \quad 2.13)$$

2.3 Plenum Chamber

Basically, the equations describing the behaviour inside the chambers are very similar to the cylinder's ones, with the exception that the volume of the chambers remains constant with respect to time.

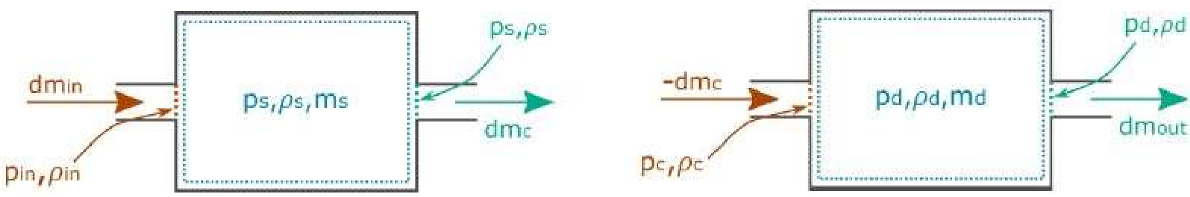

Figure 2.8 Intake and discharge plenum chambers

Referring to the notations for the suction chamber above, it is possible to write:

$$\frac{dp_s}{dt} = \frac{\gamma}{V_s}\left(\frac{p_{in}}{\rho_{in}}\left(\frac{dm_{in}}{dt}\right) - \frac{p_s}{\rho_s}\left(\frac{dm_c}{dt}\right)\right) \quad 2.15)$$

Where V_s is the volume of the suction plenum chamber.

The mass flow going in and out of the plenum chamber is linked to the mass of the gas inside the plenum chamber, which is governed by the law of conservation of mass, i.e.:

$$\frac{d\rho_s}{dt} = \frac{1}{V_s}\left(\frac{d\,m_{in}}{dt} - \frac{dm_c}{dt}\right) \quad 2.16)$$

In the Simscape environment it is possible to model the chamber with the 'constant volume' block. The chamber contains a constant volume of gas. It can have between one and four inlets. The enclosure can exchange mass and energy with the connected gas network and exchange heat with the environment, allowing its internal pressure and temperature to evolve over time. The pressure and temperature evolve based on the compressibility and thermal capacity of the gas volume.

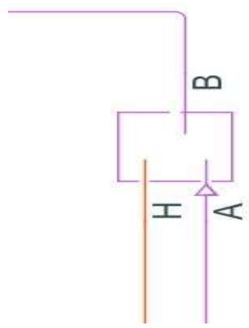

Figure 2.9 Finite Volume in Simscape library

2.4 Pipeline

The last component of the pipe system is either the intercooler or the aftercooler, depending on whether the compressor is a multi-stage or single stage. On the way along the pipe, the air is cooled before entering the second stage intake chamber or tank.

The pipe is modelled as a straight one of length L_{pipe} with a constant cross-sectional area A_{pipe}. It is assumed to be one-dimensional incompressible flow inside, the motion of which (as a gas column) is governed by Newton's second law:

$$\frac{m}{A_{pipe}^2}\frac{du}{dt} = p_1 - p_2 - \Delta p_{drop} \quad 2.17)$$

Wherein p_1, p_2 stand for the stagnation pressure in the spaces connected by the pipeline, Δp_{drop} stands for the pressure drop along the pipe which can be divided in two terms one stands for the major losses due to friction the other stands for the minor losses due to a local resistance.

$$\Delta p_{drop} = \left(\mu \frac{L_{pipe}}{D_{pipe}} + \sum K\right)\frac{1}{2}\rho u^2 = \frac{1}{2}\varepsilon\rho u^2 \quad 18)$$

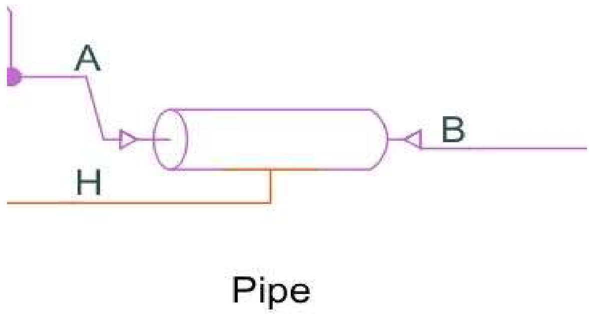

Figure 2.10 Pipe in Simscape library

2.5 Valve Modelling

Compressor valve dynamics influence valve life and compression efficiency. A compressor valve opens and closes with every compression cycle. Interaction of the flow of the compressible system and the dynamics of the mechanical system makes the mathematical modelling rather complex to understand.

Valve lift is one of the primary factors deciding the efficiency and reliability of the compressors. Since the suction process is longer than the discharge process for the same mass flow rate circumstances, the suction side valve lift must be larger than the discharge side. The lowest possible lift is normally used to achieve reliability [6] [12], while the greatest available lift is used to achieve valve efficiency. Higher valve lift, on the other hand, tends to result in higher impact velocities and, as a result, higher impact fatigue stresses in reed valves.

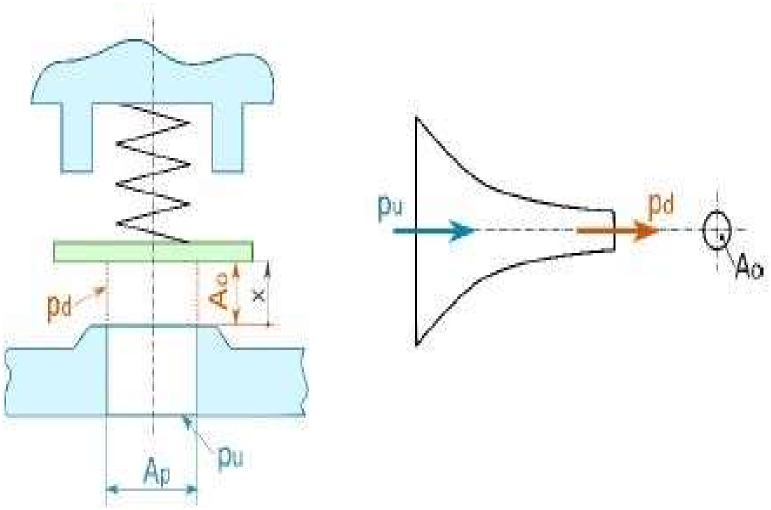

Figure 2.11 Mechanical and Fluid dynamic modeling of the valve

The maximum allowed valve lift is determined by factors such as rotational speed, operating pressure. The impact robustness of various valve plate materials (steel, polymers, etc.) determines the maximum permissible valve lift. Excessive valve lift can reduce valve life significantly owing to high-velocity impact forces, valve flutter, late closing, and other life-degrading phenomena.

The goal is to arrive at an analytical formulation of the flow through the valve as a first approximation, and then to describe the forces applied to the valve in order to analyse its dynamic.

To connect the thermodynamic systems representing the cylinder and each of the plenum chambers, equations defining the time dependent mass flow in each of the valves must be introduced. The valve should be modelled as a flow restriction with varying limited area for this purpose.

2.5.1 Valve dynamic

The assumption is made that the valve plate is a spring-loaded rigid body movable in a direction perpendicular to the plane of the seat.

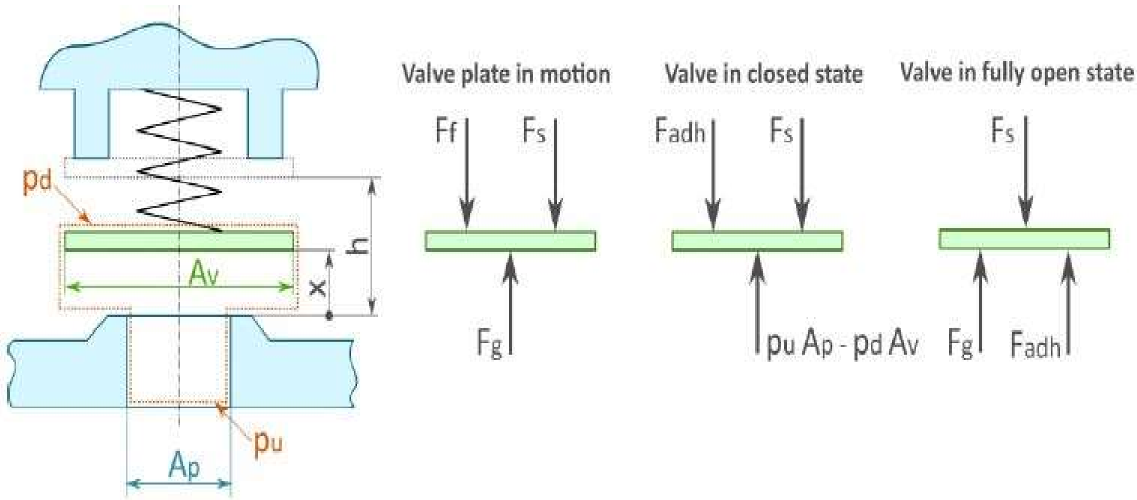

Figure 2.12 Mechanical and Fluid dynamic modeling of the valve

It is clear from that while analysing valve dynamics, it is important to represent the reed as a one-DOF model, bending beam, or plate. Calculation results may change depending on the simplified model and assumptions used. The one-DOF model is frequently used to represent the dynamic behaviour of a reed-type valve because of its cheap computing cost [6][10] [11] [7].

Where m is the mass in motion, x stands for the distance of the valve plate from the seat, Fg stands for the gas force and Fs indicates the elastic force. If the valve plate reaches an obstacle (a seat or limiter), a rebound can occur. Afterwards, the plate comes into direct contact with the seat or limiter.
The valve lift x is assumed variable over an interval 0<x<h, where h is the maximum valve lift permitted by the limiter.

The system described can be found in 3 different configurations:

- Valve plate in motion
- Valve in closed state when the valve does not allow the flow rate to pass.
- Valve in fully open state when the flow rate through the valve reaches its maximum value

The transition from one configuration to another depends on the magnitude of the forces applied to the valve plate.

If the valve is closed, then the following inequation is fulfilled:

$$p_u A_p - p_d A_v \leq F_s \quad 2.19)$$

When this inequality condition reverses, the valve plate will lift,

$$p_u A_p - p_d A_v > F_s \quad 2.20)$$

In fully open state, if the sum of the forces pushing the valve plate towards the limiter is higher than the spring force acting in the opposite direction, then the valve plate will remain in a fully open state

$$F_s \leq F_g \quad 2.21)$$

Analogously to the previous event, when the inequality is not fulfilled anymore the valve plate will then start to move back towards the valve seat.

$$F_s > F_g \quad 2.22)$$

Once the various phases of valve movement have been analysed, we can analyse the parameters in the second equation of dynamics.
The elastic force F_s considers the presence of the spring element which, depending on the kind of valve, can be represented by a real spring or by the reed that elastically deflects during the lift. In the latter case the value of the stiffness is the one of the valve reed itself [13]

With the assumption of linear characteristic, the elastic force is given by:

$$F_s = k(x_0 + x) \quad 2.23)$$

Where k is the Reed movable stiffness and x_0 is the preload displacement.

Gas force is defined as the area integral of the gas pressure load existing on both sides of a valve plate.
The valve plate may be thought of as a sharp-edged bluff body submerged in a fluid flow field that it opposes. As a result, the force pressing on the body is exerted by the fluid flow, which is caused by the unequal pressure distribution around the valve plate.
In general, calculating the pressure distribution along the surfaces of a hovering valve plate is impractical. In many papers in the literature the force due to the pressure difference is modelled as follows:

$$F_g = c_g A_v \Delta p \quad 2.24)$$

Where c_g stands for the drag coefficient, A_v is the Reed area and Δp acting upstream and downstream the reed. The drag coefficient can be extrapolated from different paper where there are some analytical treatments to show the relationship between some parameters and the drag coefficient or it can be approximated as a constant value. This aspect will be explored in more detail later when describing the type of valve that will be analysed.

2.5.2 Valve Flow Modeling

When a compressor valve is open, it provides resistance to the flow of gas, and the rate of mass flow will be a function of:

- geometrical factors (shape and dimensions of the constructional elements; momentary lift of the valve reed),
- operating conditions (state of the gas upstream and downstream of the valve)
- gas properties.

To increase the model's adaptability, it was targeted at a flow equation with the same structure for valves of any size and type, with variances compensated for by varying values of parameters in the equation. The mass flow of the gas via the valve is frequently approximated as an incompressible flow through a converging channel in compressor models available in the literature [14] using the following equation:

$$\Phi = \alpha \varepsilon A_0 \sqrt{2\rho_u (p_u - p_d)} \qquad 2.25)$$

Where :

- α , named flow coefficient, stands for all the non-ideal effect (i.e. A vena contracta can be made by separating the stream tube from the walls) , while ε is called expansion coefficient and it takes in account all the compressibility factors
- ρ_u and p_u are respectively the density and pressure of the gas upstream of the valve, p_d stands for the pressure downstream the Reed.
- The area of the channel produced between the valve reed and the seat is denoted by A_0. As mentioned earlier, since the valve has been modelled as a rigid body with one degree of freedom, the area of gas flow through the valve will also be a function of a single variable: x representing the lift of the reed multiplied by a gain that will depend on the type of valve.

Since the ε coefficient is purely experimental, the Eq. 25 has been substituted with the equation that models the flow of gas through the valve as the flow rate through a converging diverging nozzle.

$$\Phi = \alpha A_0 \sqrt{\frac{2k}{k-1} p_u \rho_u \{ \left(\frac{p_d}{p_u}\right)^{\frac{2}{k}} - \left(\frac{p_d}{p_u}\right)^{\frac{k+1}{k}} \}} \qquad 26)$$

3 Simscape Model

As mentioned above, Simscape was chosen as the software for simulating compressor operation.

In order to understand the operation of the valve, it is necessary for the valve to be connected to the pumping unit because the thermodynamic quantities between the compressor and the valve are closely interconnected.

An example of this connection is the volumetric efficiency of the compressor, a parameter that will be explained later, which depends not only on the design of the pumping unit but also on the design of the valve itself.

Unlike other predictive models in the literature [10] where in order to switch from one phase to another during the thermodynamic cycle it is necessary to write logical conditions as written in the chapter on valve dynamics, in Simscape this is not necessary because by setting up the connections between the cylinder and the two tanks in an appropriate manner, the switch from one condition to the other occurs automatically.

This greatly simplifies the model architecture and makes the model understandable and usable by others.

In the simulation workspace, the equations governing the operation of the compressor unit are differential equations with respect to time.

With the code below, once the Simscape model has been run, it is possible to calculate the number of rotations performed by the crankshaft. Eq. 3) shows a relationship between time and the angle of rotation of the crankshaft, so that the physical quantities of interest can be plotted as a function of the crankshaft.

acquiring data

```
%run simscape
stop_time=2; %sec
sample_crank_angle=1; %deg
sample_time=1/(n/60*360/sample_crank_angle); %sec

sample=360/sample_crank_angle; %# samples
crank_angle=0:sample_crank_angle:360; % deg
theta=(simOut.simlog.Slider_Crank.theta.series.values)*180/pi;
last_rotate=floor(max(theta)/360)-0.5; %# last rotation #
k=(last_rotate*360)/sample_crank_angle; %# sample seq #
```

Figure 3.1 Conversion of time in angle rotation script

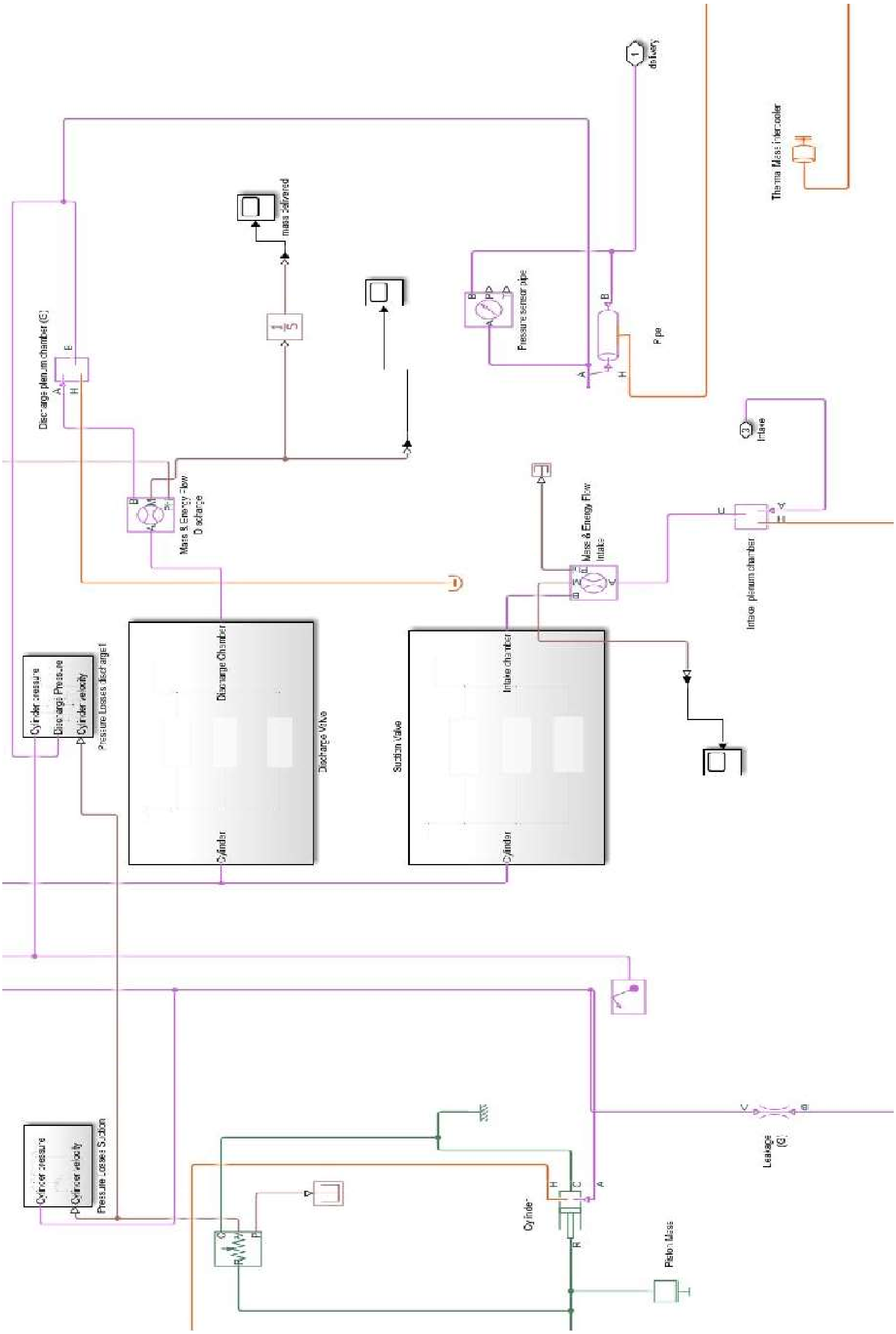

Figure 3.2 Simscape model layout

The final point is to obtain a tool able to supply a series of significant outputs representative for the performance of the compressor in order to understand which is the influence of a certain valve assembly on it.

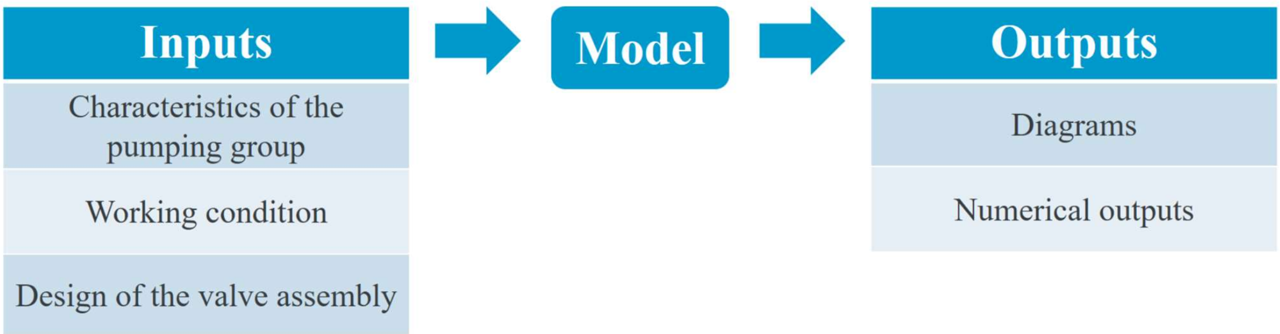

Figure 3.3 Workflow of the model

The outputs can be provided in the form of diagrams or numbers, in most cases they are efficiencies in percentage form.

The inputs, on the other hand, are parameters referring to both the compressor unit and the valve unit. The latter will be described later depending on the type of valve being studied.

3.1 Model Outputs

Model outputs can be provided either in graphical form, or in the form of efficiencies. An example is given below.
When the proposed model is subsequently applied to a real machine, it will be noticed how all outputs of the pumping unit are strongly influenced by the behaviour of the valve.

3.1.1 Graphical outputs

From the Simscape Model the trends of the all thermodynamic quantities as a function of crank angle in different part of the pumping unit can be extrapolated like:

- Pressure Volume diagram

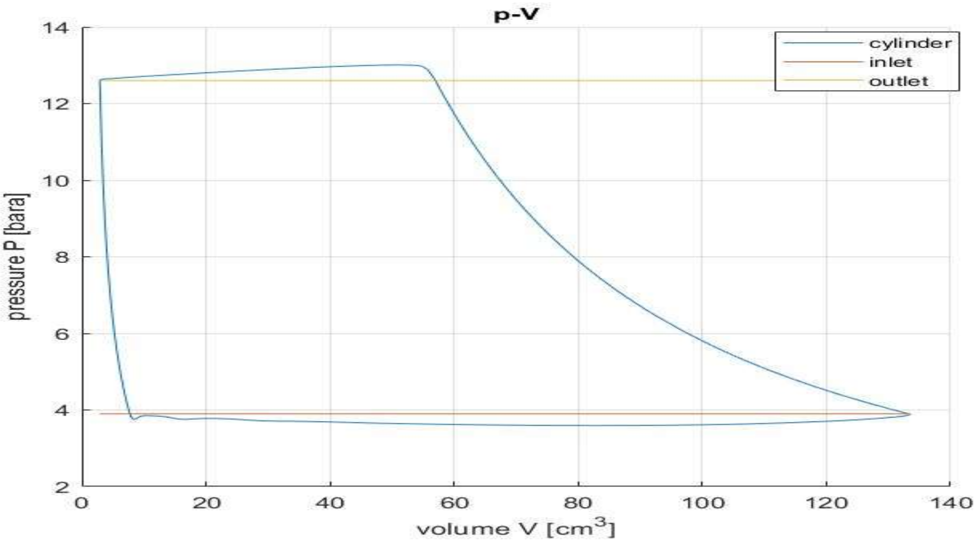

Figure 3.4 P-V Diagram

- Pressure – Crank angle diagram

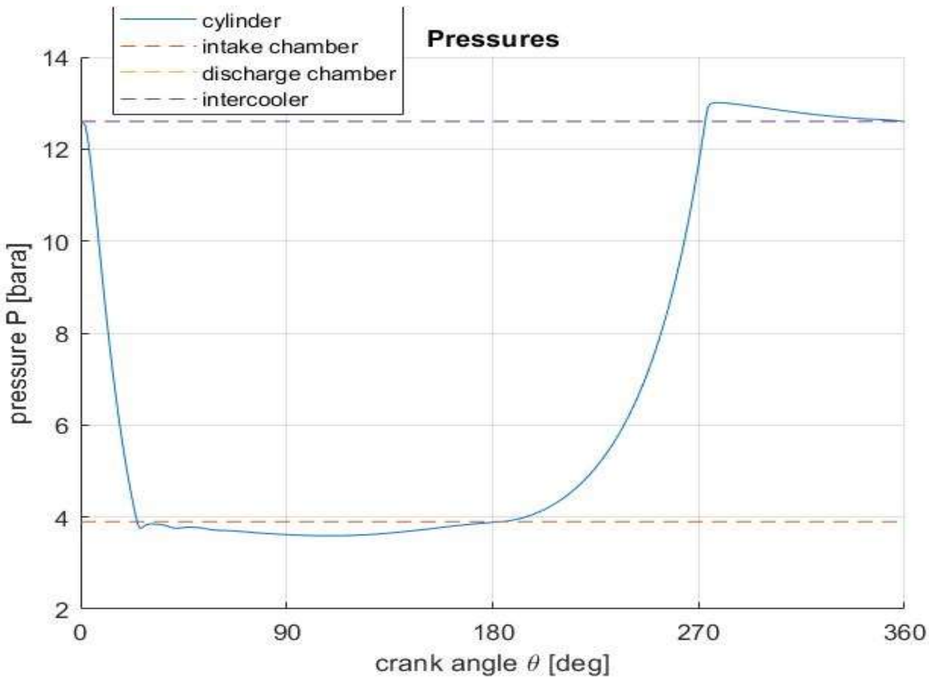

Figure 3.5 Pressure- Crank angle plot

- Discharge flow rate -Crank angle diagram

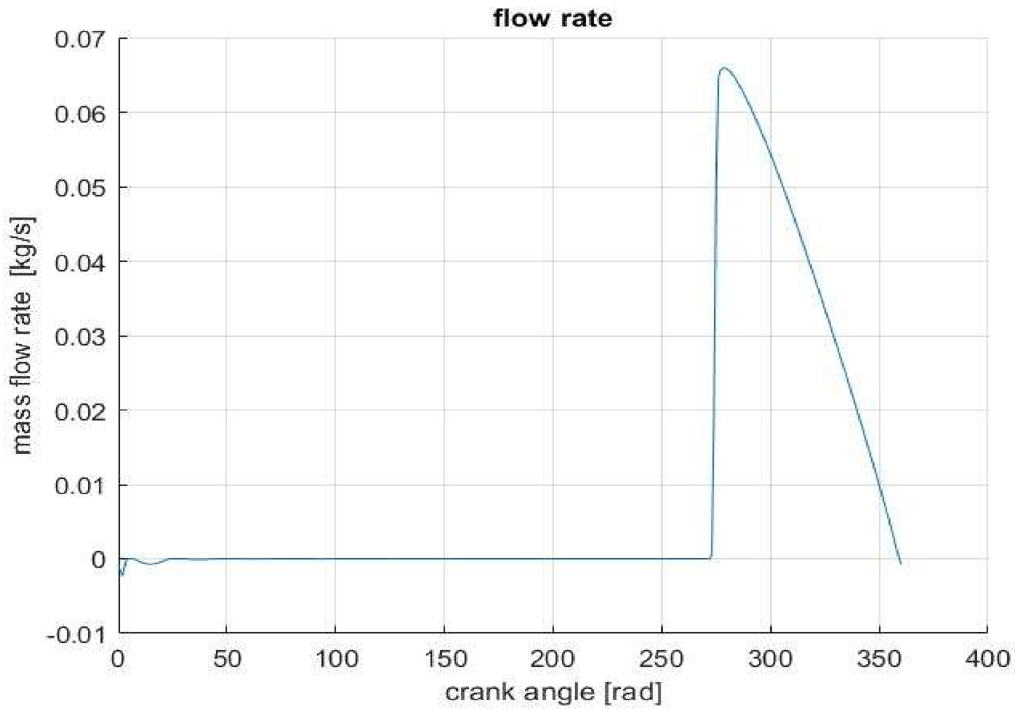

Figure 3.6 Mass flow rate-crank angle plot

- Suction plate lift -Crank angle diagram

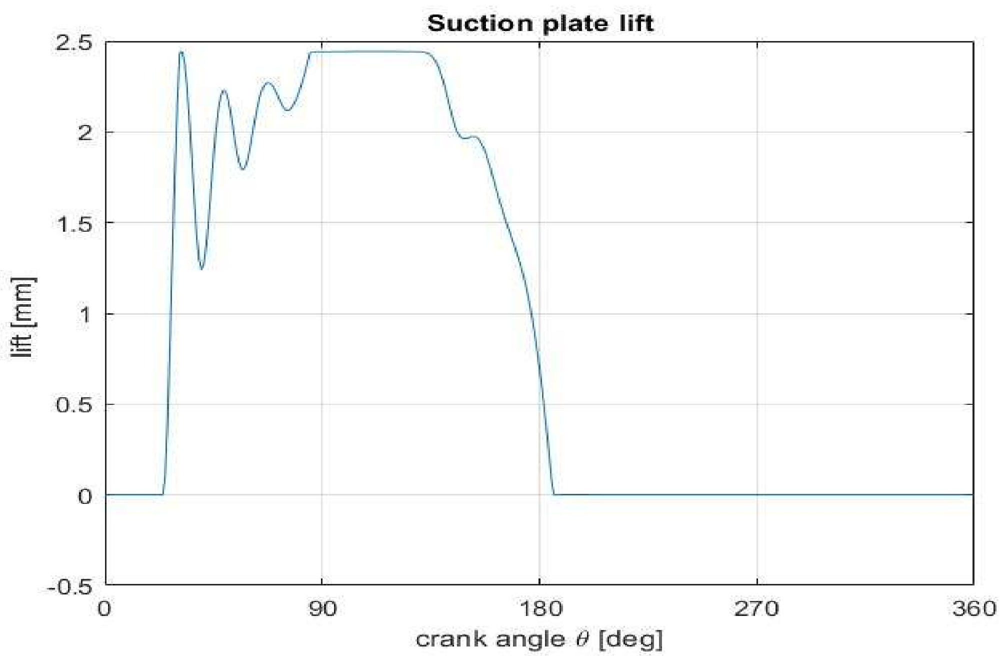

Figure 3.7 Plate lift – Crank angle plot

- Suction plate velocity -Crank angle diagram

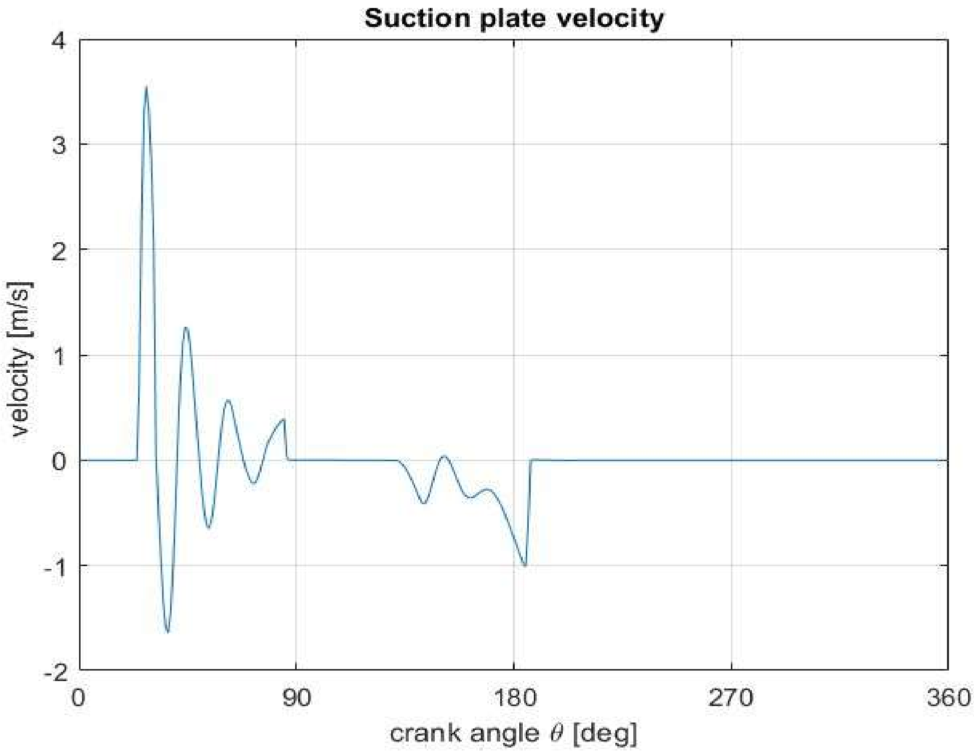

Figure 3.8 Plate velocity – Crank angle plot

3.1.2 Efficiencies Outputs

Other outputs important for the study of valve performance are represented in numerical form.

- Pressure losses
- Overpressure
- FAD
- Volumetric Efficiency
- Mechanical Power Required
- SER

The problem of efficiency of the compressor has necessitated a thorough study of losses.
the valve losses are particularly worthy of study since they so seriously lower the volumetric efficiencies.
The significance of the valve losses can be seen form the p-v diagram.

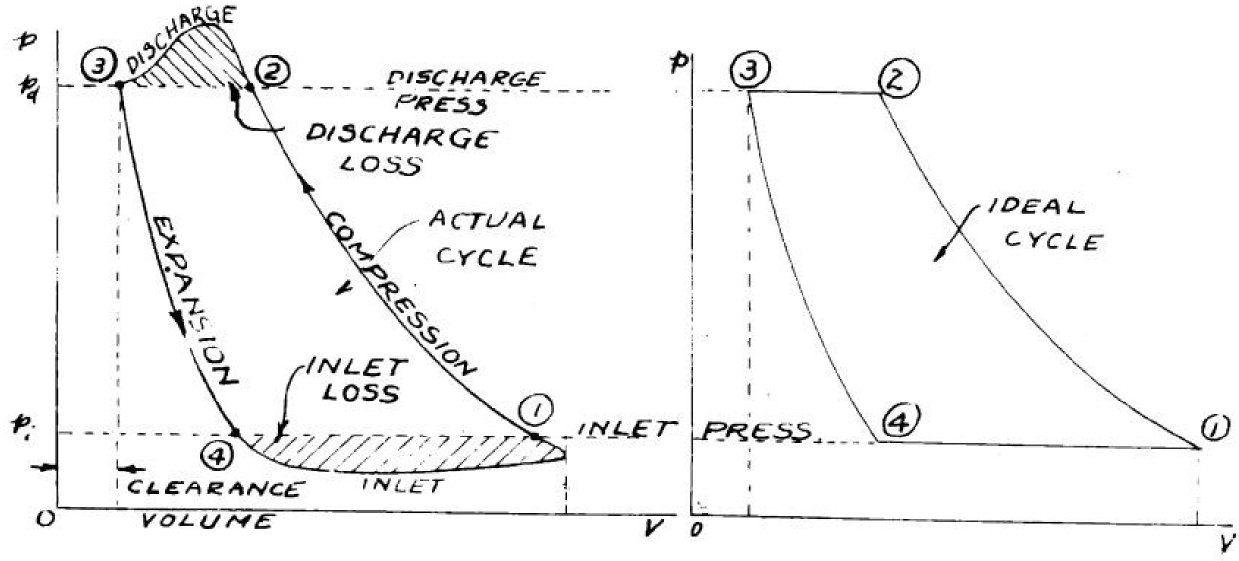

Figure 3.9 Comparison between real and ideal P-V Diagram

The inclusion of valves modifies the ideal compression cycle in two major ways. The first is caused by the preload of the springs, while the second is caused by the reduction in gas pressure as it passes through the valves. A larger compression ratio (with the same nominal suction and discharge pressures) is created just to overcome the previously indicated spring opposition.
The capacity decreases as the compression ratio increases due to two primary reasons :

- At the conclusion of the discharge phase, the overpressure creates a sucked capacity decrease for the re-expansion, which begins at a higher pressure and ends at a larger volume.
- A drop in intake pressure causes a proportionate fall in gas density, resulting in a decrease in mass flow rate.

The power expended for gas compression is increased by the contributions of the valves opposition at their opening (almost rectangular areas between the isobars, related to the nominal pressures, and the new cylinder inner and discharge pressures), and partially decreased by the smaller handled gas capacity.
Given that the opening valves provide a certain gas passage area and as a result establish no negligible pressure reductions throughout the gas passage, the second impact must now be considered. Consequently, as indicated in Figure below, the compression cycle is adjusted.

The ideal P-V diagram is also reported above: it would be obtained in a compressor traveling at infinitely low speed if it had valves which could be opened by an infinitesimal pressure difference. Thus, the gas would flow in and out of the cylinder at constant pressure along line 1-4 and 2-3 producing no valve losses.
The shaded areas constitute the added work requited to force the gas through the inlet and discharge valves and are therefore termed inlet and discharge losses since they reduce the volumetric efficiency and at the same time they cause an increasing of power required by the crankshaft.

From the p-V diagram, it can be seen that the total power is the sum of the three terms described above:

$$P_{real} = P_{ideal} + P_{loss\_discharg} \ + P_{loss\_suction} \quad 3.1)$$

these pressure losses are also related to the speed of the crankshaft. Referring to mechanical power, this can be evaluated as follows

$$P_m = \frac{1}{\eta_m} L_c n \quad 3.2)$$

Where η_m is the mechanical Efficiency, n is the crankshaft speed and $\mathrm{L_c}$ is the work for cycle which also can be described by the internal area of the PV diagram. That's why the mechanical power is related to the Valve losses.
Since in all valve manufacturers' catalogues [15] these losses are given in terms of power also in this work

- the overpressure, which indicates the pressure difference created by the presence of the valve
- Power losses which indicates the power added to the power required by thermal work (expansion and compression)

In a compressed-air system, free air delivery (FAD) is the enlarged volume of air that the compressor releases into the network within a given measure of time. To determine FAD, measurements must be made of the ambient pressure, humidity and temperature present at the air inlet of the machine.
FAD (Free Air Delivery) is the actual quantity of compressed air converted back to the inlet conditions of the compressor. The units for FAD is l/min in the SI system.
In the proposed model, this parameter was calculated by considering the average of the outflow rate divided by the density of dry air at a temperature of 15 degrees Celsius and at sea level (equivalent to a pressure of 101 325 Pa or 1 atm) it is approximately 1.225 kg/m³.

```
FAD=mean(mass_flow(k-sample:k))/1.225e-3 %L/s
```

The volumetric efficiency represents the efficiency of a compressor cylinder to compress gas. It may be defined as the ratio of the volume of gas actually delivered to the piston displacement, corrected to suction temperature and pressure. The principal reasons that the cylinder will not deliver the piston displacement capacity are wire-drawing, a throttling effect on the valves; heating of the gas during admission to the cylinder; leakage past valves and piston rings; and re-expansion of the gas trapped in the clearance-volume space from the previous stroke.

There are various theoretical formulations in the literature [2] explaining what the parameters are and how they affect volumetric efficiency, even if with simplifications (i.e. no valve pressure drops, no heat exchange)

$$\lambda_v = 1 - \mu(\beta^{\frac{1}{k}} - 1) \quad 3.3)$$

Where β stands for the pressure ratio, k is the heat capacity ratio and μ is the volume dead ratio.

The equations described above sets another limit for the maximum pressure ratio that can be obtained with a piston compressor. Setting λ_v=0, it founds out a relationship between the maximum compression ratio and the volume dead ratio.

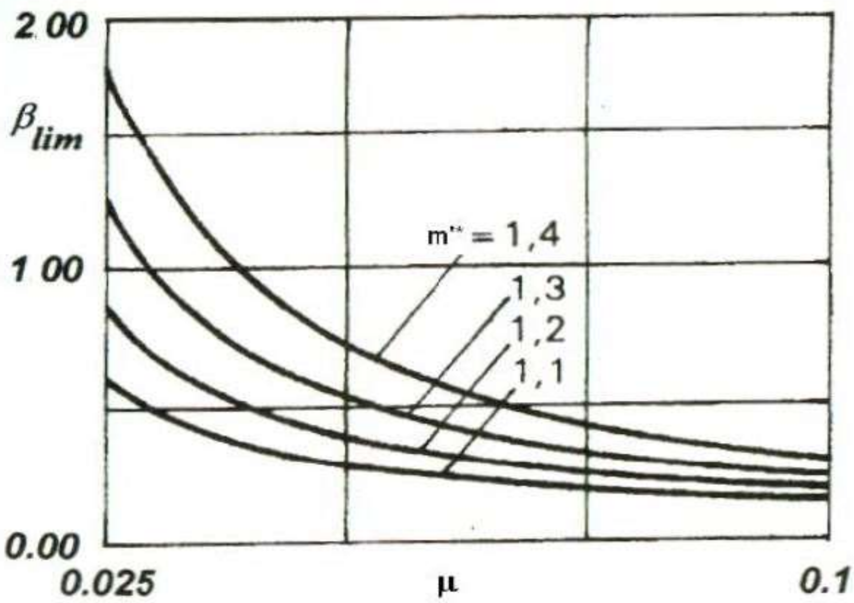

Figure 3.10 Relationship between dead volume ratio and maximum compression ratio

In this model, volumetric efficiency will be calculated as the ratio of FAD to air displacement

$$\lambda_v = \frac{FAD}{\dot{V}_c} \quad 3.4)$$

Where $\dot{V}_c$ is computed as follows:

```
volumetric_flow_rate =(max(volume)-min(volume))*P_in*n/60/1000 %L/s
```

3.2 Model inputs

Finally, lets summarize the variables, which are considered to be input parameters in the mathematical model. Bear in mind that all of them are required to be in basic SI units in the developed simulation tool.

In this section, only the variables relating to the pumping unit will be presented, as the variables relating to the valves may change depending on the type of valve being considered

Crank mechanism
Radius of crankshaft
Connecting rod length
Angular velocity of the crankshaft
Inertia crank

Cylinder parameters
Clearance length
Piston mass
Bore
Piston stroke

Steady state tanks
Reservoir Temperature
Cross section area at ports

Intake / Discharge Plenum chamber
Area at port A
Area at port B

Pipe
Pipe length
Cross sectional area
Hydraulic diameter

Some of these parameters are design parameters, while others are geometric parameters and can also be measured by the CAD

4 Application of the model to current design

In this section, the Simscape model created is applied to a real compressor built at Abac S.p.A. The compressor under study is called B5900: it is a multi-stage compressor with two cylinders in a straight configuration.
The main parameters of this compressor are summarised in the table below:

B5900 Parameters		
Suction pressure [Bara]	**0,98**	
Discharge pressure [Bara]	**12**	
	First stage	**Second stage**
Stroke [mm]	**55**	**55**
Bore [mm]	**105**	**55**
Clearance length [mm]	**1,2**	**1,2**
Conrod length [mm]	**122,5**	**122,5**

Table 4.1 Pumping Parameters

The listed parameters do not include the compressor speed because some experiments were carried out at Abac testing lab at different speeds to understand how the compressor works under different conditions and whether the valve assembly is capable of operating at increasing speeds.

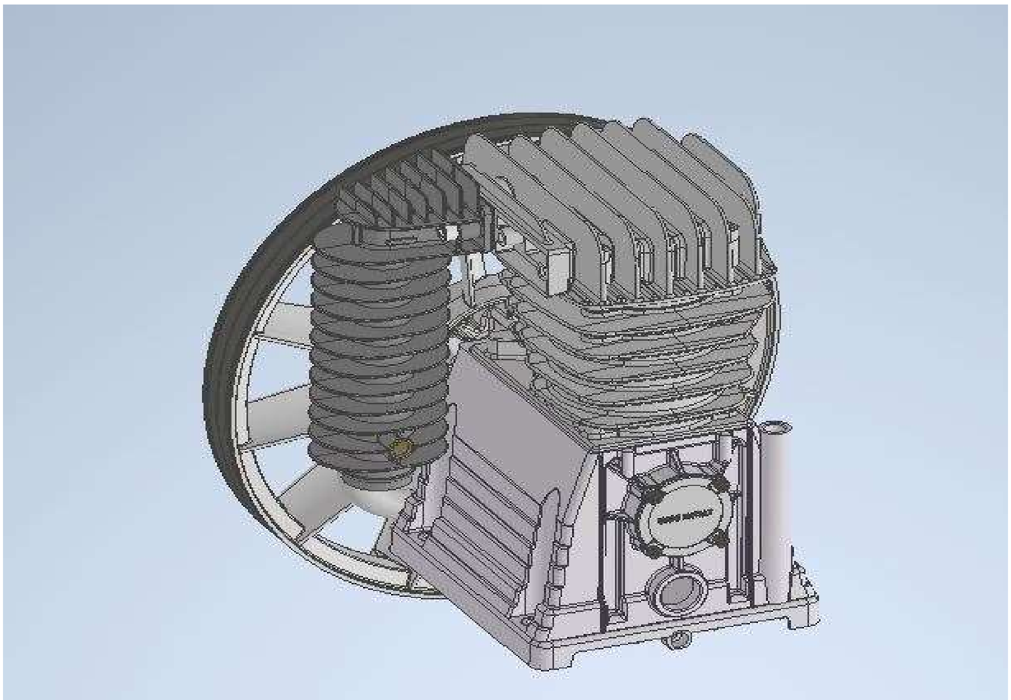

Figure 4.1 3D Compressor view

As far as the valve is concerned, in this configuration it is a valve assembly where there is suction and delivery for both compression stages.

By using Simscape as modelling software, it is possible to simulate not only the dynamic behaviour of the reed under the action of upstream and downstream pressure, but also how the number and area of air passages downstream and upstream of the reed impact on the valve's performance.
This is because these restrictions also have an impact on the overpressure and pressure drop [13] in the valve assembly and consequently on the Pumping group.

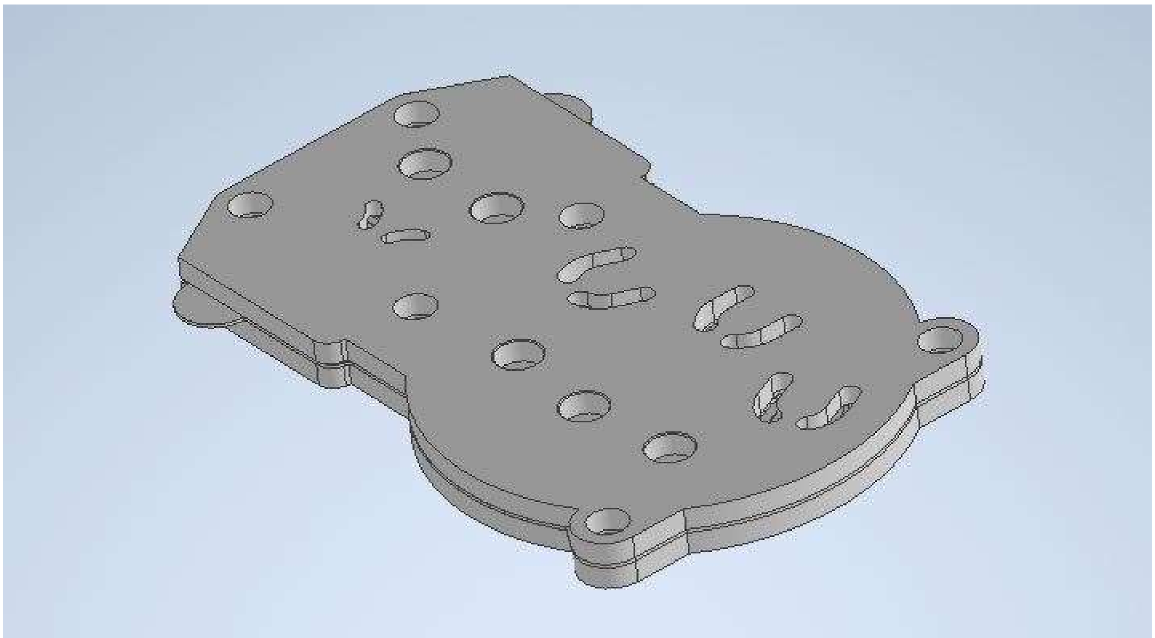

Figure 4.2 Valve Assembly

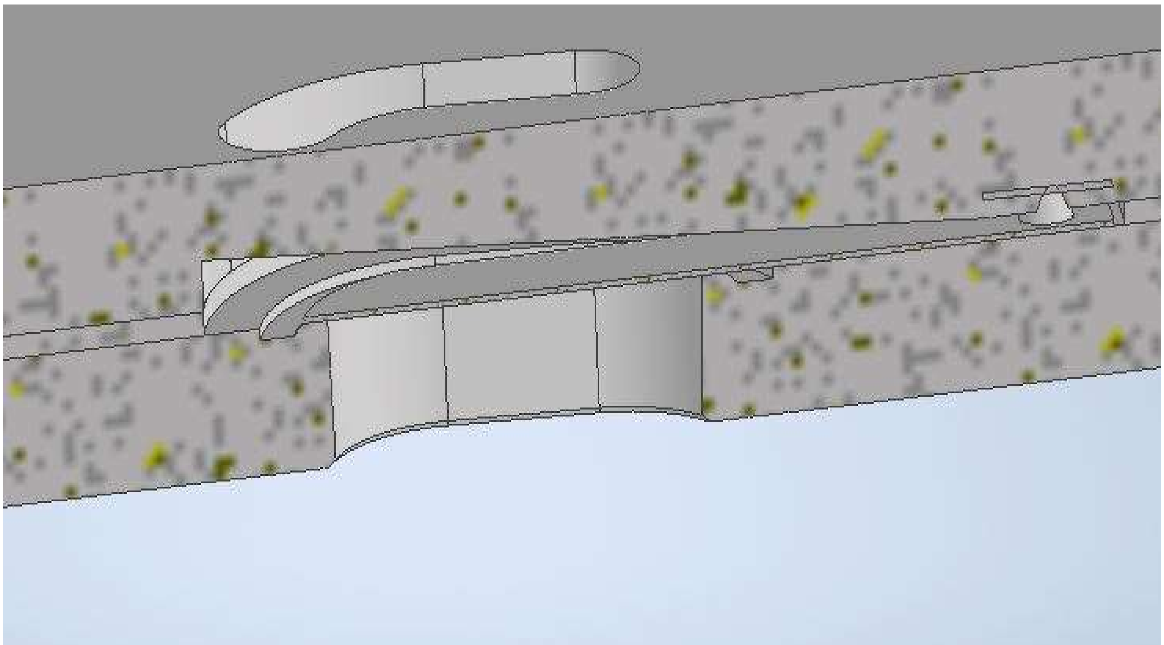

Figure 4.3 Valve plate detailed view

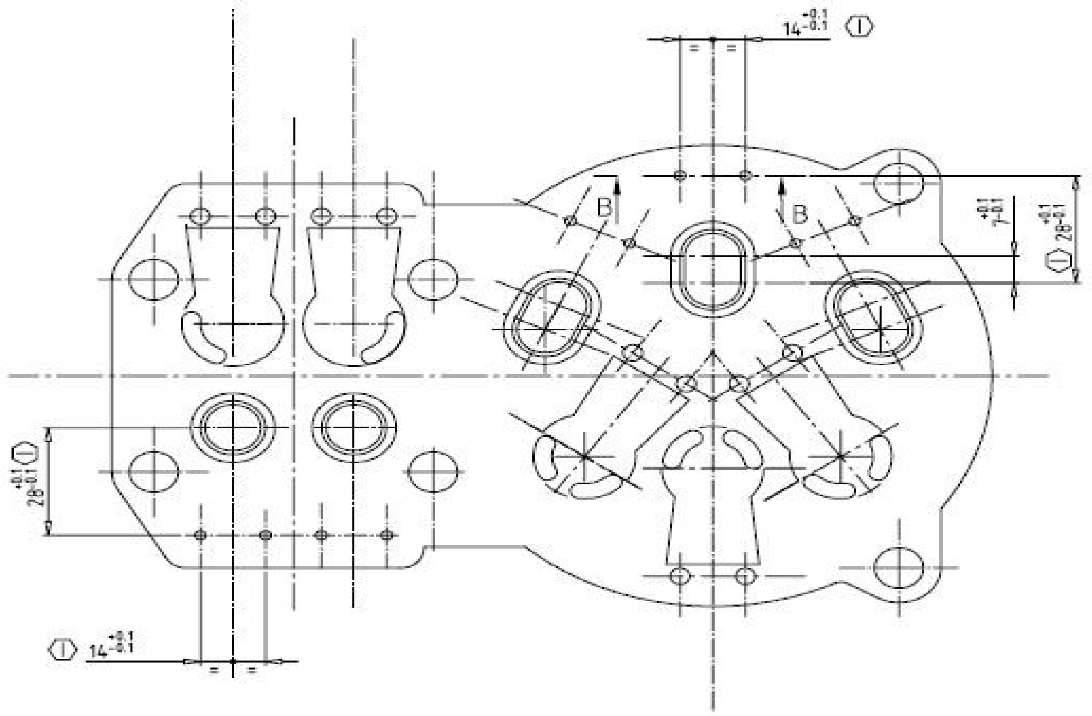

Figure 4.4 2D Drawing of the valve plate (Head side)

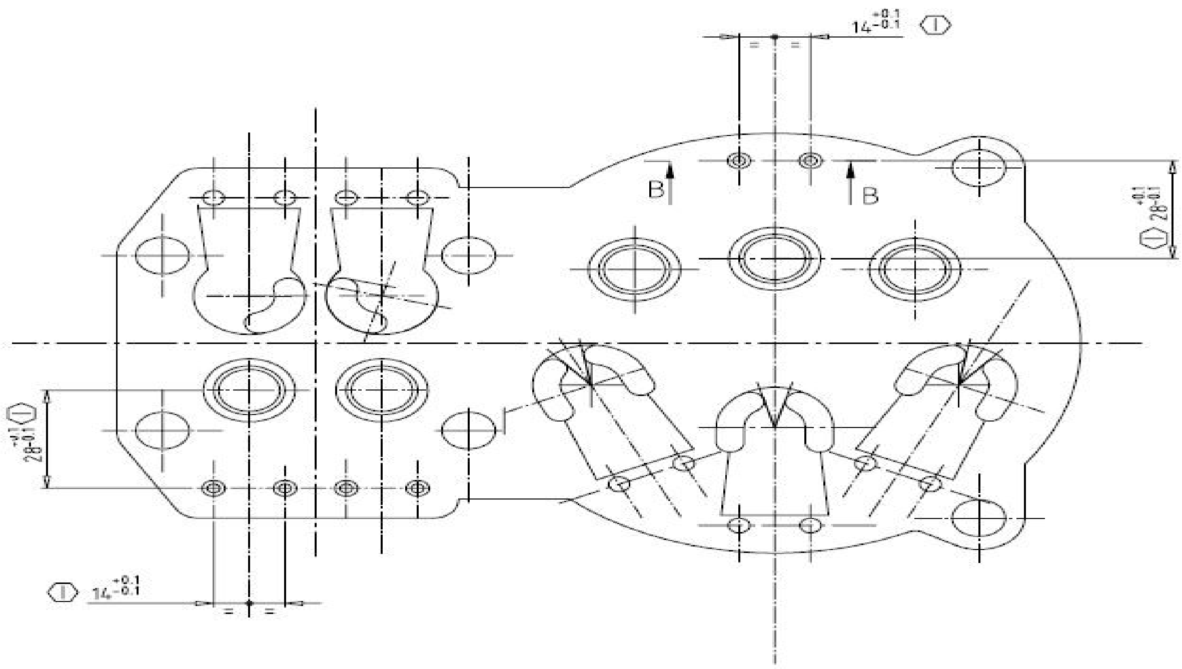

Figure 4.5 2D Drawing of the valve plate (cylinder side)

4.1 First-stage modelling

As can be seen from the 3D model made on Inventor, both the delivery and suction valves of the first stage consist of 3 reeds. For this reason, the valve model consists of 3 different sub-models, each of which simulates the dynamics of the reed and the passage of air. As mentioned above, the passage of air through the moving plate is modelled in Simscape with the 'local restriction' block but set to 'variable restriction' as can be seen from the following image. This block receives as input a physical signal, according to the syntax of Simscape, which represents an area.

In the reed valve, the passage area can be calculated with a certain degree of approximation using the following formula

$$A_{variable} = Perimeter_{Port} * x$$

where x represents the plate lift which depends on the plate dynamics.

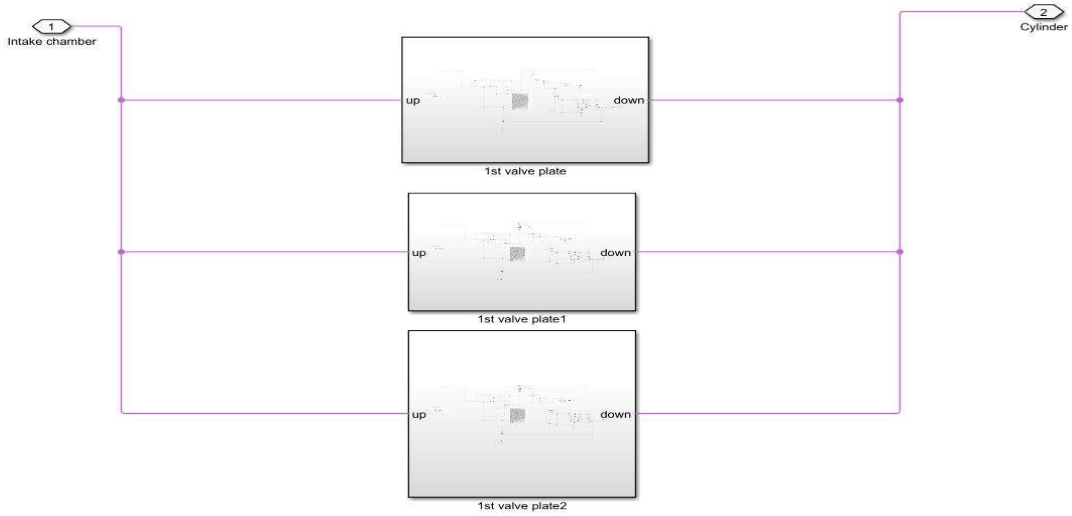

Figure 4.6 Suction valve first stage Simscape submodel

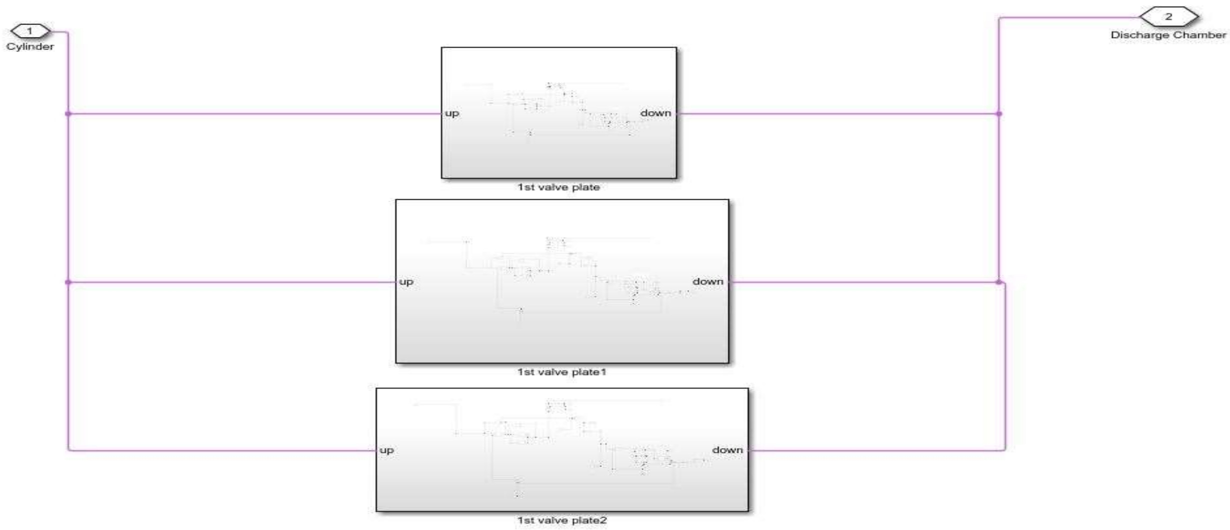

Figure 4.7 Discharge valve first stage Simscape submodel

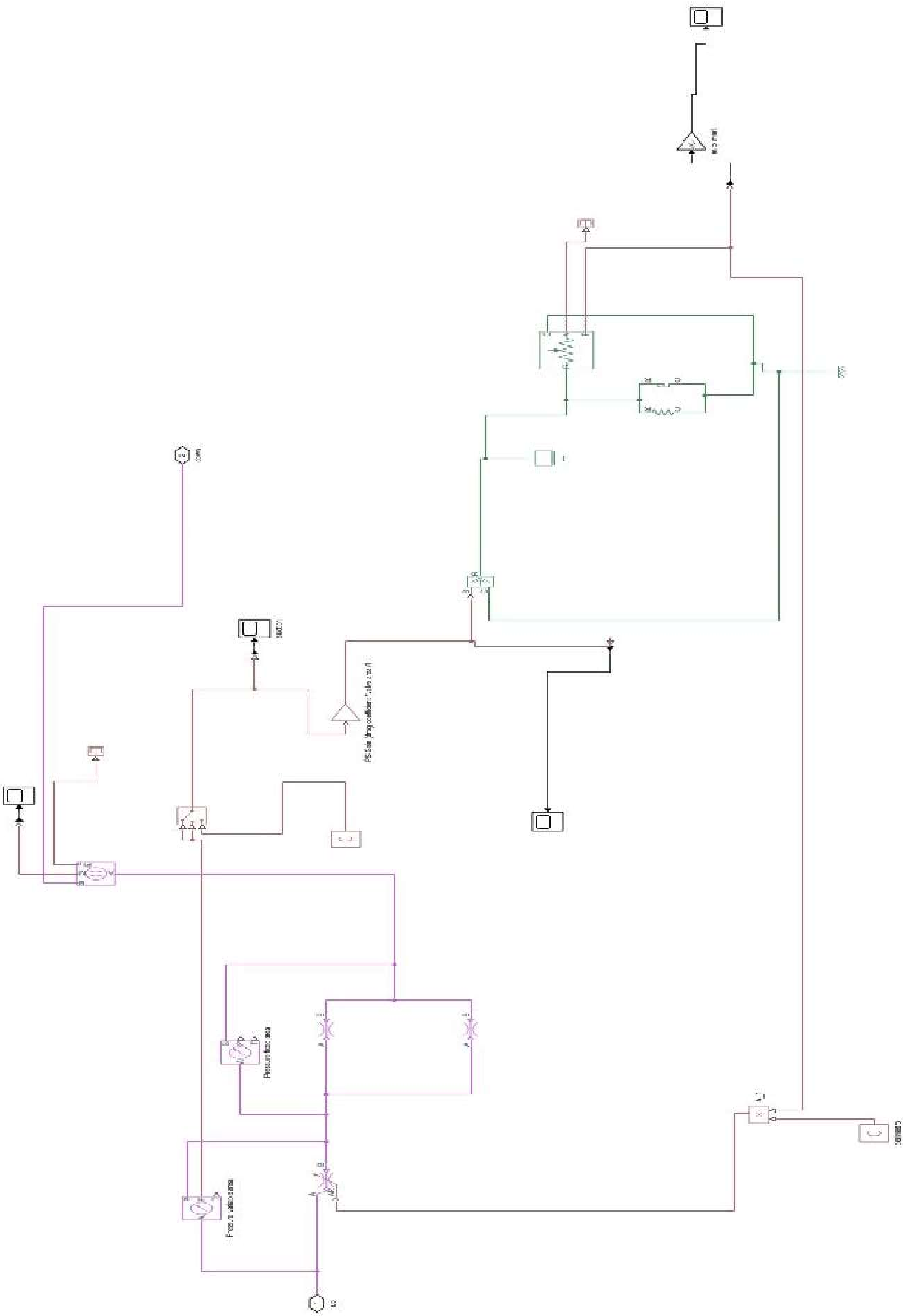

Figure 4. 8 Valve plate first stage sub model

4.2 Second-stage modelling

In the second stage, as can be seen from the image taken from the CAD software, the main difference compared to the first stage is that instead of two passage holes, there is only one. This leads to a small difference in the architecture of the model, shown below.
Another difference to the first stage is that in the second stage, for both suction and delivery, the shape of the port is circular, whereas in the first stage the suction port is circular, the delivery port has a 'slot' as its basic shape, as can be seen in the 3D drawing.
This will cause the parameters for initialising the Simscape model to be different depending on the geometry of the valve assembly

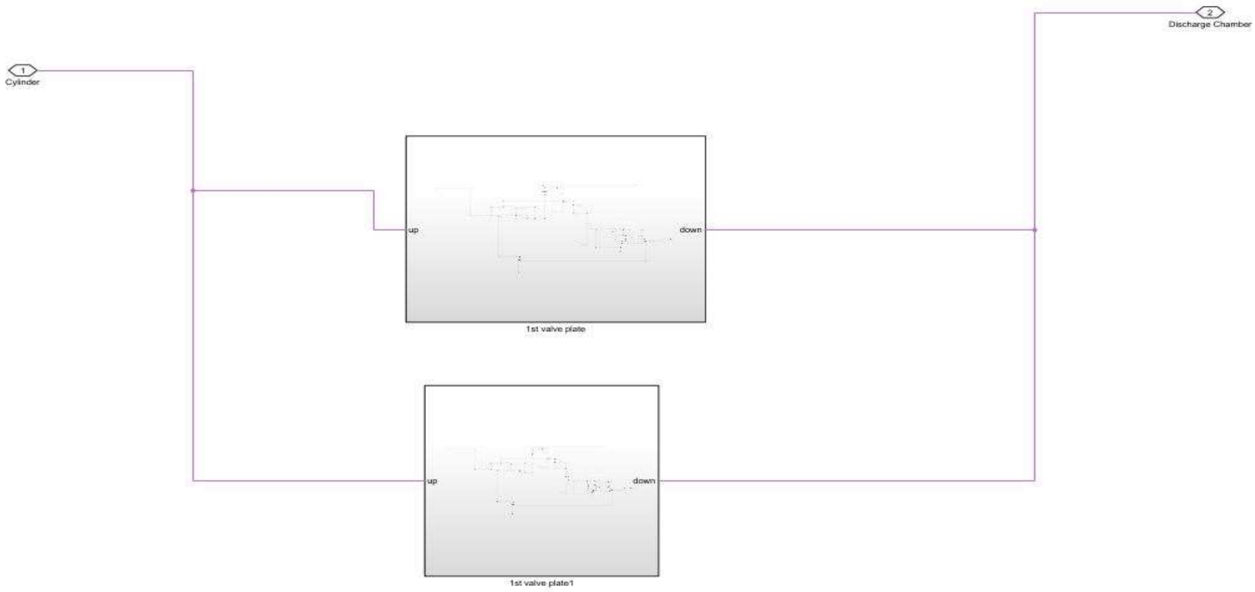

Figure 4.9 Discharge valve Second stage sub model

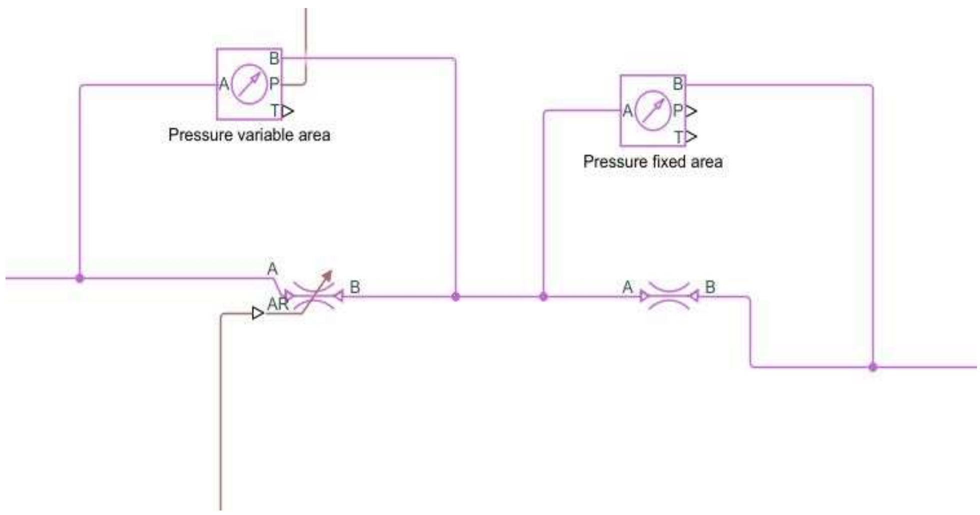

Figure 4.10 Second stage detailed view

4.3 Valve parameter

In this section, the main parameters characterising the valve assembly and how these were calculated or measured will be analysed. The first considered is the valve reed.

The valve plate is modelled as a spring-mass single degree of freedom system characterized by lumped properties whose values of stiffness and mass depends on the typology and geometry of the valve plate itself.

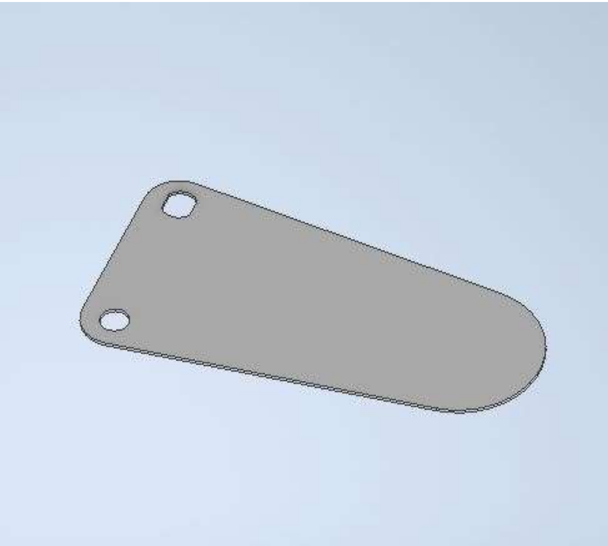

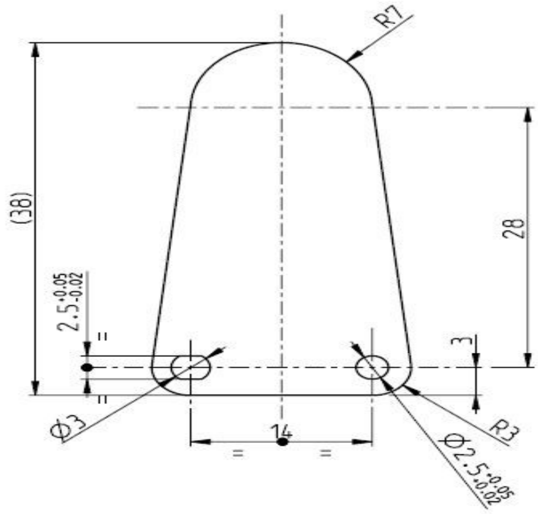

Figure 4.11a 3D Reed view *Fig. 4.11b 2D Reed drawing*

This computation is developed following two different approaches:

- Analytical calculation
- FEM calculation

There are various papers in the literature [13] [16] which state that it is possible to calculate the bending stiffness of the plate using the theory of the Bernoulli Euler beam.

In this study, only the first modal response of the beam is considered for simplicity and the load applied to the plate is assumed to be concentrated.

The following formula is used to calculate the bending stiffness:

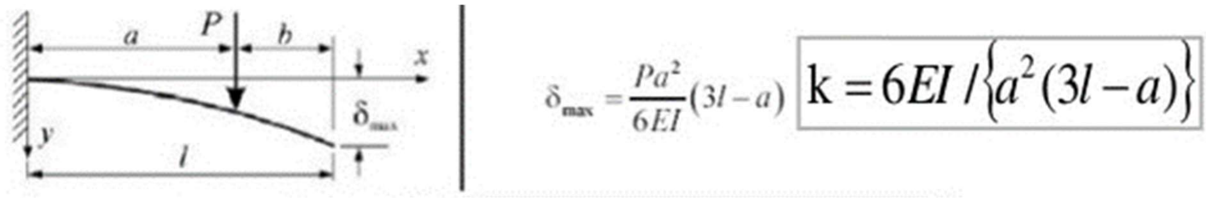

Figure 4.12 Cantilever Beam Deformation and stiffness

Where:

- E stands for the Young modulus
- I stands for the inertia of the cross section area
- L stands for the total length of the plate
- a represents the length in relation to the origin where the load is applied

whereas the following formula can be used to calculate the modal frequency

$$\omega_n = \alpha^2 \frac{h}{L^2} \sqrt{\frac{E}{12\rho}}$$

$$f_n = \frac{\omega_n}{2\pi}$$

Where α is a coefficient that can be found in the literature that depends on which modal frequency order you want to calculate. In the case of a cantilever beam whose first modal frequency is to be calculated, this coefficient is equal to 1,875.

In the mass-spring model, the natural frequency can be calculated as follows:

$$f_n = \frac{1}{2\pi} \sqrt{\frac{k}{m}} \quad [Hz]$$

By inverting the last formula, the equivalent mass of the system can be calculated

$$m_{eq} = \frac{k_{eq}}{(2\pi f_n)^2}$$

The following table shows the geometrical parameters of the plate used in the valve, which are the same for both discharge and suction stages

Parameters	Value	Unit
Thickness	0,254	mm
Total length	38	mm
Load length	28	mm
Width	19,4	mm
Analytical stiffness	552	Nm
Equivalent mass	0,45	g
Natural frequency	173	Hz
Drag Coefficient	1,28	

Table 4.2 Valve plate parameters

The drag coefficient useful to model the force acting on the reed due to gas has been taken from NASA reference [V17], assuming a drag coefficient constant varying the reed lift, this hypothesis will later be removed .The table below lists the maximum plate lift used in the B5900 compressor valve. These values were extrapolated from the CAD software and were measured from the centre of the valve plate port, as some papers suggest. As mentioned above, the discharge valves require less lift than the intake ones.

	First stage		Second stage	
	suction	discharge	suction	discharge
Valve Reed lift [mm]	2,5	2,2	2,4	2,2

Table 2.3 Reed Valve lift

In order to make a comparison with respect to the analytical calculations, a FEM analysis was carried out to calculate the bending stiffness. In the FEM analysis there is a difference between the two plates in that the port has a different shape: circular and slotted. This aspect results in slightly different values. Another aspect that has led to a slight deviation of the stiffness from the analytical calculation is that in the beam theory it is assumed that the beam has a constant cross-section while the 3D drawing shows that this is not true

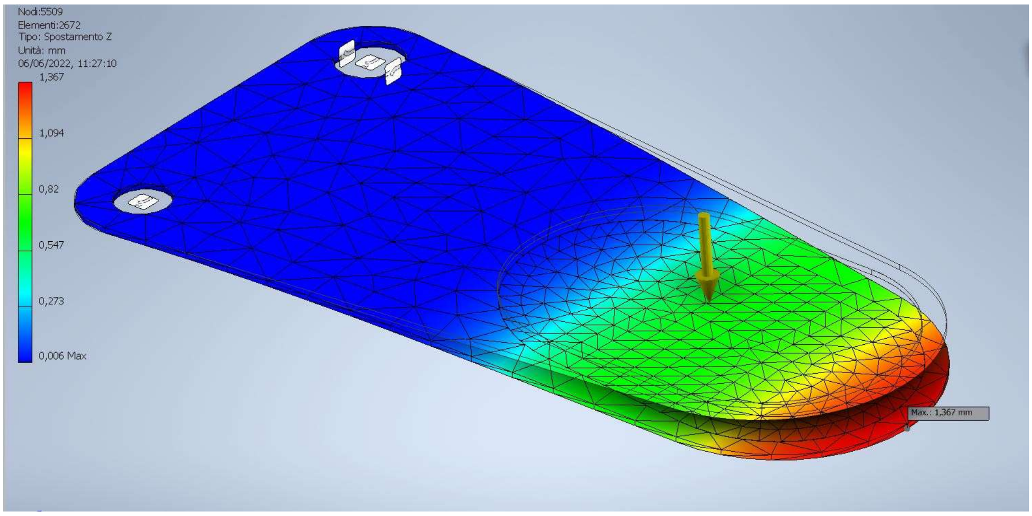

Figure 4.13 FEM calculation Discharge Reed

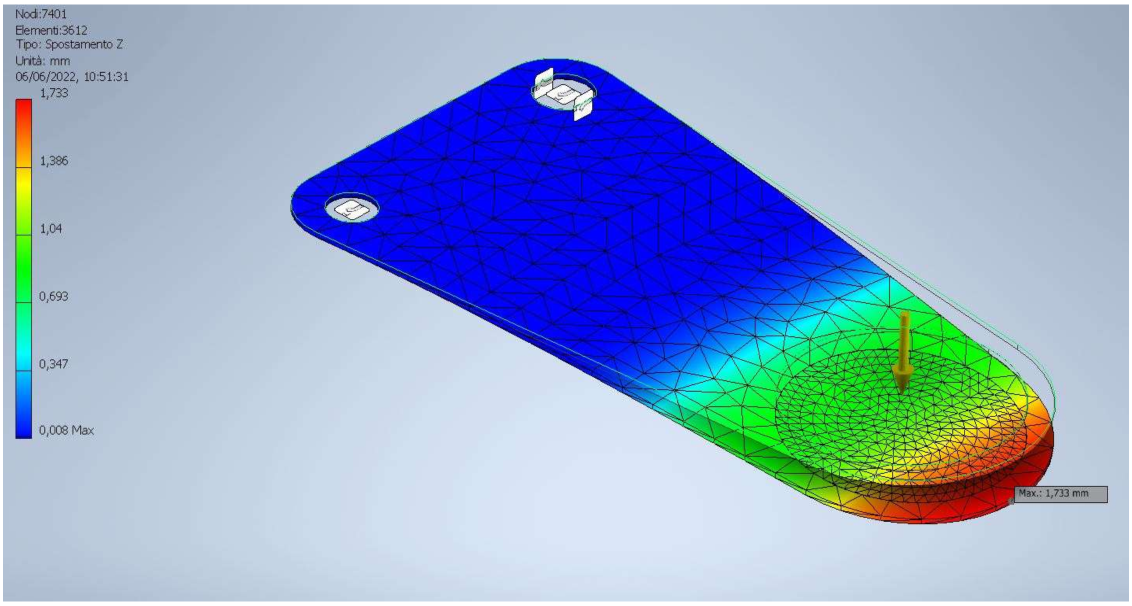

Figure 4.14 FEM calculation Suction Reed

It must be kept in mind that the first plate shown is used in the discharge valve in the first stage, while the second is used in the intake in the first stage and in both exhaust and intake in the second stage

	First stage		Second stage	
	Suction	**Discharge**	**Suction**	**Discharge**
FEM bending stiffness [N/m]	**577**	**731**	**577**	**577**
Analytical bending Stiffness [N/m]	**596,72**	**770**	**596,72**	**596,72**
Error [%]	**3,41**	**5,06**	**3,41**	**3,41**

Table 4.4 Bending Stiffness of the Reeds by FEM

Other parameters necessary to define the behaviour of the valve are the geometric parameters relating to the orifices that allow air to pass through the valve.

These orifices can be classified into two categories:

- fixed area orifices
- variable area orifices

The former model the restriction behaviour downstream of the reed, while the latter represent the restriction created by the deformation of the reed due to the pressure difference acting on the reed itself.

In the latter, the passage air depends not only on the geometric characteristics but also on the dynamics of the reed valve; in fact, as can be seen from some of the attached layouts, they receive a physical signal from the mechanical domain, thus creating model with feedback. The tables below show the geometric parameters for the above-mentioned restrictions. These parameters will influence the values of the flow rate through the valve, the Mach number (and therefore the air speed) and, above all, the pressure losses in the compressor unit that are created due to the non-ideality of the valve.

Restrictions Type	Geometric variable	Value	Unit
Variable	Port Perimeter	53.58	mm
	Port Area	212.9	mm^2
Fixed	Valve Area	191.8	mm^2
	Restriction Area	109.9	mm^2
	Discharge Coefficient	0,64	

Table 4.5 1st stage Suction valve parameters

Restrictions Type	Geometric variable	Value	Unit
Variable	Port Diameter	11.5	mm
	Port Area	103.86	mm^2
Fixed	Valve Area	191.8	mm^2
	Restriction Area	109.9	mm^2
	Discharge Coefficient	0,64	

Table 4.6 1st stage Suction discharge parameters

Restrictions Type	Geometric variable	Value	Unit
Variable	Port Diameter	11.5	mm
	Port Area	103.86	mm^2
Fixed	Valve Area	191.8	mm^2
	Restriction Area	43.56	mm^2
	Discharge Coefficient	0,64	

Table 4.7 2nd stage valve parameter

4.4 Model results

In this chapter, the object of study is the B5900 compressor performances and the valve mounted on it. As previously mentioned, this is a multi-stage compressor, which is the reason why some changes have been made to the model compared to the generic one presented previously.

At ABAC S.p.A, several measurements were carried out on this pump group to understand how its performance and valve's one change at different speeds and to try to reduce compressor noise, which is not the subject of this work.

The compressor has been run at different speeds listed below

- 1235 rpm
- 1375 rpm
- 1569 rpm
- 1667 rpm
- 1769 rom
- 1963 rpm

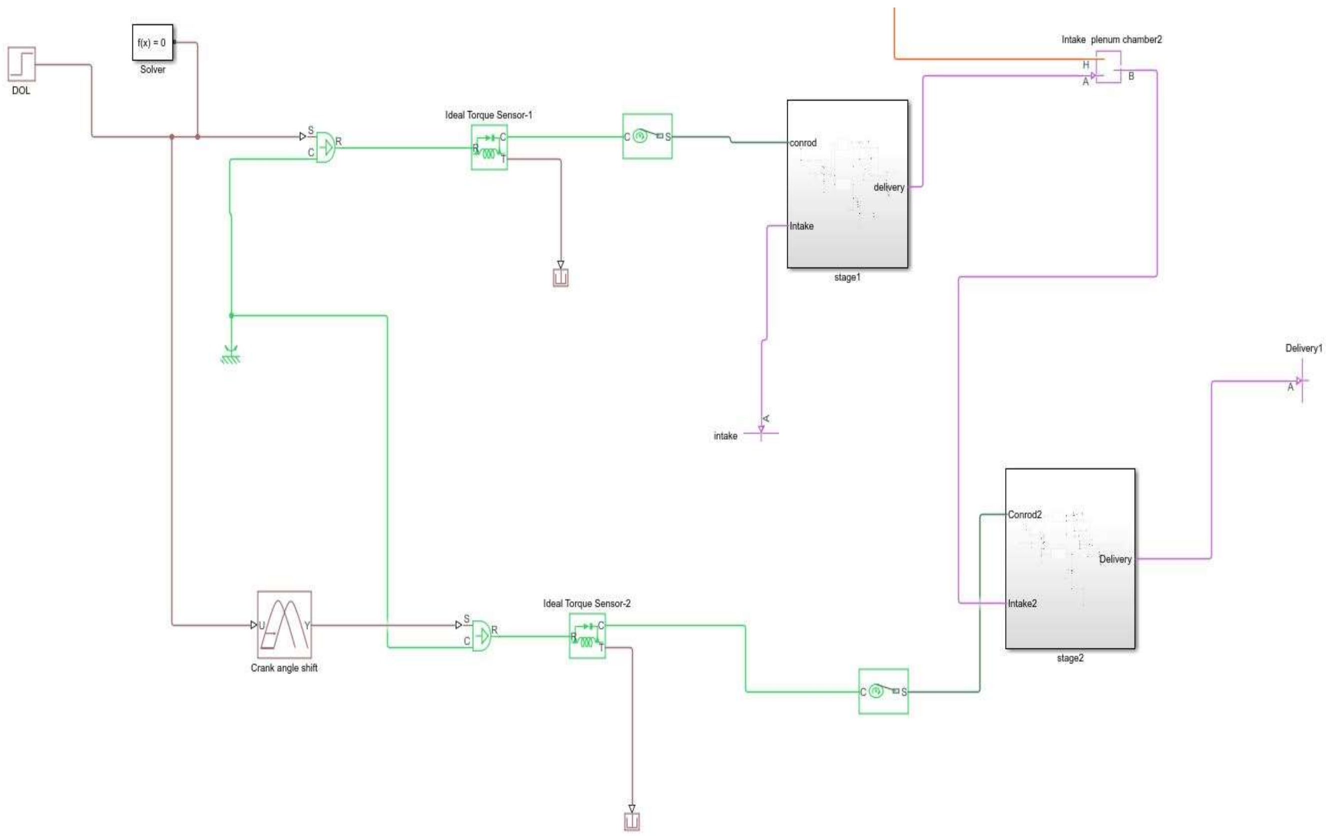

Figure 4.15 Simscape model

For the sake of brevity, the results of only a few speeds will be shown in order to show the main differences.

4.4.1 Model results @1235 rpm

- P-V Diagram

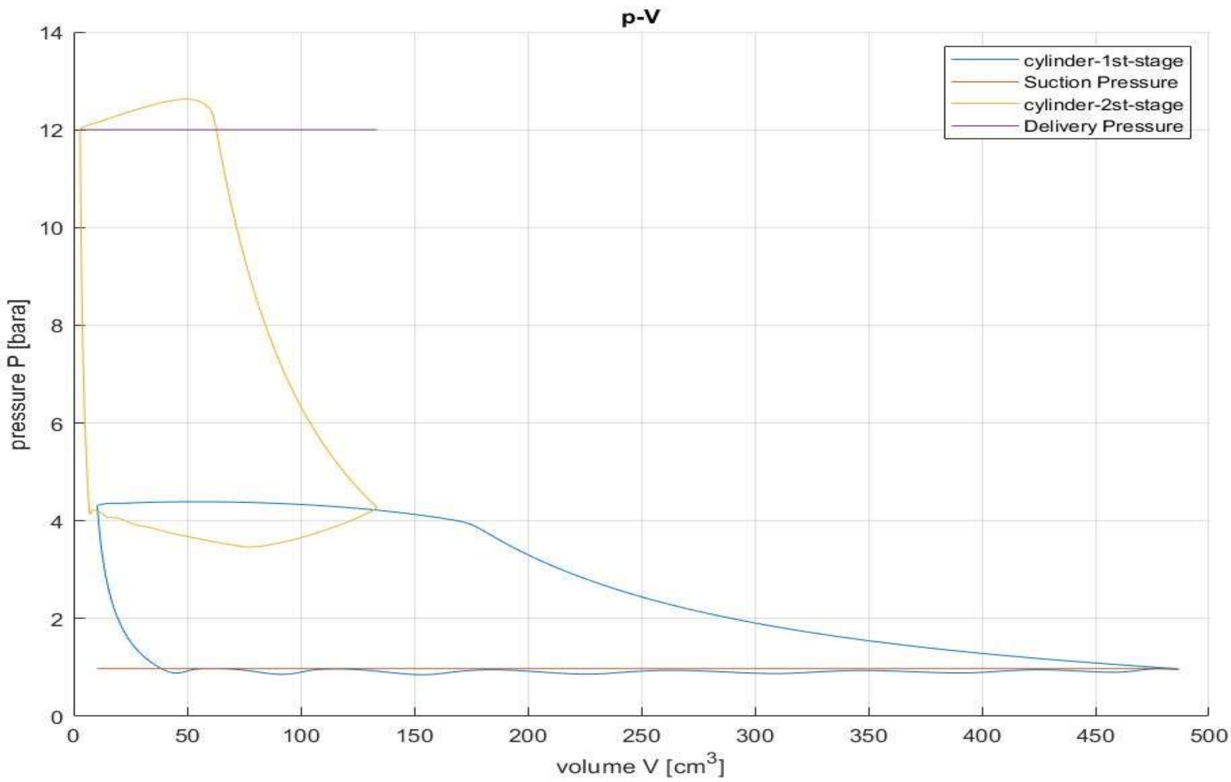

Figure 4.16 P-V Diagram

- Pressure in 1st stage – Crank angle diagram

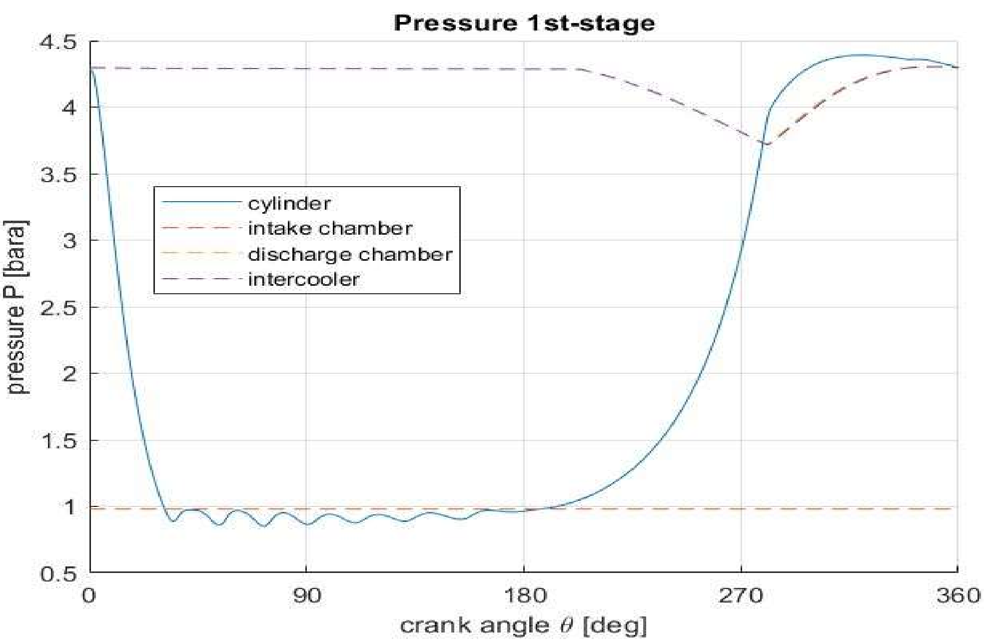

Figure 4.17 Pressure in 1st stage-Crank angle plot

- Pressure Drop in 1st stage suction valve – Crank angle diagram

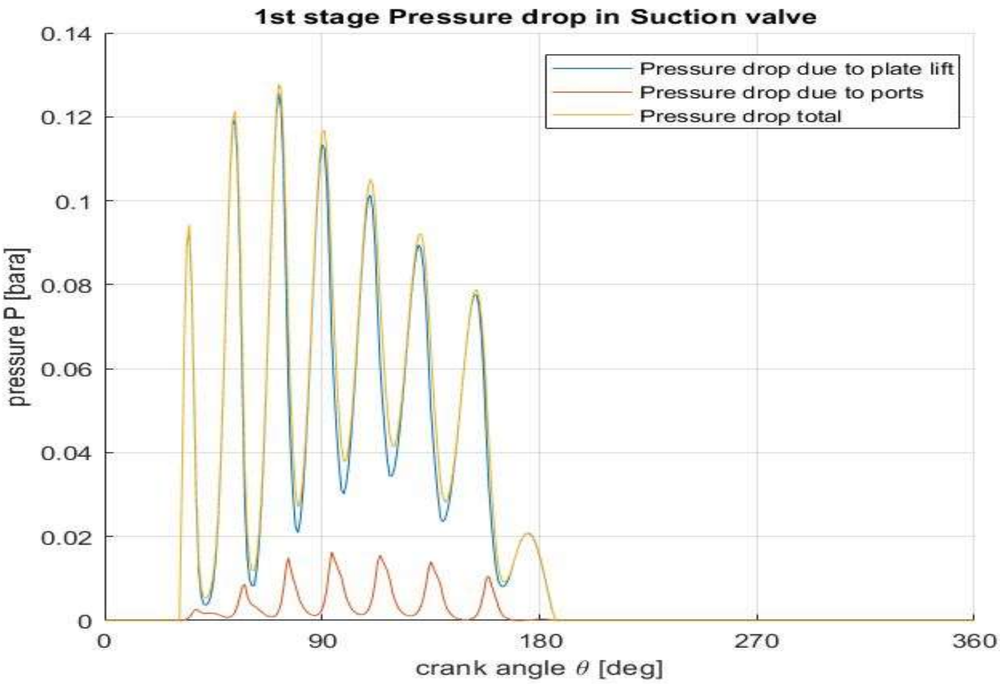

Figure 4.18 Pressure Drop in 1st stage suction valve -Crank angle plot

- Pressure Drop in 1st stage discharge valve – Crank angle diagram

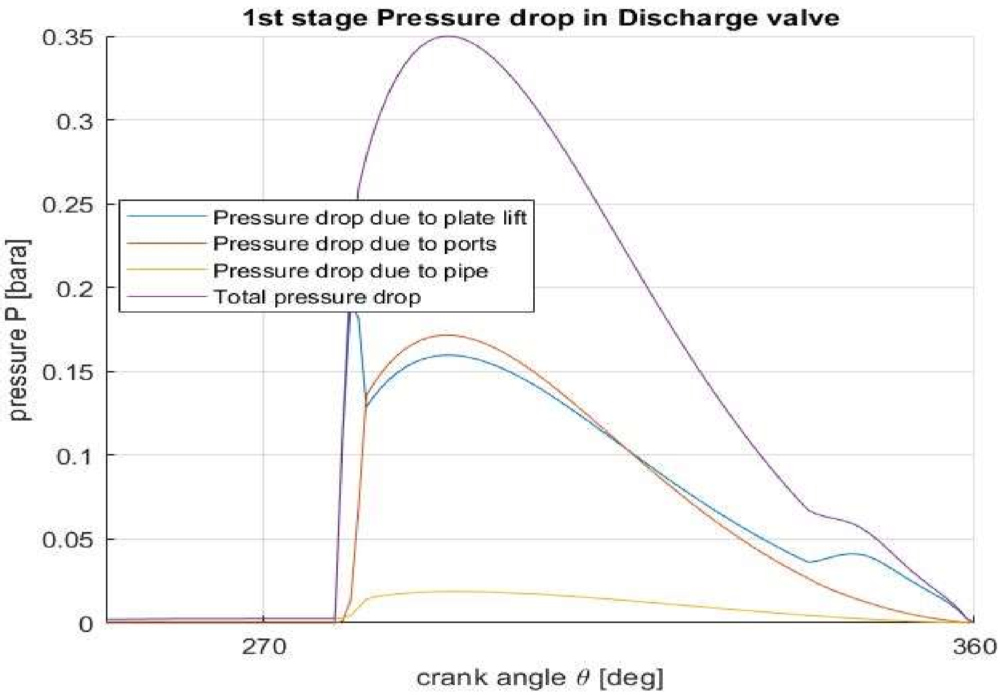

Figure 4.19 Pressure Drop in 1st stage discharge valve -Crank angle plot

- Reed kinematic quantities in 1st stage– Crank angle diagram

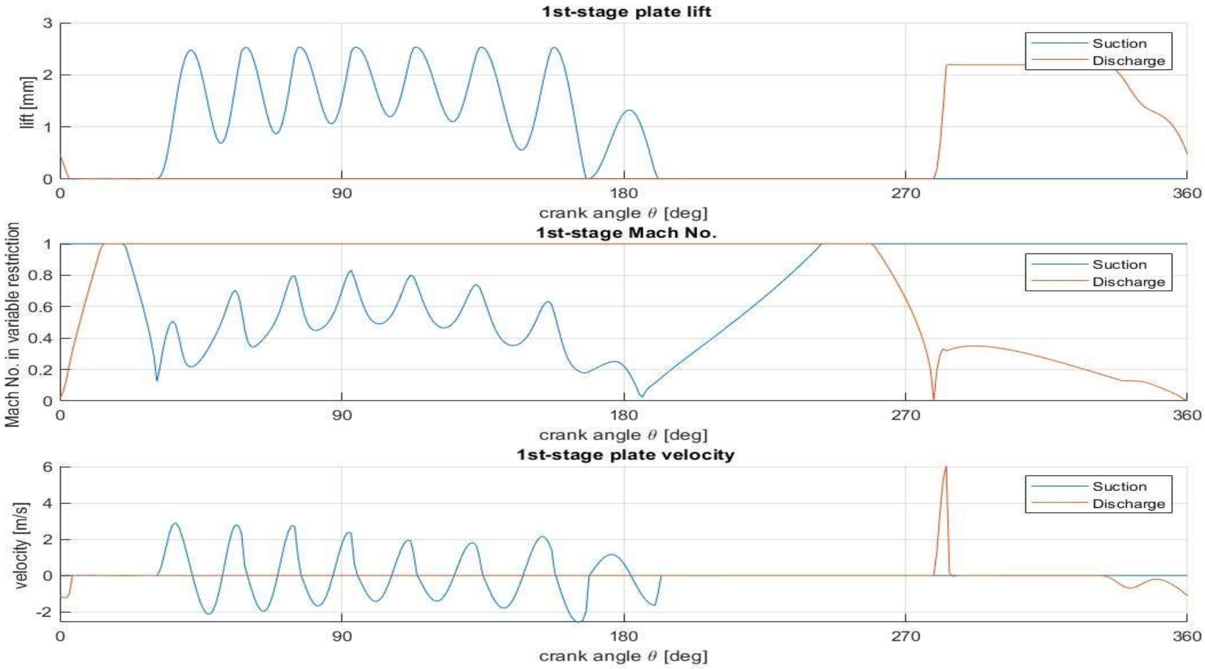

Figure 4.20 lift, velocity Reed-Crank angle plot

- Pressure in 2nd stage – Crank angle diagram

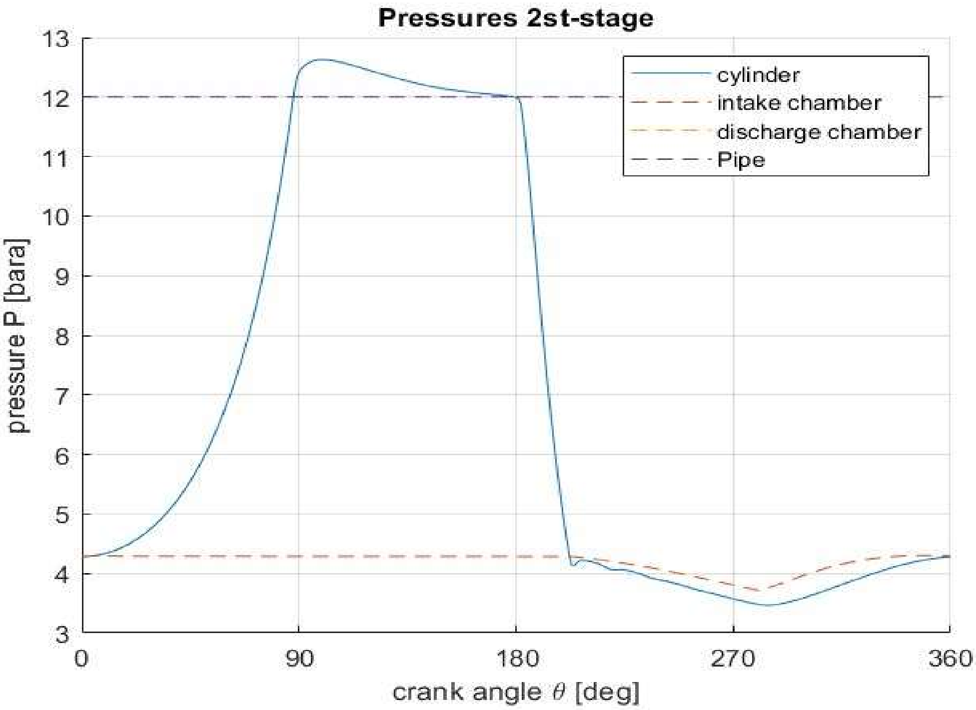

Figure 4.21 Pressure in 2nd stage-Crank angle plot

- Pressure Drop in 2nd stage suction valve– Crank angle diagram

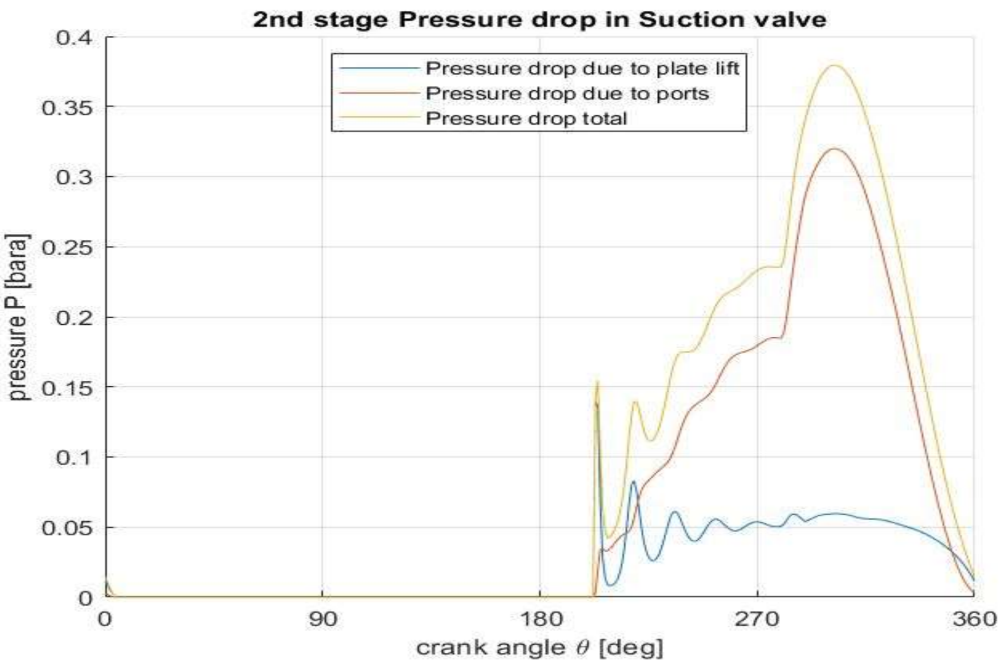

Figure 4.22 Pressure Drop in 2nd stage suction valve -Crank angle plot

- Pressure Drop in 2nd stage discharge valve– Crank angle diagram

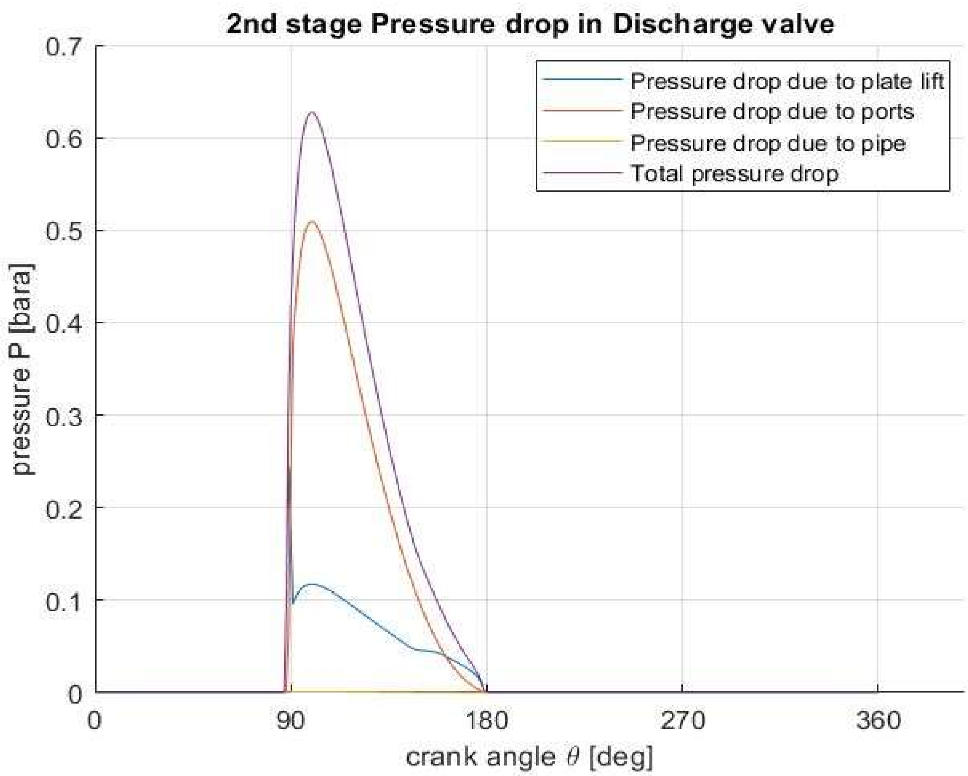

Figure 4.23 Pressure Drop in 2nd stage Discharge valve -Crank angle plot

- Reed kinematic quantities in 2nd stage– Crank angle diagram

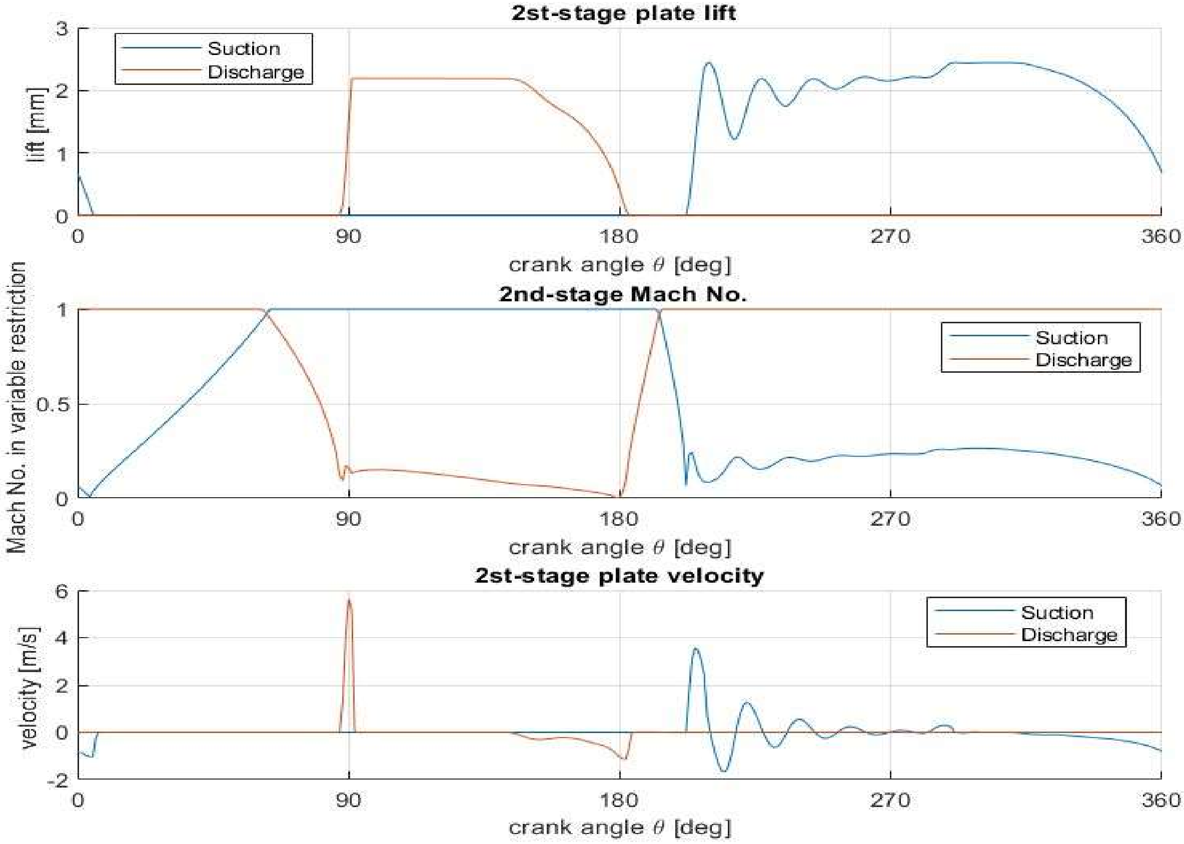

Figure 4.24 Lift, velocity Reed-Crank angle plot

As can be seen from the reed valve lift graph, in both intake valves there is the phenomenon of the reed valve bouncing against the plate cavity. As a result, the reed valve speed graph shows almost alternating behaviour, which can lead to reed valve failure through impact fatigue.
In both stages, the intake valves remain open for a greater shaft angle than the exhaust valves, in fact, higher reed valve peak velocities are observed in the exhaust valves.

The following table summarises Compressor efficiencies described above in numerical form: the first two relate exclusively to valve behaviour and how the valves impact the compressor unit. The others relate more generally to compressor behaviour.

As can be seen in the second stage, the overpressures in the second stage due to the passage of air through the valves are greater than in the first stage, from which these losses also depend on the nominal pressure acting. Despite this, the power losses are greater in the first stage because the suction valve in the first stage remains open for longer time.

	First stage		Second stage	
	Suction	**Discharge**	**Suction**	**Discharge**
Pressure losses [kW]				
Over pressure [bar]	**0,12**	**0,35**	**0,38**	**0,62**

	First stage	**Second stage**	**Overall**
FAD [l/s]	**7,90**	**7,85**	**7,85**
Air displacement [l/s]	**9,80**	**10,48**	**9,80**
Volumetric efficiency	**0,789**	**0,748**	**0,8**
Shaft Power [kW]	**2,10**	**1,84**	**3,95**
SER [J/l]	**272,25**	**234,21**	**502,56**

Table 4.8 Numerical efficiencies @1235 rpm

4.4.2 Model results @1963 rpm

- P-V Diagram

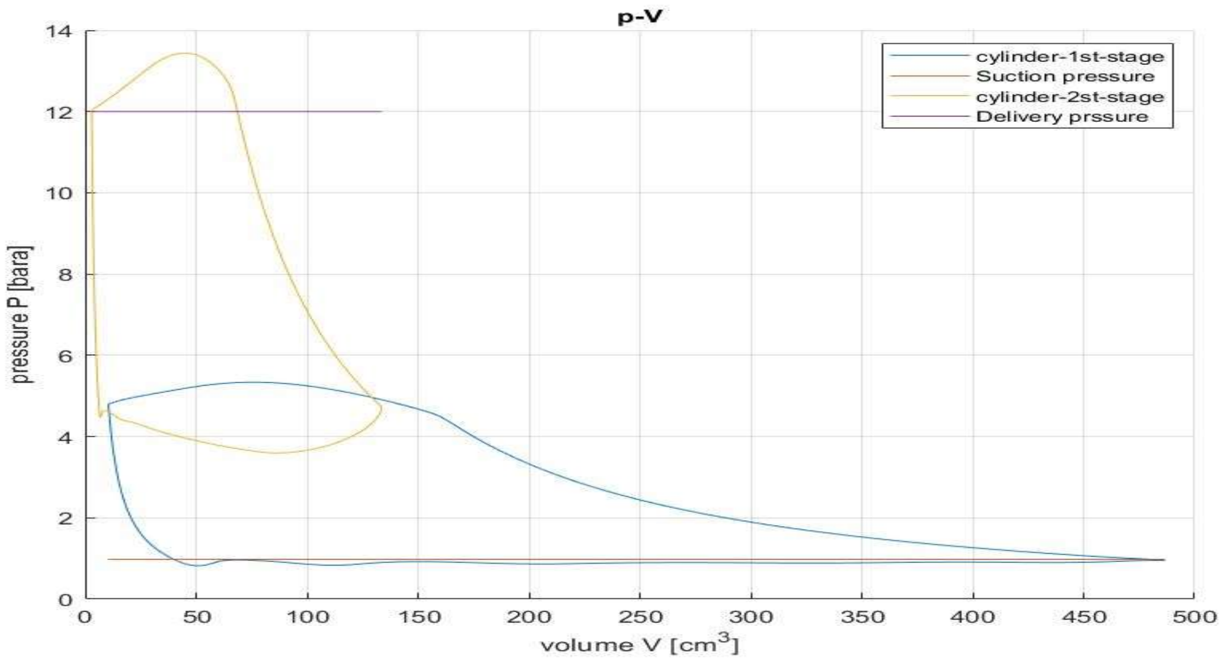

Figure 4.25 P-V Diagram

- Pressure in 1st stage – Crank angle diagram

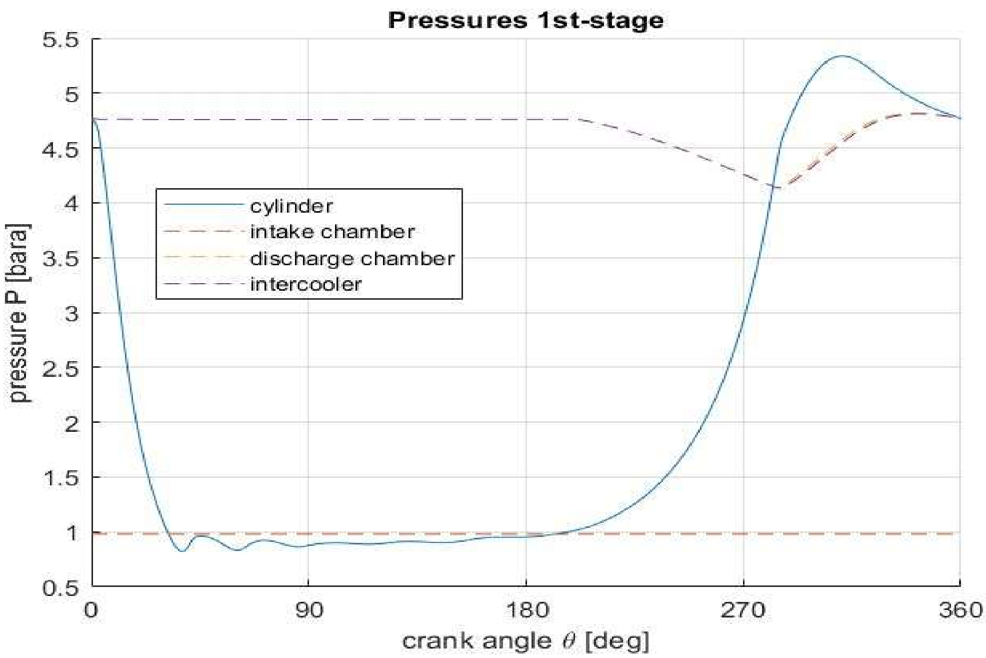

Figure 4.26 Pressure in 1st stage-Crank angle plot

- Pressure Drop in 1st stage suction valve – Crank angle diagram

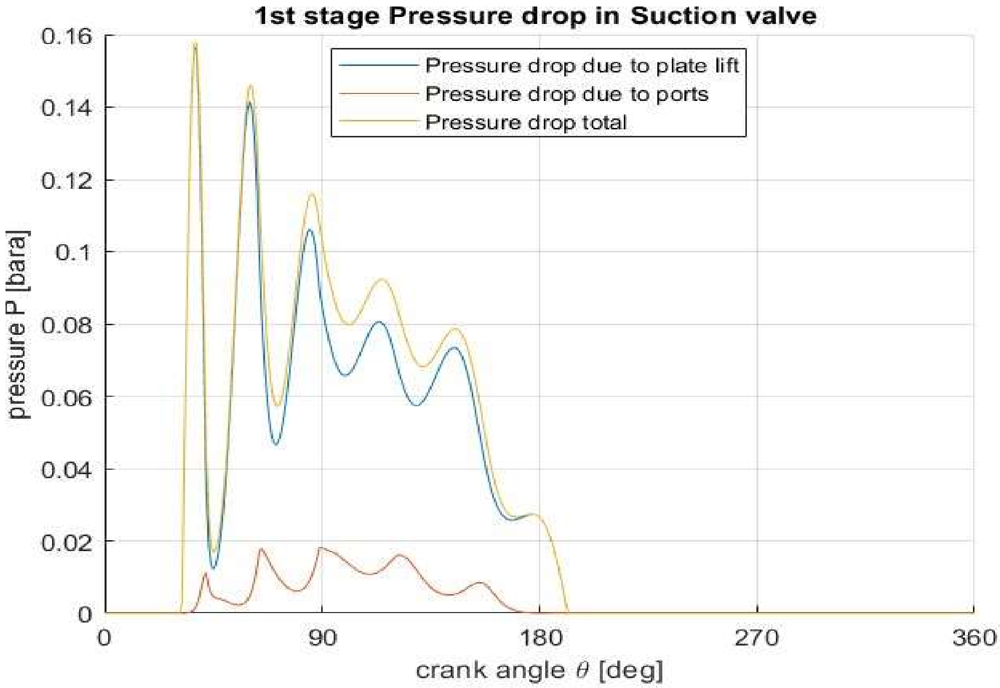

Figure 4.27 Pressure Drop in 1st stage suction valve -Crank angle plot

- Pressure Drop in 1st stage discharge valve – Crank angle diagram

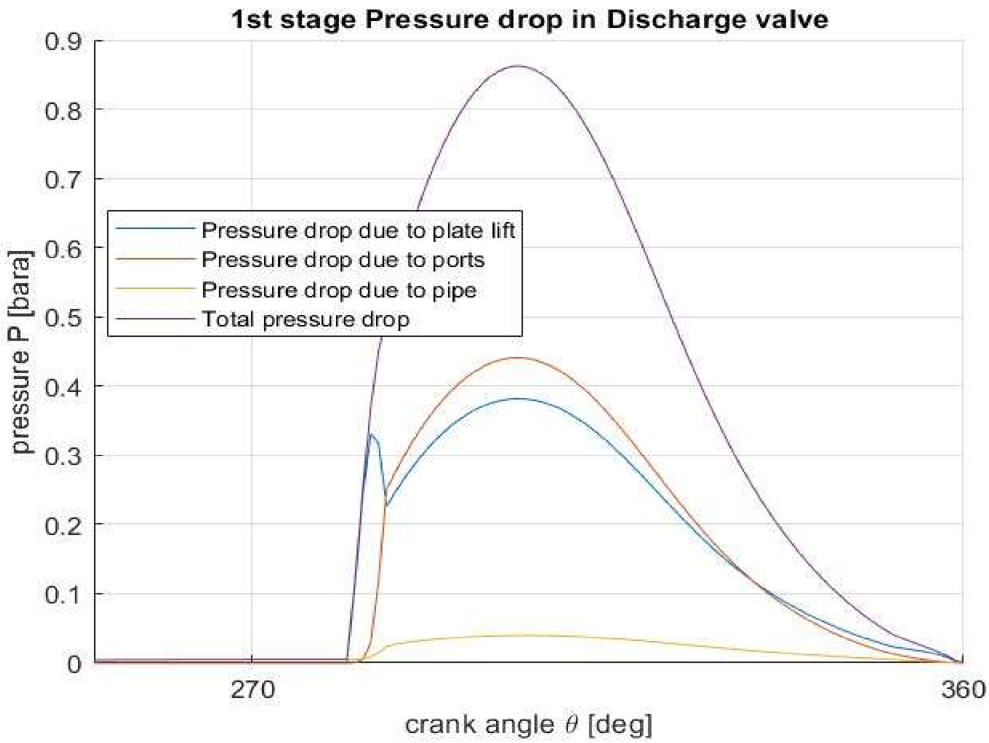

Figure 4.28 Pressure Drop in 1st stage discharge valve -Crank angle plot

- Reed kinematic quantities in 1st stage– Crank angle diagram

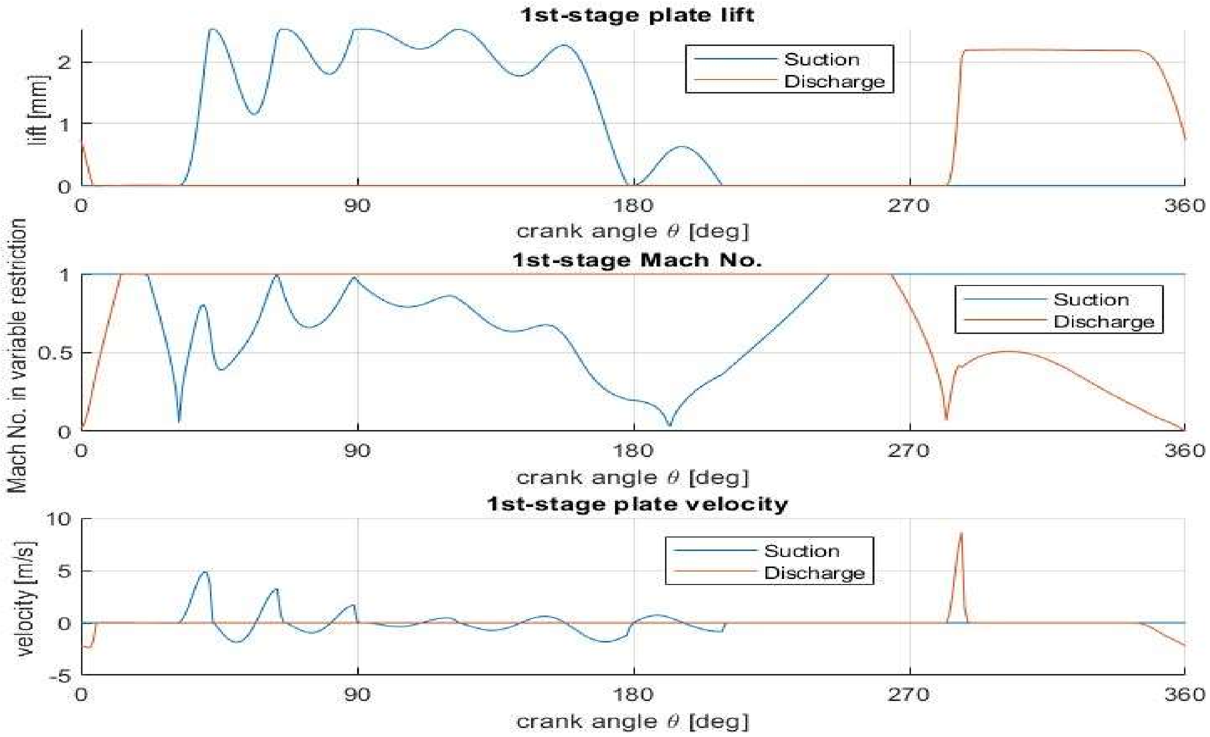

Figure 4. 29 Lift, velocity Reed-Crank angle plot

- Pressure in 2nd stage – Crank angle diagram

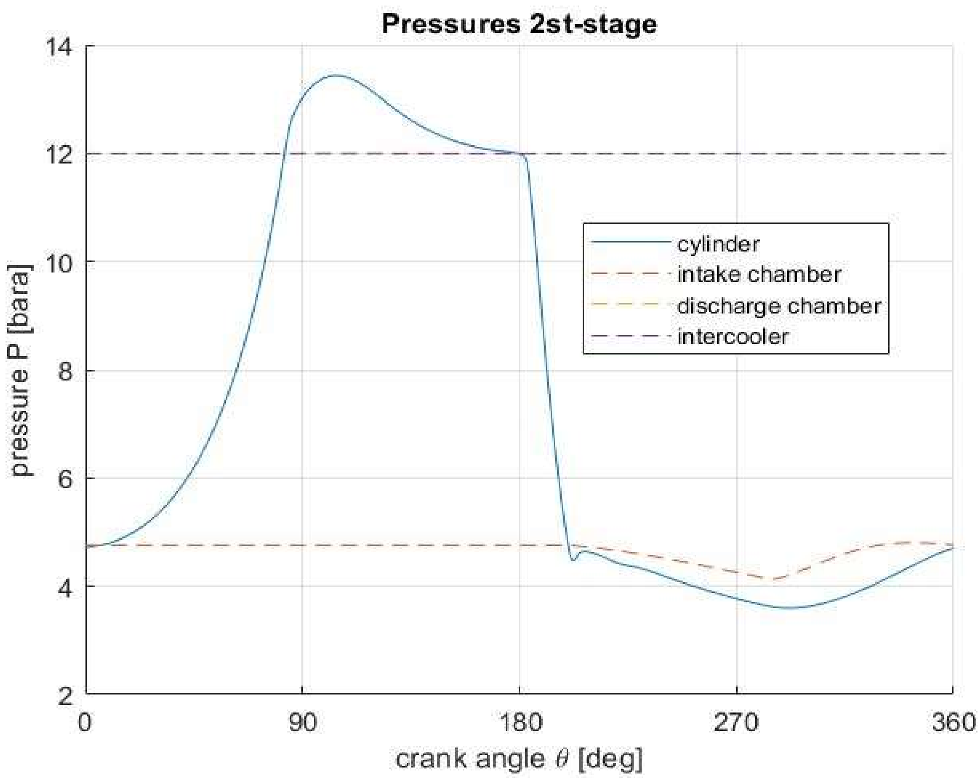

Figure 4.30 Pressure in 2nd stage-Crank angle plot

- Pressure Drop in 2nd stage suction valve– Crank angle diagram

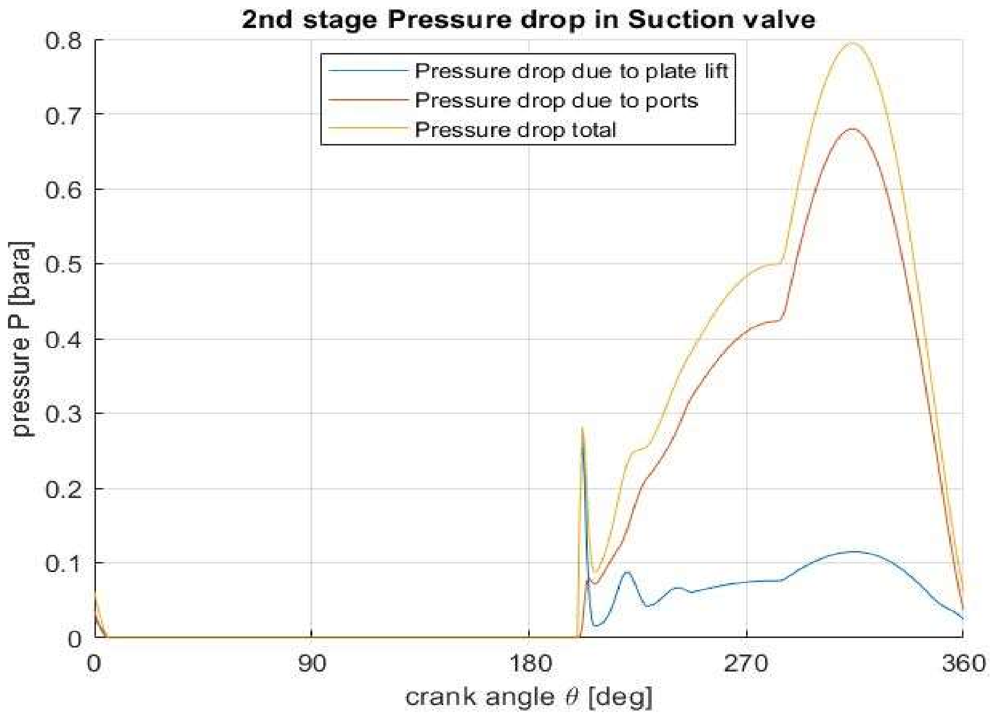

Figure 4.31 Pressure Drop in 2nd stage suction valve -Crank angle plot

- Pressure Drop in 2nd stage discharge valve– Crank angle diagram

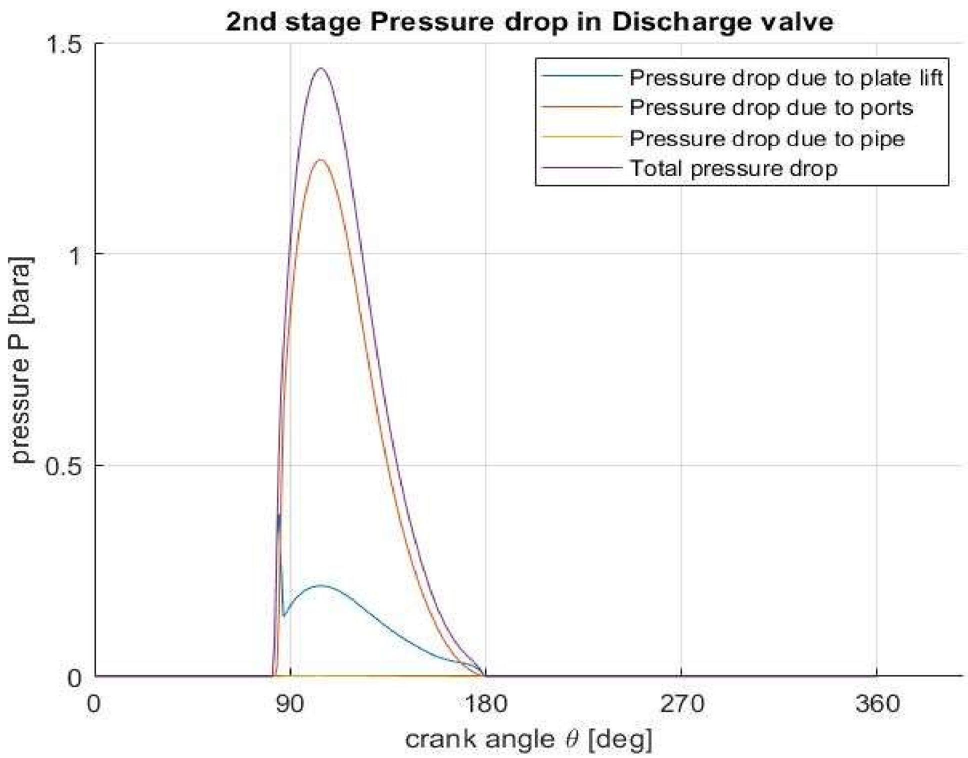

Figure 4. 32Pressure Drop in 2nd stage discharge valve -Crank angle plot

- Reed kinematic quantities in 2nd stage– Crank angle diagram

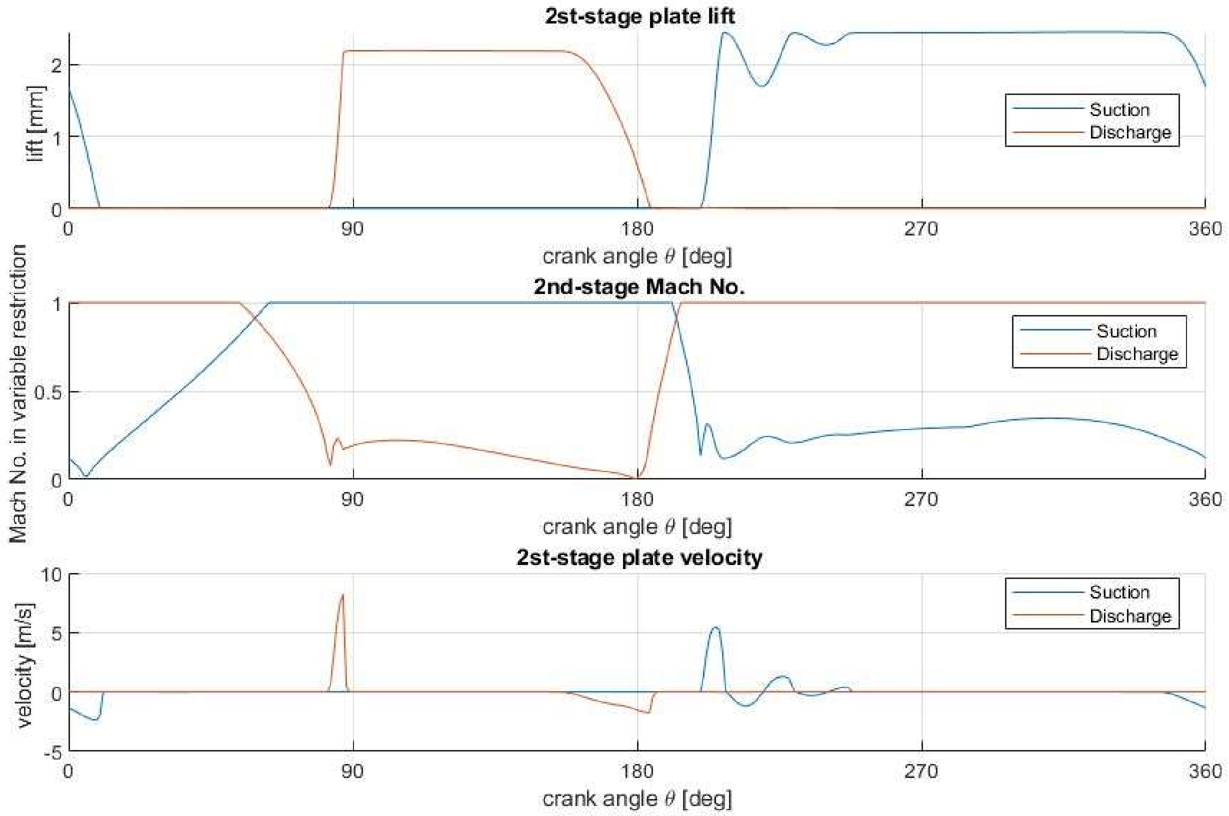

Figure 4.33 Lift, velocity Reed-Crank angle plot

As already done for the @1235 rpm model, the main compressor efficiencies are summarised below.

Obviously, increasing the crankshaft speed improves the FAD because the flow rate increases but the volumetric efficiency of the compressor drops to 76 %. This drop in volumetric efficiency is explained by the fact that in the first stage, the restriction due to the deformation of the reed modelled as a nozzle gets choked.

	First stage		**Second stage**	
	Suction	**Discharge**	**Suction**	**Discharge**
Pressure losses [kW]	**0,1188**	**0,1345**		**0,1984**
Over pressure [bar]	**0,1507**	**0,86**	**0,8**	**1,4**

	First stage	**Second stage**	**Overall**
FAD [l/s]	**11,92**	**11,86**	**11,86**
Air displacement [l/s]	**15,58**	**18,4**	**15,58**
Volumetric efficiency	**0,75**	**0,64**	**0,76**
Shaft Power [kW]	**3,55**	**3,44**	**7**
SER [J/l]	**303,71**	**289,88**	**589,45**

Table 4.9 Numerical efficiencies @1963 rm

4.4.3 Comparison between Model and Experimental Results

This subsection shows graphs of certain quantities and efficiencies as a function of crankshaft speed. Regarding the pressure difference created due to the valve, this increases almost linearly as the speed varies.
As mentioned above, this pressure difference depends on whether it is a delivery or exhaust valve and also on the compression stage. In fact, as can be seen from the graph, at maximum speed in the exhaust of the second stage there is a pressure difference of 1.4 bar, while in the first stage it reaches 0.86 bar.
The FAD, which is a parameter indicating the delivery flow rate, linearly increases with crankshaft speed, but at the same time, above a certain value of crankshaft speed, the volumetric efficiency starts to drop. Several measurement tests were conducted at ABAC in parallel with the creation of the model in order to compare the model with experimental reality.
The only parameters that were extrapolated from the measurements concerned the temperatures developing in the cylinders' chambers.
Comparing the results of the model and the measurements on the FAD there is an average error of 3 %, which is more than acceptable.

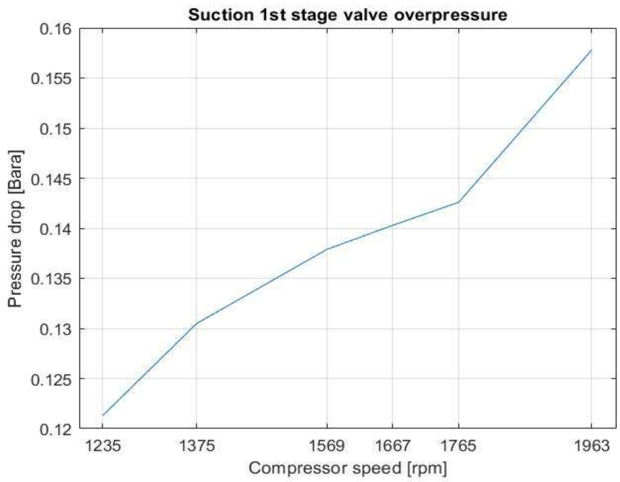

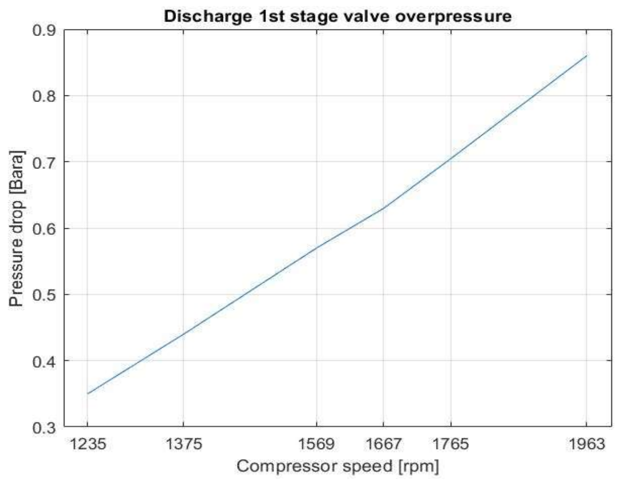

Figure 4.34 a Suction 1st stage overpressure-speed Fig. 4.34b Discharge 1st stage overpressure-speed

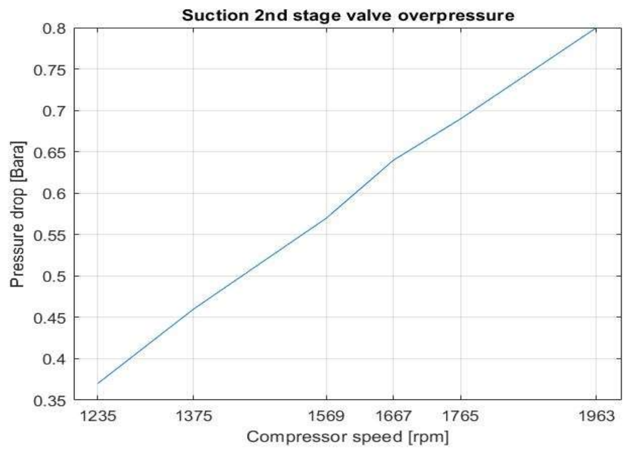

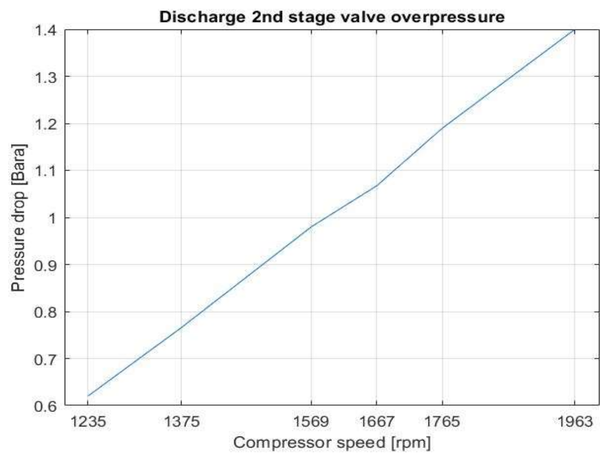

Figure 4.34 c Suction 2nd stage overpressure-speed Fig.4.34d Discharge 2nd stage overpressure-speed

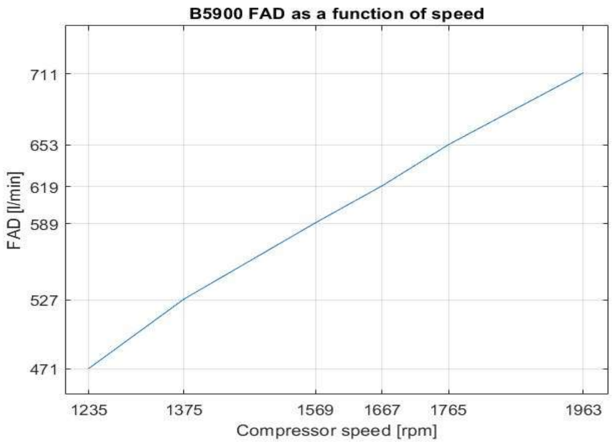

Figure 4.35 FAD- Crankshaft speed

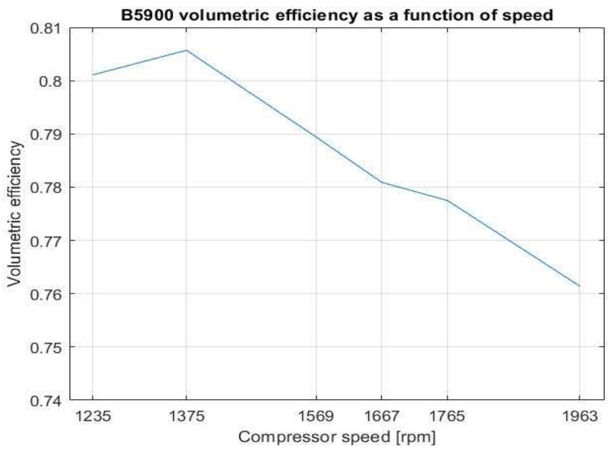

Figure 4.36FAD- Crankshaft speed

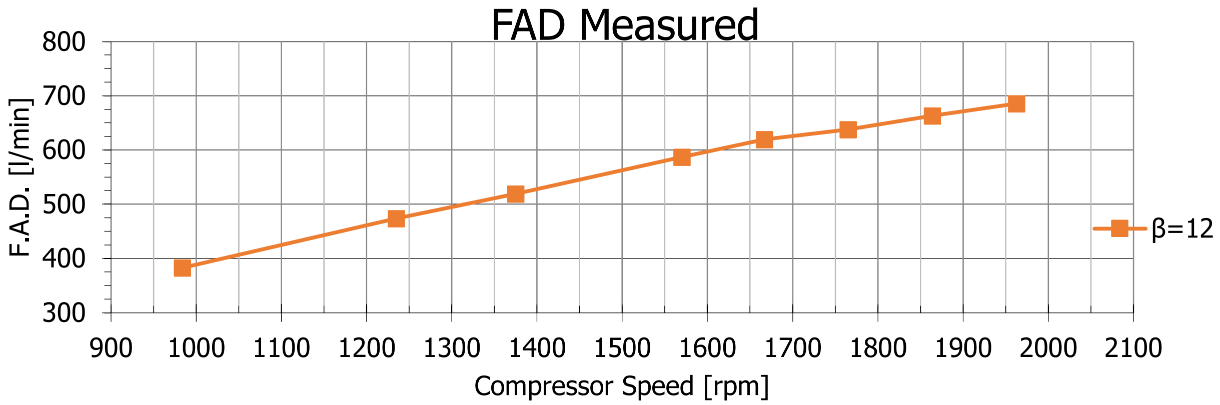

Figure 4.37 FAD -crankshaft speed Experimental

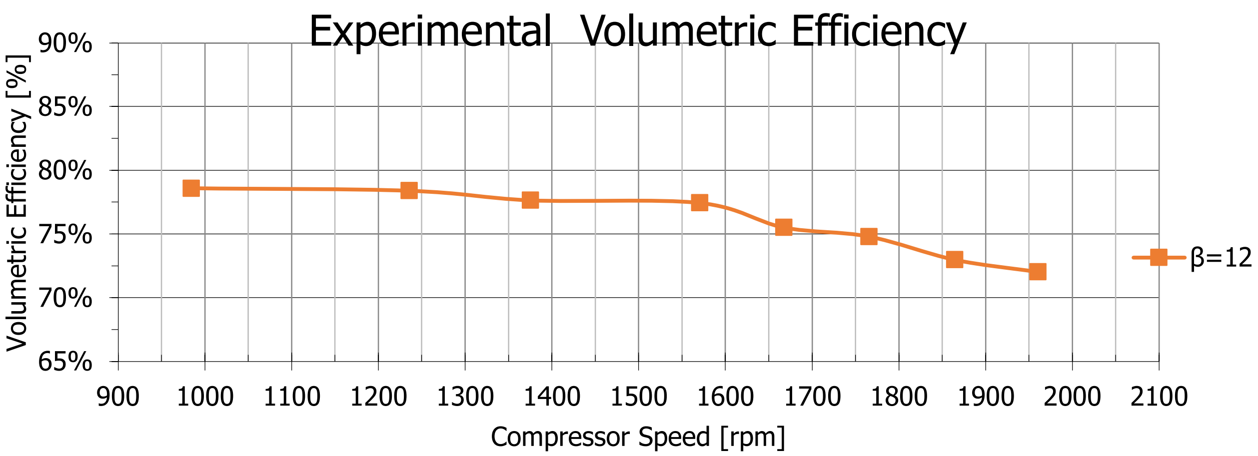

Figure 4.38 Volumetric Efficiency -crankshaft speed Experimental

From this model-laboratory comparison procedure, it can be said that it is possible to create a model on Simscape to calculate valve quantities for the Reed Leaf valve, which is a useful support during the valve design phase. In the next chapters the model will be applied on another type of valve on which there are not predictive models in literature so it was necessary to implement a CFD analysis on the valve in order to extrapolate some parameters for the Simscape model.

5 Feather Valve

This section describes the feather valve, which will be installed on the compressor whose Simscape model is being programmed and will replace the reed valve discussed in earlier chapters.

The novel valve has various properties, including a small clearance volume, low resistance, low noise, high adaptability under varying operating circumstances, a simple manufacturing procedure, and a low cost. The first part of this chapter provides a brief description of the valve's working principle and its salient features, introducing some equations that are useful in both the valve design and Simscape model development phases. The second part includes 2D drawings of the valve.

5.1 Description

Figure 5.1 depicts the "feather" valve, which is utilised in the piston compressor.

The valve is made up of a flat strip of steel that covers a slot in the seat plate. A retainer with notches for the reed ends holds the reed in place over the slot. When the valve is opened by an excess of pressure (from the cylinder side), it bends against a curved stop plate. This stop plate can be cut to a uniform arc profile or a shape composed of straight lines and arcs. The retainer plate and stop plate are normally intended to provide a little amount of uniform lift before the reed begins to bend. The design of these components has an impact, which will be discussed in more detail below, on the characteristics of the valve and consequently on the operation of the compressor.

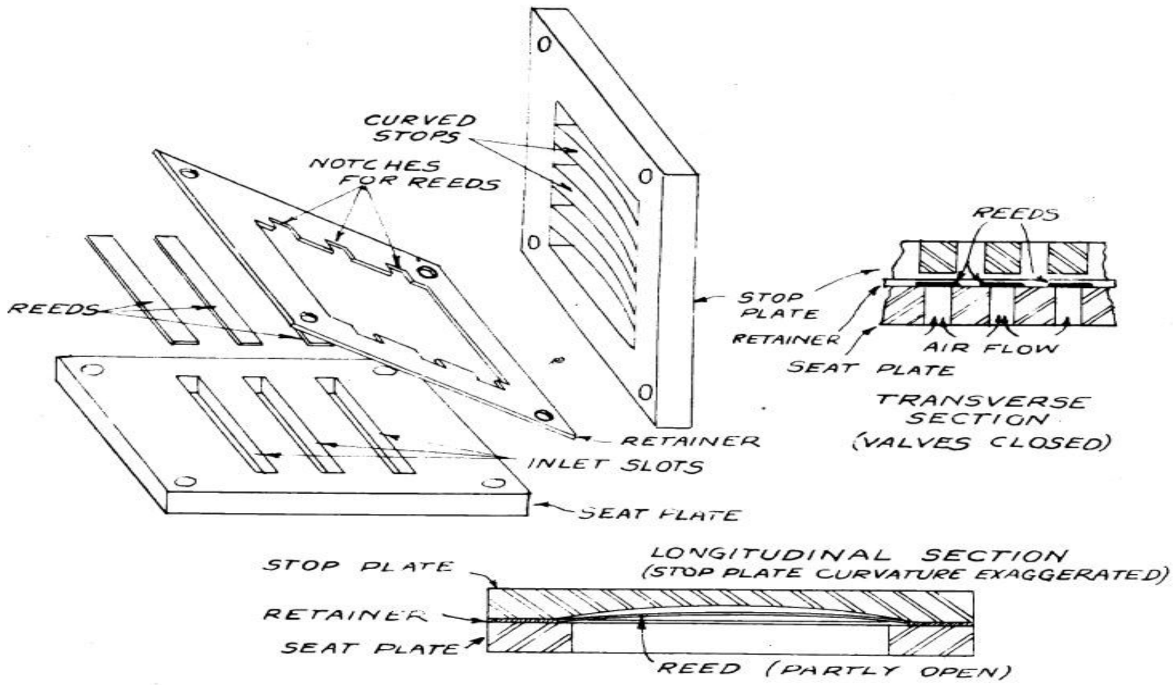

Figure 5.1 Feather valve Description [5]

The third support is made up of two short arc-bottomed keyseats, visible in Fig. 5.2 and Fig. 5.4 . The bottom surface an of the keyseat supports the feather spring, while the side surface limits the spring's lateral motion.

When there is no air flowing through the valve, the spring pushes tight to the valve seat, blocking the valve channel. When the valve is in use, the spring is pushed by air and bent, opening the valve channel and allowing air to flow into the cylinder through the valve. The feather spring lift is variable because there is no valve guard to limit the spring lift h.

When the simply supported valve is in operation, the feather spring bends as a result of the air force acting on the reed. The bending is determined by the distribution and value of this force.

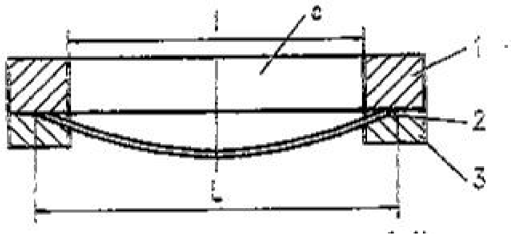

Figure 5.2 Feather valve Scheme

In [5] and [18] there is a analytical study for this type of valve. It’s assumed that, while opening, the valve has the form of its basic mode of vibration as a simply supported beam. This assumption appears acceptable since the frequency of the exciting force is low in comparison to the reed's first natural frequency. This implies that higher modes should not be occurred.

With these assumptions, the area for gas flow is proportional to the lift. As a result, the Nozzle flow equation may be used to simulate the valve flow behaviour, which is characterized by a One DOF system as done previously.

After describing the components and the principle of operation, a mathematical treatment is described below in order to assess how these components and their dimensions impact on valve performance.

As done for the reed valve modelled above, the Euler beam theory is also used for the Feather valve. The following variables are used in the following mathematical discussion, the physical meaning of which are described in Tab. 5.1

Variables		Physical Meaning
Reed Geometrical paramters	**a**	**Reed Thickness**
	B	**Reed Width**
	L	**Reed Length**
	$\boldsymbol{A_v}$	**Reed maximum Area**
Reed Structural parametrs	$\boldsymbol{\rho_S}$	**Reed Density**
	E	**Young Modulus**
	J	**Moment of inertia**
Reed Fluidodynamic Parametr	$\boldsymbol{C_g}$	**Drag coefficient**
	$\boldsymbol{\Delta P}$	**Pressure Difference along the Reed**

Table 5.1 Physical Parameter

In this case it is not possible to approximate the pushing force given by the air to a concentrated load but a well distributed loas was used to model the drag force.

$$F_g = C_g A_v \, \Delta P \quad 5.1)$$

So the well distributed load q can be calculated as follows

$$q = \frac{F_g}{L} = C_g B \Delta P \; 5.2)$$

The lift and the effective flow area depend on the spring bending function $y = y$(x,θ) . The equation of the bending of the simply supported feather spring is given by the influence of the well-distributed linear air lift q. Referring to Fig.3 the lift is composed by two terms:

$$\Delta h = L\frac{\alpha - sin\theta}{2} = \frac{5\rho_S L^4}{32Ea^3} \qquad 5.3)$$

$$y = \frac{qx}{24EJ}(L^3 - 2Lx^3 + x^4) \quad 5.4)$$

The term Δh is related to the deformation due to the gravity. For this reason, the reed will not press close to the valve seat, leading to the loss of the actual suction capacity. The Eq. 3 comes from the balance between the gravity force and the elastic force of the reed. But in most common conditions the angle α , visible in Fig.5.3, is very low, until the ratio $\frac{y_{max}}{L}$<0,1 , so the term Δh can be ignored.

Substituting $x = \frac{L}{2}$ in the Eq.5.4 becomes:

$$h = \frac{5qL^4}{384\,EI} \qquad 5.5)$$

Which represents the feather valve lift in the middle of the reed, visible in Fig. 5.3.

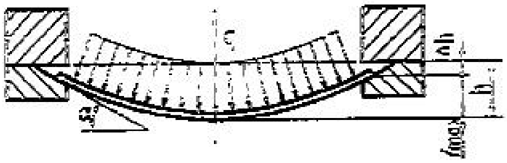

Figure 5.3 Reed Deformation under distributed load

From Eq.5.5, a first useful relation for valve design can be derived

$$\frac{h}{L} = \frac{5qL^3}{384EI} < 0{,}1 \quad 5.6)$$

From Eq.5.6 it's possible to verify the relationship between the lift and the length of the reed and also set a ratio between the length and the thickness.

For this type of valve, one of the most difficult parameters to calculate is the flow area formed by the deformation of the reed due to air pressure. In [8] an analytical treatment is proposed in order to calculate the flow area based on the elastic displacement.

The effective flow area A_v is composed of two bow shaped areas, If the number of strips is i and their lengths are L_1, L_2 and L_i then:

$$A_v = 2\sum_{n=1}^{n=i}\int_0^{L_i} y(x)dx$$

Substituting in the integral the Eq.4 and considering that the deformation is symmetric respect to the middle of the Reed, it's possible to write

$$A_v = 4\sum_{n=1}^{n=i}\int_0^{\frac{L_i}{2}} \frac{qx}{24EJ}(L^3 - 2Lx^3 + x^4) \quad dx$$

Resolving this integral and assuming that there is just one Reed having a length equal to, it's possible to write

$$A_v = \frac{qL^5}{5Ea^3} \qquad 5.7)$$

Combining Eq.5.7 and Eq.5.5 it's possible to link the lift h with the flow area A_v

$$A_v = \frac{32\ hL}{25} \quad 5.8)$$

The formulation of flow area, represented in Eq.5.8, is quite different from the formulation of flow area proposed for the previous valve study.

Another important design parameter is the arc bottom of the keyseat whose detail is shown in Fig. 5.4.

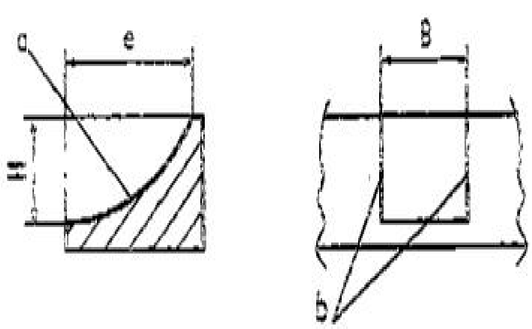

Figure 5.4 Arc Bottom of the keyseat frontal and lateral view

Denoting with λ the angle of the arc bottom it's possible to write a design criteria due to the balancing equation between the Euler load and the force generated by the drag force

$$\lambda = tg^{-1}\frac{2\pi^2 EJ}{BL^3 q_{max}} \quad 5.9)$$

5.2 New valve prototype

Being a valve mounted on a multi-stage compressor in straight configuration, the valve under consideration is an assembly consisting of the following parts listed in Tab. 5.2

Part	Quantity
Valve plate	**2**
High Pressure Reed	**2**
Low Pressure Reed	**2**
Gasket	**1**

Table 5.3 Assembly list

The same type of reed was used for both the exhaust and the intake for each compression stage: this design choice simplifies the design of the valve plate itself, as only one type of plate can be designed. The dimensions and shapes of the various channels, hollows, etc. etc. were extrapolated from the accumulated experience of ABAC S.p.A. in an initial design phase.

Subsequently, these characteristic dimensions were modified during the design of the Simscape model to improve the valve's performance. Furthermore, a FEM analysis was carried out in the following chapter to test the reeds from a structural point of view.
While the equations modelling the behaviour of the reed valve from a structural point of view have been described in this chapter, no information concerning the fluid-dynamic nature of the valve is to be found in the literature.
This necessitated a CFD analysis of the valve in order to observe how the fluid-dynamic variables (pressure, density and velocity) of the air change for the passage through the valve and to extrapolate some semi-experimental coefficients to refine the Simscape model.

Below the 2D drawings of the valve components listed in Tab. 5.2 are shown

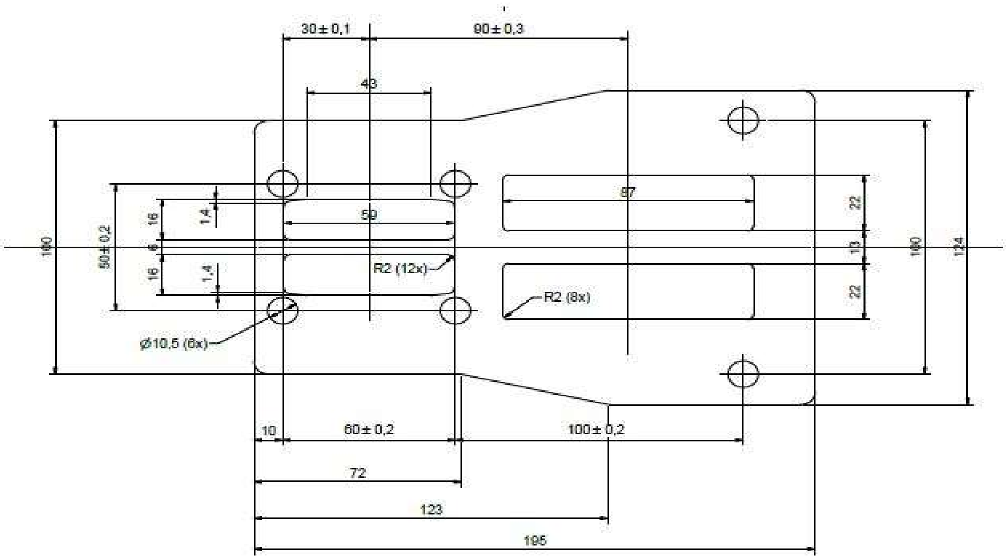

Figure 5.5 Valve Gasket

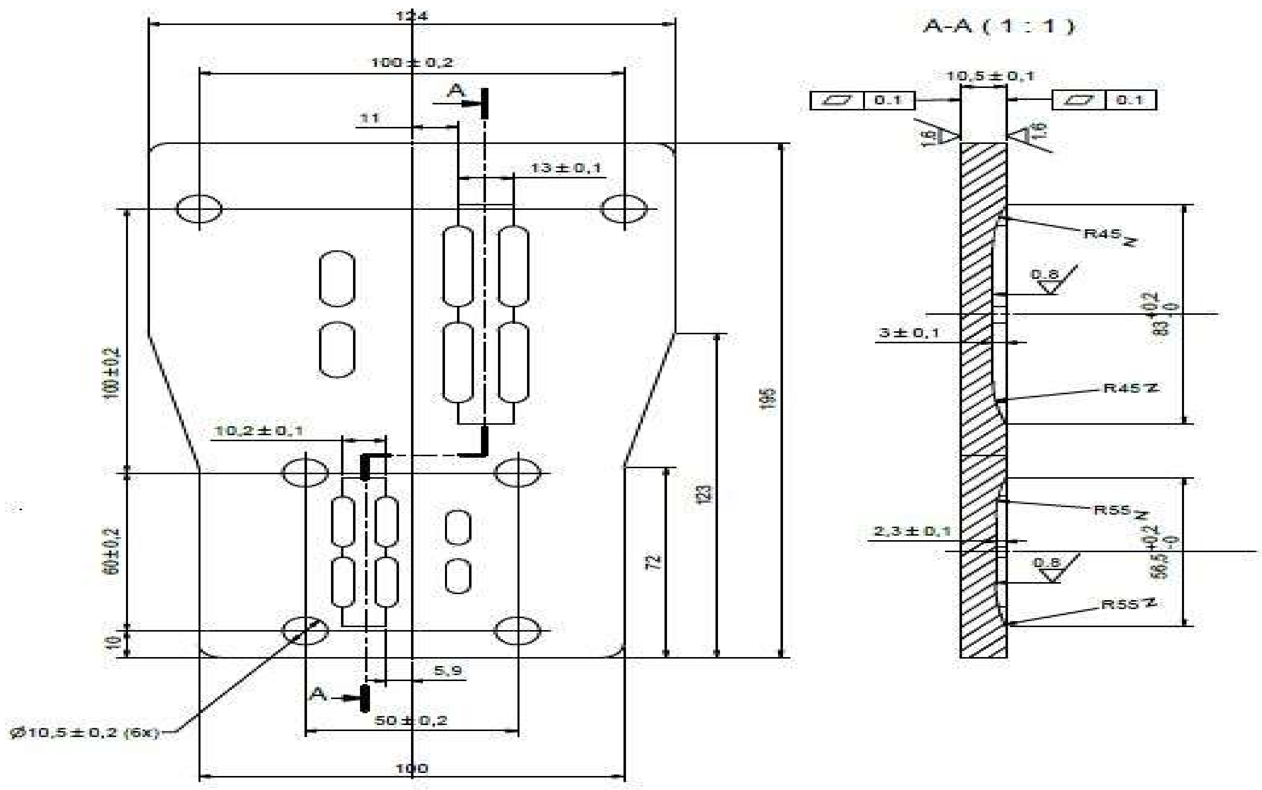

Figure 5.6 Valve Plate

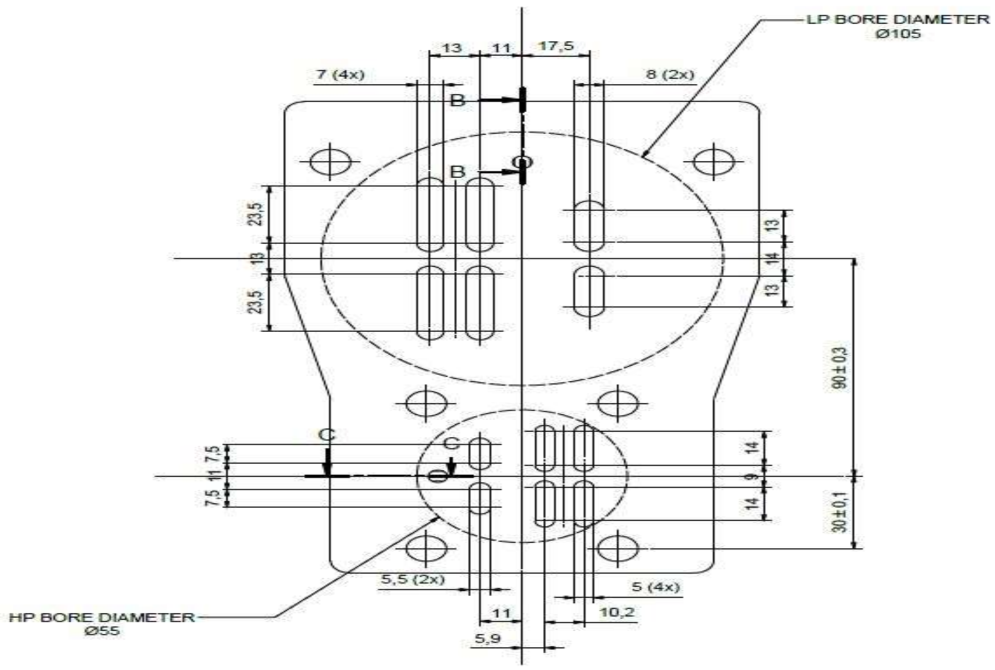

Figure 5.7 Valve Plate (Cylinder view)

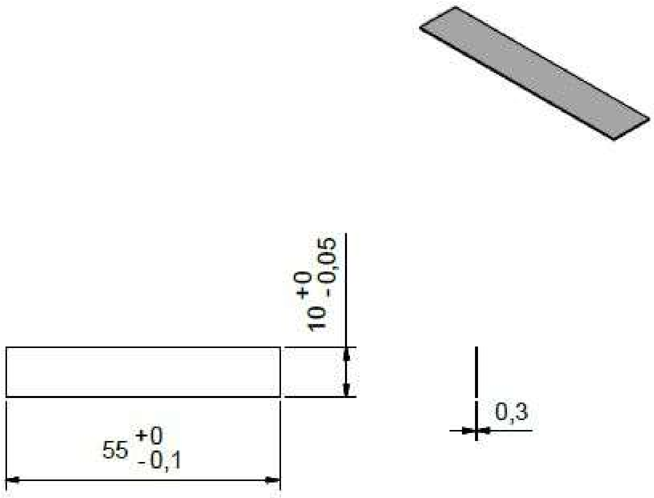

Figure 5.8 2nd stage Reed

6 CFD Analysis

6.1 Introduction

The behaviour of a flowing fluid, whether compressible or incompressible, is described by fluid dynamics, which involves the computation of various physical parameters that characterize the fluid's state.

These values must be connected to the fluid's motion and can be scalars (such as pressure, temperature, and density), vectors (such as velocity and volume forces), or tensors (such as viscous stresses).

Conservation rules are derived from physics and apply to several physical quantities connected to fluids: they declare that the fluctuation of the total amount of certain quantities inside a specific domain is equal to the balance of that quantity entering and exiting in the domain under consideration, plus the contribution from potential sources generating that amount.

Some flow quantities, such as mass, momentum, and energy, do not obey a conservation law. The combination of these three equations is sufficient to completely solve incompressible flows owing to constant density, whereas for compressible flows dissipations due to the viscous stresses impact density, a set of equations must be solved, including an equation of state and a viscosity formulation. All equations and mathematical discussion are taken from [19] [20] [21].

The governing equations of fluid flow are mathematical formulations of physics' conservation laws:

• A fluid's mass is preserved.

• Newton's second law states that the rate of change of momentum equals the total of the forces acting on a fluid particle.

• The rate of energy change is equal to the total of the rates of heat added to and work done on a fluid particle (first law of thermodynamics).

The fluid will be considered a continuum. The molecular structure of materials and molecular movements can be neglected while analysing fluid flow at macroscopic length .We characterize the fluid's behaviour using macroscopic characteristics such as velocity, pressure, density, and temperature, as well as their space and time derivatives. The smallest feasible element of fluid whose macroscopic characteristics are not impacted by individual molecules is a fluid particle or point in a fluid.

We examine a tiny fluid element with sides x, y, and z shown in Fig. 6.1. The first step in developing the mass conservation equation is to create a mass balance for the fluid element for each face. This yields to the following formula:

$$\frac{\partial \rho}{\partial t} + \frac{\partial(\rho u)}{\partial x} + \frac{\partial(\rho v)}{\partial y} + \frac{\partial(\rho w)}{\partial z} = 0$$

Or in a more compact form it can be written as :

$$\frac{\partial \rho}{\partial t} + \mathrm{div}(\rho \mathbf{u}) = 0$$

Equation is the unsteady, three-dimensional mass conservation or continuity equation at a point in a compressible fluid.

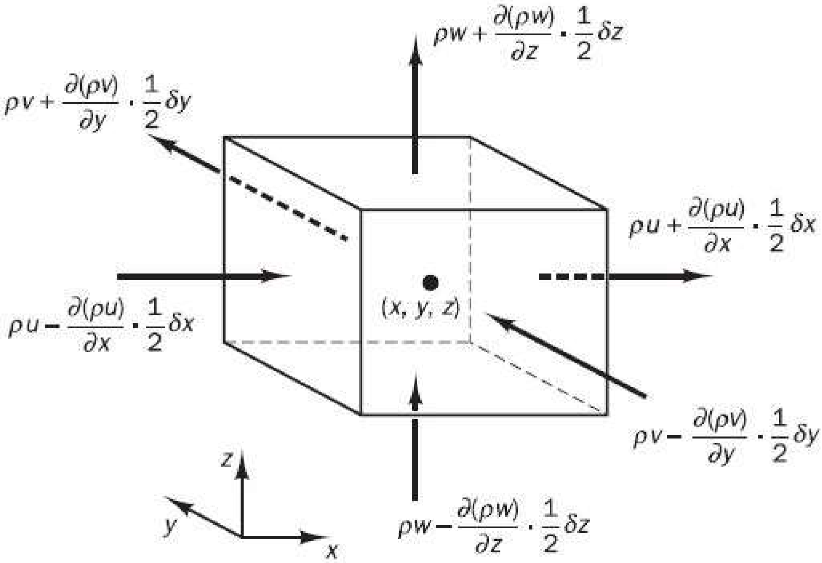

Figure 6.1 Infinitesimal Fluid Element

The momentum equation correlates to Newton's second rule of motion, which states that the forces exerted on an object are proportional to its acceleration multiplied by its mass.

External volume forces (such as gravity or applied forces) and internal forces both contribute to the source terms in this scenario (stress). The momentum conservation equation has the following integral formulation:

$$\frac{\partial}{\partial t}\int_{\Omega} \rho\vec{U}d\Omega + \oint_{S} (\rho\vec{U})\vec{U} \cdot d\vec{S} = \int_{\Omega} \vec{f}_e d\Omega + \oint_{S} \bar{\bar{\sigma}} \cdot d\vec{S}$$

Where $\overrightarrow{f_e}$ accounts for external volume forces and expresses stress, which indicates a fluid's internal deformability. Stress $\vec{\sigma}$ may be split into an isotropic component (pressure) and a viscous shear stress tensor that describes the internal friction force of fluid layers against each other, assuming the fluid is Newtonian.

$$\bar{\bar{\sigma}} = -p\bar{\bar{I}} + \bar{\bar{\tau}}$$

Using Newton's rule for viscous fluids, the viscous shear stress tensor may therefore be represented in terms of flow velocity:

$$\bar{\bar{\tau}} = 2\mu\bar{\bar{D}} - \frac{2}{3}\mu\nabla(\vec{\nabla}\cdot\vec{U})$$

$$\bar{\bar{D}} = \frac{1}{2}(\nabla\vec{U}^T + \nabla\vec{U})$$

Where μ is the dynamic viscosity and $\overline{\overline{D}}$ is the strain rate tensor.

Substituting these terms into the equation results in the following formulation

$$\frac{\partial(\rho\vec{U})}{\partial t} + \vec{\nabla}\cdot\left(\rho\vec{U} * \vec{U}\right) = \rho\vec{g} - \nabla p + \mu\nabla^2\vec{U} + \frac{1}{3}\mu\nabla(\vec{\nabla}\cdot\vec{U})$$

According to the energy equation, total energy e_t, defined as the sum of fluid internal energy plus kinetic energy per unit mass, conserves. In this case, the equation includes both conductive and diffusive fluxes, while the volume source terms are the work of the volume forces f_e and the heat sources q_h, and the surface sources are the result of the work done on the fluid by the internal shear stress acting on the surface of the control volume. The integral version of the energy equation using these premises is:

$$\frac{\partial}{\partial t}\int_\Omega \rho e_t d\Omega + \oint_S \rho e_t\vec{U}\cdot d\vec{S} = \oint_S k\vec{\nabla}\mathrm{T}\cdot d\vec{S} + \int_\Omega \left(\rho\vec{f_e}\cdot\vec{U} + q_H\right)d\Omega + \oint_S \left(\bar{\bar{\sigma}}\cdot\vec{U}\right)\cdot d\vec{S}$$

where *k* is the thermal conductivity of the fluid.

One of the most crucial in CFD study phase is the discretization of the domain, which results in the generation of the computation grid and equations via the formulation of the numerical method used. During the discretization process, geometrical and mathematical models are converted into numbers. The computation grid (or mesh) is generated via domain discretization, which replaces the continuity of actual space with a set of points or components.

The goal of equation discretization is to convert all mathematical operators into arithmetic operations on the values of the mesh points. It is possible to execute it using the finite difference technique or the finite volume method.

The software used in this study was Ansys Fluent which is based in finite volume method which is described below.

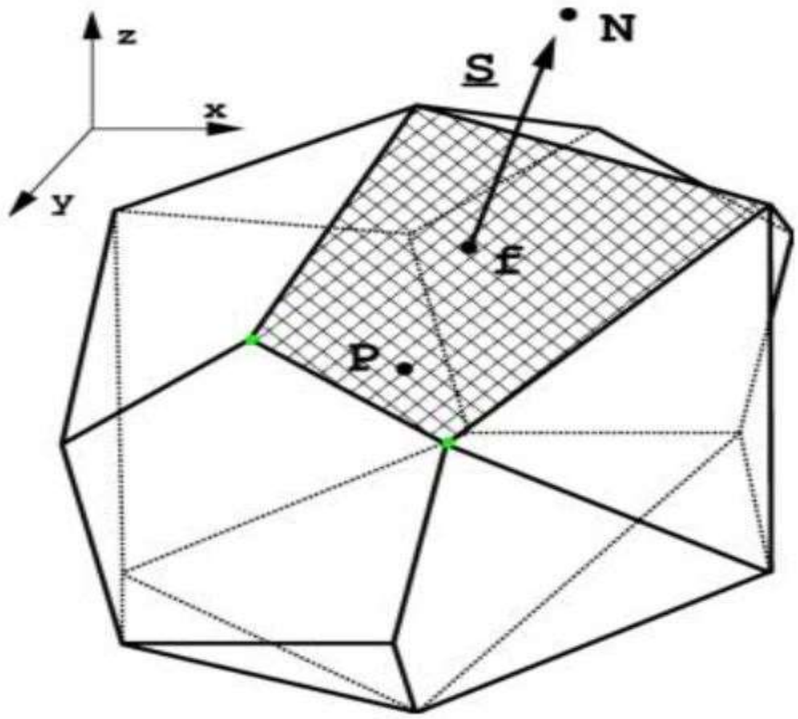

Figure 6.2 Finite Volume Method

The whole domain is split into cells in finite volume discretization (Fig.6.2), with each cell sharing an internal face with a neighbour cell. The values of the fields are kept in the centroid of each cell, denoted by N, whereas P signifies the centroid of the adjoining cell.

The discretisation of the domain under study is called Meshing. The precision and stability of the numerical calculation are greatly influenced by the mesh quality.

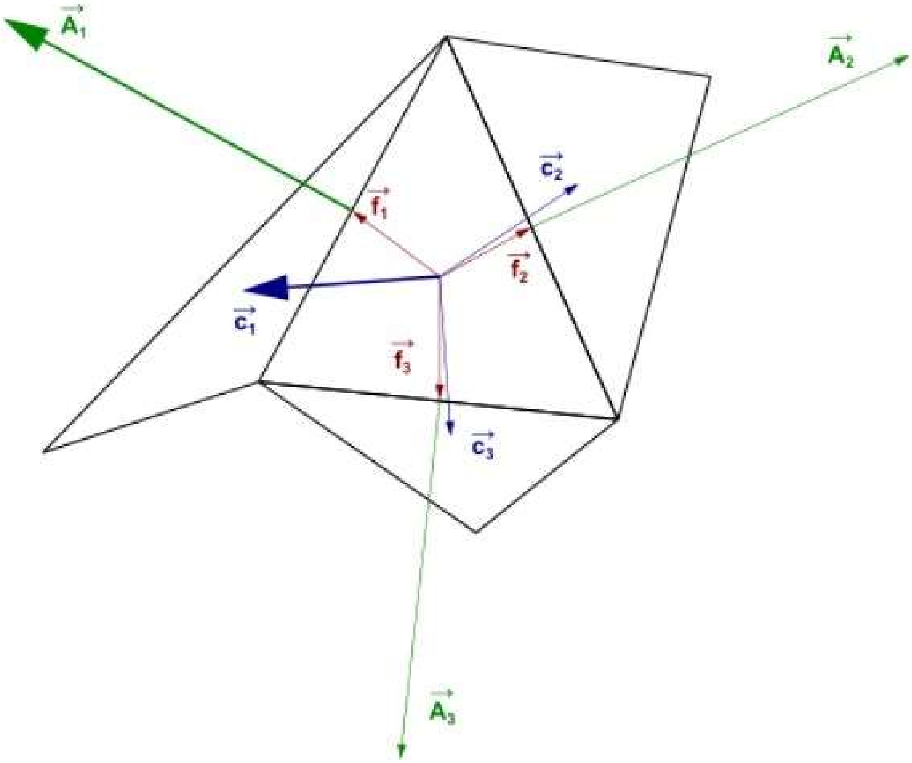

Figure 6.3 Orthogonal quality

The orthogonal quality is an essential measure of mesh quality that ANSYS Fluent allows you to examine.

Another important parameter for the mesh accuracy is the Skewness.

Skewness is a measure of the grid's distortion. It is determined as the distance between the face centre and the face intersection point of the vector linking the centroids of surrounding cells, normalised by their distance. High skewness values reduce the inaccuracy for the convection terms.

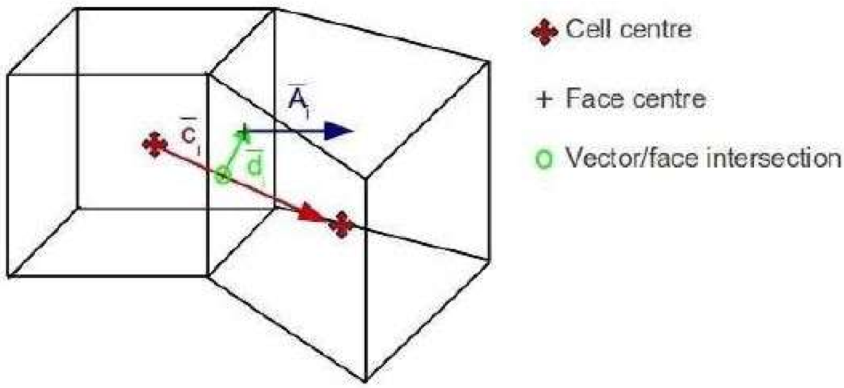

Figure 6,4 Face area vector and cell centroid vector

The recommended values of these two parameters are summarised in the following table, which was used as a reference for the meshing procedure in Ansys Fluent software.

Skewness mesh metrics spectrum

Excellent	Very good	Good	Acceptable	Bad	Unacceptable
0-0.25	0.25-0.50	0.50-0.80	0.80-0.94	0.95-0.97	0.98-1.00

Orthogonal Quality mesh metrics spectrum

Unacceptable	Bad	Acceptable	Good	Very good	Excellent
0-0.001	0.001-0.14	0.15-0.20	0.20-0.69	0.70-0.95	0.95-1.00

Table 6.1 Table for orthogonal and skewness quality

6.2 Valve study

The main components of the case study valve are described in the previous chapter and a 3D view of it is shown below.

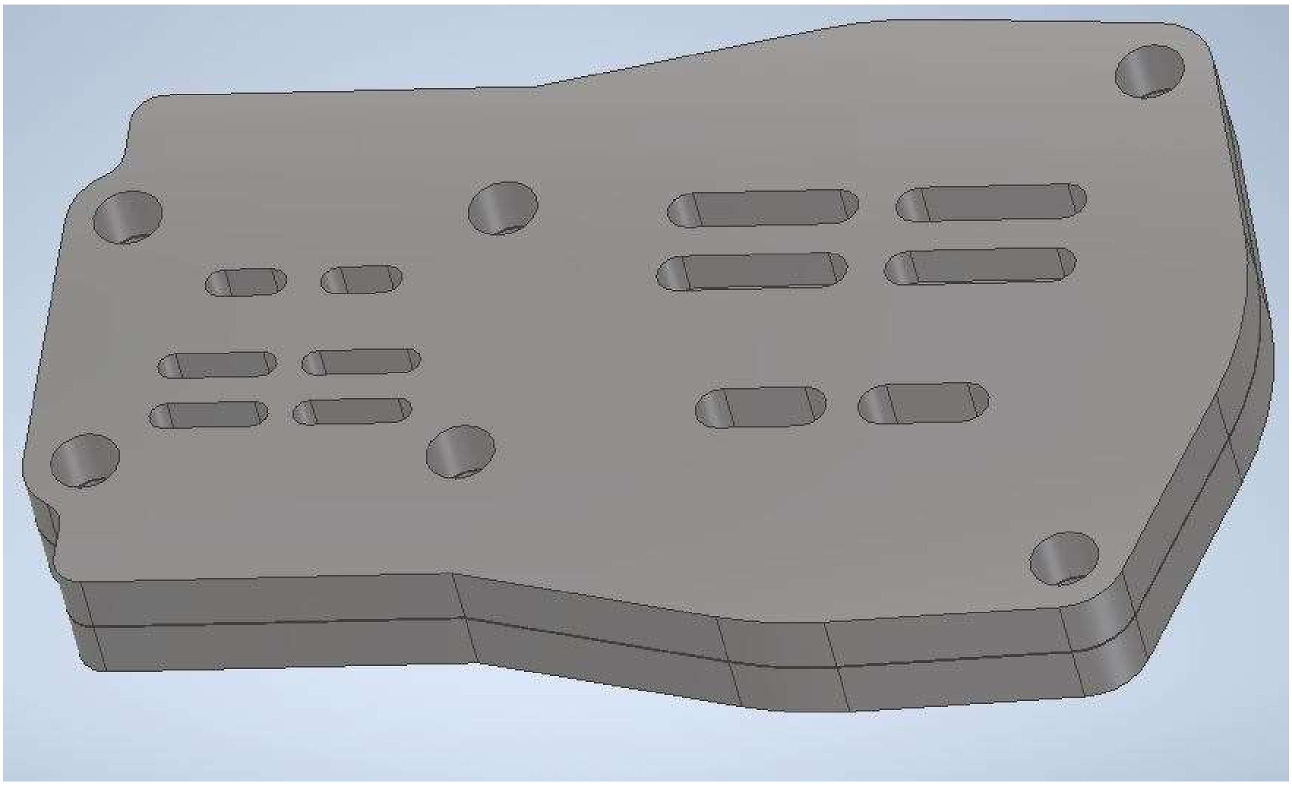

Figure 6.5 3D view of the valve under study

Since the action of the fluid passing through the valve channels causes the deformation of the reed, which in turn allows the passage of air from the intake chamber to the cylinder (in the case of the intake valve), a study is required in two different physical domains: structural and fluid. In order to link these two domains of a different nature, there are various procedures in the literature which are applicable within Ansys based on fluid-structure interaction (FSI). This interaction can be modelled with the following procedures:

The FSI technique described above is very computationally expensive, as FSI requires a transient study. In [22] [23] [24] [25], another procedure named "sequential one-way coupled FSI procedure" is described in order to be able to analyse fluid domain quantities as a function of reed deformation with a certain degree of accuracy. In the cited documents, the time variable is not taken into account, so the movement of the fluid in a steady state is considered.
In order to be able to export the deformed reed to Ansys Fluent, as shown in Fig.8a and Fig.8b, and study how it affects the velocity and pressure profiles, it is first necessary to carry out a structural FEM (finite element analysis) with the assumption that the pressure acting on the reed is homogeneously distributed, an assumption that will later be disproved by showing the pressure profile acting on the surface of the reed.

This assumption is very conservative from a design point of view, but is able to provide indications on the sizing of the Reed from a structural point of view.
Since the fluid domain is very complex, it is not possible to perform a 2d analysis, but at the same time representing the results of the analysis in 3d form is not easy to read. For this reason, as done in [22] and [25] all results are shown by dissecting the fluid domain according to two planes as in Fig.6.7a and Fig. 6.7b.

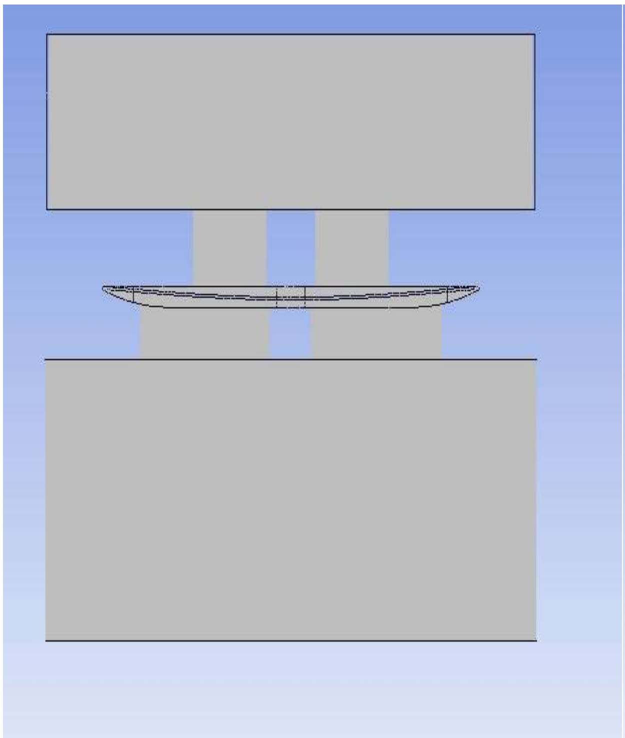

Figure 6..6 a Fluid Domain Section ZX

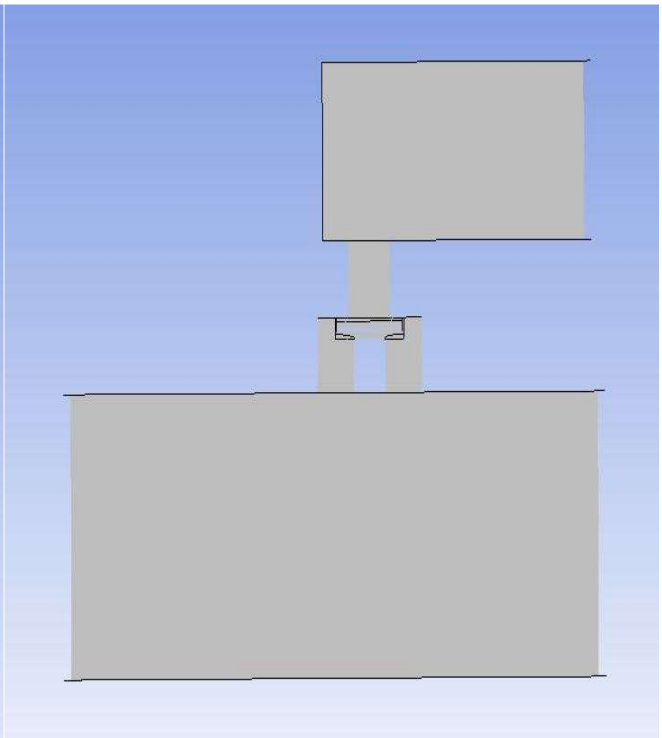

Fig. 6.6b Fluid Domain Section ZY

6.3 FEM analysis

In the structural environment of the Ansys software, the first step is to choose the material to be assigned to the components. For the reed, 'mild steel' was chosen as the material, the structural characteristics of which are summarised in Fig.6.7.

Once the materials have been assigned, we proceed to mesh generation, focusing mainly on the reed mesh and the plate hollow mesh(Fig.6.8a, 6.8b), which allows the deformation of the reed itself. The generation of the mesh of these two components, visible in Fig. 6.8a and Fig.6.8b, is fundamental in order to have a high accuracy of the calculations.

Structural	
Isotropic Elasticity	
Derive from	Young's Modulus and Poisson's Ratio
Young's Modulus	2,2e+05 MPa
Poisson's Ratio	0,27500
Bulk Modulus	1,6296e+05 MPa
Shear Modulus	86275 MPa
Isotropic Secant Coefficient of Thermal Expansion	12,000 1/°C
Tensile Ultimate Strength	345,00 MPa
Tensile Yield Strength	207,00 MPa

Figure 6.7 Reed Structural Data

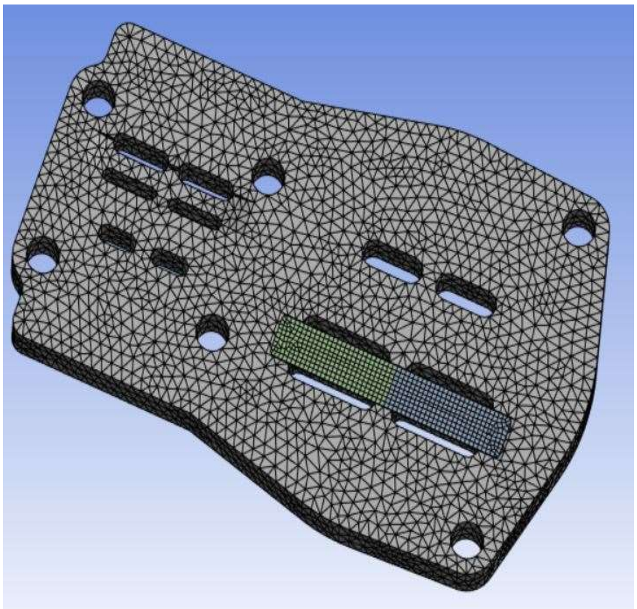

Figure 6.8a Valve Plate Mesh

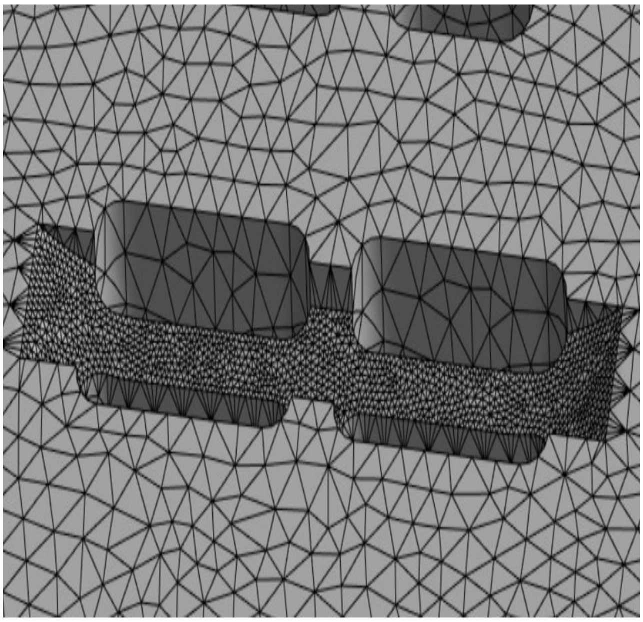

Fig.6.8b Detail of Valve plate hollow

In order to achieve a high degree of accuracy in the calculations, the structural study was carried out on the valve assembly rather than on a single part, which is why it is necessary to introduce certain constraints in the study to limit the deformation of the reed and certain contact constraints summarised in the table Fig.6.9 whose physical meaning can be consulted in [26].

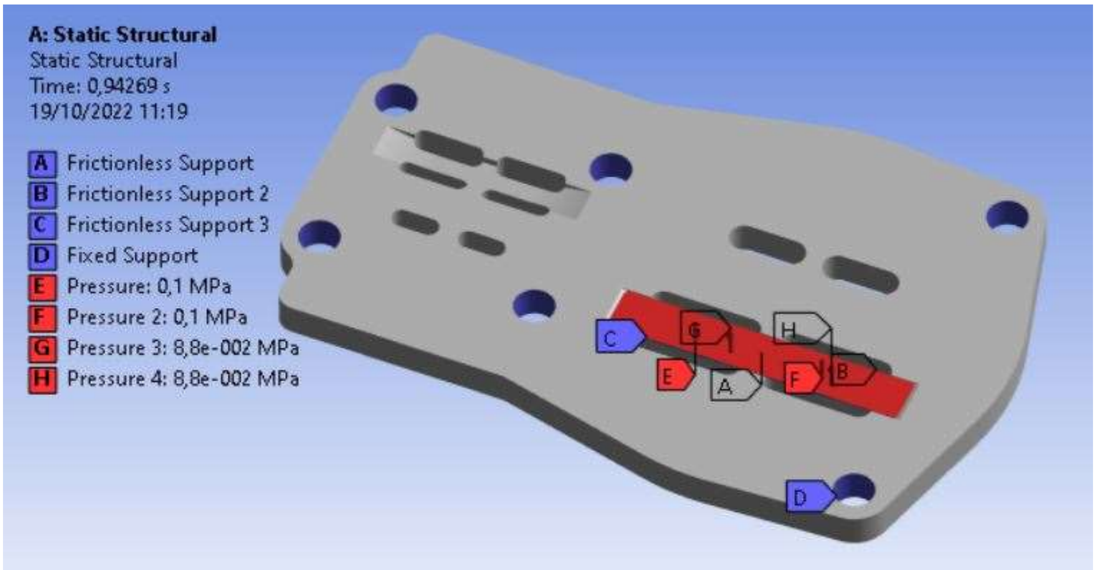

Figure 6.9 Boundary conditions in Ansys Mechanical

Contact type	**Conctat Bodies**	**Target Bodies**
No Separation	Reed	Plate Hollow Support
No Separation	Reed	Plate Hollow Support
Frictionless	Reed	Plate Hollow

Table 6.2 Contact List

After defining the constraints and the type of contact, it is possible to carry out the FEM analysis, shown in the images below.
In the suction and delivery valves of the first stage, the maximum possible lift is 2.6 mm, while for those of the second stage, the maximum possible lift has been reduced to 2 mm.
The reason for this choice comes from the fact that the pressures involved in the compressor's second stage are higher than in the first one, and during the initial stages of dimensioning and calculation of the quantities (pressure, velocity), it was noted that, with the same maximum lift, the impact velocities of the second stage reed on the plate were excessively high, which could lead to reed failure due to impact fatigue, a subject which will not be mentioned in this work.
Since both the structural analysis and the fluid-dynamic analysis, as mentioned above, are conducted from a static and a steady-state point of view respectively, it is necessary to discretise the movement of the valve in different lifts.

6.3.1 FEM Fist stage suction valve

The first stage's Reed movement inside the hollow was discretized in the following way:

- 2,6 mm
- 2,1 mm
- 1,57 mm
- 1 mm
- 0,45 mm
- 0,16 mm

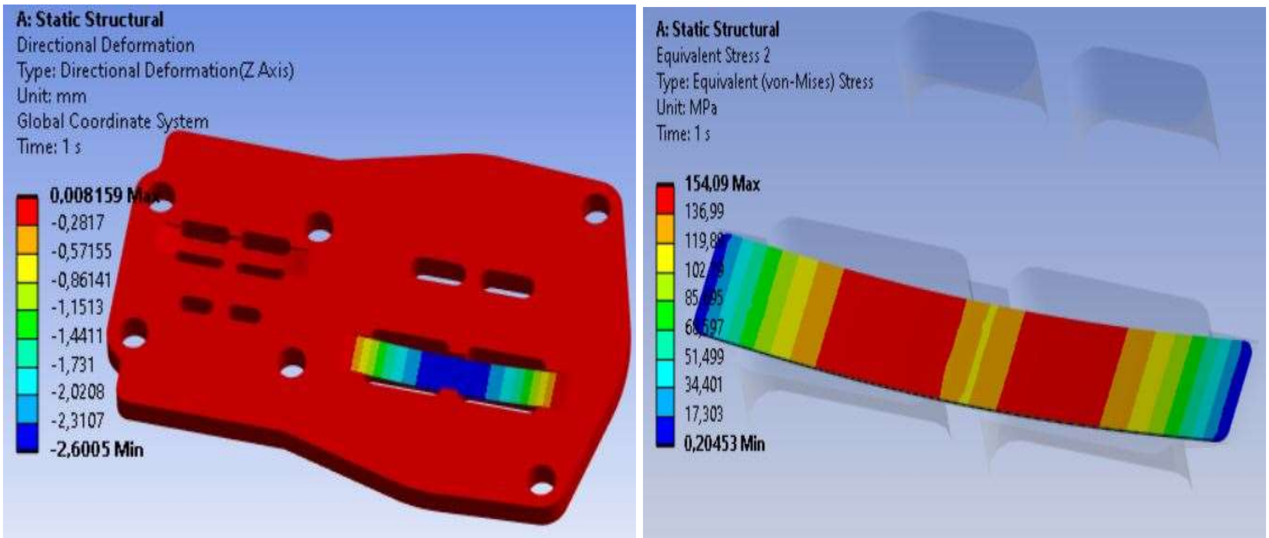

Figure 6.10 Stress and deformation of the Reed @2,6 mm

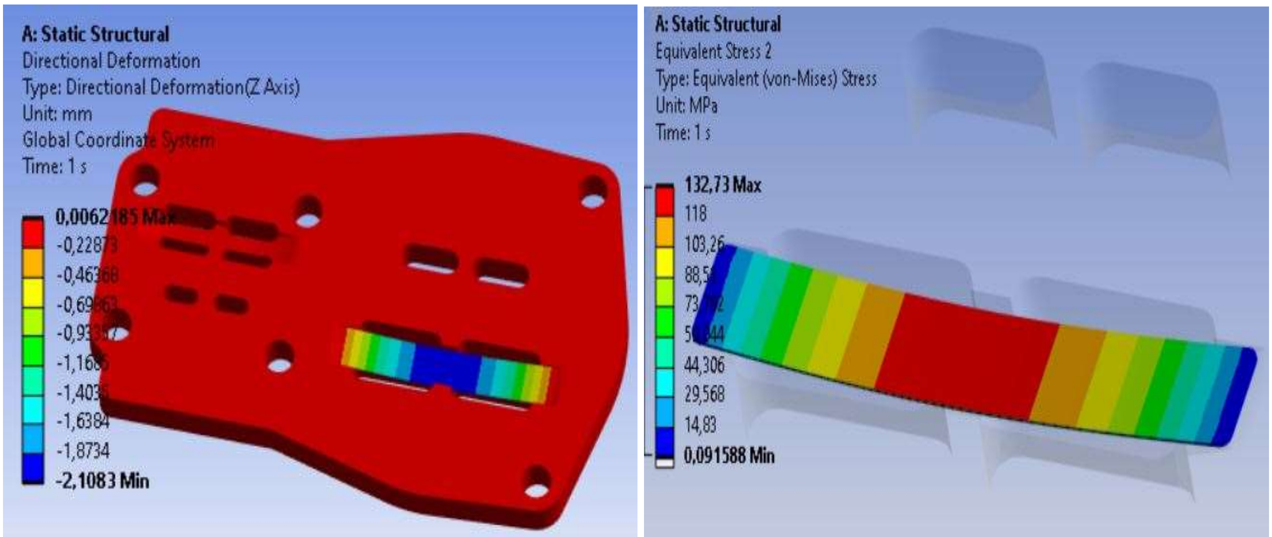

Figure 6. 11 Stress and deformation of the Reed @2,1 mm

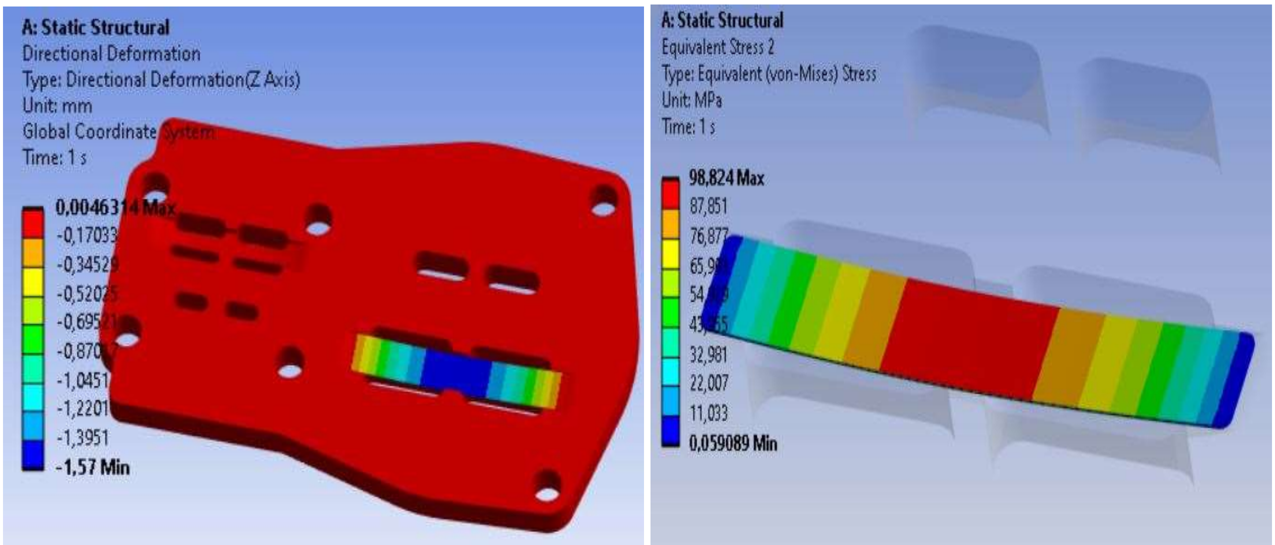

Figure 6.12 Stress and deformation of the Reed @1,6 mm

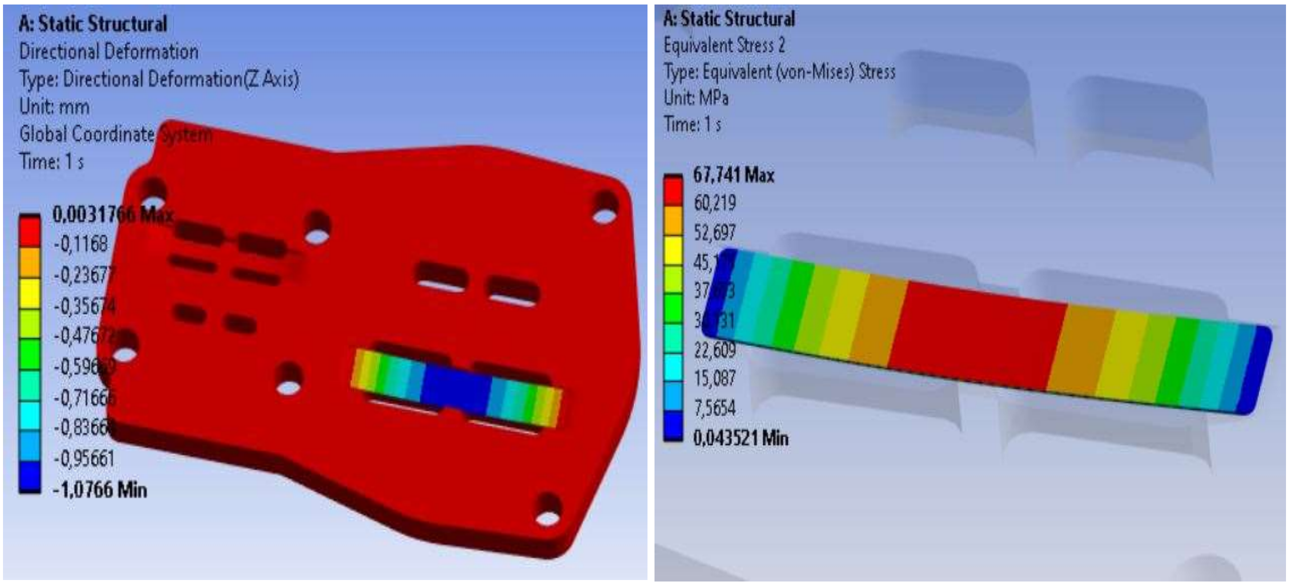

Figure 6.13 Stress and deformation of the Reed @1 mm

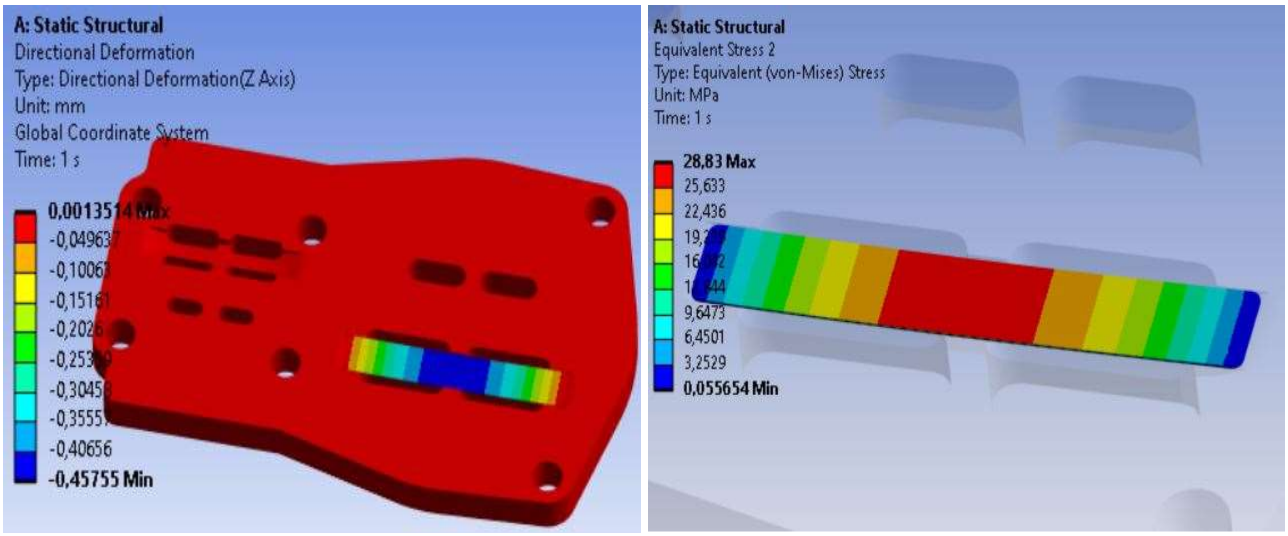

Figure 6.14 Stress and deformation of the Reed @0,45 mm

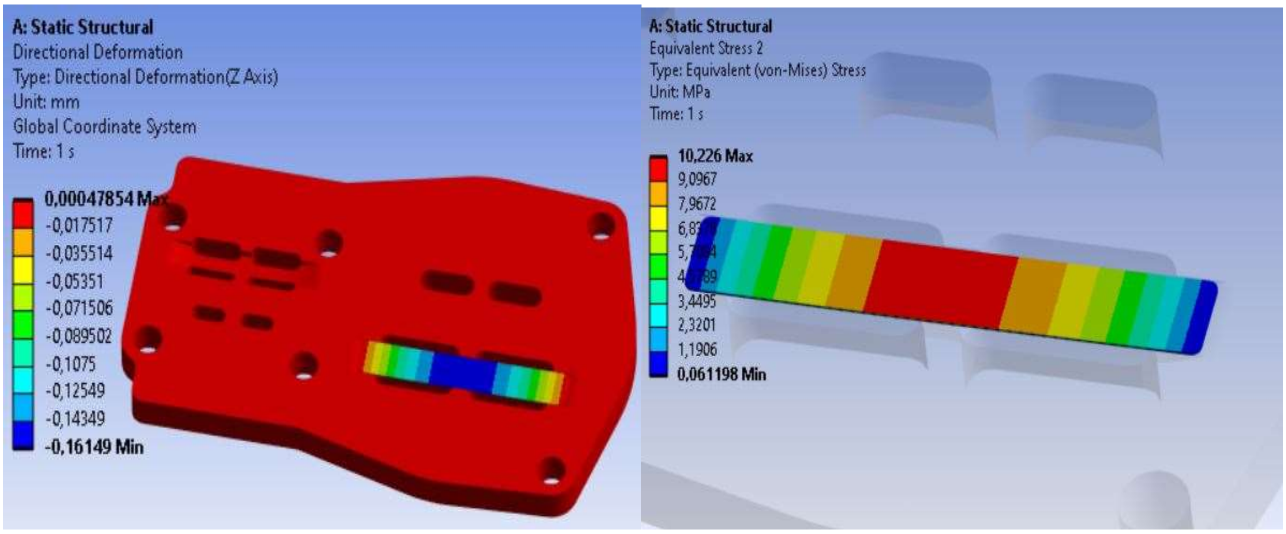

Figure 6.15 Stress and deformation of the Reed @0,16 mm

6.3.2 FEM Second stage Discharge valve

The second stage's Reed movement was discretized in the following way:

- 2 mm
- 1,6 mm
- 1 mm
- 0,6 mm
- 0,16 mm

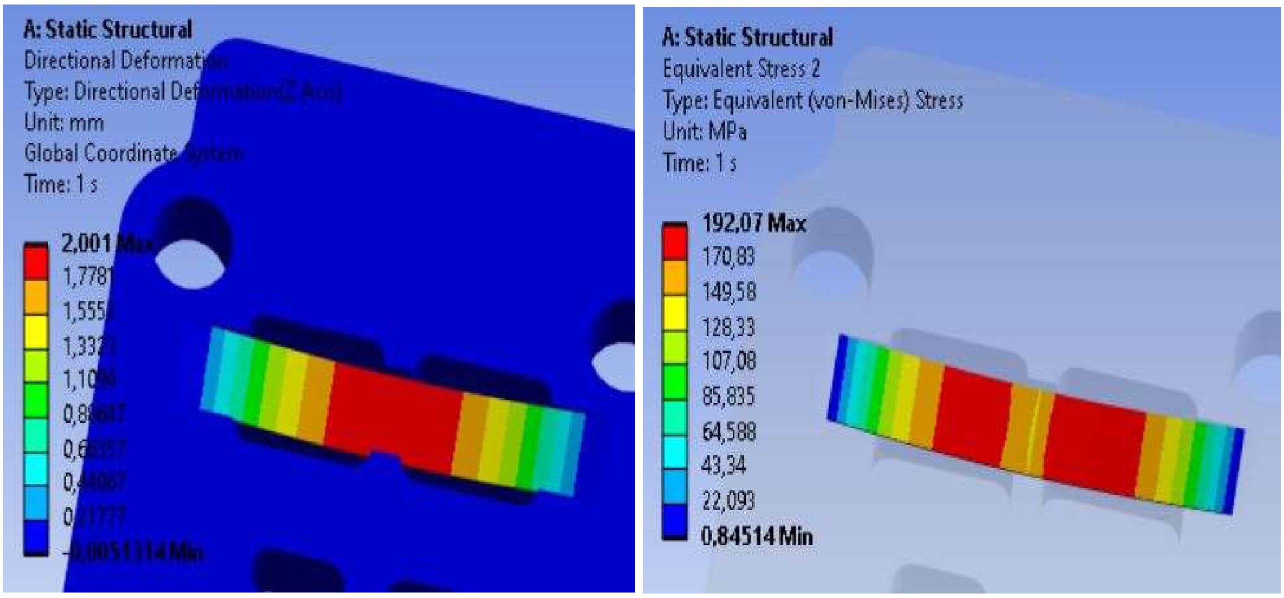

Figure 6.16 Stress and deformation of the Reed @2 mm

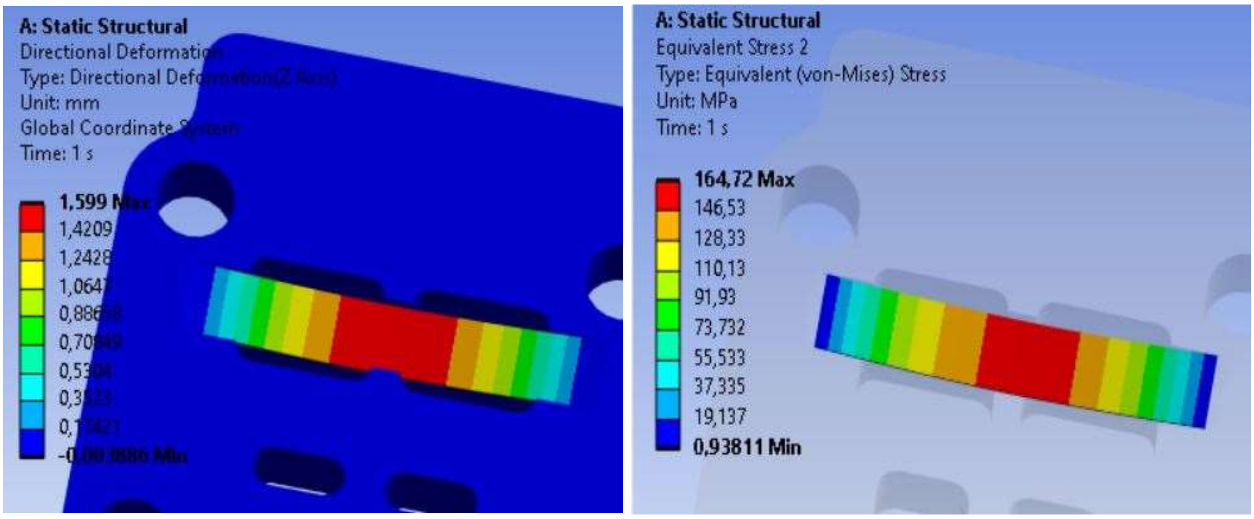

Figure 6. 17 Stress and deformation of the Reed @1,6 mm

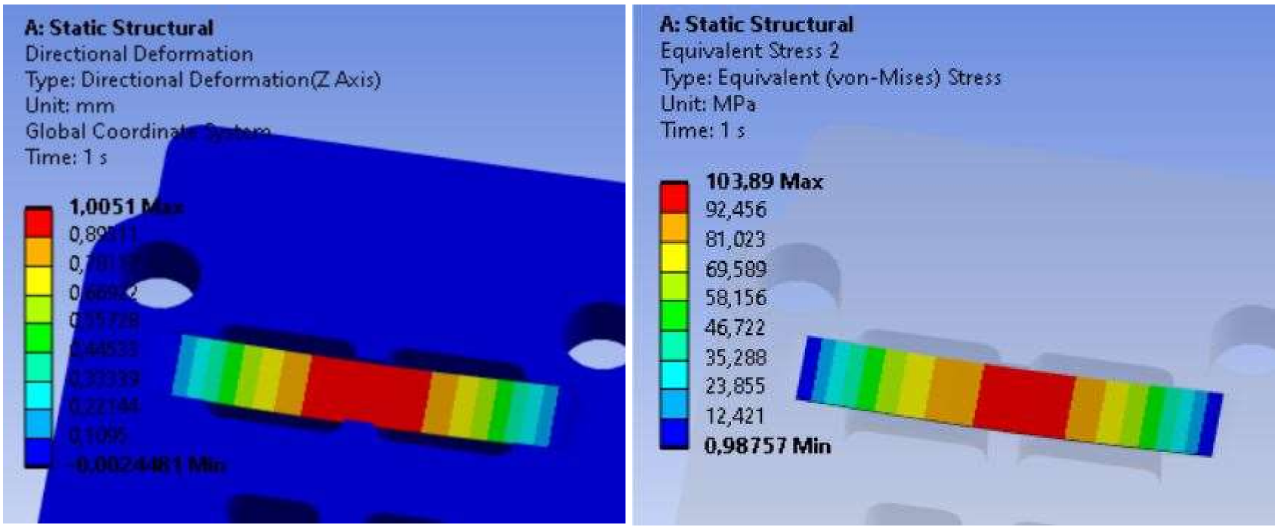

Figure 6.18 Stress and deformation of the Reed @1 mm

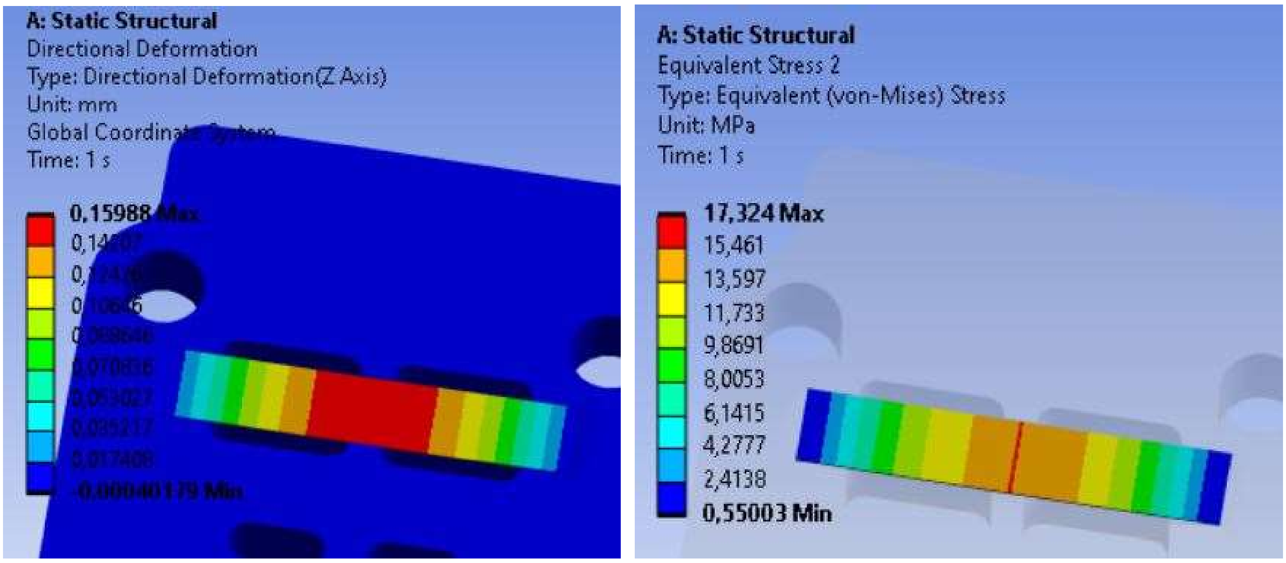

Figure 6.19 Stress and deformation of the Reed @0,16 mm

6.4 CFD study

6.4.1 Fluid domain creation

Starting from the valve assembly, visible in Fig.6.5 , it is possible to create the volume that the air will pass through. In this CFD analysis, only the fluid domain will be analysed, while the solid part of the valve will not be considered. Consequently, the heat exchange that takes place between the air and the surrounding material during the suction and delivery phases will also not be considered in this discussion.

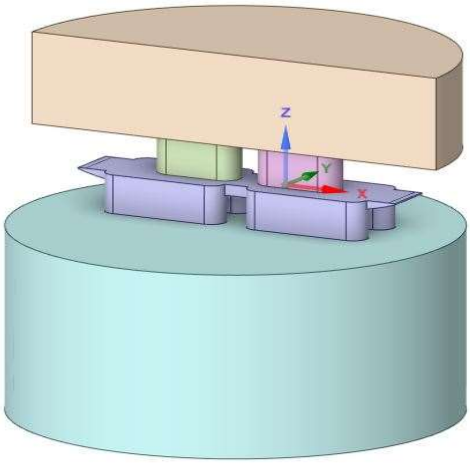

Figure 6.20a 1st stage Suction valve Fluid Domain

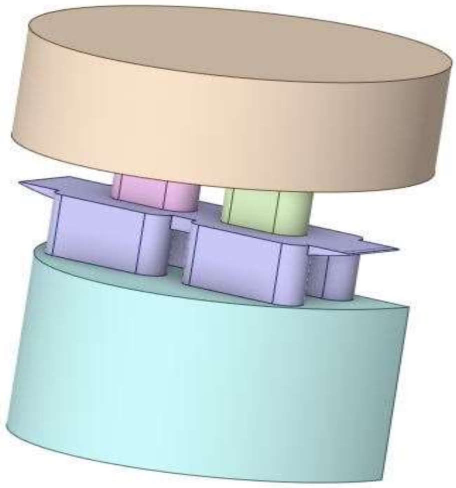

Fig. 6.20b 2nd Discharge valve Fluid Domain

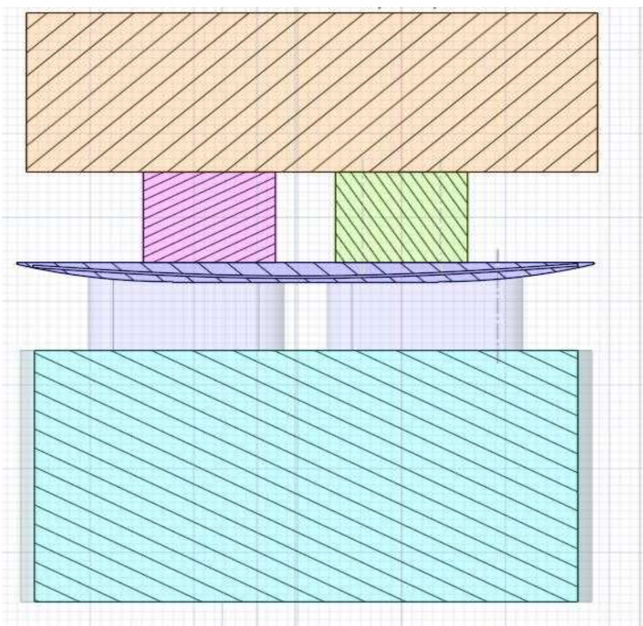

Figure 6.21a Fluid domain Section ZX

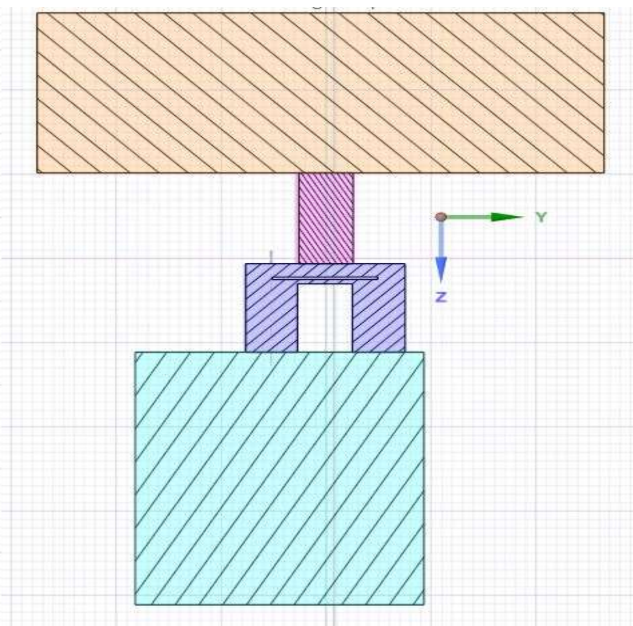

Fig. 6.21b Fluid domain Section ZY

In order to optimally generate the mesh, the fluid domain is composed of several parts, always starting with the valve geometry and the compressor geometry in general.

The fluid domain is composed as follows:

- Intake or Discharge Chamber
- 2 Ports
- Valve Domain
- Cylinder

one of the first steps in fluid modelling on the Ansys software is to set some physical parameters of the fluid analysed summarised in Tab.6.3

Physical Properties	Value	Unit
Density	Ideal gas [variable]	Kg/m^3
Specific Heat	1006.43 [constant]	[J/(kg K)]
Thermal Conductivity	0,0242 [constant]	[W/(m K)]
Viscosity	1,7894 e-05 [constant]	[kg/(m s)]
Molecular Weight	28,966 [constant]	[kg/kmol]

Table 6.3 Physical Properties of the air

The fluid domain was discretized in order to improve the mesh quality and to make the mesh as fine as possible in those sections where the characteristic dimensions could have influenced the physical quantities of air.

Elements	497672
Nodes	113457

Table 6.4 Meshing Characteristics

This mesh resulted in the orthogonal quality and asymmetry values shown in Fig.6.15a and Fig.6.15b which according to the reference values shown above in Tab.6.1 are quite acceptable.

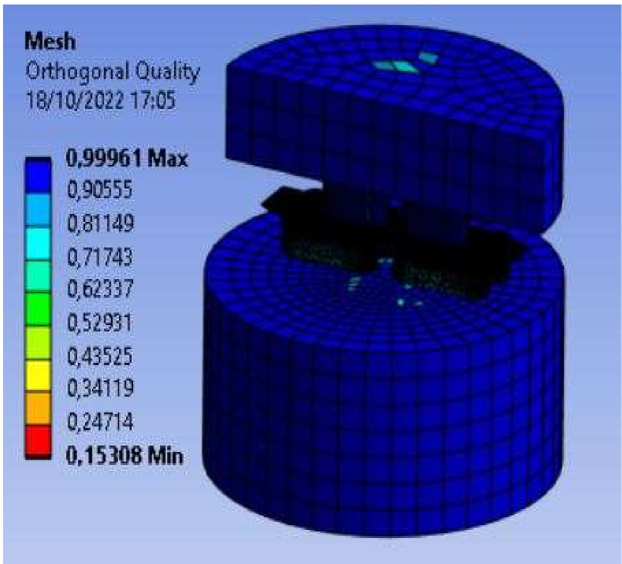

Figure 6.22a Orthogonal quality Fluid Domain

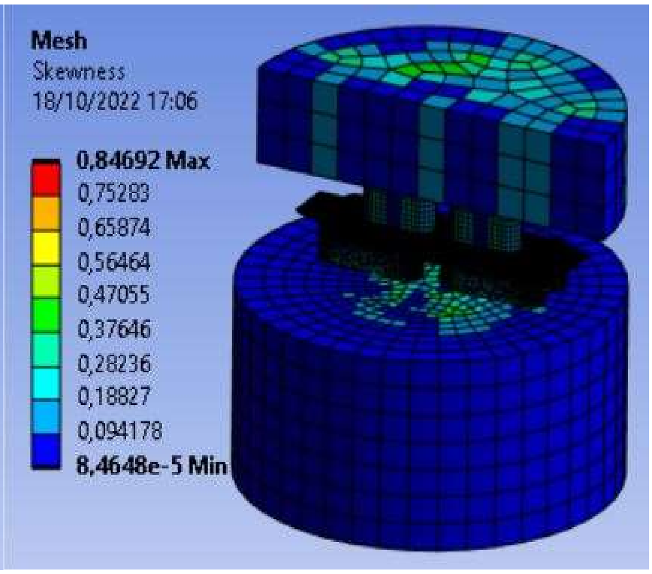

Fig. 6.22b Skewness Fluid Domain

6.4.2 CFD Boundary Conditions

There is a standard set of boundary conditions for compressible flows that are widely utilised in internal flows studies [27] [24] [25] :

- Upstream Total pressure, total temperature
- Downstream Static pressure

To achieve robustness in incompressible cases, it is common practise to couple upstream total pressure and total temperature and downstream mass flow rate, but this approach is impractical for compressible flows where chocking can occur and limit the delivered mass flow, resulting in failed convergence. On the contrary, the previously indicated combination of boundary conditions ensures that the issue is well-posed even if it chocks.

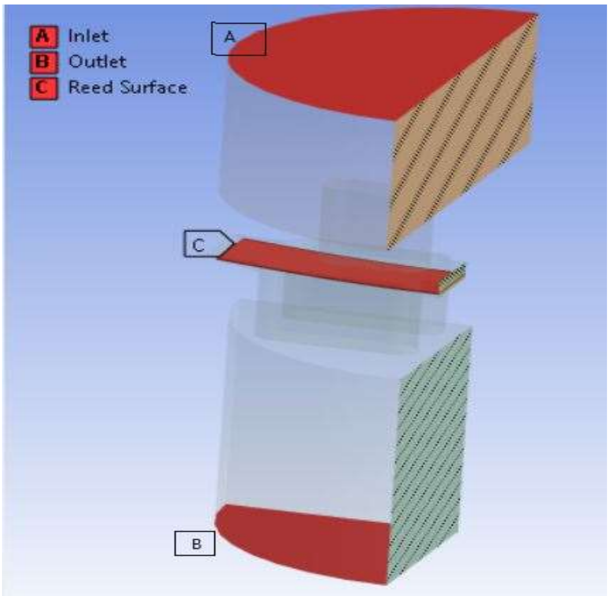

Figure 6.23 Named Selection

In order to set the boundary conditions, it is first necessary to set the 'named selections' during the meshing generation phase.

The named selections, visible in Fig.6.23, also include the deformed reed, which will be useful later in order to calculate the drag coefficient during iterations.

The pressure and temperature values required, visible in Tab.6.5 and Tab.6.6 , to calculate the pressure and velocity Contour were initially taken from the Simscape model of the compressor, then the coefficients extrapolated from the CFD analysis were applied to the Simscape model, which will be described in the following chapter, thus creating an iterative procedure until convergence between the two analysis is achieved.

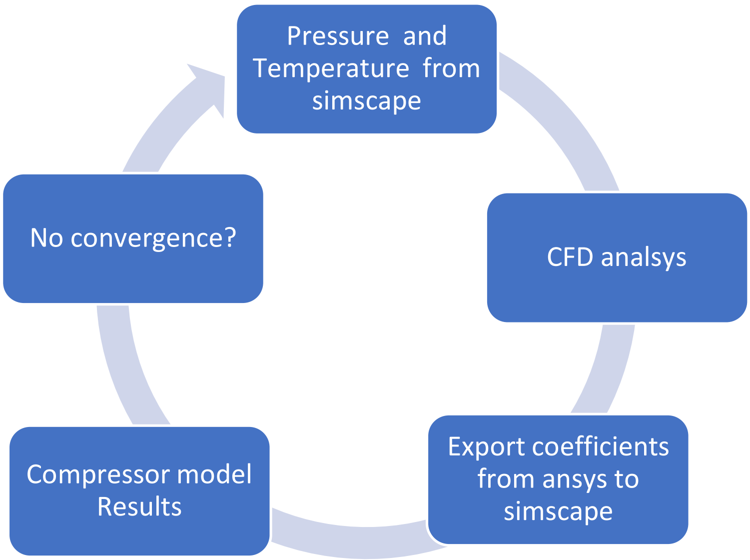

Figure 6.24 Iterative procedure for setting boundary conditions

Lift [mm]	Boundary Conditions	
	Inlet	Outlet
2,6	P_0=1 bara T_0=310 K	P_0=0.87 bara
2,1	P_0=1 bara T_0=310 K	P_0=0.92 bara
1,6	P_0=1 bara T_0=310 K	P_0=0.961 bara
1	P_0=1 bara T_0=310 K	P_0=0.978 bara
0,45	P_0=1 bara T_0=310 K	P_0=0.983 bara
0,16	P_0=1 bara T_0=310 K	P_0=0.996 bara

Table 6.5 Boundary Conditions Suction Valve Table

Lift [mm]	Boundary Conditions	
	Inlet	Outlet
2	P_0=12.32 bara T_0=470 K	P_0=12 bara
1,6	P_0=12.24 bara T_0=469,4 K	P_0=12 bara
1	P_0=12.16 bara T_0=469 K	P_0=12 bara
0,6	P_0=12.11 bara T_0=467,5 K	P_0=12 bara
0,16	P_0=12.06 bara T_0= 467K	P_0=12 bara

Table 6.6 Boundary Conditions Discharge Valve Table

The algorithm used is the Coupled. This approach offers some advantages over the non-coupled or segregated approach. The coupled algorithm solves the momentum and pressure-based continuity equations together. For the CFD simulation, an iteration number was chosen which, on the one hand, did not require a high computational cost and, on the other hand, a number of iterations such that the residuals of physical quantities such as continuity k and w values for modelling turbulence and energy were stabilised. For this analysis it was chosen a number of iterations equal to 600 (Fig.6.25).

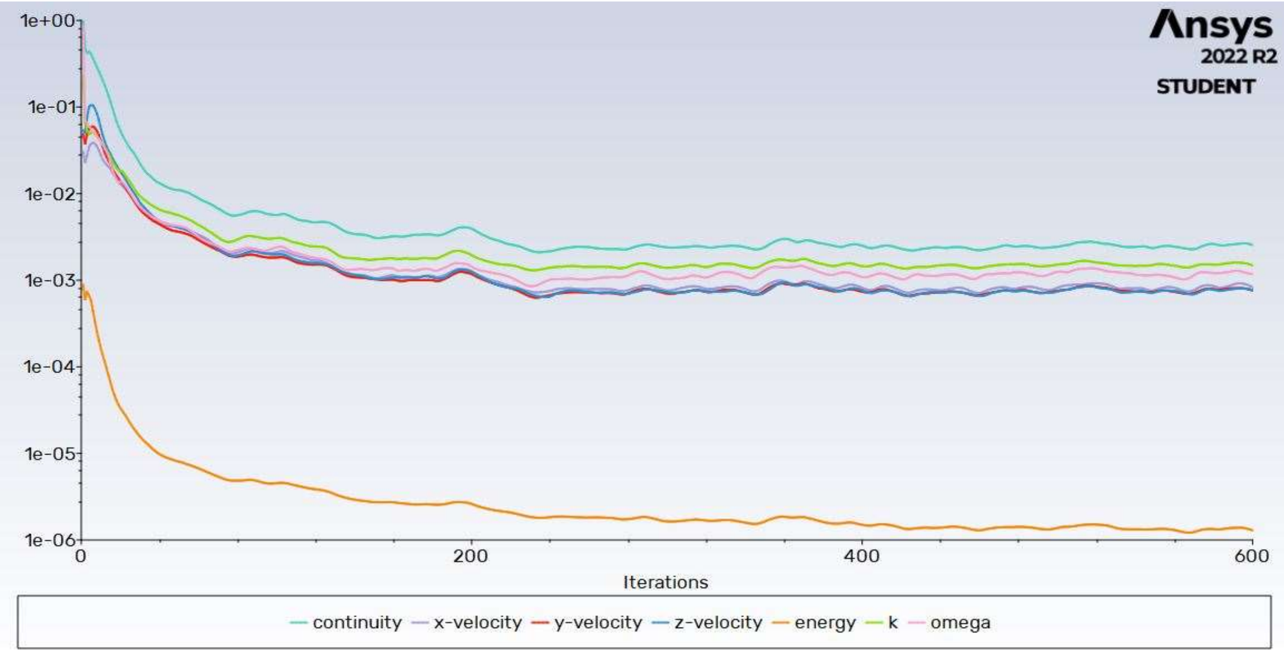

Figure 6.25 CFD Residuals

In the next page some CFD results are shown for both the valves related to a certain reed lifts.

6.4.3 Suction Valve CFD Results

- Lift 2,6 mm

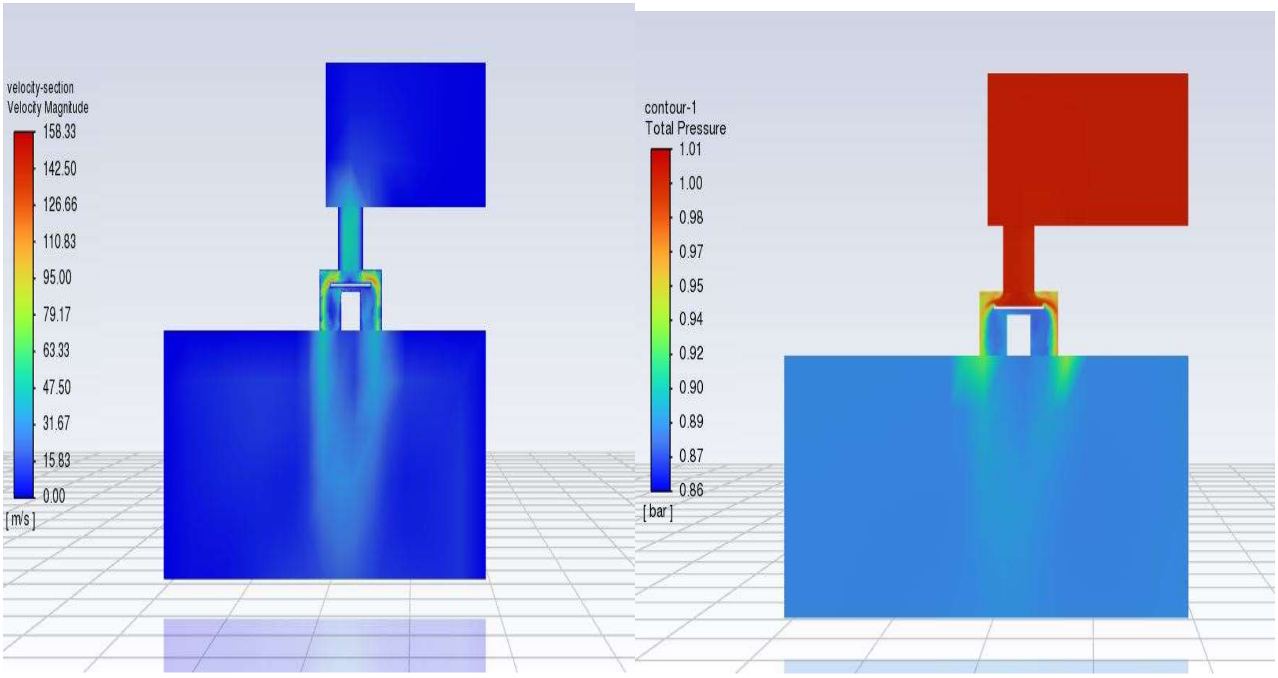

Figure 6,26 Velocity-Pressure Contour

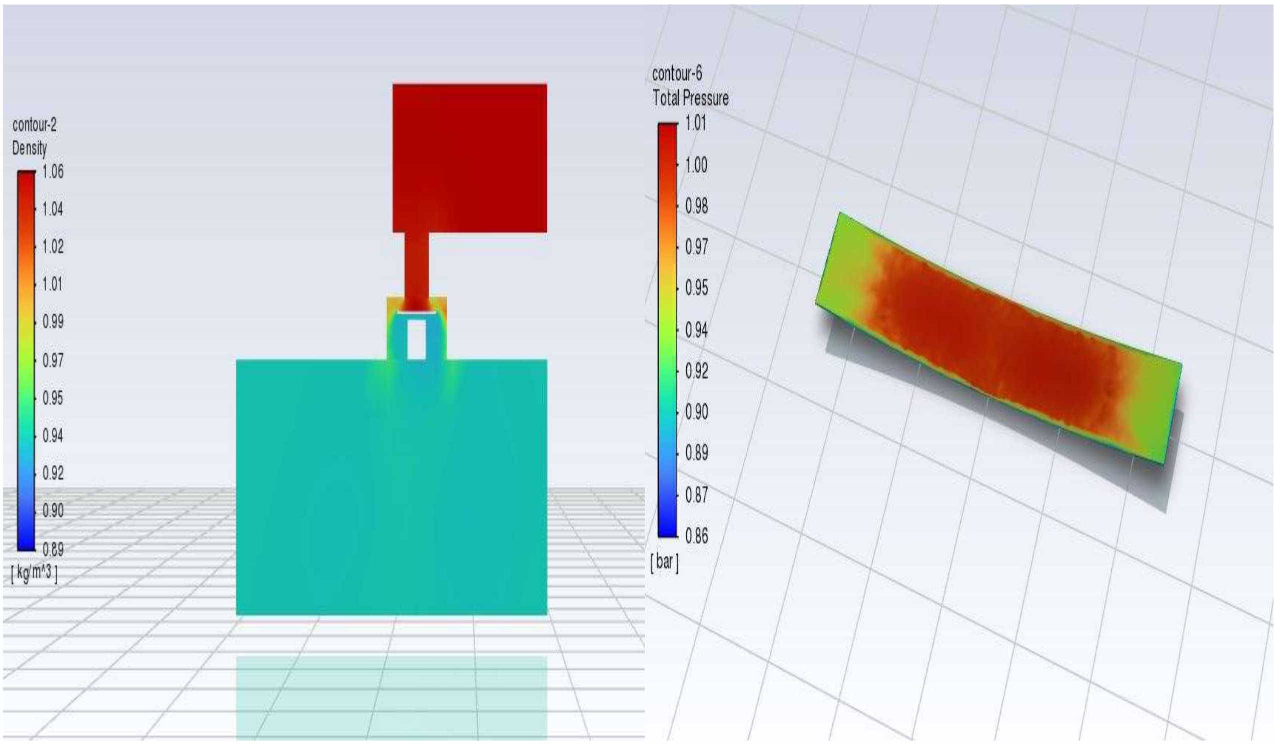

Figure 6.27 Density Contour -Pressure on Reed

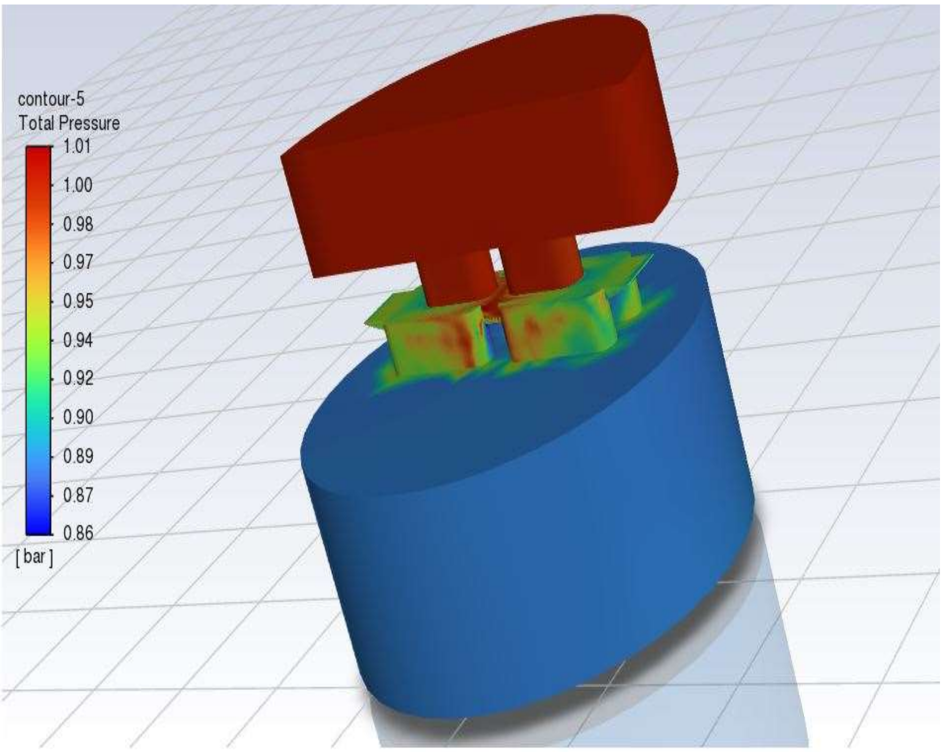

Figure6. 28 Global Pressure Contour

- Lift 0,16 mm

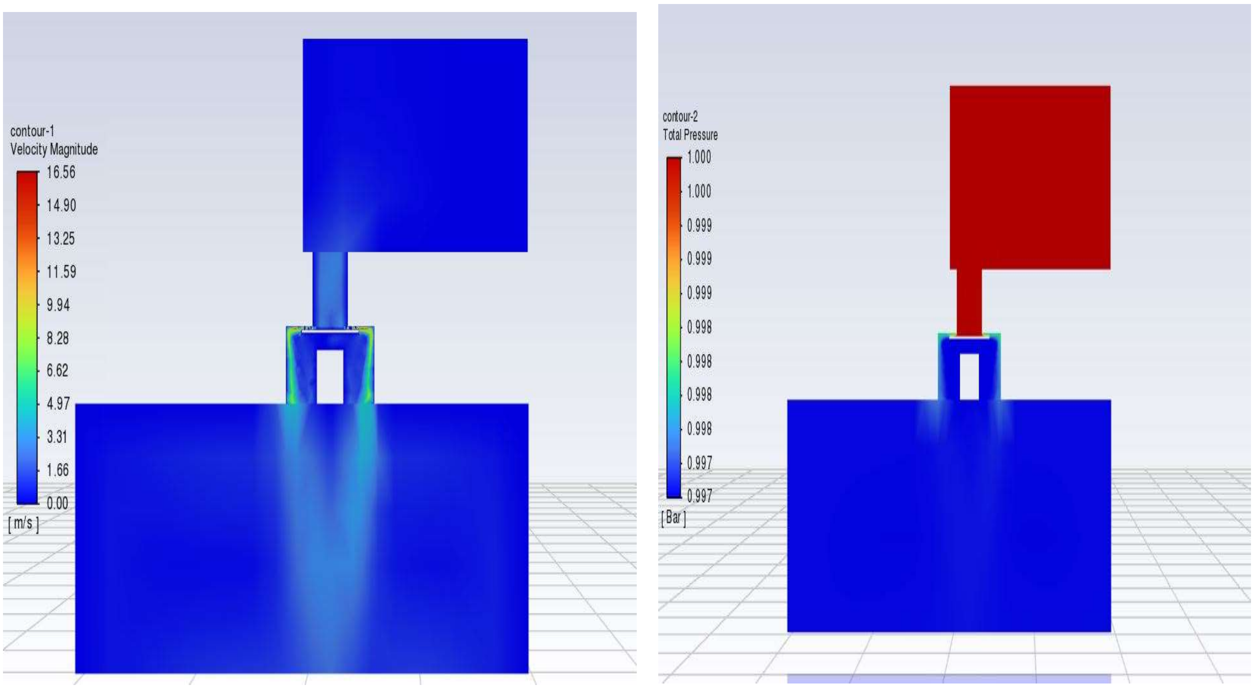

Figure 6.29 Velocity-Pressure Contour

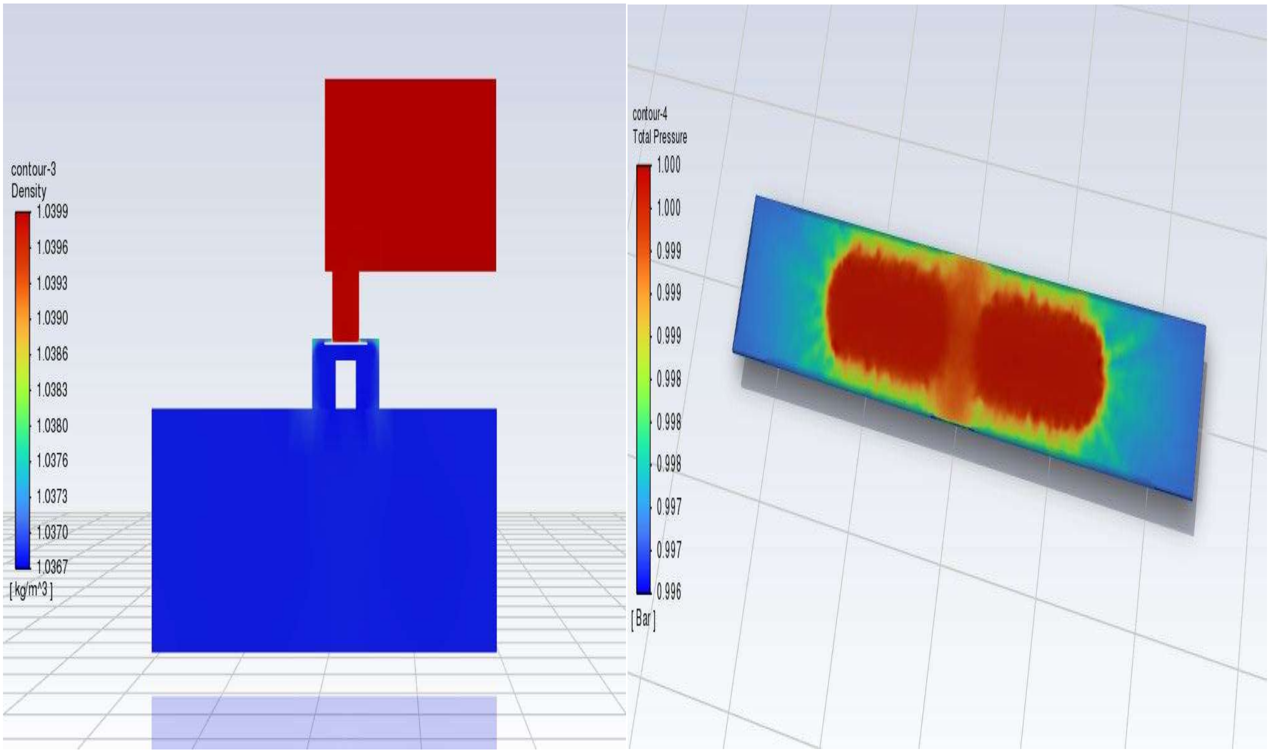

Figure 6.30 Density-Pressure on Reed Contour

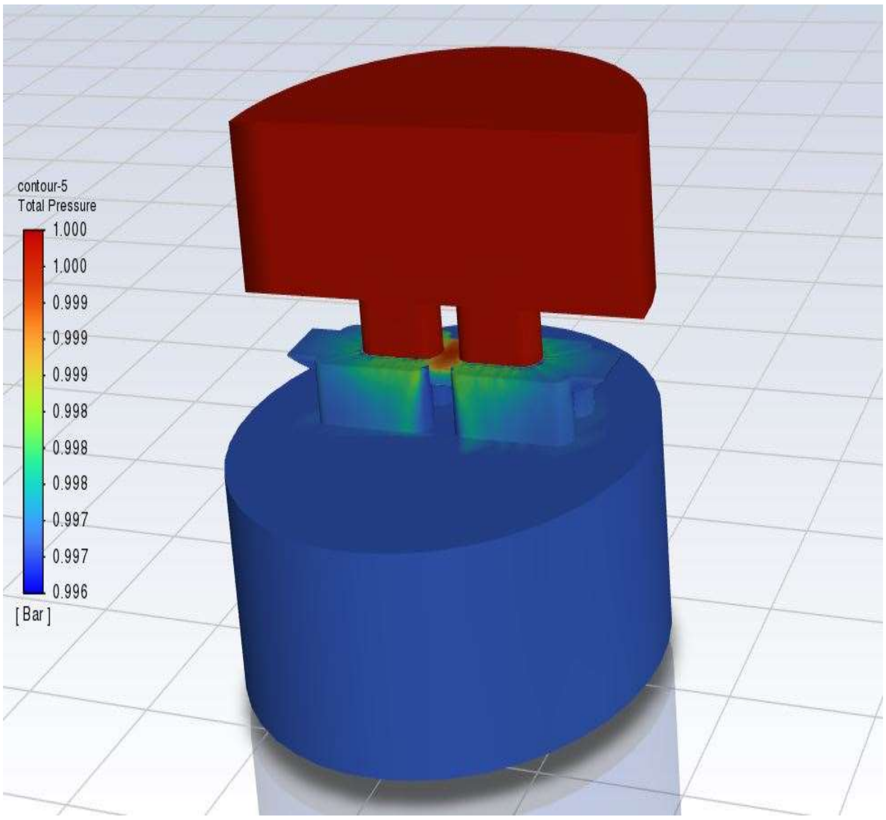

Figure 6.31 Global Pressure Contour

6.4.4 Discharge Valve CFD Result

- Lift 2 mm

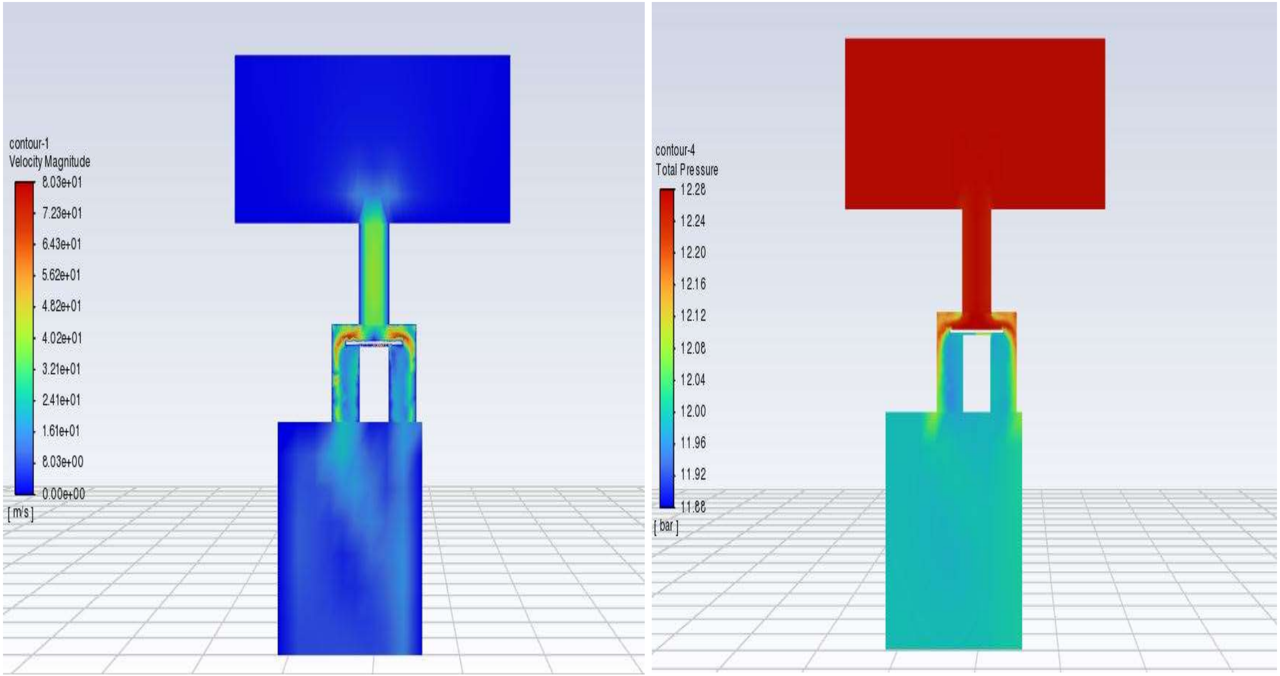

Figure 6.32 Velocity-Pressure Contour

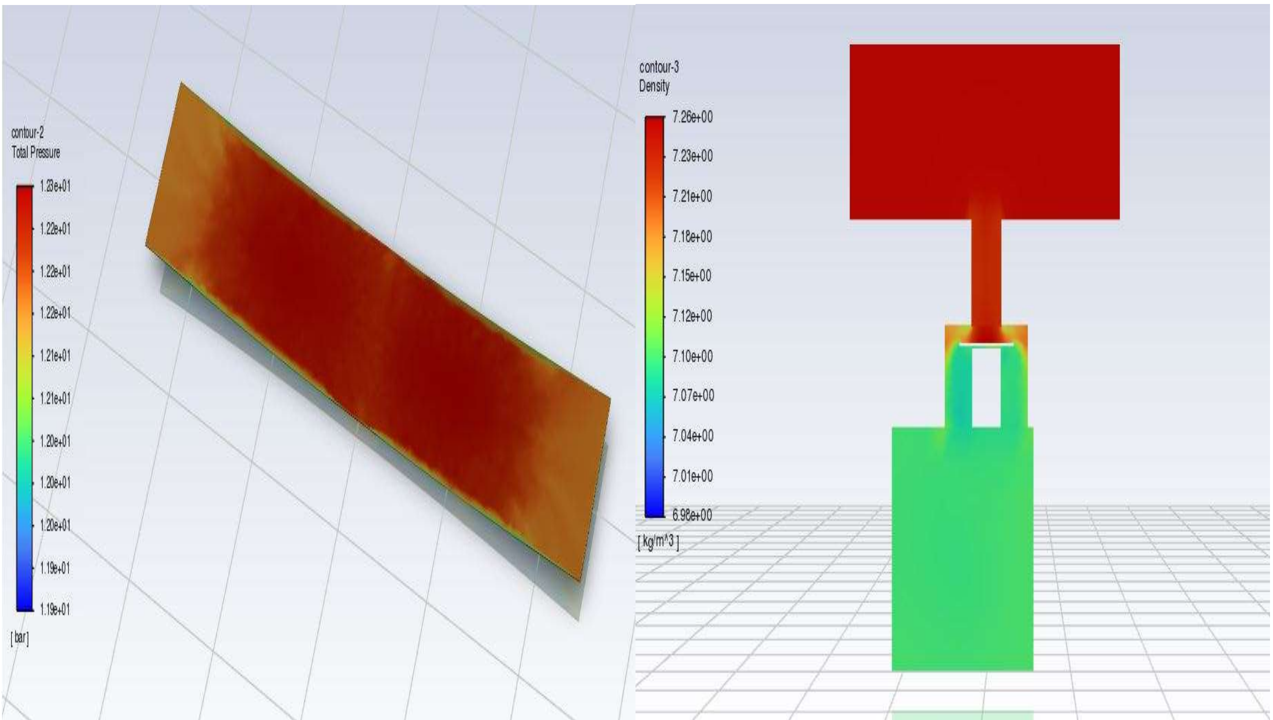

Figure 6.33 Density-Pressure on Reed Contour

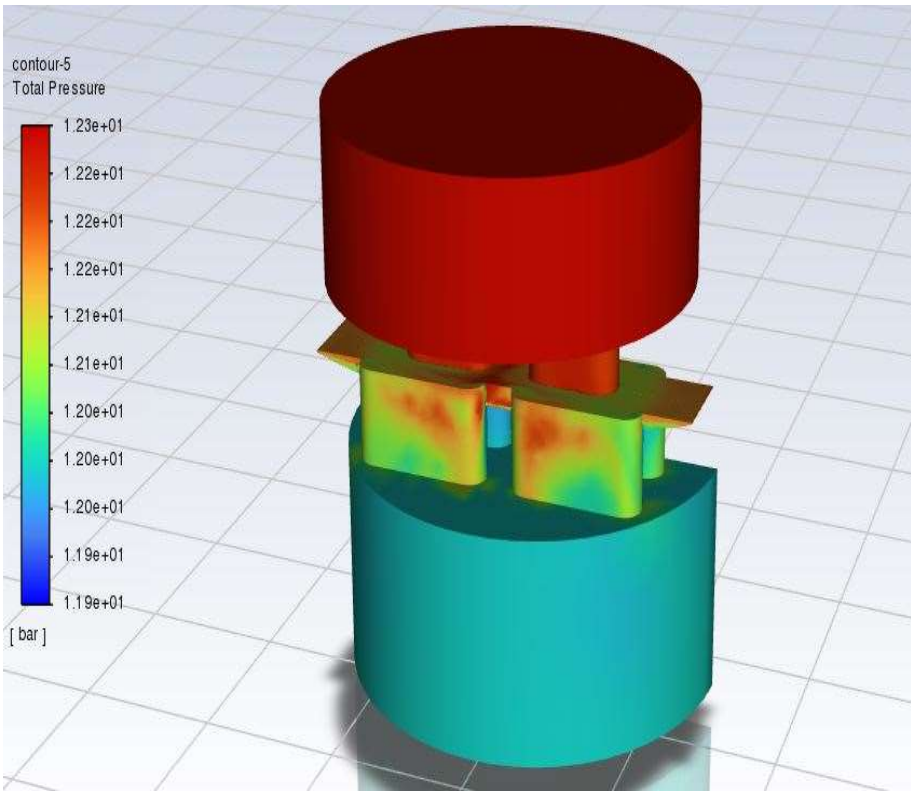

Figure 6.34 Global Pressure Contour

- Lift 1 mm

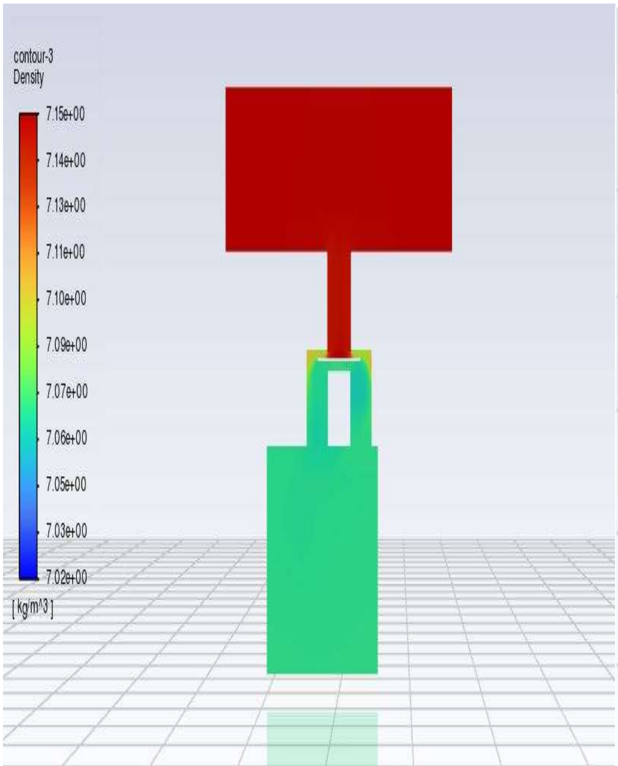

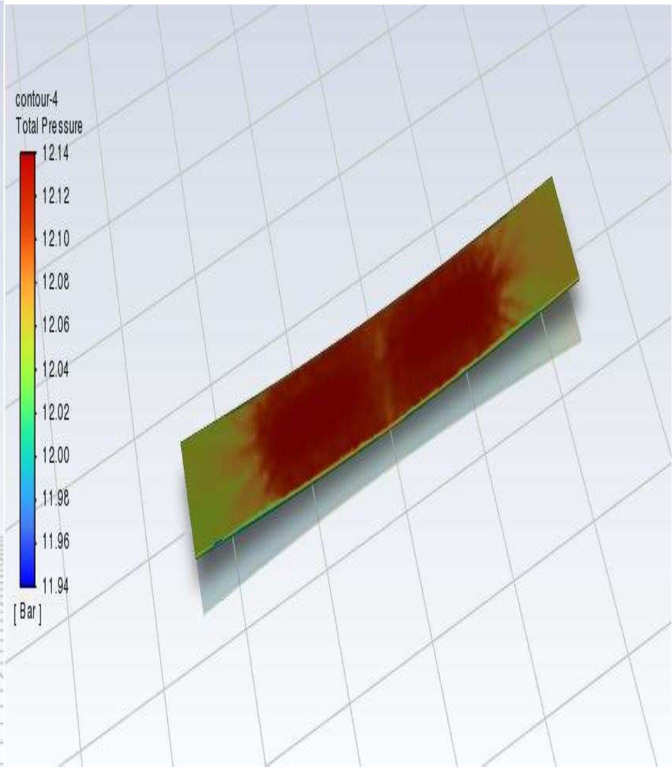

Figure 6.35 Density-Pressure on Reed Contour

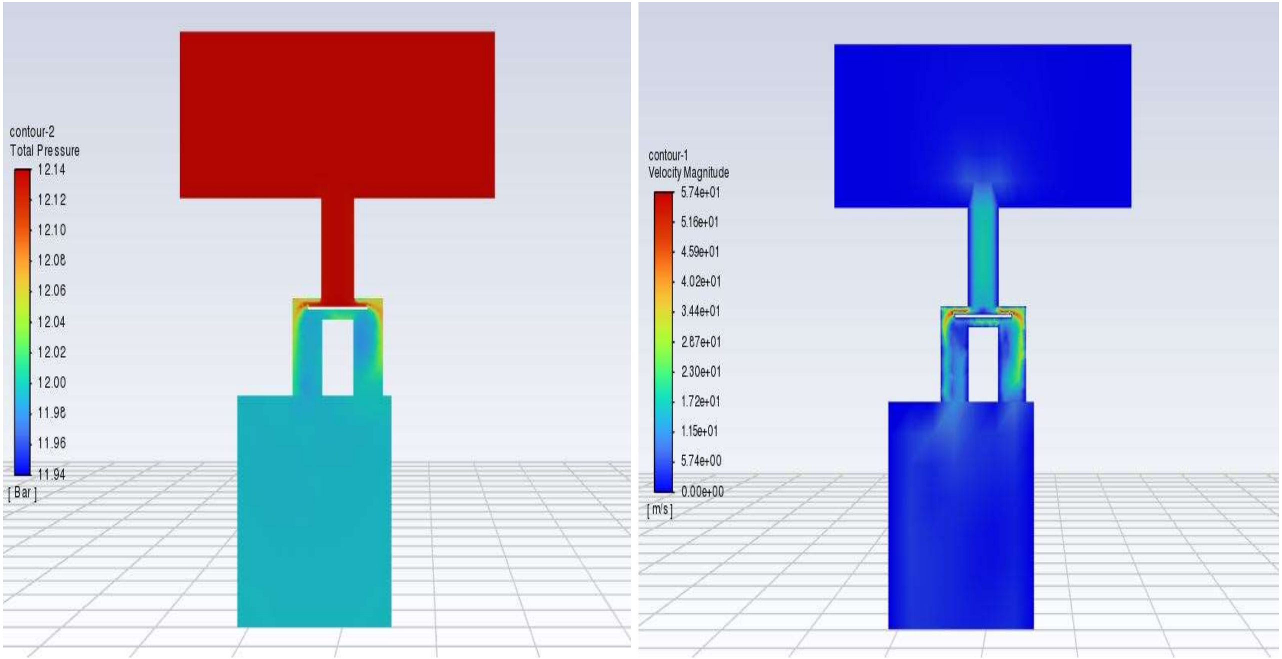

Figure 6.36 Pressure -Velocity Contour

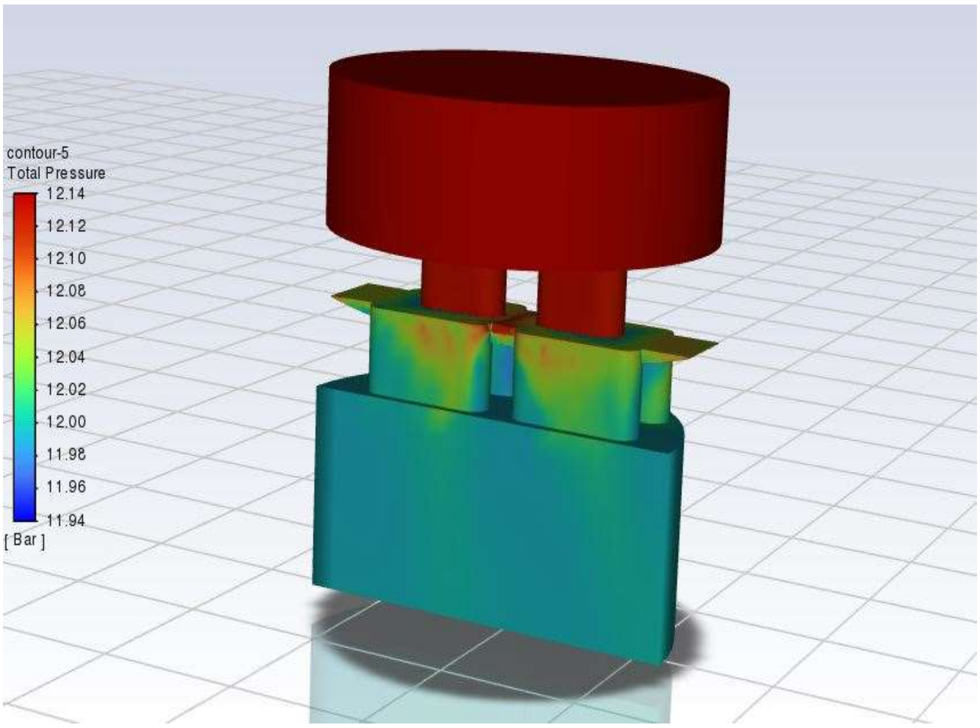

Figure 6.37 Global Pressure Contour

6.4.5 Simscape Coefficients

The main results of the CFD analysis are summarised below, which will be used to implement the compressor model on Simscape.
From the two graphs below it is possible to see how the velocity in the restriction created between the deformed reed and the plate hollow assumes the highest value within the fluid domain and how these increases in value as the deformed reed increases.
The difference in velocity values between the first stage intake valve and the second stage exhaust valve can be explained by the law of continuity. In fact, as can be seen from the various contours reported, the density in the second stage is approximately 7 times greater than that in the first stage. This causes the velocities reached in the first stage to be higher than the velocities in the second stage, with the same reed lift.

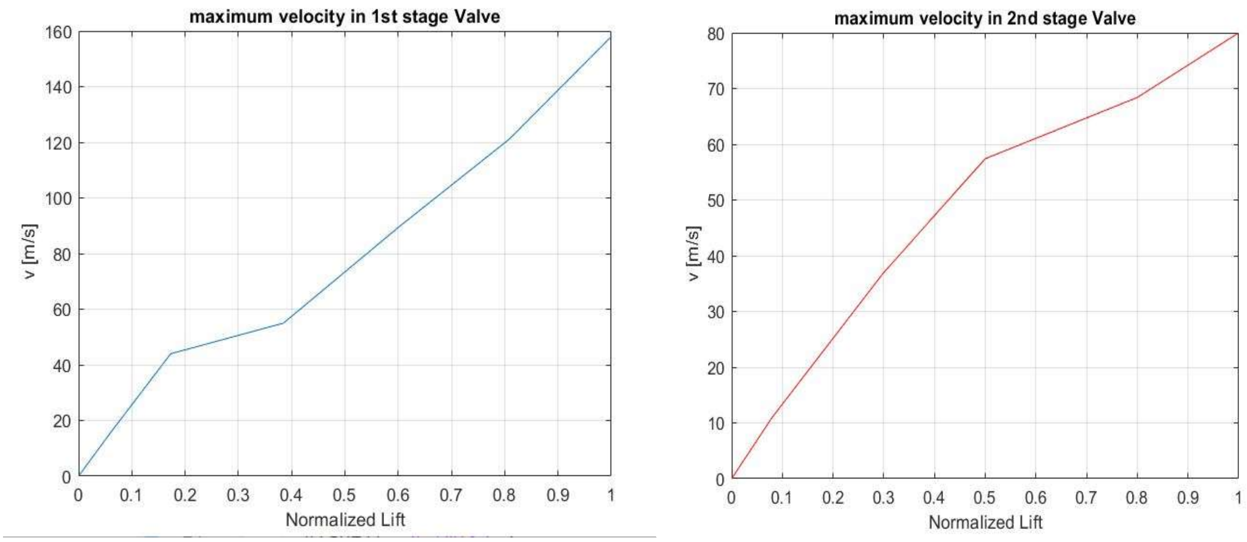

Figure 6.38 Maximum velocity as a function of lift

The drag coefficient, a fundamental parameter for calculating the force produced by the air on the reed can be calculated automatically in the ANSYS software.
Reading the graphs on the drag coefficient demonstrates a preliminary hypothesis of the CFD analysis: this parameter is minimally influenced by the pressure difference acting on the reed, which is because only two valves out of four were analysed.
Unlike other works in the literature [9] where the drag coefficient can be considered almost constant, here this coefficient varies depending on the lift. It must be noted that the works already present in the literature describe ring valves where the reed only translates in the vertical direction without deforming. The variation of this parameter can therefore be explained by this aspect.

Table 6.7 and Fig.6.39 summarise the results of the drag coefficient analysis performed on the exhaust valve when the valve is fully open with a lift of 2mm.

	Pressure	Viscous	Total
Drag Force [N]	**9,0264698**	**2,99 e-3**	**9,0268**
Drag Coefficient	**1,924**	**6,39 e-5**	**1,924**

Table 6.7 Drag Coefficient and Drag Force @2mm

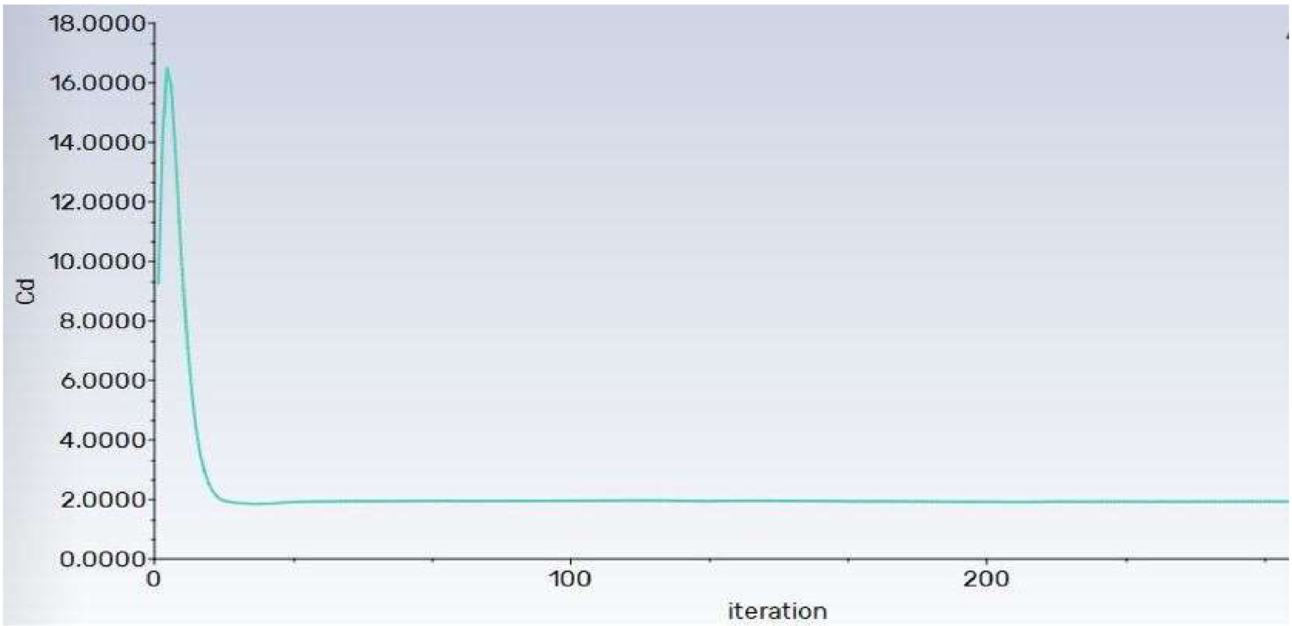

Figure 6.39 Drag Coefficient Iterations

The plots in Fig.6.40 summarise the behaviour of the drag coefficient for both valves varying the lift.

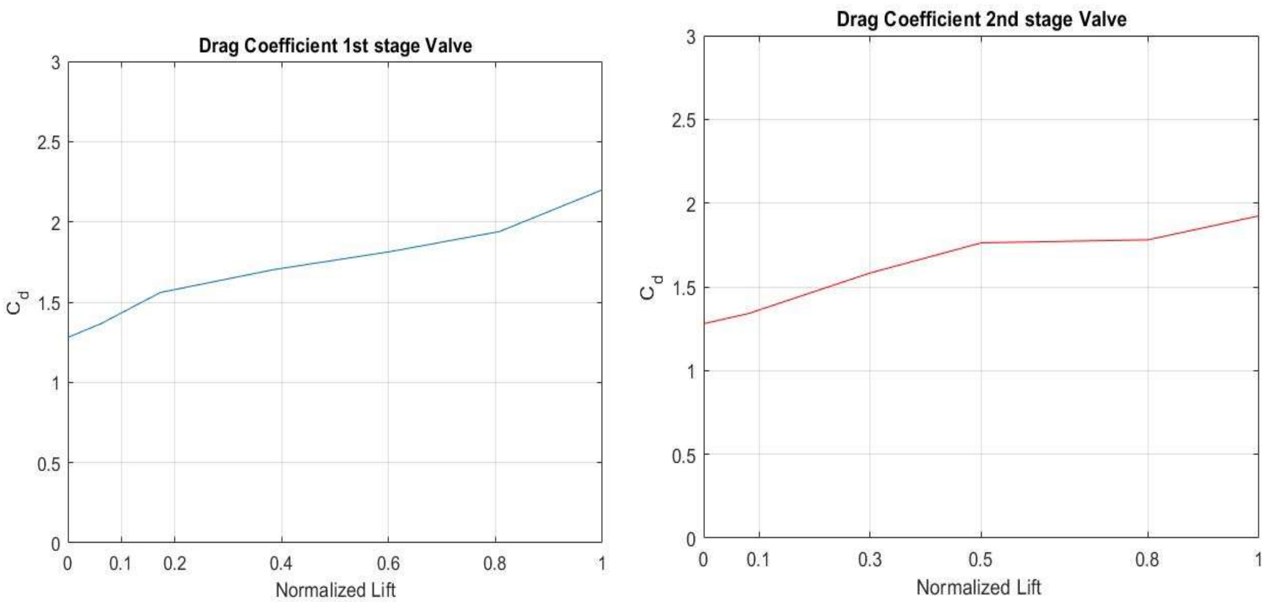

Figure 6.40 Drag coefficient as function of lift

The formula that allows an analytical treatment of the air force acting on the reed is as follows:

$$F_g = C_g A_v \Delta p$$

As can be seen from the CFD analysis and as mentioned above in the structural part, the pressure given by the passage of air over the reed is not uniformly constant. This aspect is also noted in [9]. It is therefore possible to link both the drag coefficient and the reed area to the deformation of the reed itself. In the absence of other data, the area can be approximated using a linear function with two known values: when the lift is zero, the area over which the pressure acts is equal to the area of the two channels visible in the 3D drawing of the assembly, while when the lift is maximum, the area is equal to the area of the reed.

The formula of gas Force has been modified as shown below

$$F_g = C_g A_v \; a \; \Delta p$$

A dimensionless coefficient was inserted to express the percentage of reed area as a function of reed lift, as represented in Fig.6.41

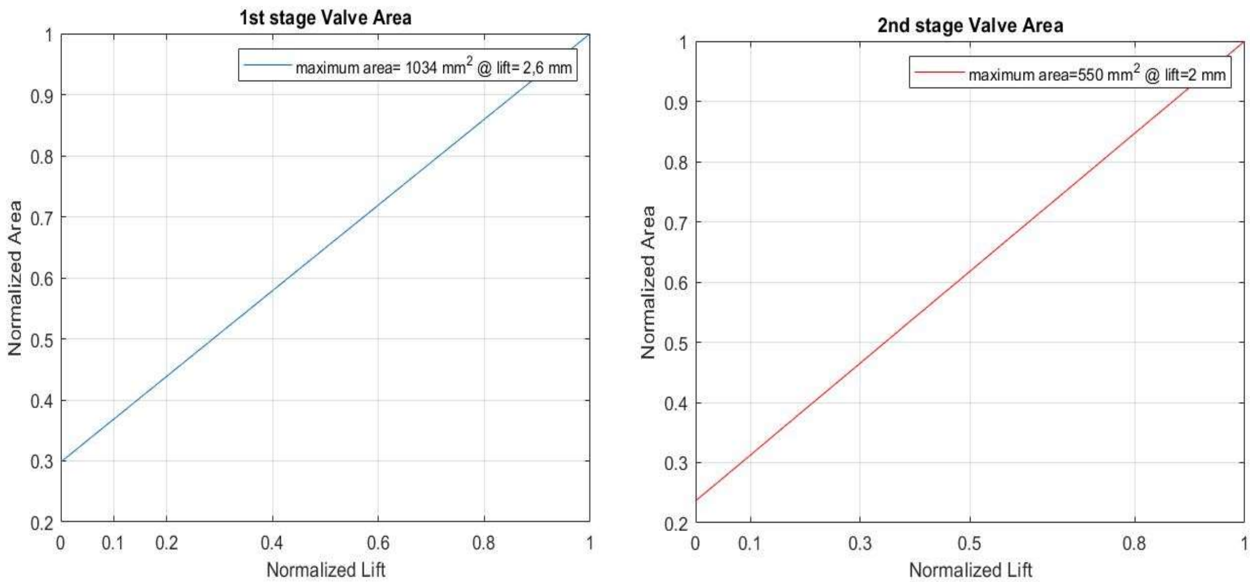

Figure 6.41 Valve Area as function of lift

The last parameter that can be extrapolated from the CFD analysis is the discharge coefficient. It is defined as the ratio of the actual to the theoretical mass flow rate through the restriction. The discharge coefficient is an empirical parameter used to account for non-ideal effects such as those due to restriction geometry.

The restriction consists of a contraction followed by a sudden expansion in flow area. The gas accelerates during the contraction, causing the pressure to drop.

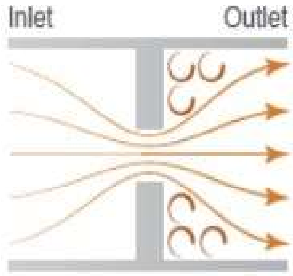

Figure 6.42 Gas restriction Layout

This coefficient goes from a value of 0.5 to a maximum of 0.70 for the valve under study. this behaviour is present in both the intake and exhaust valve.

Since the valve during its operation remains fully open or fully closed most of the time and Simscape requires a constant value to model the variable restriction's coefficient, the maximum value of 0.70 and 0.72 was entered for the first and second stage valves respectively.

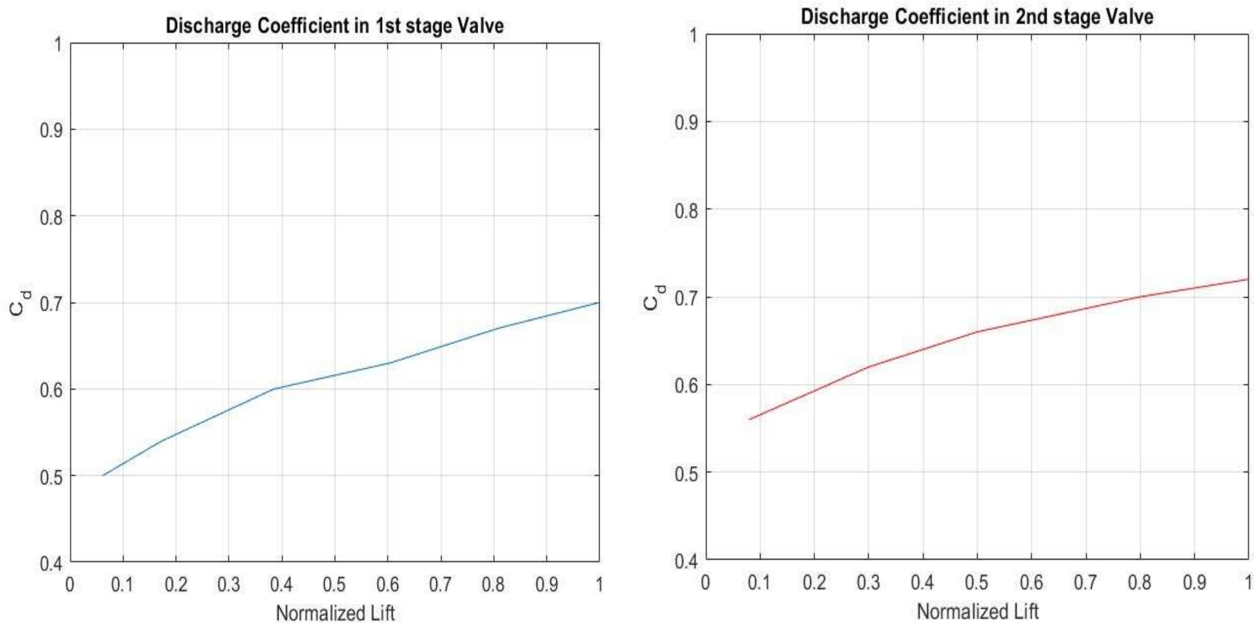

Figure 6.43 Discharge coefficient as function of lift

7 Feather Valve Model

The feather valve is mounted in the compressor assembly between the two cylinders and the cylinder head. The compressor type is the same as that analysed in Chapter 4: it is a multi-stage piston compressor in a straight configuration. An intercooler is placed between the two compression stages in order to lower the air temperature.

As can be seen in Fig.7.1 , sensors have been inserted at the outlet and inlet of the chambers and in the bottom plate of the valve to measure pressure and temperature at different points of the compressor assembly. The main compressor parameters are summarised below

Compressor Parameters		
Suction pressure [Bara]	**1**	
Discharge pressure [Bara]	**12**	
	First stage	**Second stage**
Stroke [mm]	**55**	**55**
Bore [mm]	**105**	**55**
Conrod length [mm]	**122,5**	**122,5**

Table 7.1 Compressor parameters

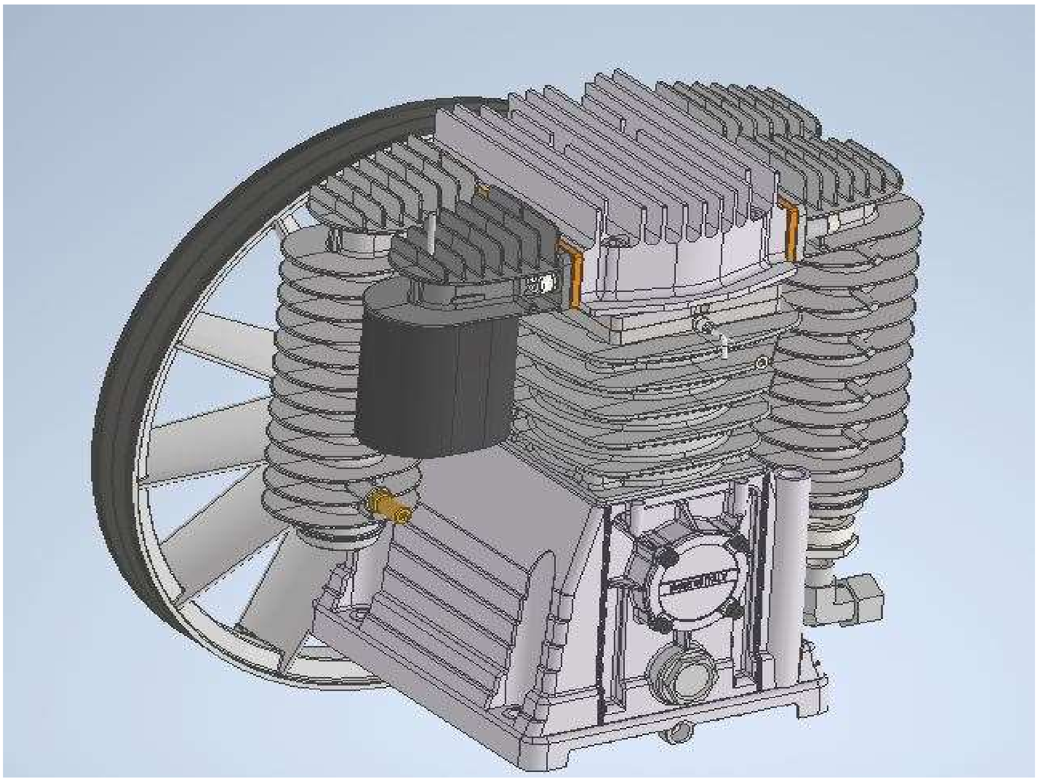

Figure 7.1 Piston Compressor prototype

7.1 Stage Modeling

The Simscape components that compose the valve sub-model, shown in fig.7.2 and fig.7.3, are the same as in the previous model, initialised in an appropriate manner. One of the main differences from the previous model is that in the 'Reed' valve there were three reed per stage, whereas in the 'Feather' valve there is only one reed that regulates the air flow.

In this model, the feedback signal is not only used to adjust the passage area due to valve deformation, but is also implemented to make the drag coefficient and the area of the reed valve on which the air is pressed vary as a function of reed lift, as can be seen from the Simscape sub-model visible in Fig.7.3

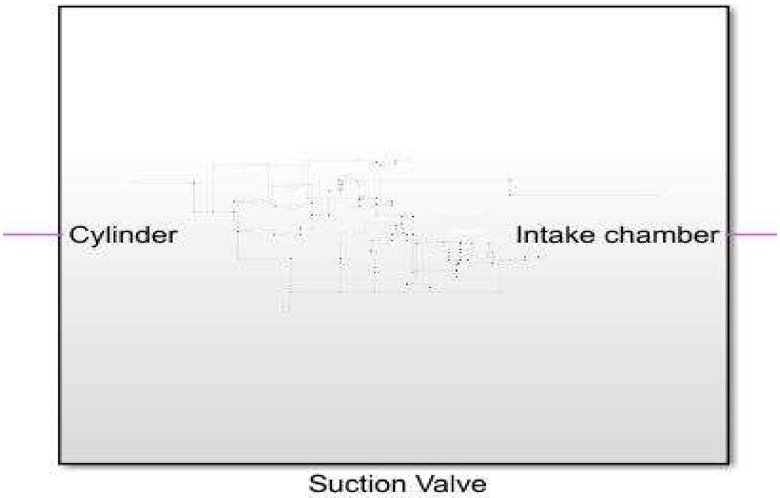

Figure 7.2 Suction Valve Submodel

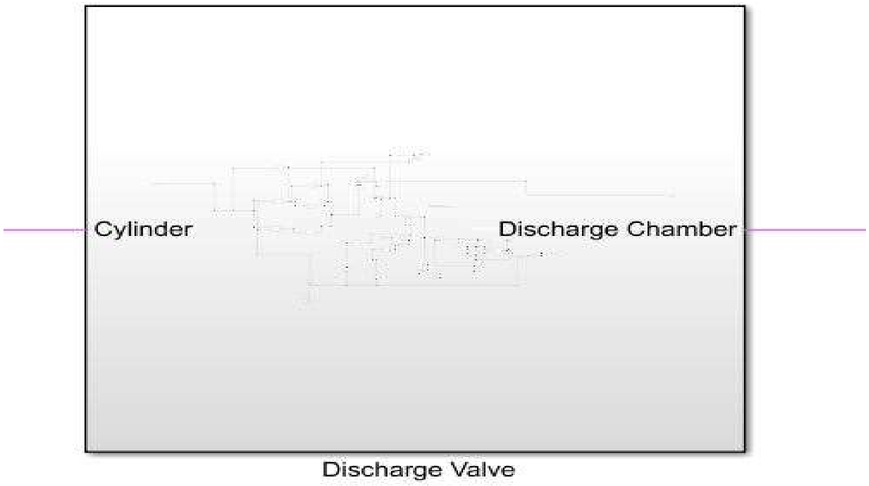

Figure 7.3 Discharge Valve Submodel

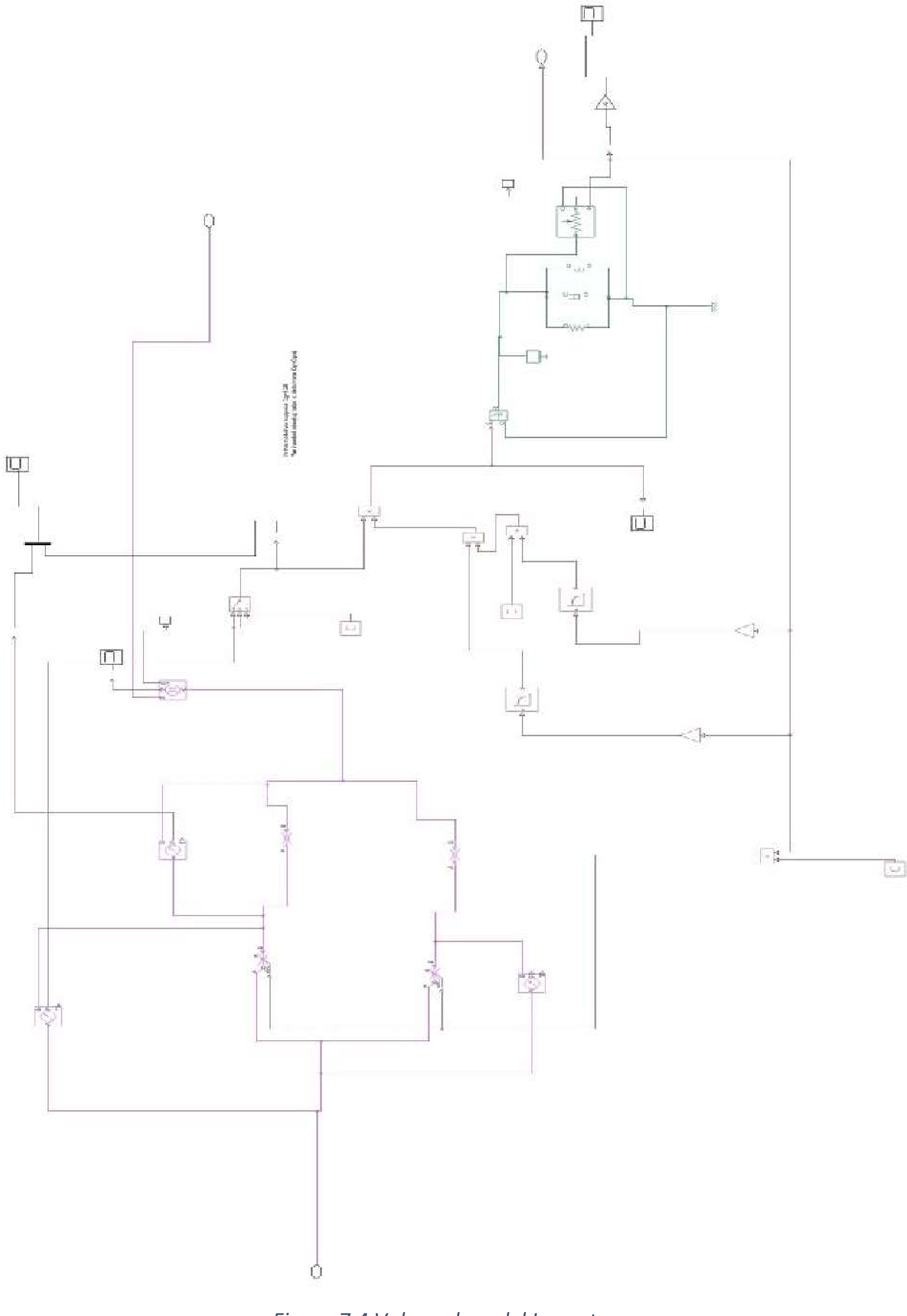

Figure 7.4 Valve submodel Layout

7.2 Valve Parameters

After describing the layout of the model, this section describes the main components of the 'Valve' sub-model.

First, the geometric parameters of the reed whose deformation due to gas pressure allows the passage of air are given. As previously mentioned, the same reeds were used for intake and exhaust, so two types of reeds are used: one for the first stage and another for the second compression stage. The dimensions that characterise the two reeds are shown in Tab 7.2 and Tab.7.3

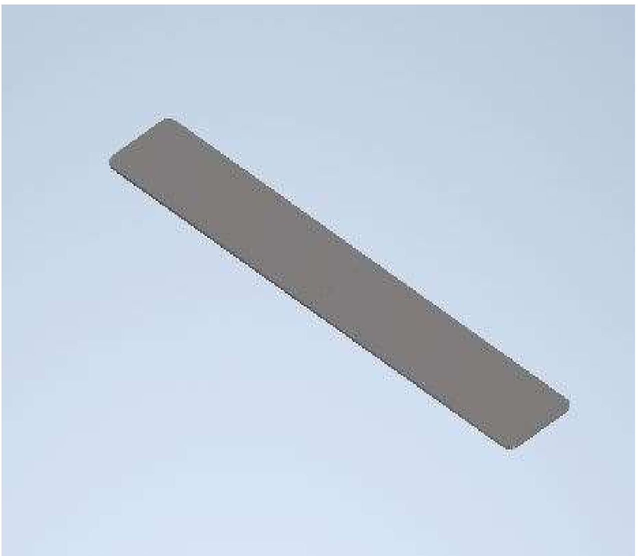

Figure 7.5 1^{st} stage Reed

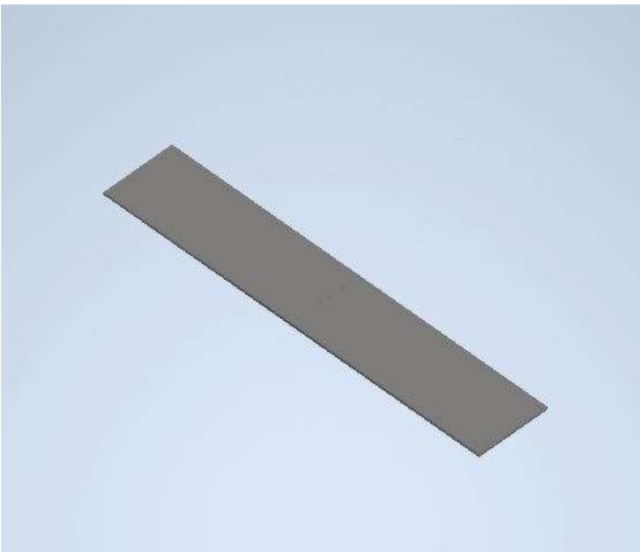

Figure 7.6 2^{nd} stage Reed

Parameters	Value	Unit
Thickness	**0,4**	**mm**
Total length	**81**	**mm**
Width	**12,80**	**mm**
Equivalent mass	**0,79**	**g**
Natural frequency	**242**	**Hz**

Table 7.2 1st stage Reed Parameters

Parameters	Value	Unit
Thickness	**0,3**	**mm**
Total length	**55**	**mm**
Width	**10**	**mm**
Equivalent mass	**0,29**	**g**
Natural frequency	**393**	**Hz**

Table 7.3 2nd stage Reed parameter

Geometrical parameters such as length, width and thickness influence the bending stiffness of the reed, which is a fundamental parameter for modelling the dynamics of the one-degree-of-freedom reed.

As with the previously analysed valve, the bending stiffness of the reed was calculated analytically and via FEM .For both calculations, the model of the beam simply supported at the ends was used.

Instead of using the formula to calculate the deformation of a beam supported under a point load, the case of a beam subjected to a uniformly distributed load was used to best model the behaviour of the valve, instead of using the stiffness according to [13]

$$k = \frac{384EI}{5L^3} \qquad 7.1)$$

The Tab.7.4 summarises the flexural stiffness values for the two reeds used in the valve assembly calculated analytically and via FEM.

	First stage		**Second stage**	
	Suction	**Discharge**	**Suction**	**Discharge**
FEM bending stiffness [N/m]	**2071**	**2071**	**1935**	**1935**
Analytical bending Stiffness [N/m]	**1837**	**1837**	**1773**	**1773**
Error	**11,3 %**	**11,3 %**	**8,37 %**	**8,37 %**

Table 7.4 Analytical and Fem Stiffness

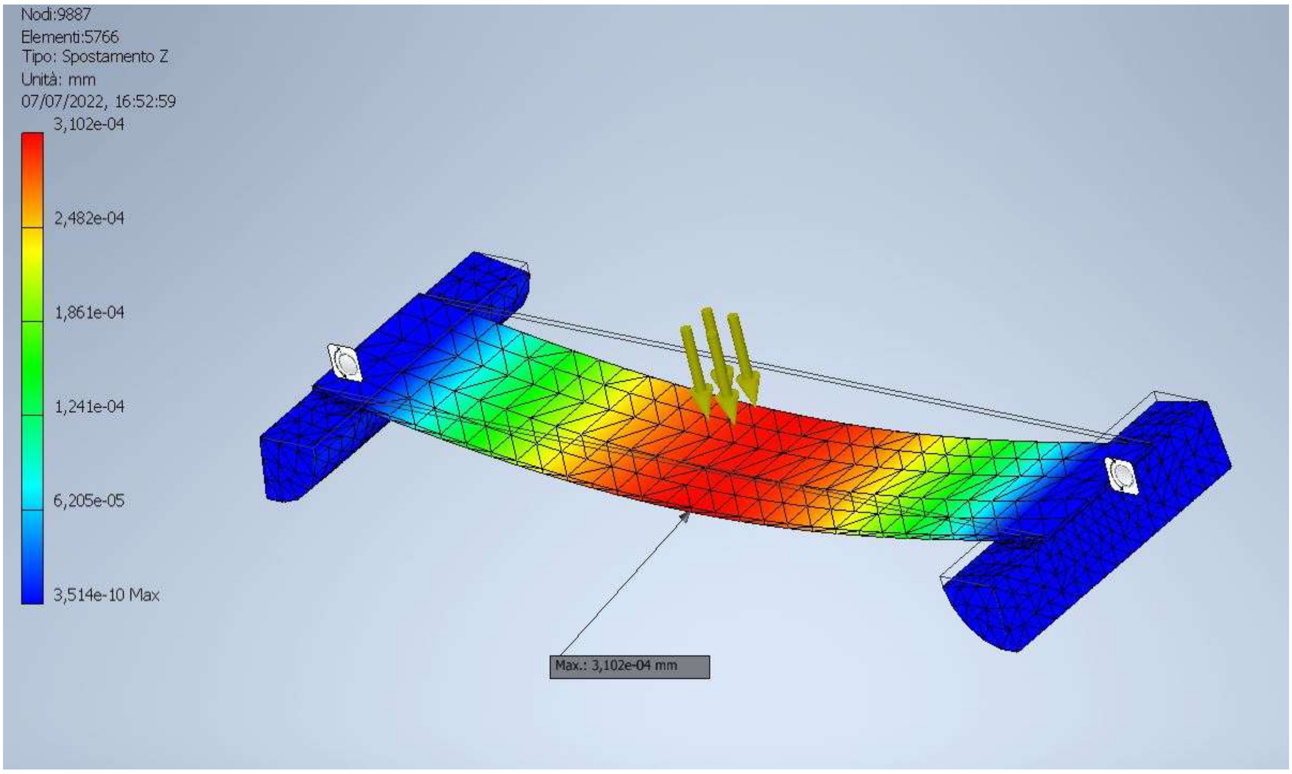

Figure 7.7 FEM analysis

Since this prototype valve was in the design phase at the same time as the modelling phase, the maximum permissible reed lift was chosen. A compromise had to be found for this parameter.
By increasing the maximum lift, the flow rate can be increased, but, as noted during the structural FEM analysis carried out in the previous chapter, at the same time the stresses to which the valve was subjected increase.
Since a technical constraint on the maximum stress of 200 MPa had to be met, the maximum lifts visible in Tab. 7.5 were chosen.

	First stage		Second stage	
	suction	**discharge**	**suction**	**discharge**
Valve Reed lift [mm]	**2,6**	**2,6**	**2**	**2**

Table 7.5 Reed Lift

One of the main parameter describing compressor performance is volumetric efficiency. This parameter depends on the dead volume ratio and the compression ratio, as described in the formula explained above and given below.

$$\lambda_v = 1 - \mu(\beta^{\frac{1}{k}} - 1) \quad 7.2)$$

The dead volume ratio is defined as follows .

$$\mu = \frac{V_o}{\Delta V} \quad 7.3)$$

ΔV is the compressor displacement and V_0 is the volume remaining in the cylinder when the piston is at TDC . This volume depends on two design factors, which can be seen in Fig.7.8 and Fig.7.9.

- Volume of air present between valve bottom plate and cylinder in TDC position

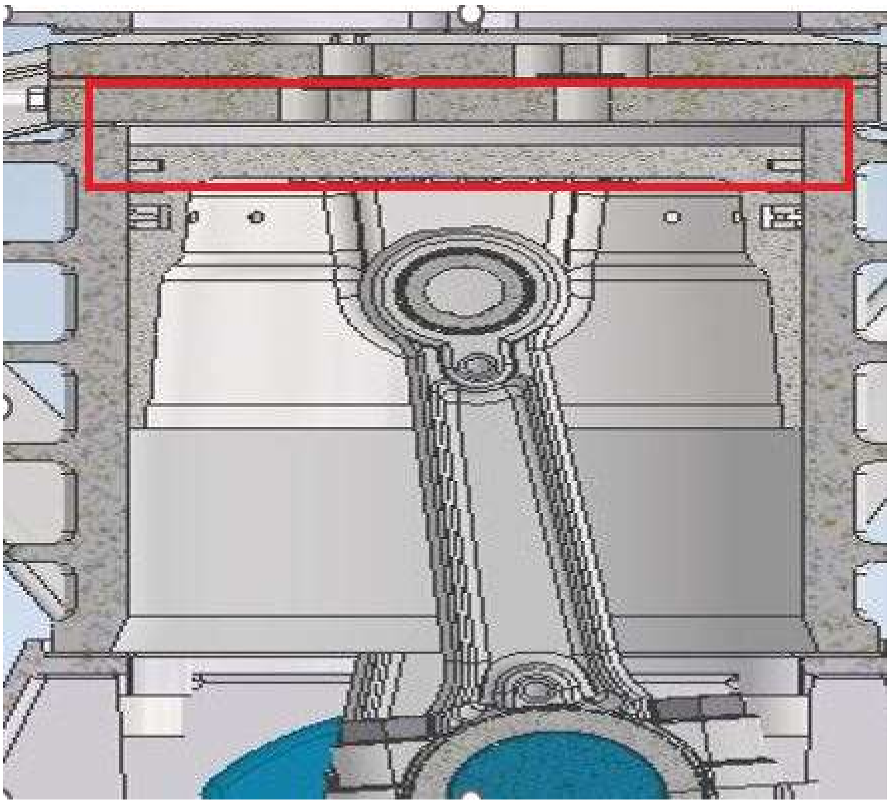

Figure 7.8 Dead volume between piston and Valve plate

- Volume of air trapped in the cylinder-side valve channels when the valve is closed.

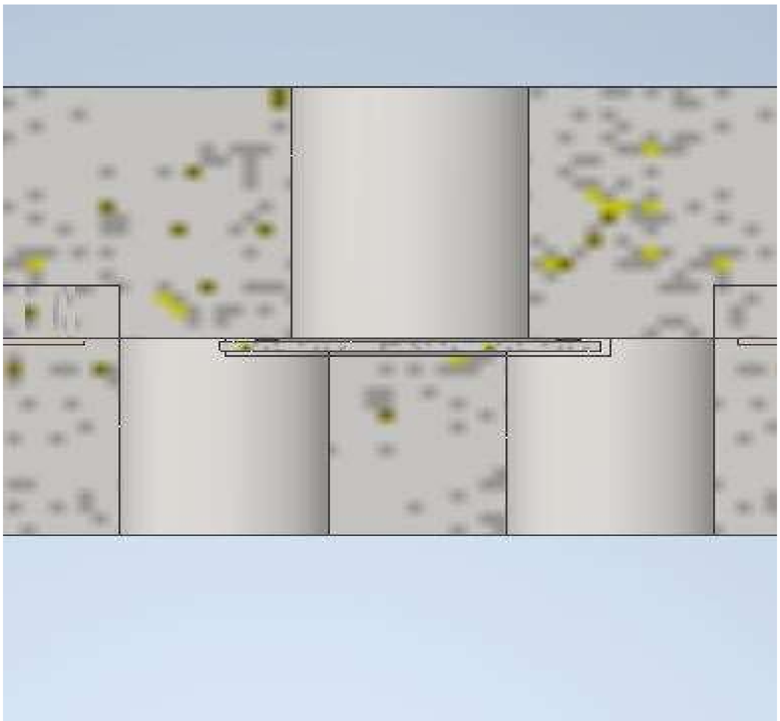

Figure 7.9 Dead Volume in Valve plate

These two volumes will characterise the "dead volume" parameter of the cylinder block. To be able to easily model this dead volume, it is easiest to use the parameter c_{eq} , called the equivalent clearance length, which can be derived from the following formula

$$c_{eq} = \frac{V_0}{\pi \frac{B^2}{4}} \quad 7.4)$$

The Tab.7.5 shows the equivalent clearance lengths for both stages, calculated both analytically and using CAD software Inventor

	1st stage equivalent clearance length	**2nd stage equivalent clearance length**
Clearance between cylinder and plate [mm]	**1,2**	**1,2**
Clearance due to valve Ports [mm]	**1,75**	**2,35**
Total analytical Clearance [mm]	**2,95**	**3,56**
CAD Equivalent Length [mm]	**2,7**	**3,65**
Error between analytical and CAD	**8,47 %**	**-2,52 %**

Table 7.6 Equivalent Clearance Lengths

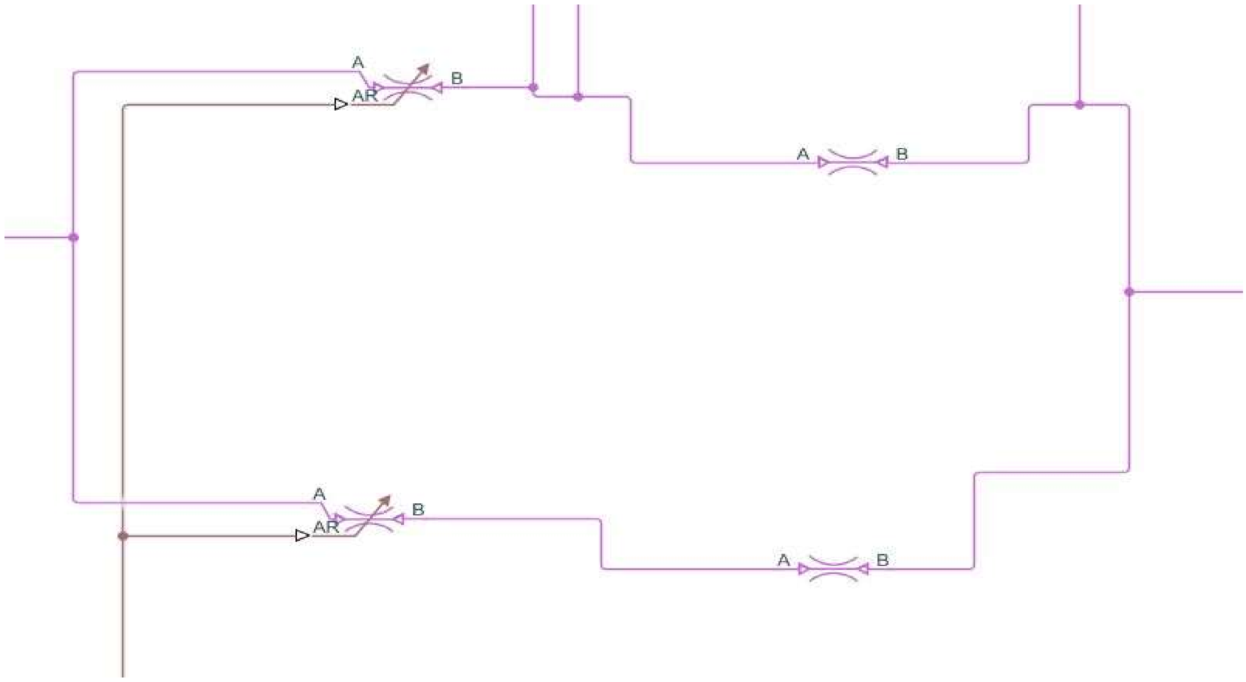

Figure 7.10 Orifices Layout in Simscape

As far as the passage through the valve is concerned, this was modelled on the Simscape software via the 'gas restrictions' block as done for the previous valve, with an appropriate configuration.

As mentioned in the descriptive chapter of the Feather valve, the passage area due to the bending of the reed valve can be approximated to two arcs and then the air passes through the channels downstream of the reed. The two tables summarise the parameters characterising the passage of air through the valve. Since the valve is designed symmetrically with respect to suction and discharge, there are two tables for the first and second stage respectively.

Restrictions Type	**Geometric variable**	**Value**	**Unit**
Variable	**Maximum area**	**134,78**	mm^2
	Discharge Coefficient	**0,7**	
Fixed	**Valve Area**	**308,5**	mm^2
	Restriction Area	**156,6**	mm^2
	Discharge Coefficient	**0,7**	

Table 7.7 1st stage Valve Parameters

Restrictions Type	Geometric variable	Value	Unit
Variable	**Maximum area**	**70,4**	mm^2
	Discharge Coefficient	**0,72**	
Fixed	**Valve Area**	**139**	mm^2
	Restriction Area	**76**	mm^2
	Discharge Coefficient	**0,72**	

Table 7.8 2nd stage Valve Parameters

One of the assumptions made in order to proceed was to consider the equal exhaust coefficient within the same stage for both exhaust and intake.

7.3 Model Results

As done previously for the reed valve model, this section shows the results of the model as a function of crankshaft speed. This is because at ABAC S.p.A., laboratory measurements were carried out at :

- 1274 rpm
- 1744 rpm

7.3.1 Model results @1274 rpm

- P-V Diagram

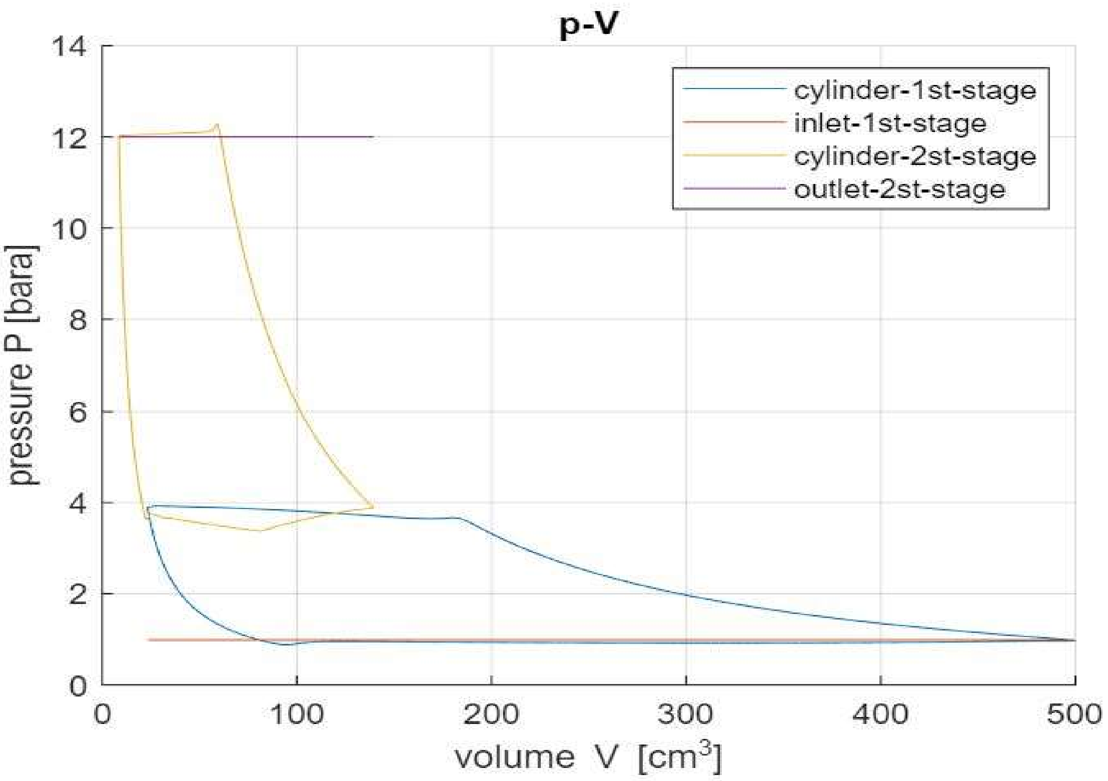

Figure 7.11 P-V Diagram

- 1st stage Pressure - Crank angle Diagram

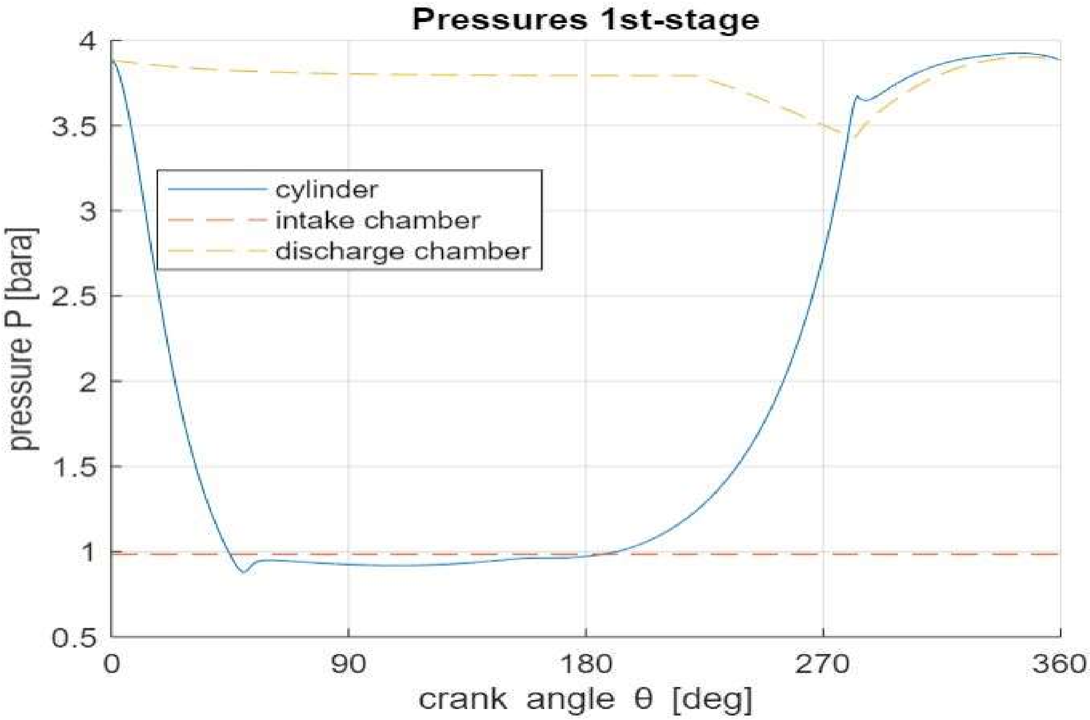

Figure 7. 12 Pressure in 1st stage-Crank angle plot

- Pressure drop in 1st stage Suction valve – Crank angle Diagram

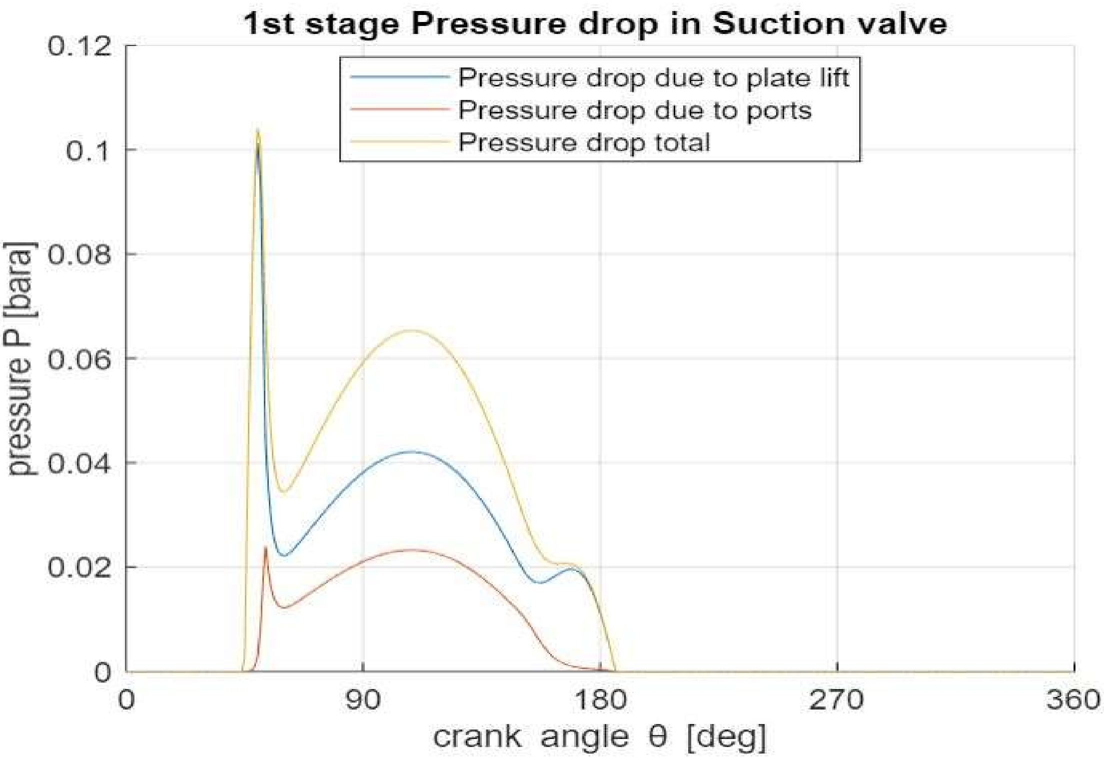

Figure 7. 13 Pressure drop in 1st stage suction valve-crank angle plot

- Pressure drop in 1st stage Discharge valve – Crank angle Diagram

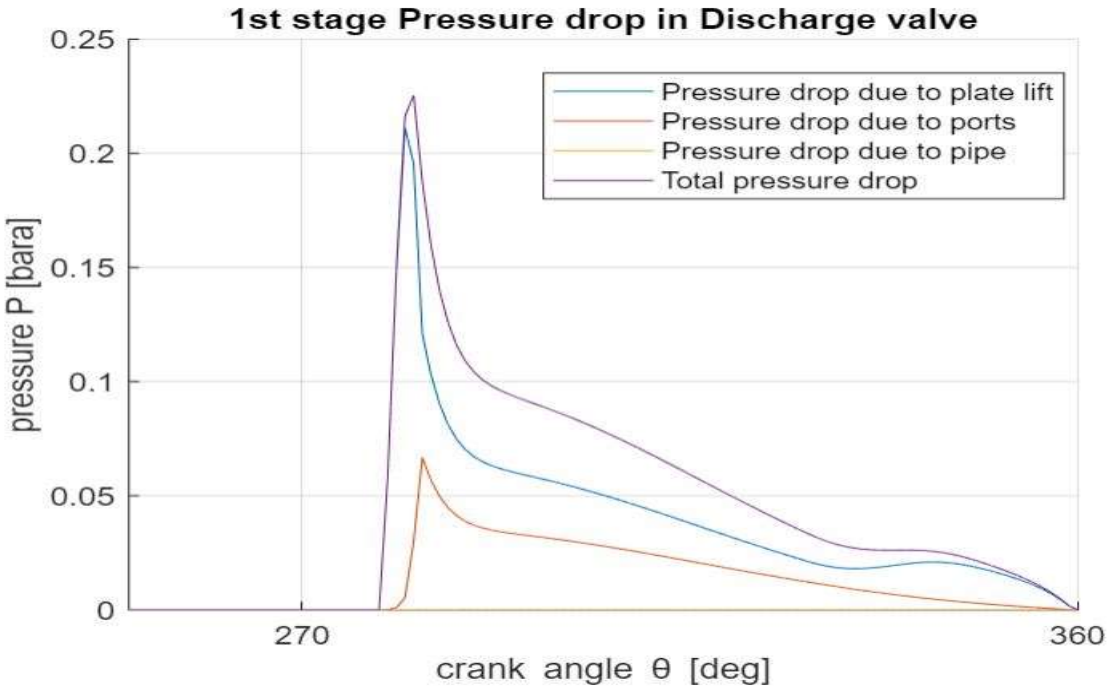

Figure 7.14 Pressure drop in 1st stage discharge valve-crank angle plot

- 1st Reed kinematic quantities – Crank angle Diagram

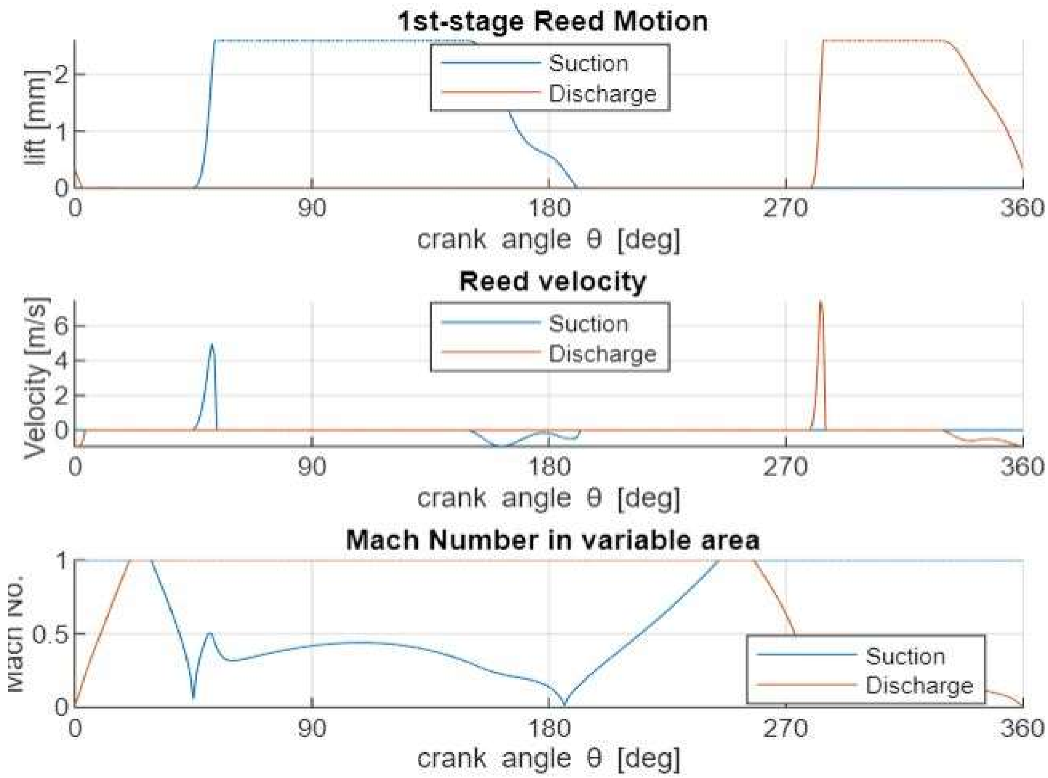

Figure 7.15 1st Reed lift -crank angle plot

- 2^{nd} stage Pressure - Crank angle Diagram

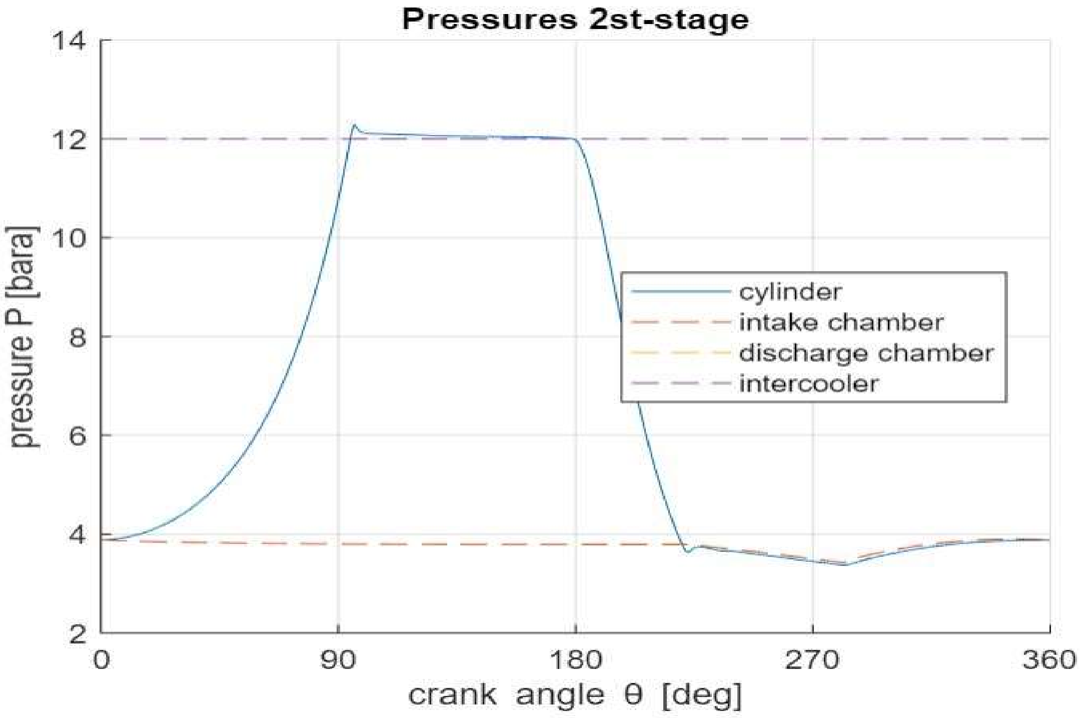

Figure 7.16 Pressure in 2^{nd} stage-Crank angle plot

- Pressure drop in 2^{nd} stage Suction valve – Crank angle Diagram

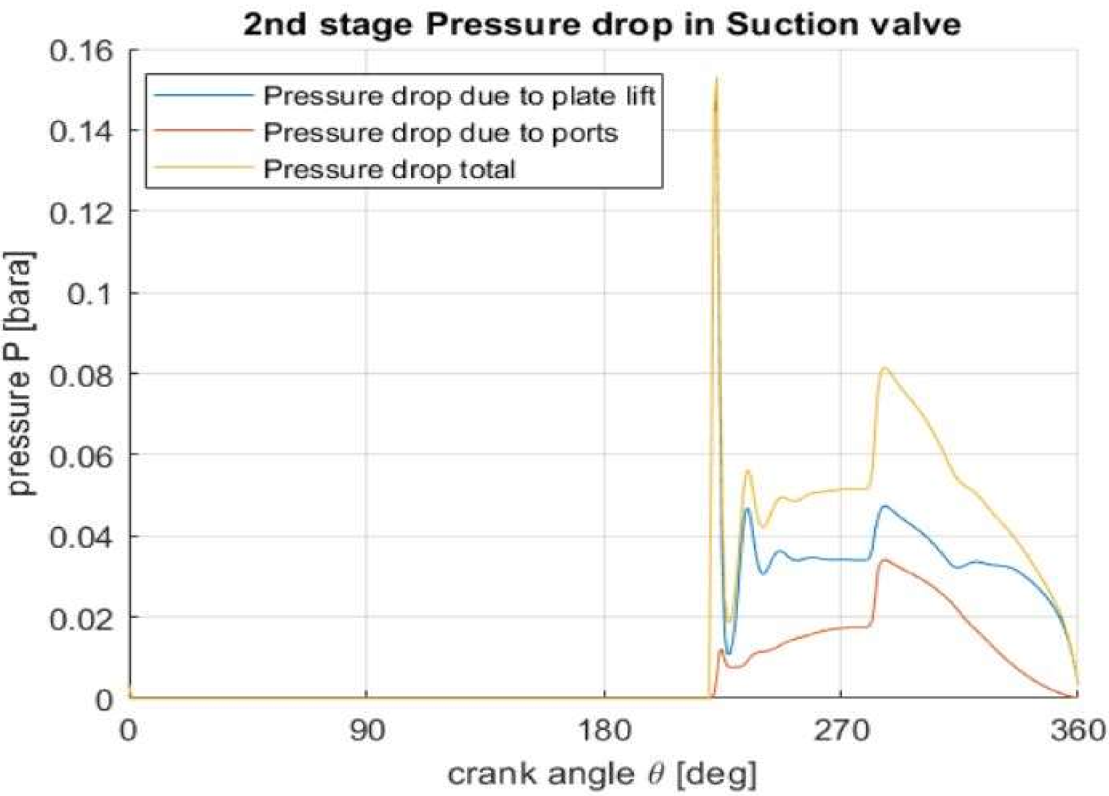

Figure 7.17 Pressure drop in 2^{nd} stage suction valve-crank angle plot

- Pressure drop in 2nd stage Discharge valve – Crank angle Diagram

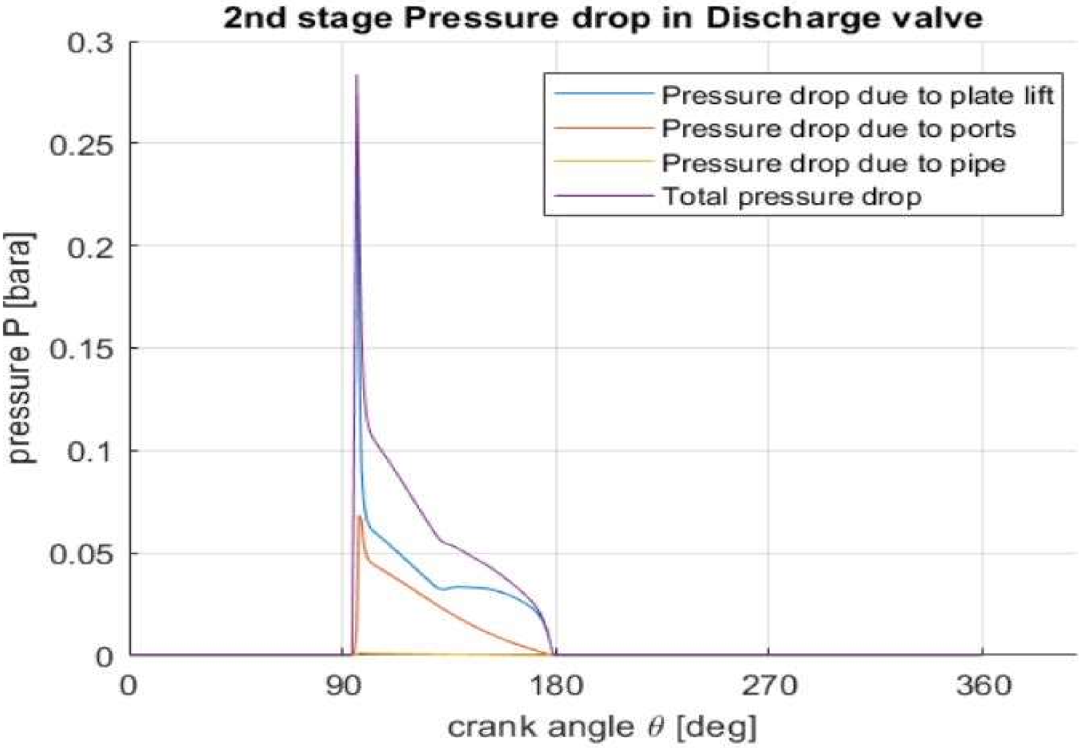

Figure 7.18 Pressure drop in 2nd stage discharge valve-crank angle plot

- 2nd Reed kinematic quantities – Crank angle Diagram

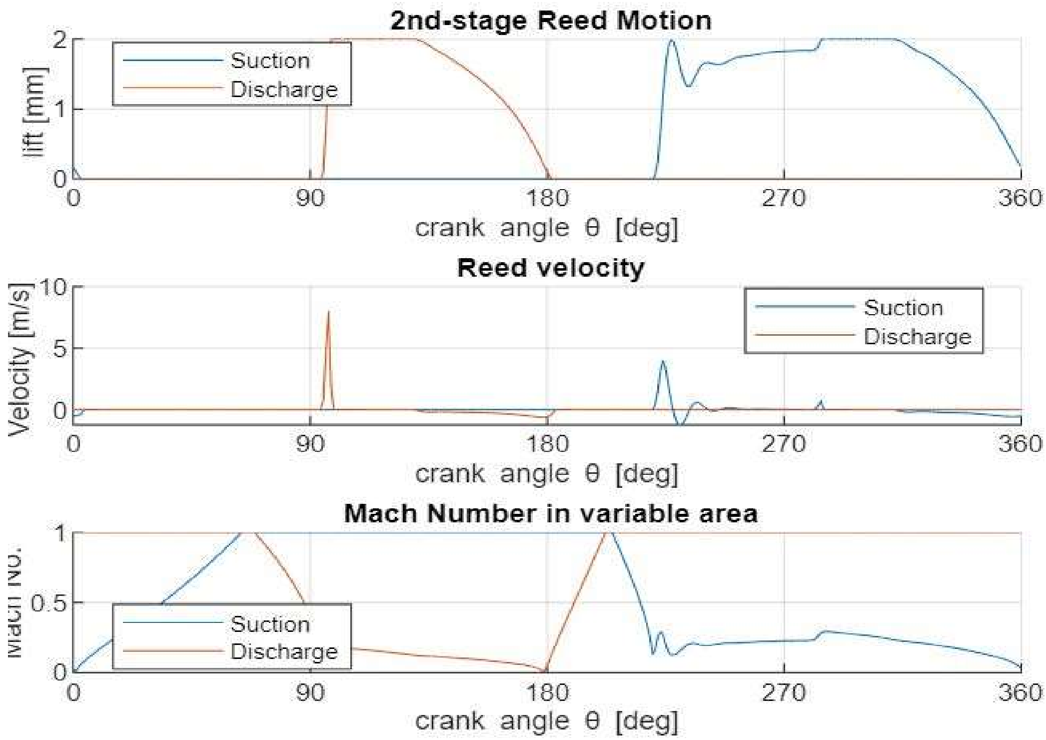

Figure 7.19 2nd Reed lift -crank angle plot

As can be seen from the results of the model @1274 rpm and @1744 rpm this valve is characterised by low pressure drops as the air passes through the valve compared to the reed, but at the same time with these parameters it allows a lower flow rate, this aspect has been summarised in Tab.7.8 and Tab.7.10 where the improvements of the new valve deisgn are underlined.

In Tab.7.7 and Tab.7.9 the main numerical efficiencies are listed as previously done for the reed valve. As stated before a lower pressure drop inside the valve results in lower mechanical power.

	First stage		Second stage	
	Suction	Discharge	Suction	Discharge
Pressure losses [kW]	0,0462	0,0301	0,0134	0,0089
Over pressure [bar]	0,1	0,21	0,15	0,25

	First stage	Second stage	Overall
FAD [l/s]	7,08	7,07	7,07
Air displacement [l/s]	10,11	9,16	10,11
Volumetric efficiency	0,70	0,77	0,70
Shaft Power [kW]	1,97	1,81	3,78
SER [J/l]	278,16	255,9	534,45

Table 7.9 Numerical Efficiencies @1274 rpm

Efficiencies	Feather Model				Reed Model			
	Fist stage		Second stage		First Stage		Second Stage	
	S	D	S	D	S	D	S	D
Overpressure [bar]	0,1	0,21	0,15	0,25	0,12	0,35	0,37	0,62
Pressure losses [kW]	0,0462	0,0301	0,0134	0,0089	0,0560	0,0822	0,0624	0,0501
Shaft Power [kW]	3,78				3,95			
FAD [l/s]	7,07				7,85			
Volumetric Efficiency	0,70				0,80			
SER [J/l]	534,45				502			

Table 7.10 Comparison between the two valves

7.3.2 Model results @1744 rpm

- P-V Diagram

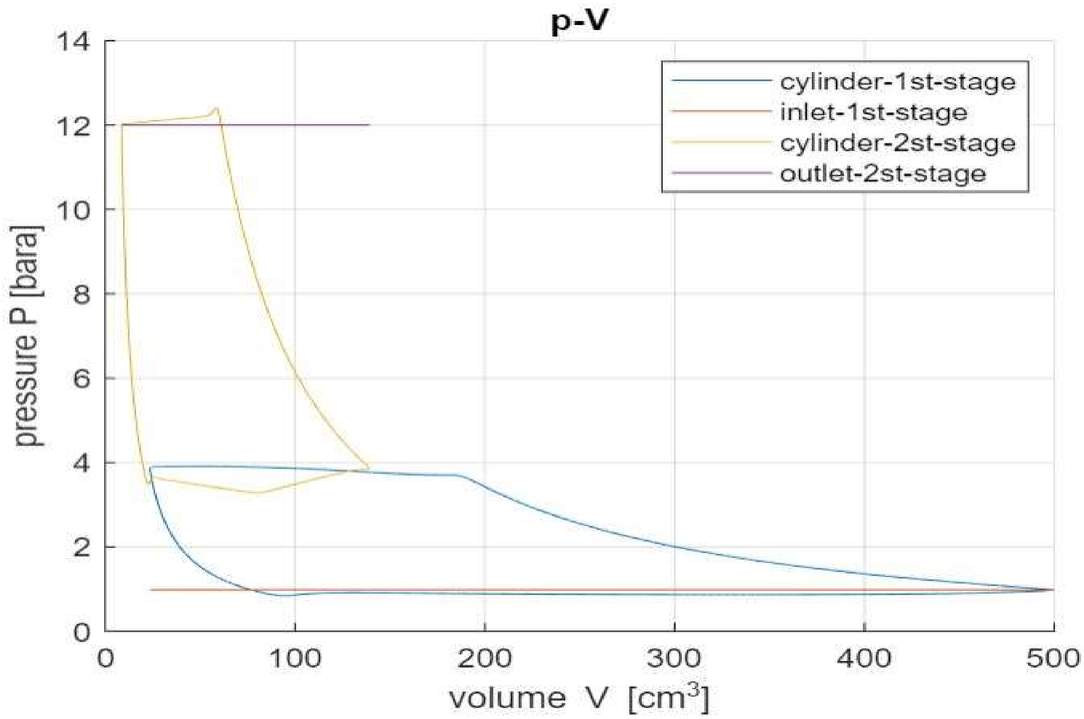

Figure 7.20 P-V Diagram

- 1st stage Pressure - Crank angle Diagram

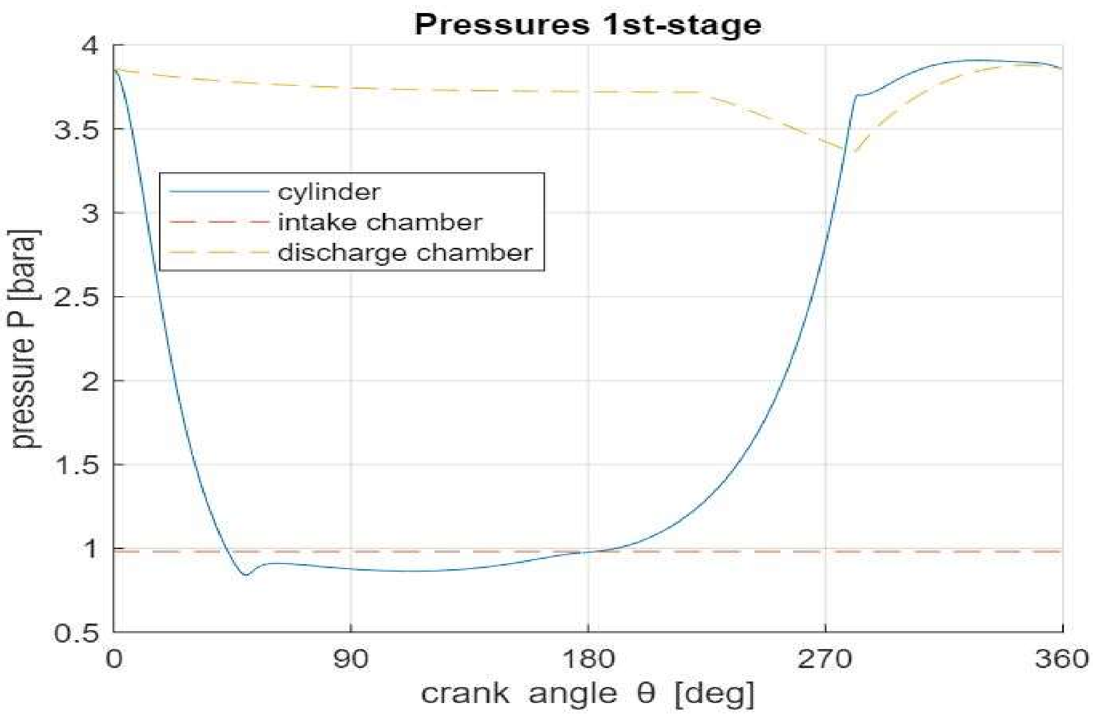

Figure 7.21 Pressure in 1st stage-Crank angle plot

- Pressure drop in 1st stage Suction valve – Crank angle Diagram

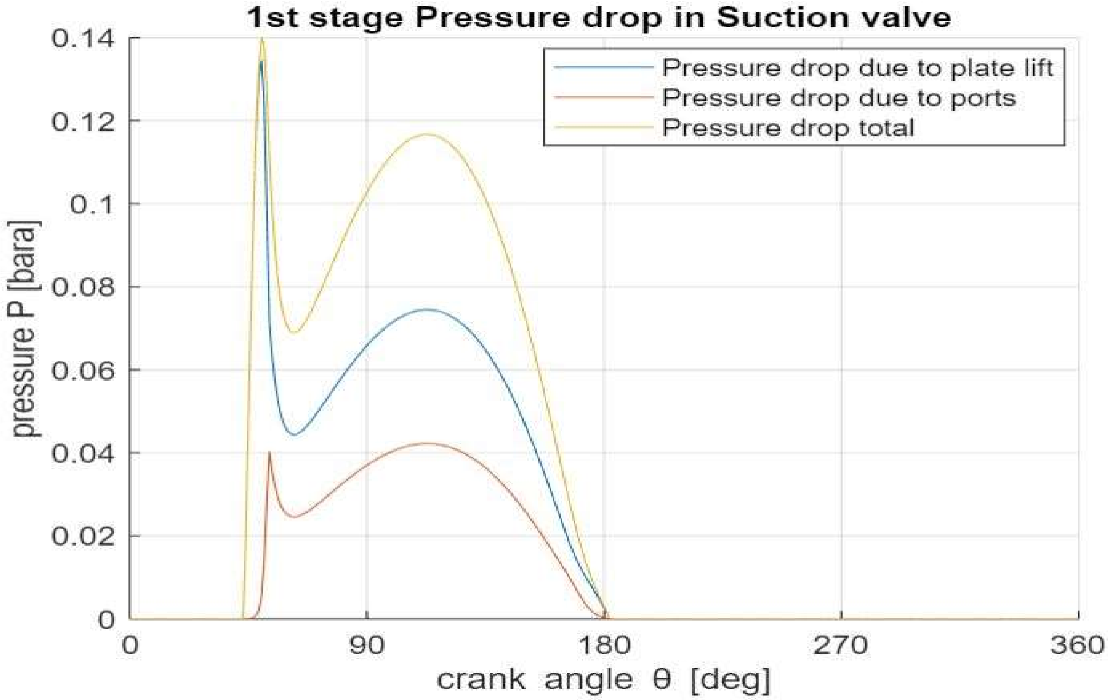

Figure 7.22 Pressure drop in 1st stage suction valve-crank angle plot

- Pressure drop in 1st stage Discharge valve – Crank angle Diagram

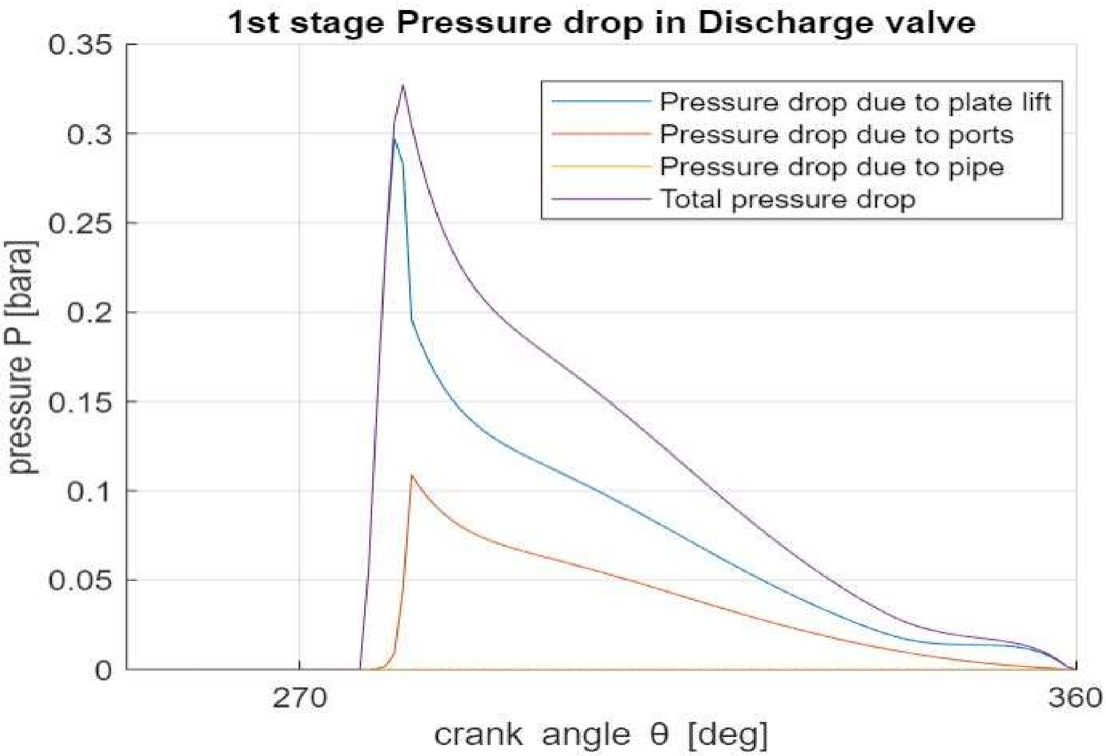

Figure 7.23 Pressure drop in 1st stage discharge valve-crank angle plot

- 1st Reed kinematic quantities – Crank angle Diagram

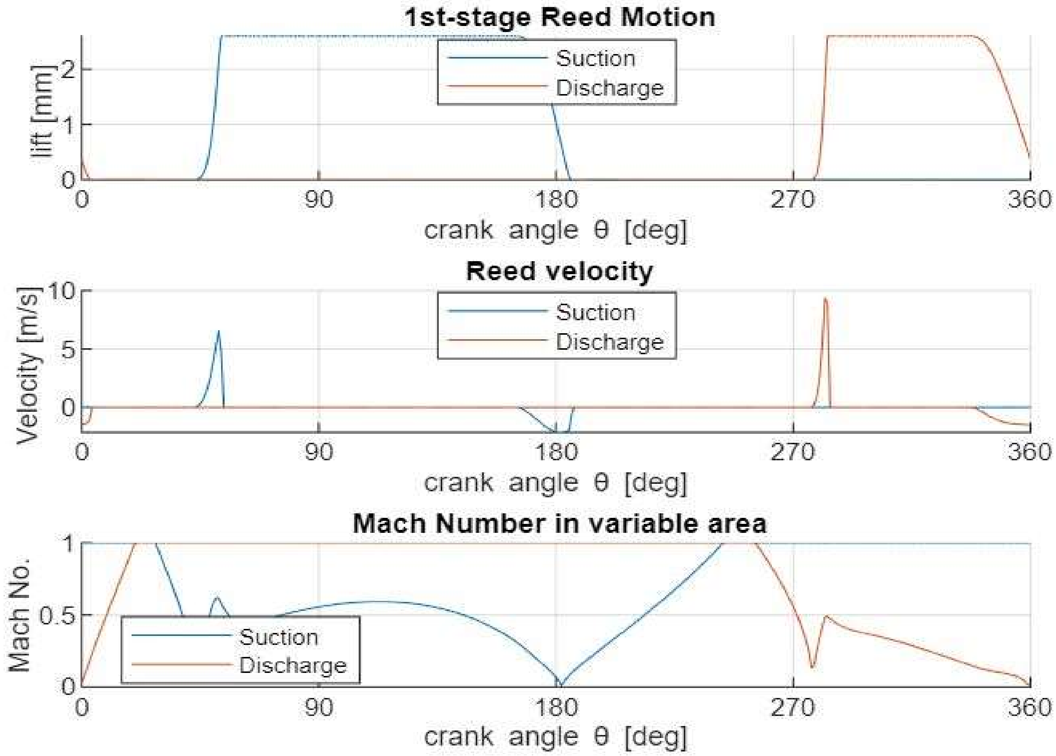

Figure 7.24 1st Reed lift -crank angle plot

- 2nd stage Pressure - Crank angle Diagram

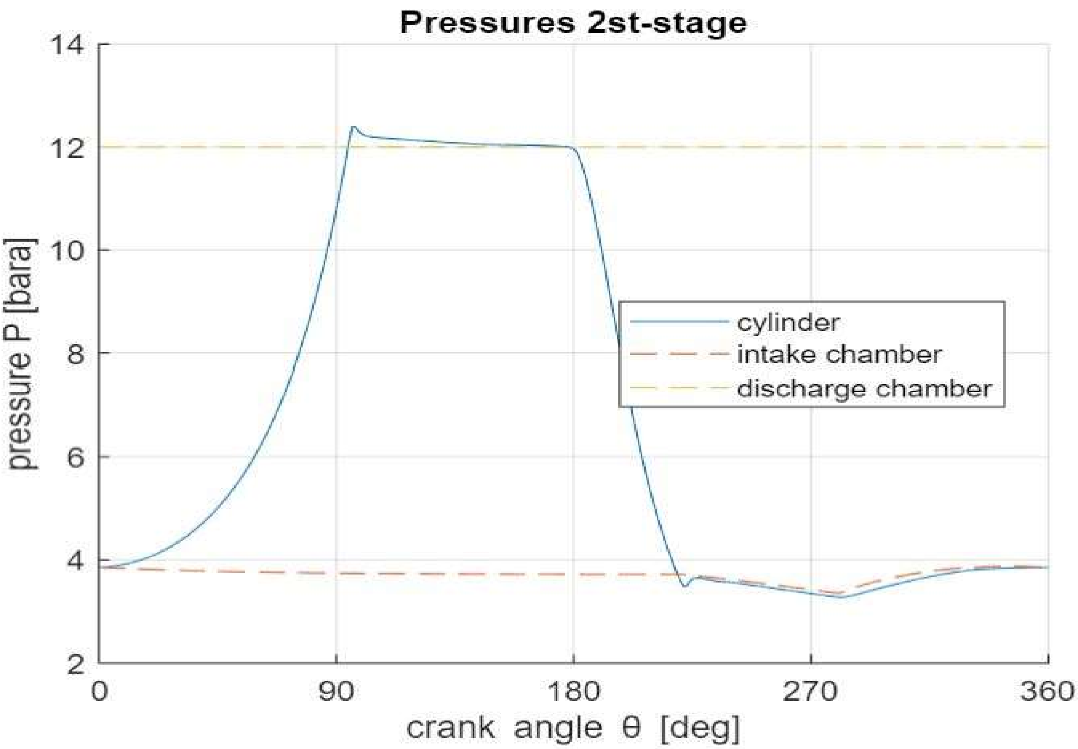

Figure 7.25 Pressure in 2nd stage-Crank angle plot

- Pressure drop in 2nd stage Suction valve – Crank angle Diagram

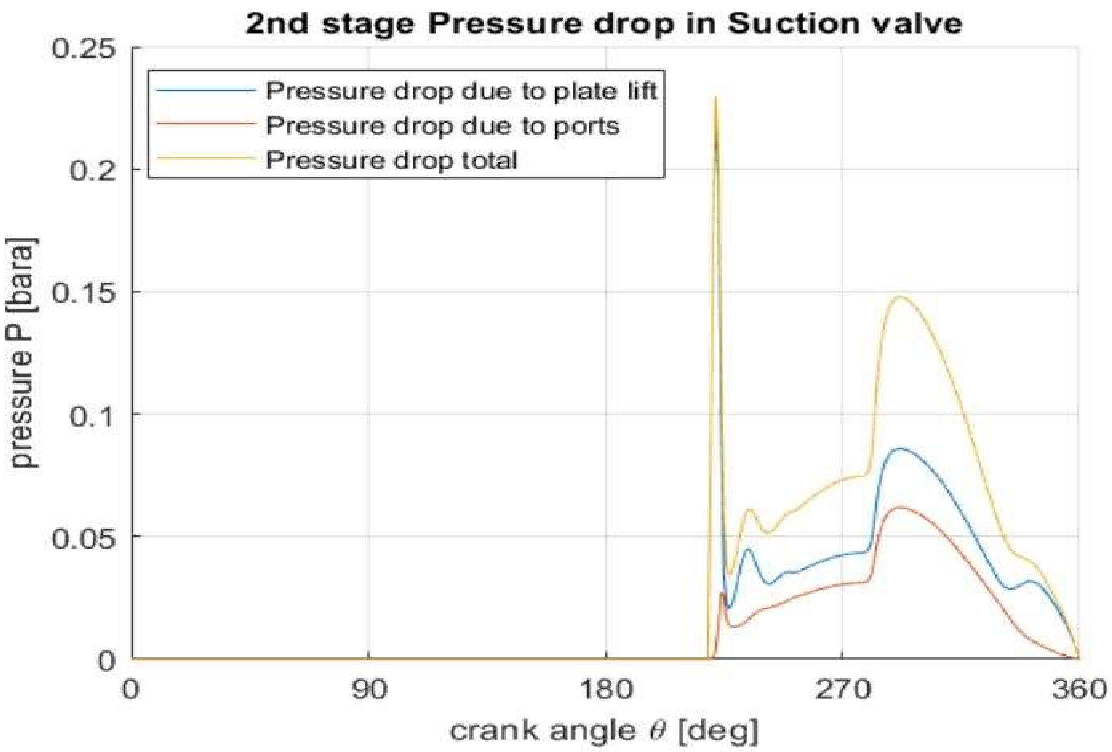

Figure 7.26 Pressure drop in 2nd stage suction valve-crank angle plot

- Pressure drop in 2nd stage Discharge valve – Crank angle Diagram

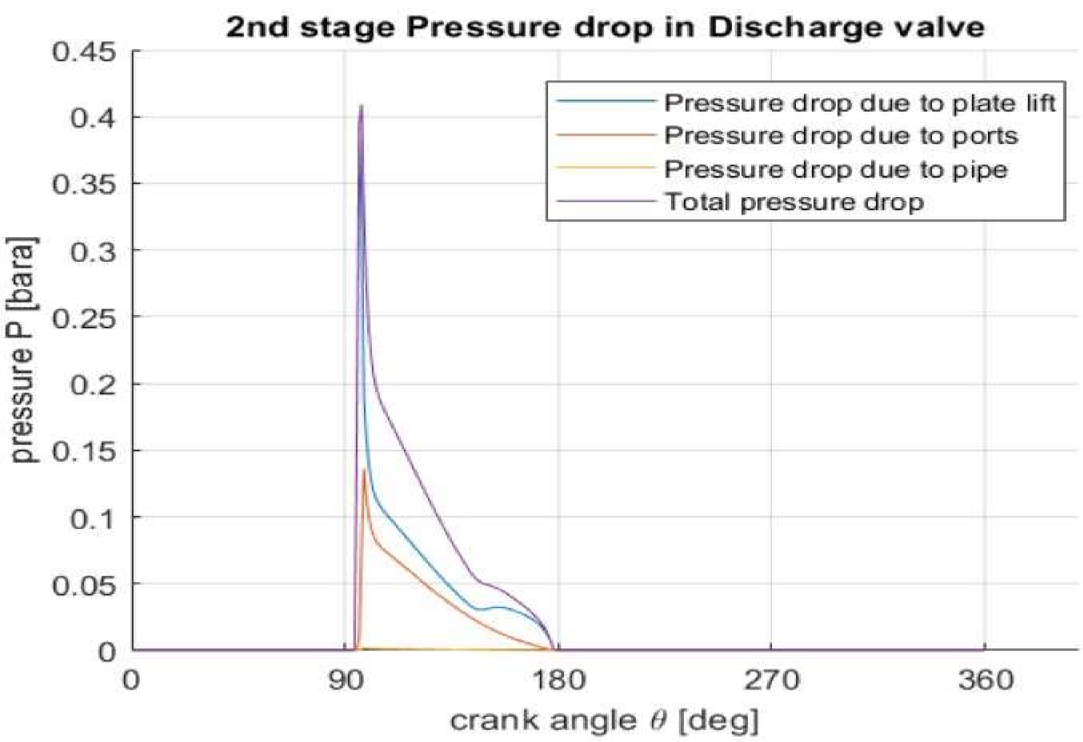

Figure 7.27 Pressure drop in 2nd stage discharge valve-crank angle plot

- 2nd Reed kinematic quantities – Crank angle Diagram

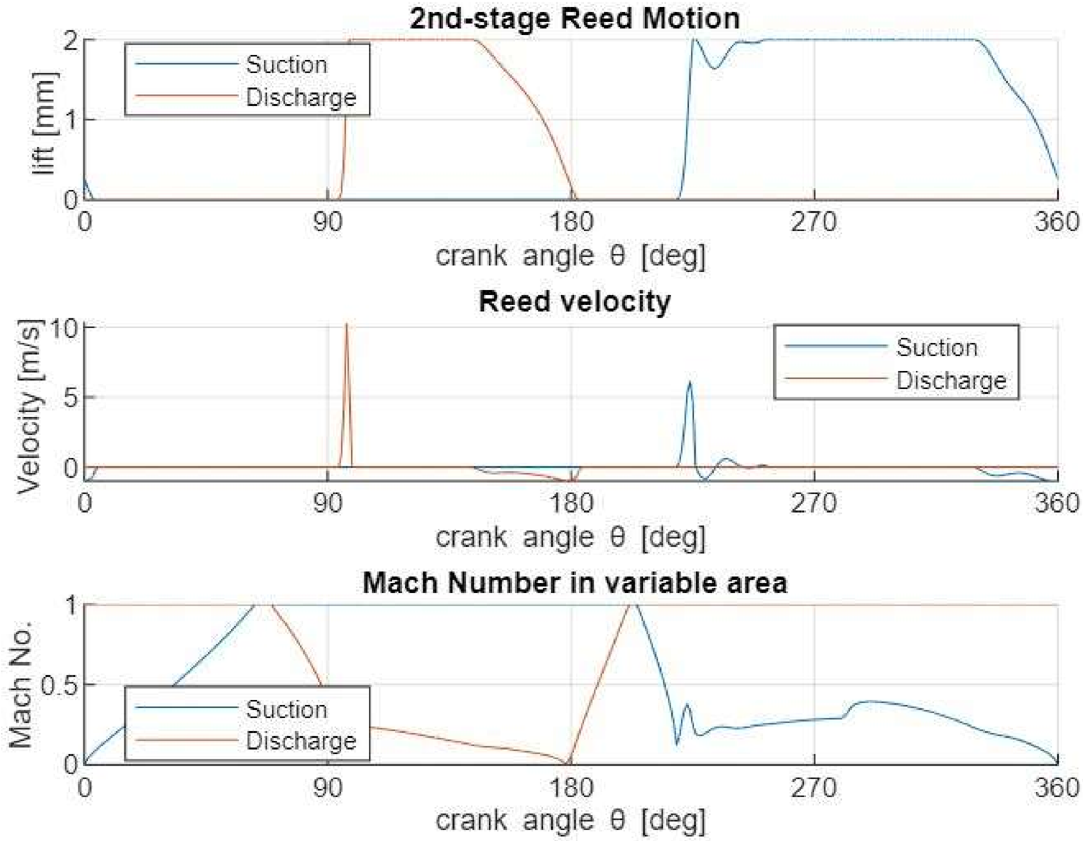

Figure 7.28 2nd Reed lift -crank angle plot

	First stage		Second stage	
	Suction	**Discharge**	**Suction**	**Discharge**
Pressure losses [kW]	**0,1157**	**0,0795**	**0,0299**	**0,0212**
Over pressure [bar]	**0,135**	**0,3**	**0,21**	**0,38**

	First stage	Second stage	Overall
FAD [l/s]	**9,58**	**9,24**	**9,24**
Air displacement [l/s]	**13,84**	**12,533**	**13,84**
Volumetric efficiency	**0,6922**	**0,74**	**0,67**
Shaft Power [kW]	**2,85**	**2,54**	**5,40**
SER [J/l]	**297,5**	**274,9**	**572,4**

Table 7.11 Numerical Efficiencies @1744 rpm

Efficiencies	Feather Model				Reed Model			
	Fist stage		Second stage		First Stage		Second Stage	
	S	D	S	D	S	D	S	D
Overpressure [bar]	0,134	0,3	0,23	0,38	0,15	0,72	0,69	1,2
Pressure losses [kW]	0,1157	0,095	0,0299	0,0212	0,1010	0,22	0,16	0,15
Shaft Power [kW]	5,40				6,3			
FAD [l/s]	9,24				10,88			
Volumetric Efficiency	67 %				77 %			
SER [J/l]	572,4				565,6			

Table 7.12 Comparison between the two valves

7.3.3 Comparison between model and experimental results

For the previous valve the measurements taken were exclusively for the flow rate (FAD), for the prototype analysed in this chapter the measurements also concerned the temperature and pressure in certain areas of the compressor unit .
This is because, as seen during the modelling phase, temperature plays an important role in the calculation of the quantities.
Especially if the analysis concerns a multi-stage compressor in which cooling takes place between the two compression stages so some thermal constraints must be set. In the flow diagram, visible in Fig.7.29, the main compressor components are represented as follows

- The components 2A 2B 2C and 2D stands for the chamber placed downstream and upstream of the valves
- 4A and 4B stand for the two Cylinders
- 5A and 5B stand for respectively for the intercooler and the cooler before the delivery tank
- 3A 3B 3C and 3D stand for the valves placed downstream and upstream of the two cylinders
- 7 stands for the delivery tank

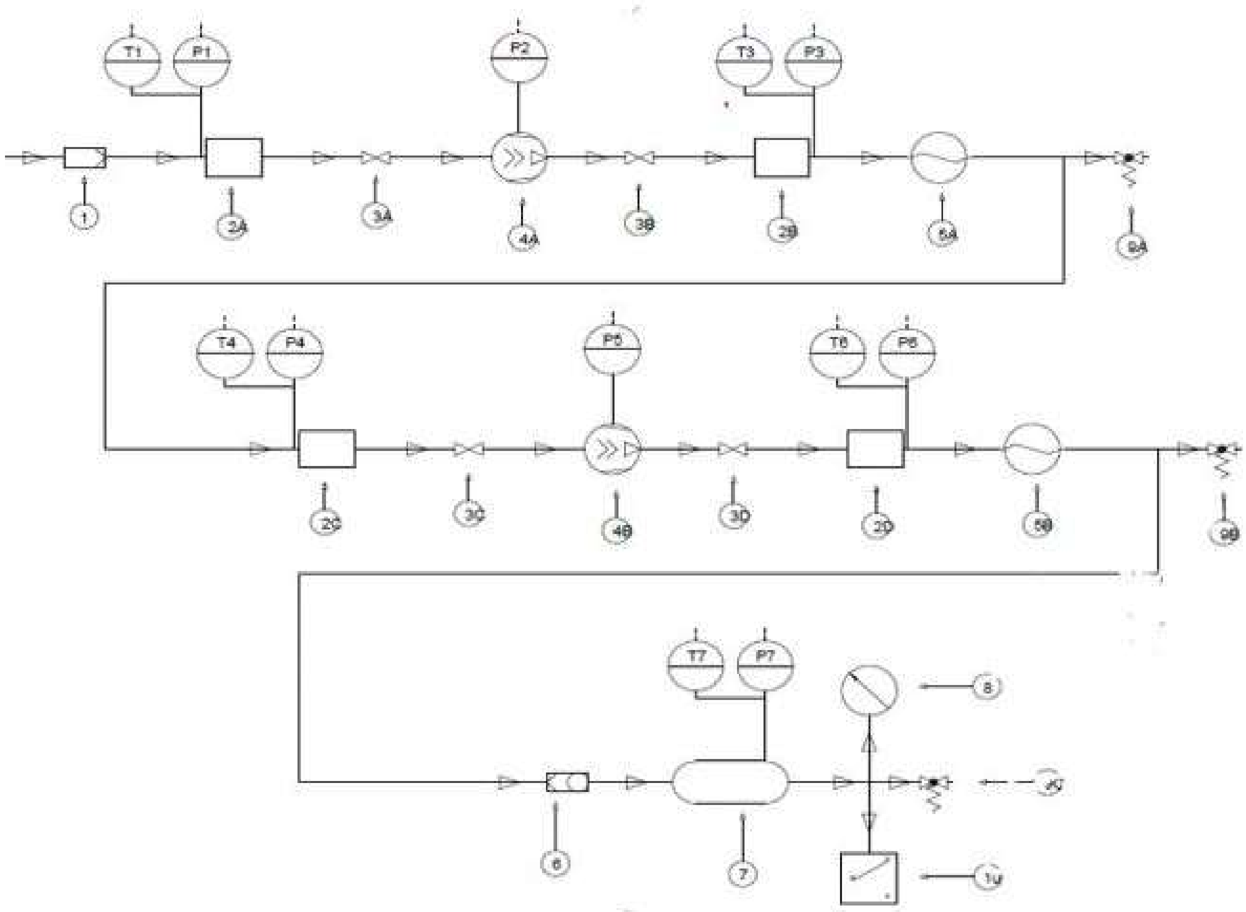

Figure 7.29 Measurements flowchart

The thermodynamic quantities (pressure and temperature), according to the flowchart in Fig.7.29, are measured downstream and upstream of the chambers mounted on the cylinders.

The tables below show the results of the measurements taken and those of the model, varying the compressor speed.

Comparing model and experimental results, the relative error in absolute value for all quantities remains below 5% except for the temperature at the inlet of the second stage @1274 rpm.
As stated the heat transfer aspect was not dealt with in depth in this work, the temperatures were set using the same procedure, in order to standardise the model, for both speeds .

	Model Results	**Experimental results**	**Error**
Air Displacement [l/s]	**606**	**606,72**	**-0,12%**
Mechanical Power [kW]	**3,78**	**3,96**	**-4,55 %**
T inlet [degC]	**29,55**	**29**	**1,90%**
T outlet 1st stage [degC]	**168,4**	**170**	**-0,94 %**
T inlet 2nd stage [degC]	**90,77**	**83**	**9,36 %**
T outlet 2nd stage [degC]	**175**	**168**	**4,17 %**
FAD [l/s]	**424,2**	**441**	**-3,81 %**
Volumetric efficiency	**70%**	**73 %**	**-4,11 %**

Table 7.13 Numerical Efficiencies @1274 rpm

	Model Results	**Experimental results**	**Error**
Air Displacement [l/s]	**830,76**	**830,5**	**0,03 %**
Mechanical Power [kW]	**5,40**	**5,78**	**-6,57**
T inlet [degC]	**31,63**	**31**	**2,03 %**
T outlet 1st stage [degC]	**196,4**	**201**	**-2,29 %**
T inlet 2nd stage [degC]	**95,15**	**98**	**-2,91 %**
T outlet 2nd stage [degC]	**205**	**197**	**4,06 %**
FAD [l/s]	**554**	**536**	**3,36 %**
Volumetric efficiency	**67 %**	**64 %**	**4,69 %**

Table 7.14 Numerical Efficiencies @1744 rpm

7.4 Sensitivity analysis and design phase

As was previously demonstrated, the kind of valve can provide entirely distinct lift and pressure patterns, as well as numerical outputs. The design of a particular configuration's geometrical aspects, such as the thickness of the valve plate or the ports area, may now be changed to show that this aspect also occurs.

The research that was completed to determine how a group of independent factors affect some dependent variables is known as a sensitivity analysis.

By changing the thickness of the reed in the valve assembly, the two main parameters that are affected by this variation are :

- The bending stiffness of the valve
- The reed inertia
- The maximum lift of the reed within the cavity of the plate on which it is supported, considering the hollow dept is kept constant

In order to best appreciate the variations in efficiency due to the single change in thickness, this analysis was only conducted on the second stage intake valve.

The current thickness is for the second stage valve is 0.3 mm, in this sensitivity study the following thicknesses have been analysed:

- 0,15 mm
- 0,25 mm
- 0,4 mm
- 0,5 mm
- 0,6 mm
- 0,8 mm

0,15 mm

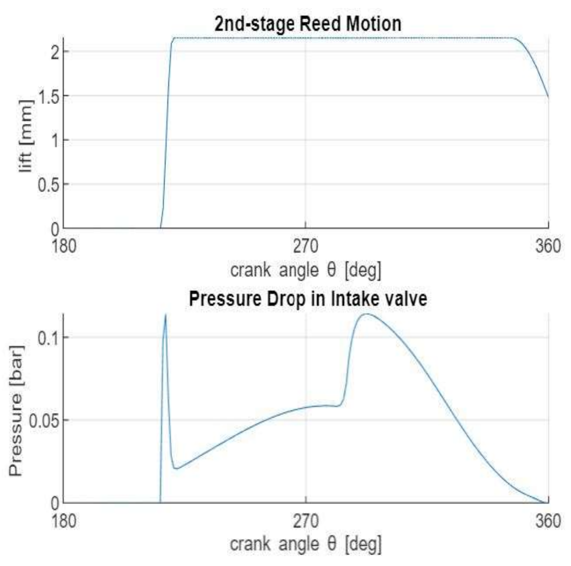

0,25mm

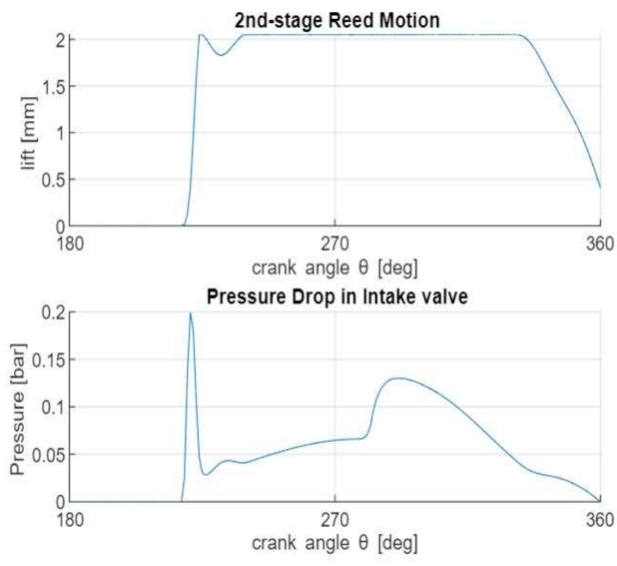

Figure 7.30 Reed lift and Pressure drop

0,4 mm **0,5 mm**

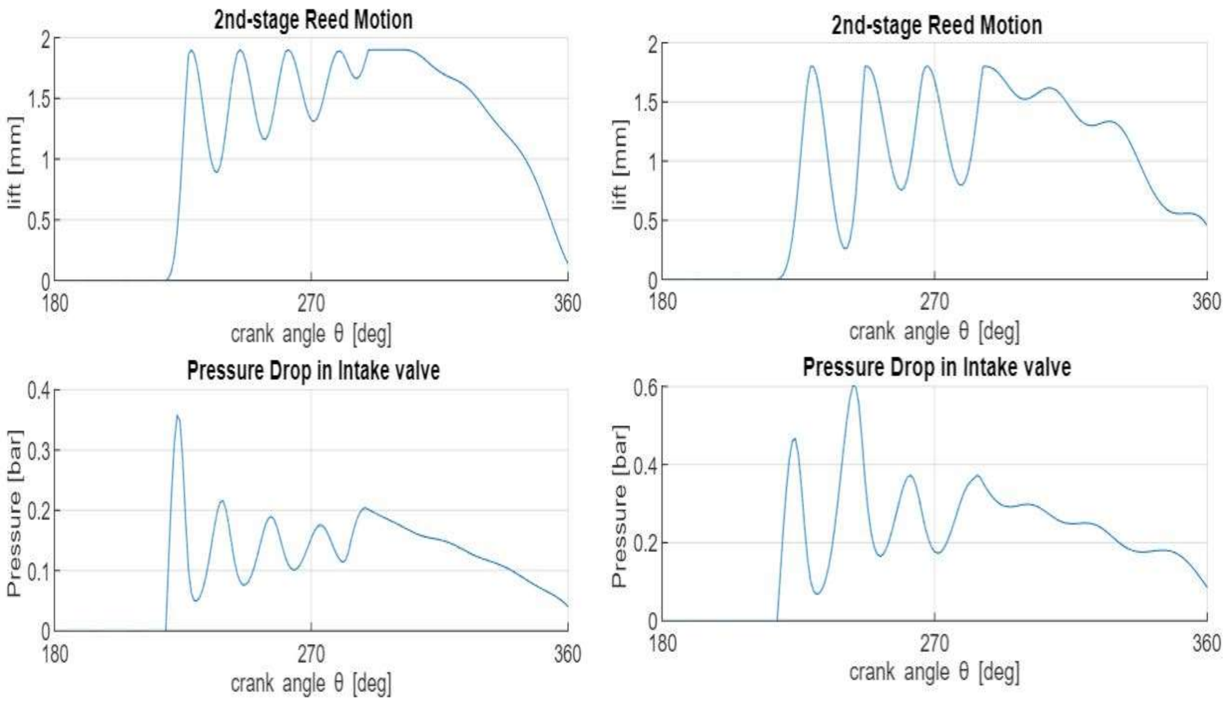

Figure 7.31 Reed lift and Pressure drop

0,6 mm **0,8 mm**

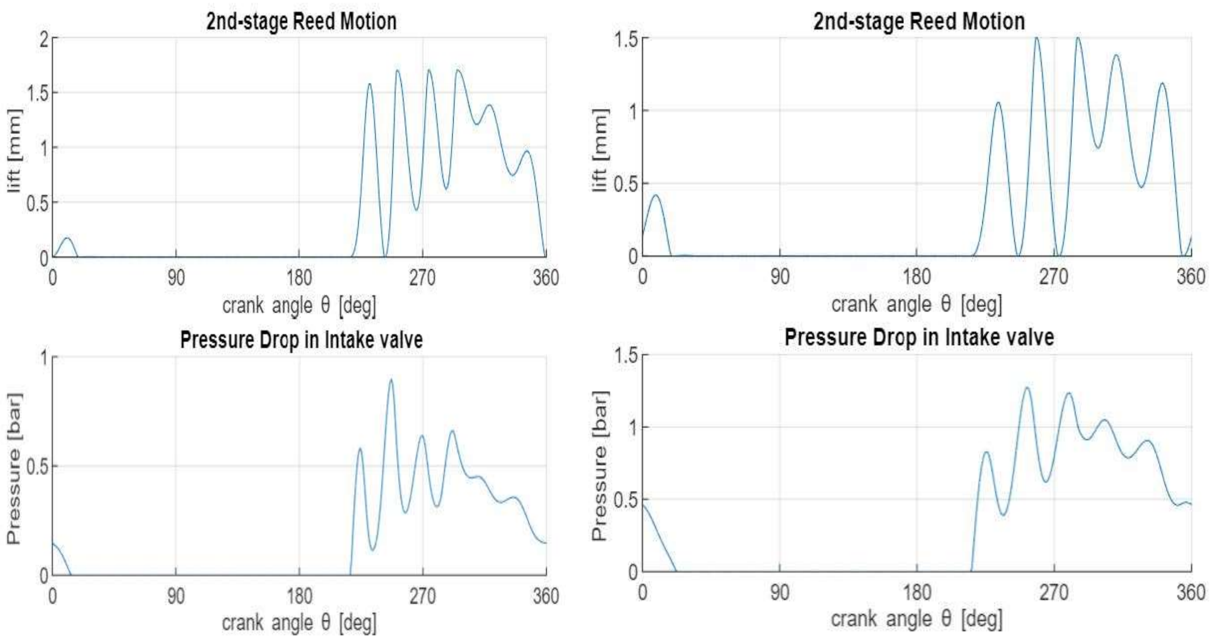

Figure 7.32 Reed lift and Pressure drop

The model outputs can now be computed for each of these configurations.

- Shaft Power

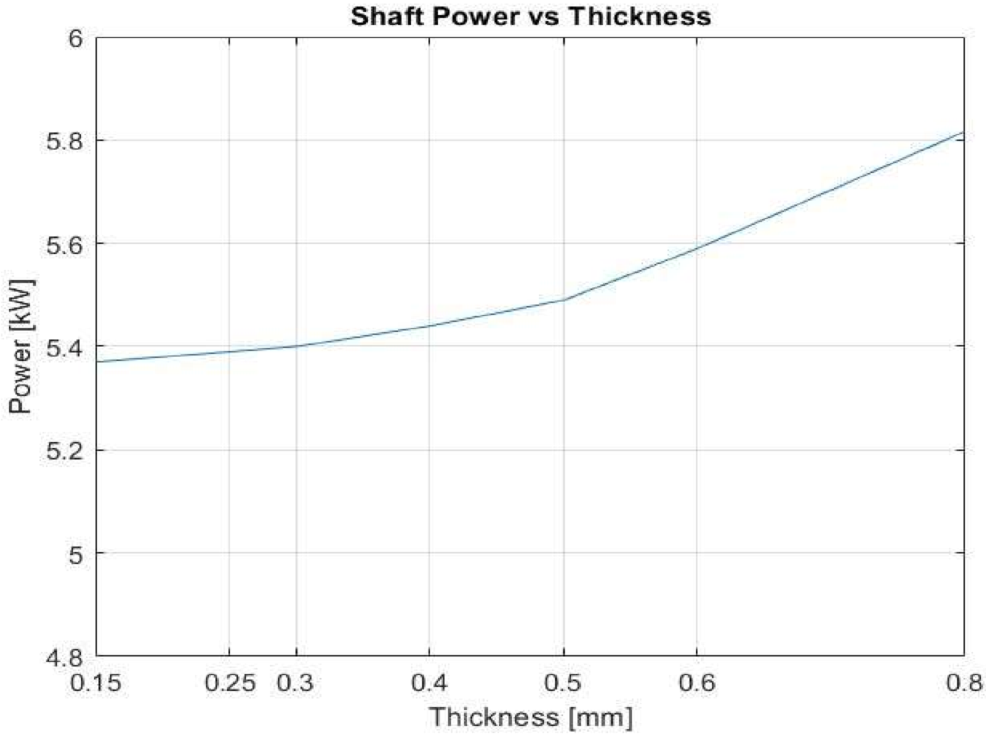

Figure 7.33 Shaft Power vs Thickness

- Reed Impact velocity

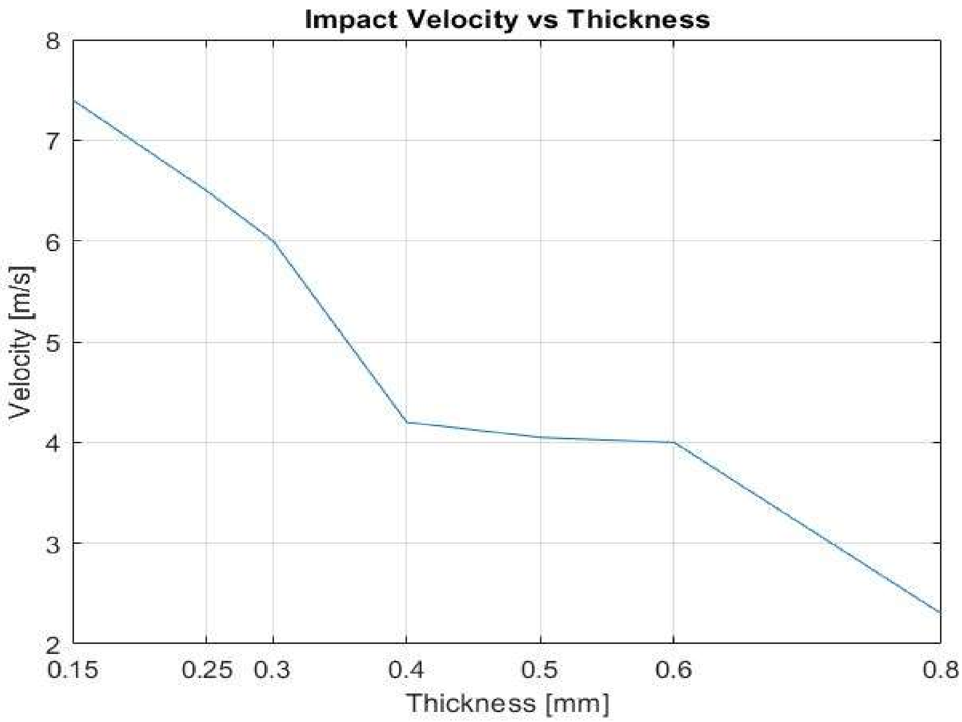

Figure 7.34 Impact Velocity vs Thickness

- Valve Pressure losses

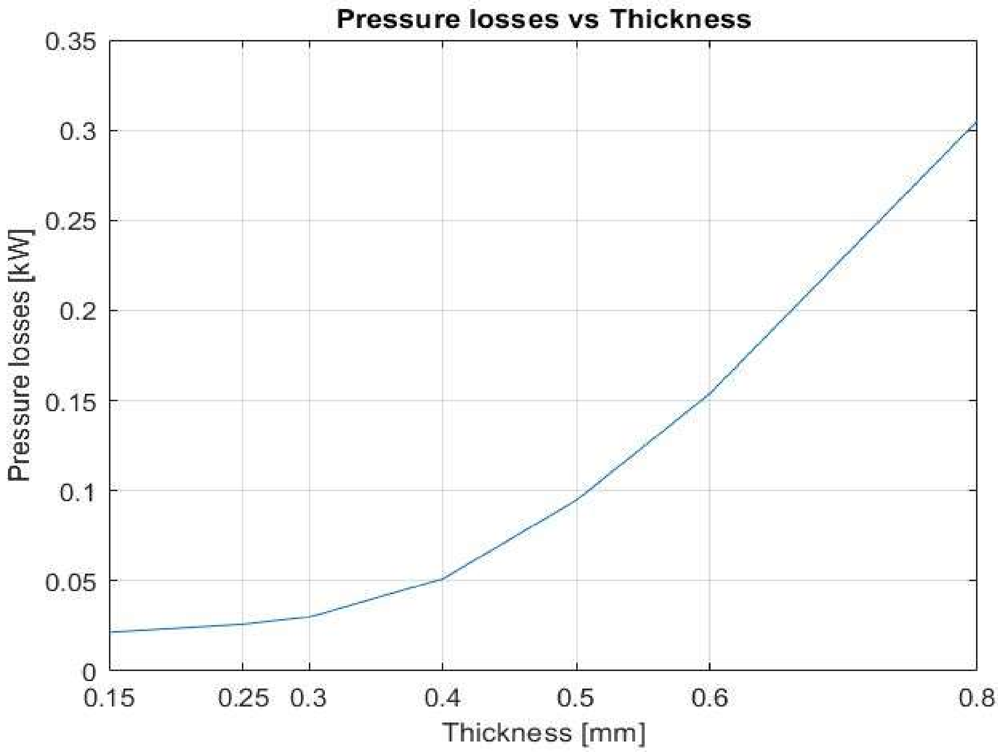

Figure 7.35 Pressure Losses vs Thickness

- Overpressure

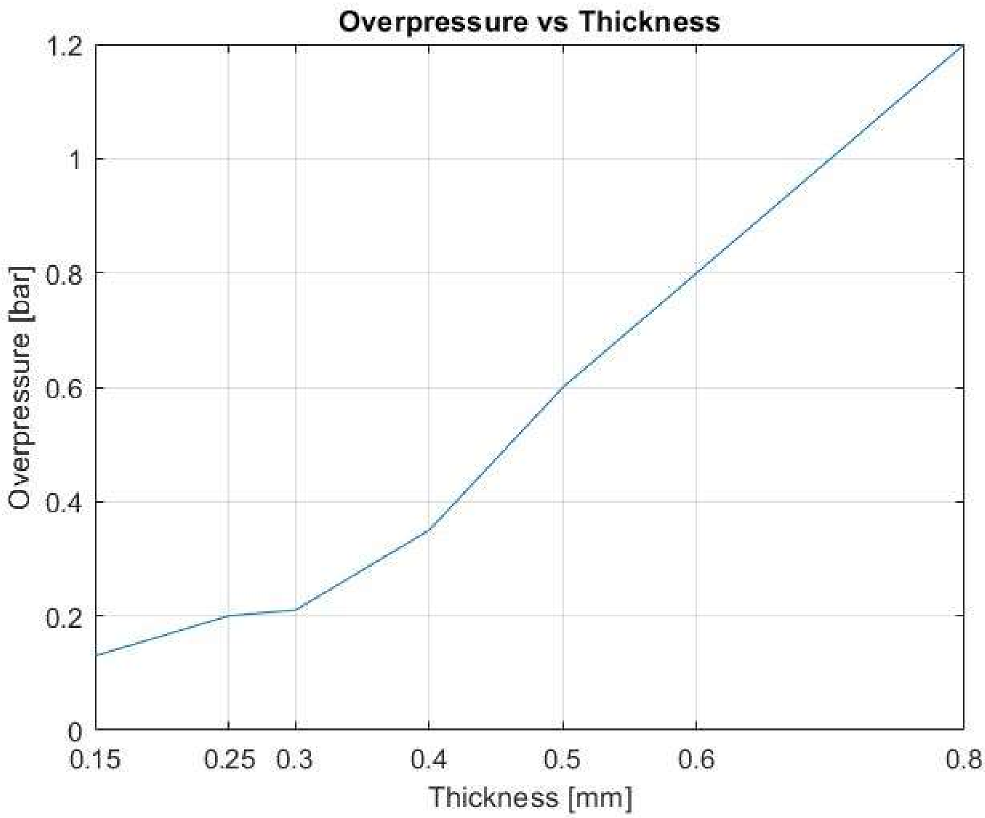

Figure 7.36 Overpressure vs Thickness

- Compressor FAD

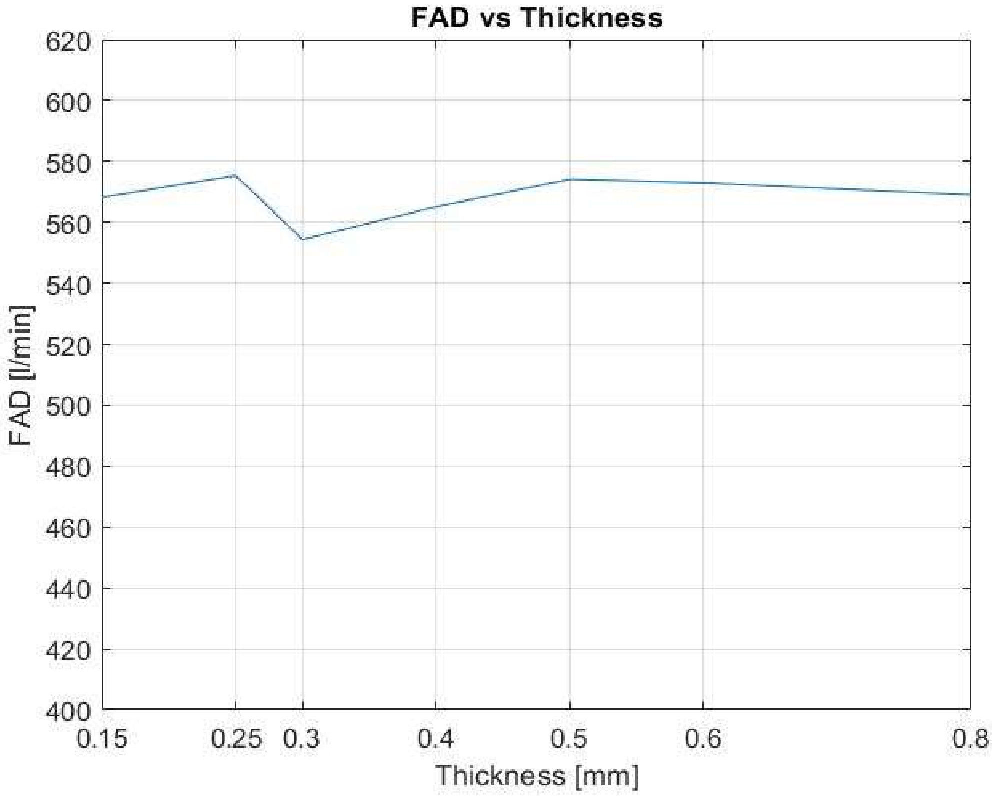

Figure 7.37 FAD vs Thickness

- Volumetric Efficiency

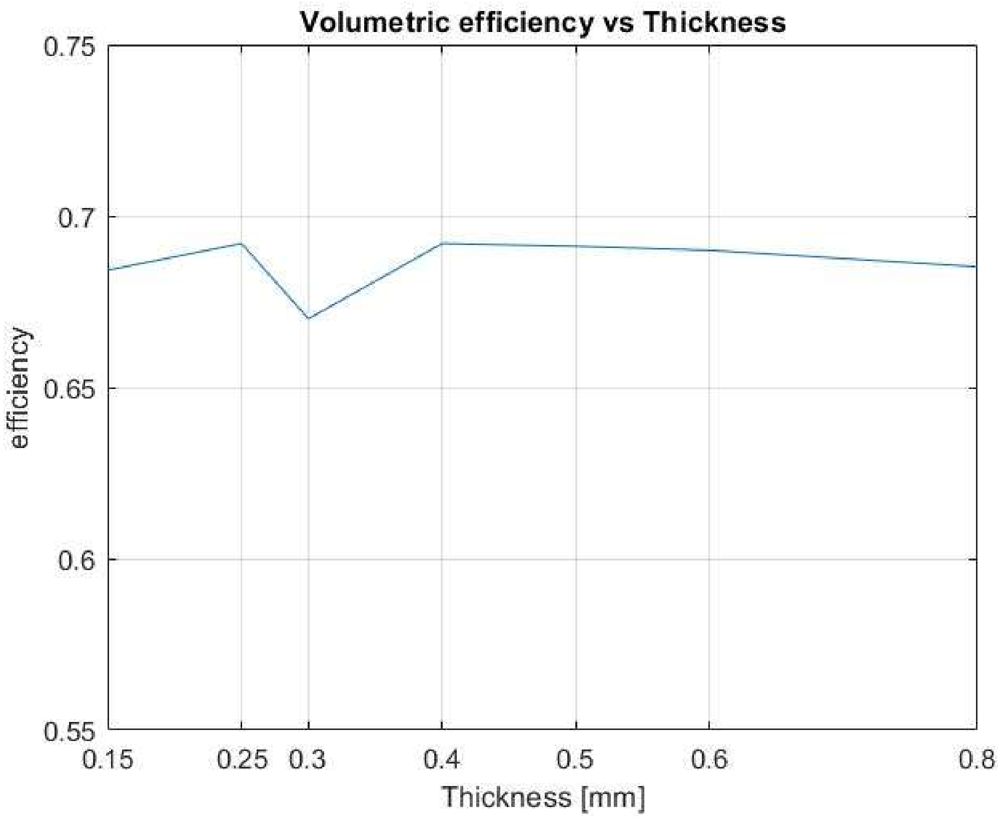

Figure 7. 38 Volumetric Efficiency vs Thickness

The analysis shows how increasing the thickness of the reed during lift-up causes the reed to "flutter" and on the other hand decreases the speed at which the reed valve impacts on the plate cavity. Another aspect that can be noted is that by increasing the thickness of the valve, the pressure drops due to the presence of the valve increase accordingly.

As mentioned above, the second parameter on which a sensitivity analysis can be conducted is the area of the ports through which air enters in the valve .
Changing this parameter will partly affect the dynamics of the reed inside the valve, the pressure drops due to the passage inside the valve and finally the equivalent Clearance length, which is why differences in volumetric efficiency can be expected.

A strong assumption for this study is that the discharge coefficient remains equal to the value calculated through the CFD analysis that was performed on the current valve design.
The design value of the ports Area is equal to 130 mm^2. In this sensitivity study the following Ports Area have been analysed:

- 76,152 mm^2
- 77,12 mm^2
- 99,25 mm^2
- 146,52 mm^2
- 152,52 mm^2

Area 76,152 mm^2 **Area 77,12 mm^2**

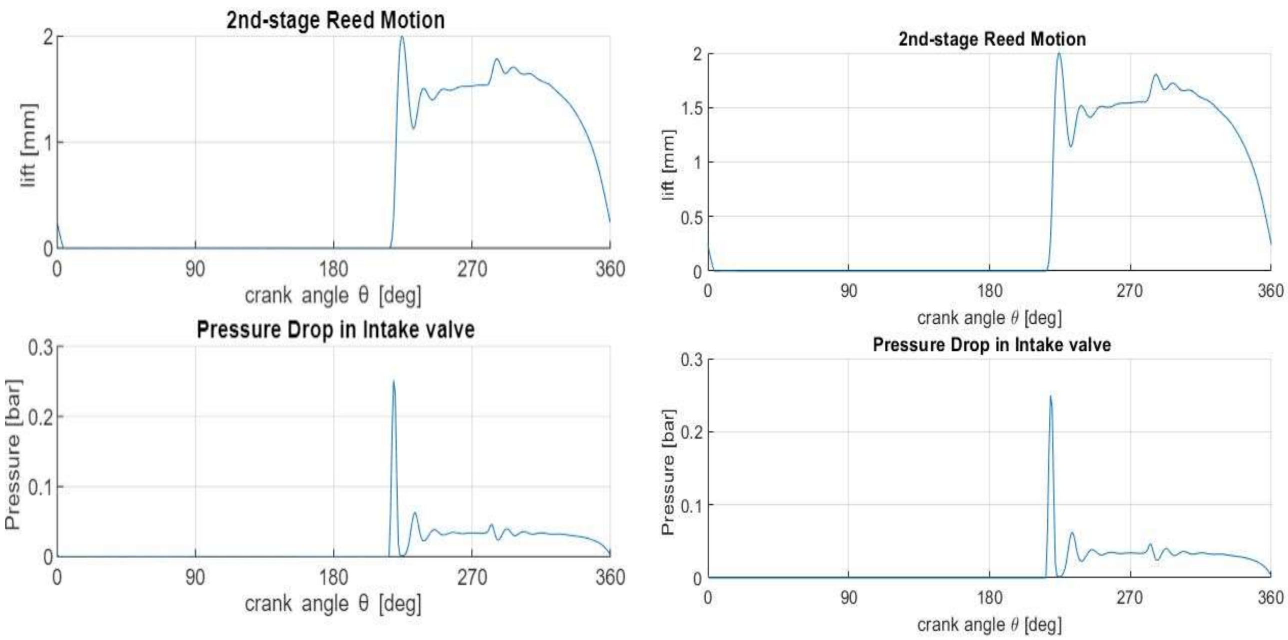

Figure 7.39 Lift and Overpressure

Area 99,25 mm^2

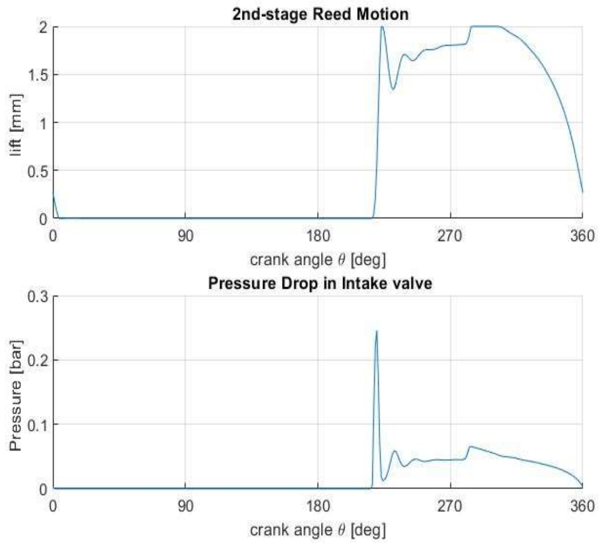

Area 146,52 mm^2

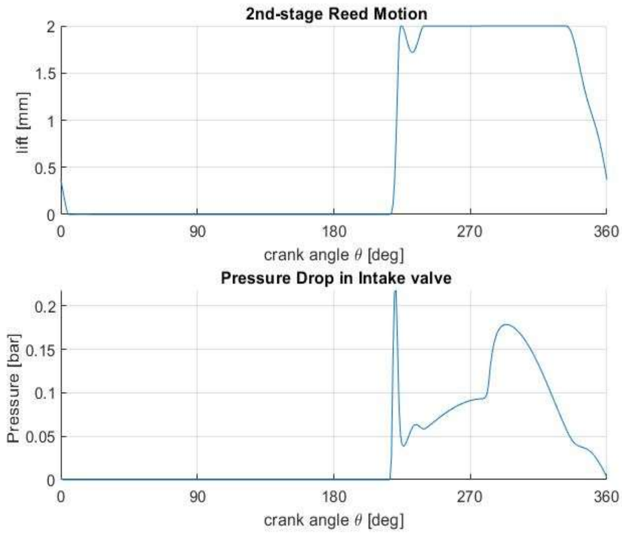

Figure 7.40 Lift and Overpressure

Area 152,52 mm^2

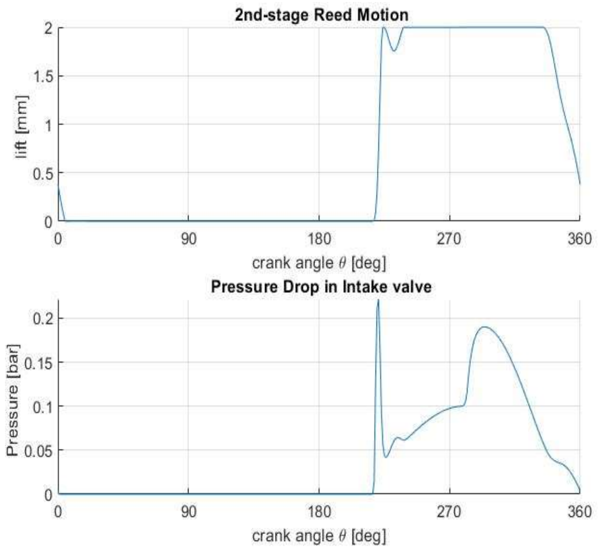

Figure 7.41 Lift and Overpressure

The model outputs can now be computed for each of these configurations.

- Shaft Power

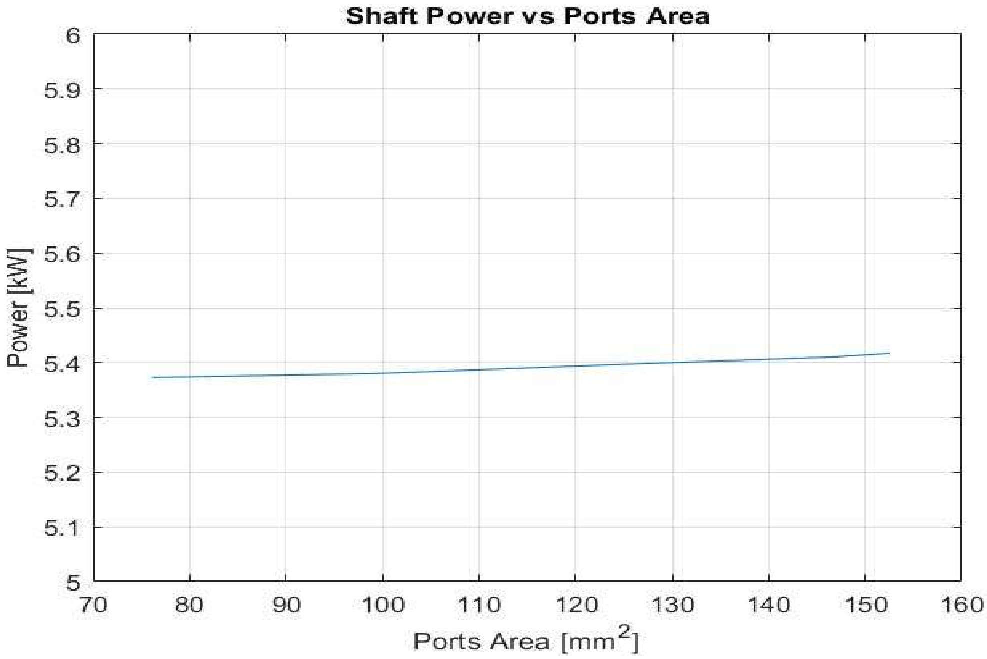

Figure 7.42 Shaft Power vs Ports Area

- Impact Velocity

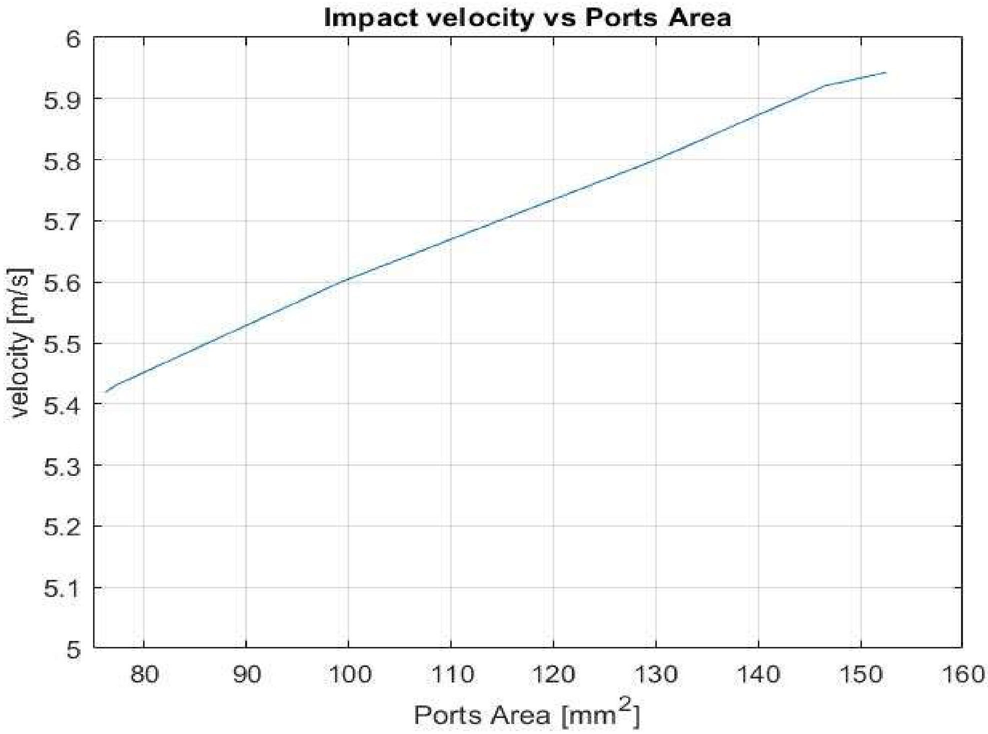

Figure 7.43 Impact Velocity vs Ports Area

- Pressure Losses

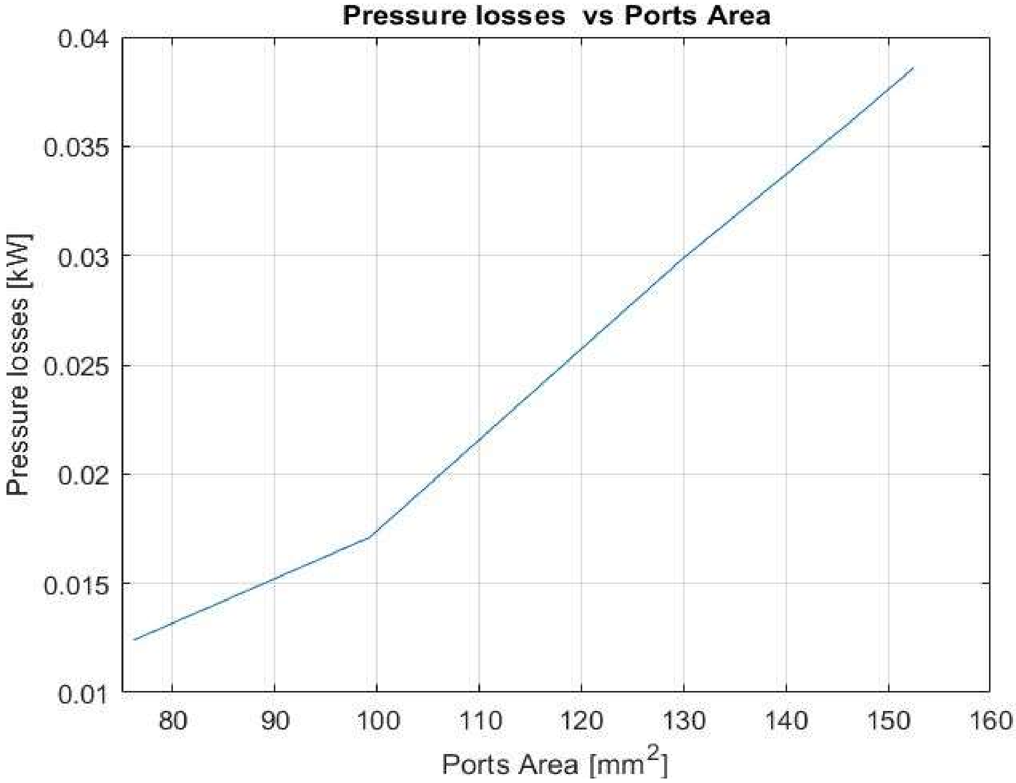

Figure 7.44 Pressure Losses vs Ports Area

- Overpressure

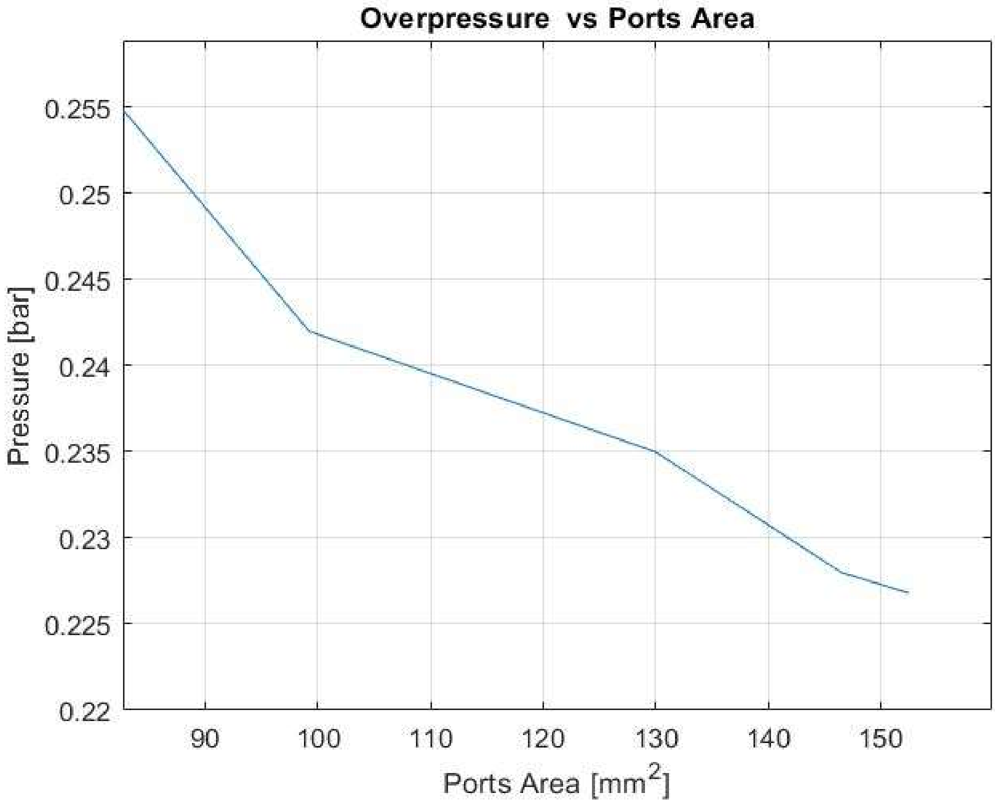

Figure 7.45 Overpressure vs Ports Area

- Equivalent Clearance Length

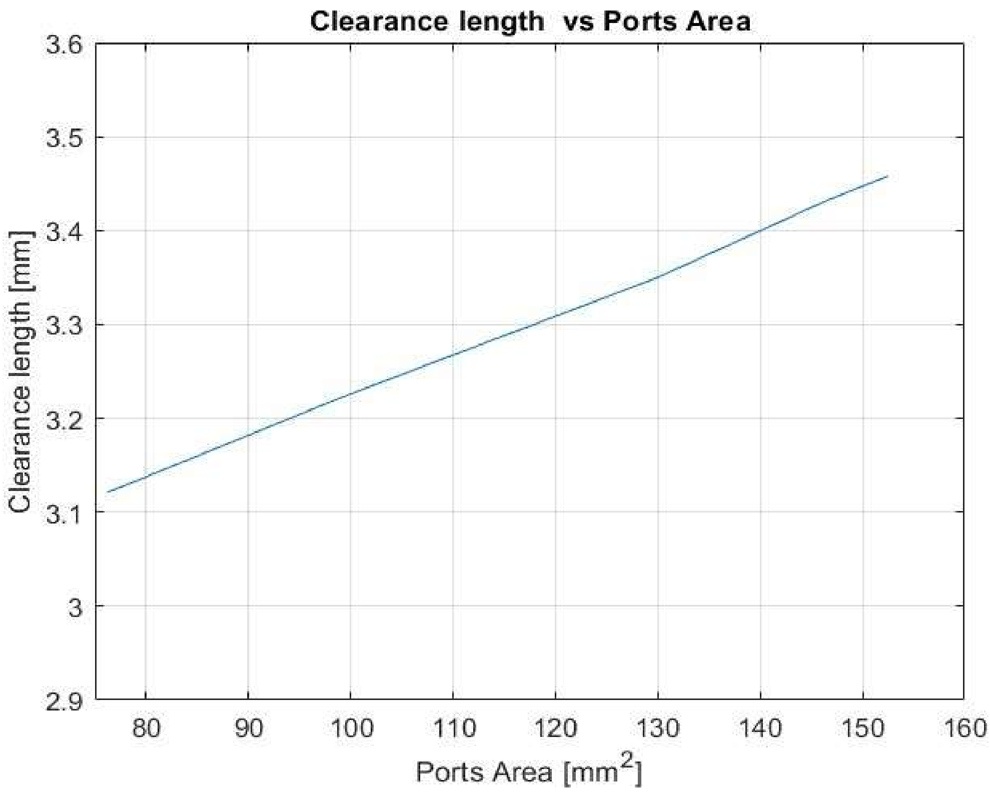

Figure 7. 46 Clearance length vs Ports Area

- Equivalent Clearance Length

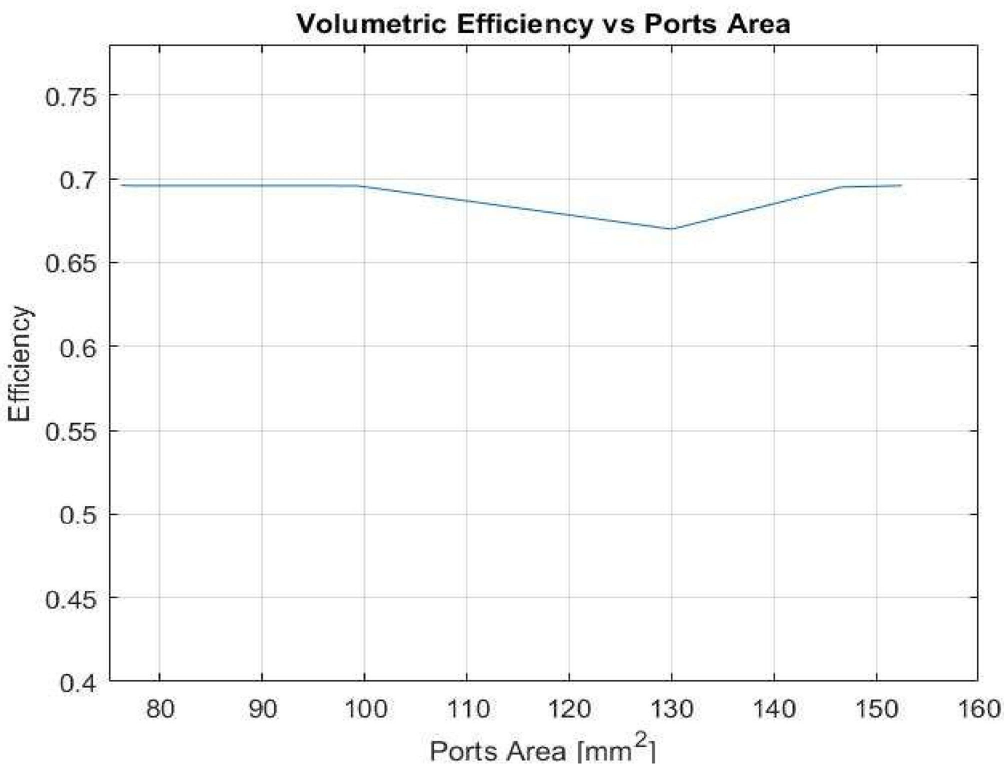

Figure7. 47 Volumetric efficiency vs Ports Area

Although it has been said previously that volumetric efficiency decays as the dead volume ratio increases from this sensitivity analysis, it can be seen that by varying the area of the valve ports, the length c increases linearly with respect to the area while the volumetric efficiency remains essentially constant.

As mentioned at the beginning about the influence of the area of the ports on performance, increasing the area of the ports has repercussions in the first instance on the dynamics of the reed in fact as can be seen from the Fig.7.39, the impact velocity of reed increases as the area of the ports increases.

In this instance, the two most representative factors have been taken into account, but the impact of each model input might theoretically be examined in a similar manner, as done before varying the crankshaft speed.

Once the valve model has been compared and possibly validated with experimental results, the sensitivity analysis may be a very helpful tool for understanding a phenomenon's behaviour and the importance of the factors that control the valve and piston compressor performance and the Simscape model can be a tool to support the design phase of compressor valves.

.

8 Conclusion and Future developments

During the development of this work, certain simplifications were accepted which at the same time did not substantially affect the quality of the results.

First of all, the heat exchange that takes place between the air inside the compressor and the surrounding environment was not fully developed.

Due to the working fluid being overheated, heat transfer inside the cylinder of a reciprocating compressor reduces volumetric efficiency. In order to obtain greater efficiency, it is vital to comprehend the heat transport phenomena inside the cylinder. There are now a number of empirical correlations that can be found in the literature that are used in simulation tools because they are simple to use and offer quick results with high accuracy compared to more intricate numerical models for heat transport. In literature [28] the authors utilised correlations based on the Reynolds number and the non-dimensional Nusselt number. The expression of characteristic velocity for Reynolds number, together with coefficients a, b, and c, are the primary distinctions between all correlations.

$$Nu = aRe^b Pr^c$$

$$Re = \frac{uD}{\nu}$$

$$St = f(C_f)$$

Woschni	$Nu = 0.035\mathrm{Re}^{0.7}$	$\mathrm{Re} = \frac{uD}{\nu}$	$u = 6.618 \cdot u_p$ - opened valves $u = 2.28 \cdot u_p$ - closed valves
Annand	$Nu = 0.7\mathrm{Re}^{0.7}\mathrm{Pr}^{0.7}$	$\mathrm{Re} = \frac{uD}{\nu}$	u_p
Adair	$Nu = 0.053\mathrm{Re}^{0.8}\mathrm{Pr}^{0.6}$	$\mathrm{Re} = \frac{uD_e}{\nu}$, $D_e = \frac{6 \cdot \text{Cylinder volume}}{\text{Cylinder area}}$	$u = 2\omega[1.04 + \cos(2\alpha)]$ $\quad \frac{3}{2}\pi < \alpha < \frac{1}{2}\pi$ $u = \omega[1.04 + \cos(2\alpha)]$ $\quad \frac{1}{2}\pi < \alpha < \frac{3}{2}\pi$
Disconzi *Compression*	$Nu = 0.08\mathrm{Re}^{0.8}\mathrm{Pr}^{0.6}$	$\mathrm{Re} = \frac{uD}{\nu}$	$u = u_p$
Disconzi *Discharge*	$Nu = 0.08\mathrm{Re}^{0.8}\mathrm{Pr}^{0.6}$	$\mathrm{Re} = \frac{uD}{\nu}$	$u = u_p + {u_p}^{0.8}{u_{c(t)}}^{0.2}$
Disconzi *Expansion*	$Nu = 0.12\mathrm{Re}^{0.8}\mathrm{Pr}^{0.6}$	$\mathrm{Re} = \frac{uD}{\nu}$	$u = u_p$
Disconzi *Suction*	$Nu = 0.08\mathrm{Re}^{0.9}\mathrm{Pr}^{0.6}$	$\mathrm{Re} = \frac{uD}{\nu}$	$u = u_p + {u_p}^{-0.4}{u_{c(t)}}^{1.4}$
Aigner	$St = \frac{h}{\rho c_p u} = \frac{Nu}{\mathrm{Re}\,\mathrm{Pr}}$	$St = \frac{C_f}{2\,\mathrm{Pr}^{2/3}}$	$C_f = 0.078\,\mathrm{Re}^{-0.25}$ $C_f = 0.046\,\mathrm{Re}^{-0.2}$

Table 8.1 Empirical correlation for heat transfer prediction

where u_p is the mean piston speed, α is the crank angle and ω is the angular velocity of crankshaft.

Table 8.1 shows how the heat exchange aspect is closely linked to the dynamics of the piston inside the cylinder and the dynamics of valve opening and closing.

Heat transfer from the walls inside the cylinder, including the piston, cylinder head, and along the suction line both contribute to the rise in gas temperature.

A rise in gas temperature of 1 °C at the start of compression results in a 0.3% reduction inefficiency. Therefore, preventing the gas from superheating and improving compressor performance might be accomplished by having a solid understanding of heat transmission inside the compressor as well as the development of innovative materials.

Additionally, there is a chance that lubricating oil would catch fire or that compressor parts will degrade quickly. This aspect on the lubricant not only affects the compressor from a thermal point of view, but also the dynamics of the reed generating an adhesion force, which has not been included in this work.

Both lubricated and non-lubricated machines exhibit adhesion. However, the impact is significantly more obvious in the former, and the situation is far more difficult, because it is primarily produced by the distortion of a lubricating oil layer in the space between the valve plate and the limiter, as can be seen in Fig.8.1.

Stiction can impair compressor performance by increasing the recommended work and decreasing volumetric efficiency. When the valve plate leaves the seat in most compressor valves, a stiction effect occurs. Stiction may also occur when the valve plate exits the limiter.

The stiction effect is accounted for only in cases where the valve plate is pressed against the obstacle for a finite time, When the valve plate collides with an object and instantly rebounds, the oil film has no noticeable adhesive effect.

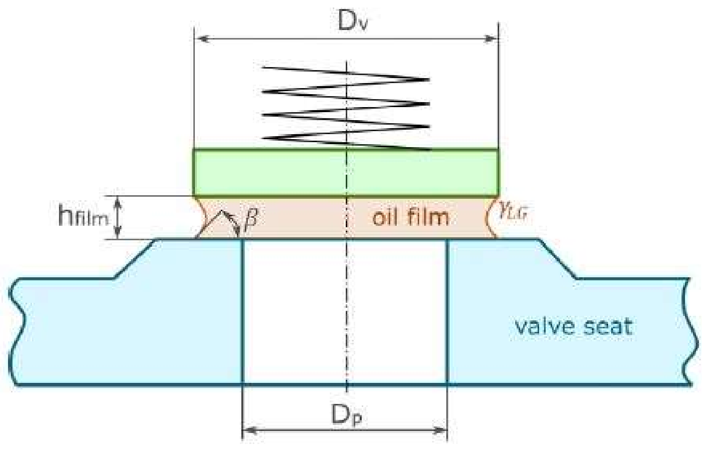

Figure 8.1 Oil Film

It was not possible to measure the reed lift in the laboratory, which requires very precise instrumentation. In the documentation provided by the valve manufacturers, a sperimental diagram of the reed lift in combination with the pressure inside the cylinder is attached (Fig.8.2).

A more irregular behaviour is observed in the experimental results of the lift [15]. This aspect with respect to the analytical model proposed in this paper is due in part to the assumption that only the first modal frequency was considered in the analysis of the valve dynamics

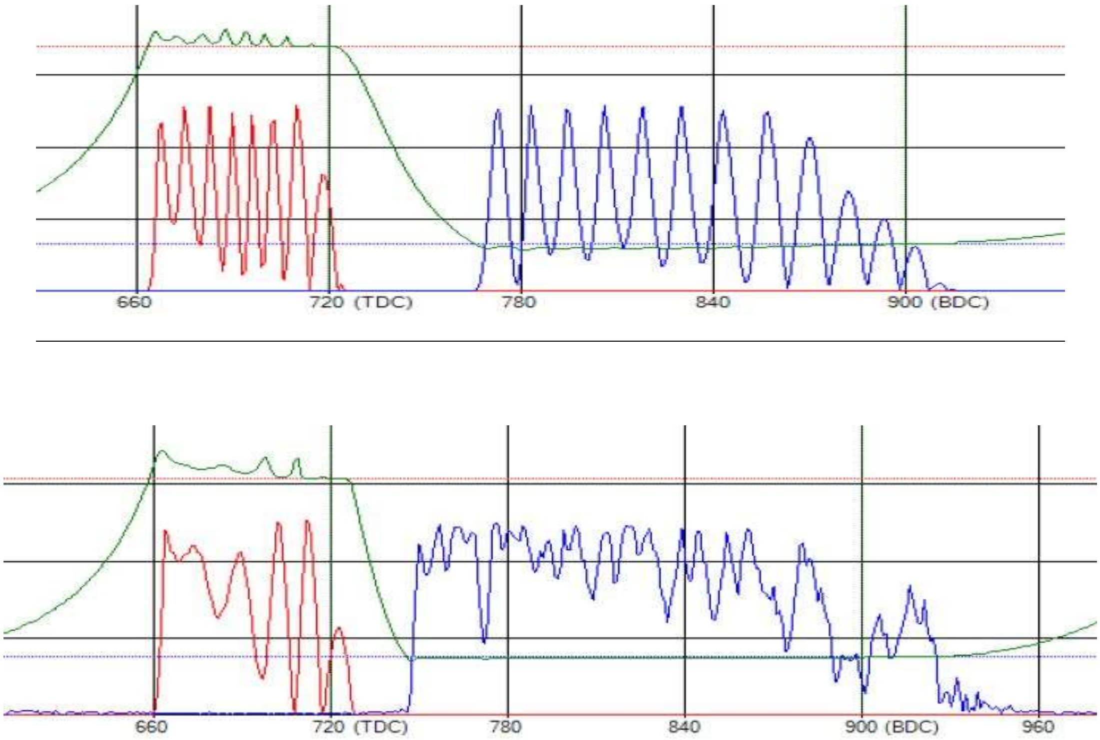

Figure 8.2 Valve lift Experimental

The mathematical model established in this thesis proved to be a useful tool for studying the behaviour of automated valves in the context of a reciprocating piston compressor.

This enables not only the analysis of various valve assembly configurations and the selection of the most suited for the desired application, but also the implementation of a preliminary design phase by identifying the best project solution in terms of performance.
Therefore, a possible development of this work would be to carry out a CFD analysis in a transient state taking into account all the aspects described so far (fluid-structure interaction, flow losses in the valve and in the cylinder, backflow, heat exchange) after defining a set of parameters that maximise the valve's performance by means of a sensitivity analysis.

Bibliography

[1] Atlas Copco. Compressed Air Manual 8th edition. 2015.

[2] Claudio Dongiovanni , " Thermal and Hydraulic Machines : Positive Displacement Machines" ,2019-2020

[3] Compressor Valves and Unloaders for Reciprocating Compressors 2002.

http://d-rco.com/techpapers/tp015.pdf.

[4] Tutorial: Compressor valves, EFRC Recip, https://www.recip.org/tutorial-compressor-valves/

[5] Michael Costagliola, "Dynamics of a reed type valve" Massachusetts Institute of Technology. Dept. of Mechanical Engineering, Thesis (Sc.D.) 1949.

[6] Simon Touber , " A contribution to the improvement of compressor valve design", University of Technology, Department of mechanical engineering,1976

[7] K. Fornitz Rasmus ,F. Hansen, " Numerical Modelling of a Suction Reed Valve from a Reciprocating Compressor using Fluid Structure Interaction", Aalborg University Esbjerg, Master Thesis ,2018.

[8] Documentation - MATLAB & Simulink ,"Simscape User's Guide",2021, https://www.mathworks.com/help/.

[9] Cristiana Delprete, Carlo Rosso, "Powertrain Component Design Engine: Crank Mechanism" 2014.

[10] Michal, Roman, "Modeling reciprocating compressor valve dynamics", AIP Conference Proceedings, 2017.

[11] Luca Romani , " Advanced methodology for the characterization of reciprocating compressors", School of engineering - Department of industrial engineering of Florence, Master's Thesis, 2013.

[12] Mu et al, " Dynamic modeling and analysis of compressor reed valve based on movement characteristics", Applied Thermal Engineering, 2019

[13] A. Saraf , J. Shah, "MATHEMATICAL MODELLING OF REED VALVE LIFT WITH CRANK ANGLE IN PISTON COMPRESSORS", Journal of Emerging Technologies and Innovative Research, Vol.7 ,2020.

[14] R. Habing , " Flow and Plate Motion in Compressor Valves", University of Twente , 1975.

[15] Hoerbiger, "Documentation of valve design ",2022.

[16] Mu et Al. ," An investigation of pressure loss and dynamical model of reed-type valves in compressors based on Euler–Bernoulli beam theory", Archive of Applied Mechanics, 2020.

[17] NASA, " Shape Effects on Drag" , https://www.grc.nasa.gov/www/k12/VirtualAero/BottleRocket/airplane/shaped.html

[18] Qian Xinghua, "The Development of the Simply Supported Feather Spring Vave", INTERNATIONAL COMPRESSOR ENGINEERING CONFERENCE ,1996.

[19] H K Versteeg and W Malalasekera, " Introduction to Computational Fluid Dynamics", Pearson Education, 2005.

[20] ANSYS Fluent User's Guide, Ansys Inc., 2013.

[21] R. Banfi, " Development of a CFD model to simulate the compressible flow within a pressure-relief safety valve", Politecnico di Milano, 2019.

[22] Jaroslav Šustek, " Analysis of Pressure Losses through Valve Plate in Compressor with CO2", Slovak University of Technology in Bratislava, AIP Conference Proceedings,2016.

[23] Sachin Pagnis, "Compressor Valve Simulation Using ANSYS and CFX", 2008 International ANSYS Conference,2008.

[24] Wang et Al., " Modeling the valve dynamics in a reciprocating compressor based ontwo-dimensional computational fluid dynamics numerical simulation", Proc IMechE Part E: J Process Mechanical Engineering227(4) 295–308, 2012

[25] H. Kerpicci, " Transient Modeling of Flows Through Suction Port and Valve Leaves of Hermetic Reciprocating Compressors", International Compressor Engineering Conference, 2006.

[26] Ansys Contact Guide , ANYS Inc., 2014.

[27] Zhao et Al. , " Application of CFD Method to Investigate the Evolution of the Thermodynamic Parameters of a Hyper Compressor and Its Pipelines", MDPI, 2022.

[28] J. Tuhovcak, "Heat Transfer Analysis in the Cylinder of Reciprocating Compressor", International Compressor Engineering Conference,2016.